eman ta zabal zazu

Universidad del País Vasco

Euskal Herriko Unibertsitatea

Aplicación de procesos de micro fabricación de alta productividad para la fabricación de componentes poliméricos funcionales de interés en el sector biomédico

"Application of high throughput microfabrication manufacturing processes for the fabrication of functional polymeric components of interest in the biomedical sector"

Dissertation presented to the department of Mining and Metallurgy Engineering and Materials Science (UPV/EHU) by

Xabier Mendibil Blasco

for the degree of Doctor of Philosophy

2023

Thesis advisors:

Dr. Iban Quintana Fernández

Dr. Jose-Ramon Sarasua Oiz

Agradecimientos

Quiero agradecer a Jose-Ramon Sarasua, miembro del Departamento de Ingeniería Minero-Metalúrgica y Ciencia de los Materiales de la Universidad del País Vasco, y a Iban Quintana, miembro de la Fundación Tekniker, por haberme dado la oportunidad de acceder a este programa de doctorado y haber podido realizar el trabajo de investigación en colaboración con estas dos entidades. Gracias Iban por la confianza depositada en mí, por tu paciencia, apoyo y consejo. No me puedo olvidar de Rocío Ortiz, gracias por tu ayuda y paciencia con las revisiones. Quiero también agradecer a Jone M. Ugartemendia, Ester Zuza y resto del personal del departamento de la universidad por vuestra disposición, colaboración y ayuda. Gracias también a los compañeros y compañeras de Tekniker que de algún modo me habéis acompañado y ayudado durante estos años, no solamente en las tareas referentes al trabajo de tesis, y me habéis hecho sentir que el trabajo es menos trabajo. En especial gracias Estibaliz Aranzabe, Miren Blanco y Cristina Monteserín por haberme "prestado" la extrusora para hacer mis cosas. Gracias Ana Aranzabe por tu consejo, comprensión, guía y motivación y gracias, Santos Merino, por haberme incluido en el equipo internacional e interdisciplinar con el que se han conseguido tan buenos resultados y me ha permitido aprender tanto.

Gracias a mi familia y amigos por acompañarme de manera incondicional y en especial a Araceli, Lander y Mattane, por estar a mi lado, colmar de positividad mi tiempo y redirigir siempre mi atención a lo que realmente importa.

Resumen y Estructura de la Tesis

El presente trabajo de tesis está estructurado en cuatro secciones principales: alcance y objetivos; introducción; resultados y discusión; y conclusiones generales. La sección de resultados y discusión, a su vez dividida en tres capítulos, describe de manera secuencial las actividades de investigación troncales vinculadas a la consecución de los objetivos definidos. El objetivo principal es establecer las bases de conocimiento científico-técnico que garanticen el desarrollo de componentes tubulares miniaturizados y micro-estructurados, cumpliendo con los requerimientos funcionales establecidos por la aplicación objetivo: la regeneración de nervios periféricos. El estudio se ha focalizado en el desarrollo de una metodología de procesado de polímeros bio-absorbibles, bajo las premisas de eficiencia, fiabilidad y escalabilidad industrial, considerando tecnologías de micro-replicación de alta productividad. En particular, dicha metodología contempla la combinación de la tecnología de micro-extrusión y la selección de poliésteres avanzados, tanto de origen sintético como bacteriano, demostrando la idoneidad de esta en la obtención de dichos componentes. Los resultados obtenidos demuestran la viabilidad de la fabricación de componentes tubulares implantables, bio-absorbibles y micro-estructurados, considerando la micro-extrusión como tecnología de fabricación clave en términos de productividad y funcionalidad del componente final.

La introducción, recogida en el Capítulo 1, resume el estado del arte actual, presentando los retos asociados al desarrollo de implantes poliméricos que promueven procesos regenerativos en lesiones de nervio periférico, tanto desde el punto de vista de fabricación, como funcional. Posteriormente se introduce una revisión de los materiales bio-absorbibles más empleados en términos académicos y a nivel comercial en dicha aplicación, destacando entre ellos los poliésteres. Finalmente, se describen los retos asociados a la implementación de tecnologías de fabricación de componentes bio-miméticos miniaturizados y micro-estructurados, susceptibles de ser empleados en la aplicación objetivo del presente trabajo de tesis.

La revisión del estado del arte establece que las características geométricas a escala micrométrica impactan drásticamente en las propiedades funcionales de los implantes de

nervio periférico (Nerve Guidance Conduits (NGC)). En particular, la micro-estructuración interna del componente, en forma de micro-porosidad de tamaño y proporción controlada, mejora la biocompatibilidad del implante y promueve los procesos regenerativos del nervio nativo. Esta micro-porosidad conforma una barrera permeable protectora en torno al tejido que se está regenerando, protegiéndolo y aislándolo del entorno al mismo tiempo que posibilita el intercambio de nutrientes y de productos de deshecho. La geometría del implante en su conjunto, incluyendo la presencia de paredes de espesor micrométrico, micro-porosas y/o micro-estructuradas no influyen únicamente en la interacción con el tejido, sino también en sus propiedades mecánicas, químicas y de bio-absorción, que a su vez son dependientes de la naturaleza del biopolímero seleccionado. Para cumplir con las especificaciones dimensionales establecidas en la fase de diseño de la aplicación, es necesario seleccionar una tecnología de fabricación adecuada. Esta tecnología debe garantizar la obtención de componentes cuyas dimensiones satisfagan los requerimientos de precisión establecidos en la fase de diseño, así como las demandas industriales en términos de productividad. Actualmente, la selección de esta tecnología es el principal desafío en el desarrollo de NGCs. Las tecnologías de fabricación de componentes poliméricos micro-estructurados que a priori cumplen con dichos requerimientos son aquellas basadas en la replicación: el hot-embossing, el micro-moldeo por inyección y la micro-extrusión. Esta última se posiciona como la más adecuada para la fabricación de componentes tubulares, como son los NGCs. Para superar las limitaciones en la fabricación de componentes mediante micro-extrusión, es necesario adquirir conocimiento sobre las magnitudes críticas que afectan a las propiedades de micro-replicación. Esto permitirá establecer una metodología de fabricación que garantice la precisión en la replicación en diferentes escenarios, incluyendo el uso de bio-polímeros y la inclusión en la matriz polimérica de porogeneradores para inducir la micro-porosidad deseada. En relación con la selección de dichos biopolímeros, los poliésteres son una de las familias de polímeros bio-absorbibles más utilizados e investigados en el ámbito biomédico, pudiéndose encontrar en una multitud de aplicaciones. La gran diversidad de formulaciones, copolimerizaciones y mezclas (blends) poliméricas susceptibles de ser desarrolladas favorece la versatilidad en la selección de la configuración más adecuada en función de los requerimientos mecánicos, biocompatibilidad y degradabilidad establecidos por la aplicación objetivo. La revisión del estado del arte se focaliza en aquellos poliésteres que han mostrado unas propiedades específicas adecuadas para su

empleo en el desarrollo de NGCs. En particular, el análisis se centra en la familia de poliésteres termoplásticos, debido a su mayor coexistencia con la tecnología de micro-extrusión.

El Capítulo 2 se centra en el estudio de las magnitudes características comunes de procesos de replicación, esto es, la temperatura y la presión, así como su influencia en la precisión de replicado de micro-estructuras con geometrías características de aquellas requeridas por la aplicación objetivo. Dicho estudio se realizó considerando la tecnología de micro-inyección de plástico como banco de ensayos de procesos de micro-replicación, dado sus características intrínsecas que permiten la implementación de sensores en la estación de trabajo, pudiendo correlacionar los parámetros de proceso seleccionados y las características geométricas de los motivos replicados. El conocimiento de dicha correlación permitió la implementación de una metodología de control y monitorización del proceso bajo el paraguas de una estrategia de cero defectos en fabricación. Se determinó una metodología novedosa de diseño correspondiente al emplazamiento de los sensores en el sistema y se logró correlacionar, de manera unívoca, los parámetros de entrada del proceso, las magnitudes medibles durante el mismo y el grado de replicación de las micro-estructuras del componente. Dichos resultados permitieron adquirir nuevo conocimiento sobre la influencia de dichas magnitudes y validar las hipótesis planteadas. En este sentido, se observó que la consigna de la temperatura en la entrada de la cavidad influía fuertemente en la calidad de la replicación al condicionar directamente la temperatura del polímero en el comienzo del llenado de la cavidad y de las micro-estructuras. La medida de la temperatura en la cavidad no se observó que variara significativamente con las temperaturas de entrada del polímero, indicando que el polímero fundido se atemperaba rápidamente a la temperatura del molde debido a su baja masa y alta relación superficie-volumen característica de la presencia de los micro-motivos. Los parámetros de proceso que pudieron correlacionarse con cambios críticos en la calidad de la replicación y, por lo tanto, esenciales para optimizar el proceso, fueron las consignas de temperaturas correspondientes a la boquilla y a la parte fija del molde. Estos parámetros son equivalentes a la temperatura del cilindro y de la boquilla en un sistema de extrusión, posicionándose como parámetros principales de estudio en el desarrollo de la investigación central del presente trabajo de tesis: La optimización de la tecnología de extrusión como herramienta única y confiable para la fabricación de NGCs bio-absorbibles, caracterizados por su geometría tubular y la presencia de estructuras

micrométricas que promuevan una mejora en las propiedades regenerativas de dichos implantes.

El Capítulo 3 se focaliza en el proceso de extrusión de un poliéster identificado como un copolímero 70/30 de poli (L-lactida) (PLLA) y poli (ε-caprolactona (PCL), el cual fue aditivado con micro-partículas (porogeneradores) de cloruro sódico (NaCl) de tamaño y proporción controlada. Dicho estudio se centró en analizar cómo el tamaño y la proporción de las partículas del porogenerador sólido afectan a las propiedades mecánicas, a la cristalización y a la variación de tamaño de las muestras de poliéster extruido una vez se retiran mediante lixiviación. Este análisis se realizó como un paso previo para generar conocimiento en el desarrollo de componentes tubulares micro-porosos hechos de poliésteres biocompatibles, que cumplan con los requerimientos mecánicos y geométricos establecidos por la aplicación objeto de estudio. A partir de la investigación realizada se logró confirmar la viabilidad de la extrusión para procesar poliésteres biocompatibles con cargas altas de porogeneradores sólidos. Se analizó la influencia de la porosidad en las propiedades mecánicas en función de las variables de tamaño y proporción del porogenerador, así como el efecto que tienen en la eficacia de la lixiviación de las partículas porogeneradoras y la variación del tamaño debido a la absorción de disolvente. El conocimiento obtenido del estudio permitió establecer pautas para seleccionar la proporción y tamaño del porogenerador para fabricar NGCs con el tamaño, porosidad y propiedades mecánicas deseadas. Este conocimiento, junto con la selección de parámetros de proceso identificados en el Capítulo 2, se materializó en la obtención de un tubo de copolímero de PLLA y PCL con una alta carga (70% en peso) de porogenerador y extruido con paredes delgadas, como demostrador de la capacidad de la extrusión para fabricar NGCs, asentando la extrusión como plataforma para la obtención de los NGCs fabricados y validados en términos funcionales en el Capítulo 4.

El Capítulo 4 añade un factor crítico más en el desarrollo industrial de implantes de nervio periférico: el uso de poliésteres de origen bacteriano como factor crítico en la dotación de una mejora en la biocompatibilidad y propiedades regenerativas de los NGCs. Los materiales seleccionados son los polihidroxialcanoatos (PHAs), los cuales han demostrado su idoneidad en términos biológicos respecto a sus propiedades de adhesión y crecimiento celular, siendo de gran interés en el ámbito de ingeniería de tejidos. En particular, dichos poliésteres ofrecen

mejoras sustanciales frente a aquellos de origen sintético en cuanto a la regeneración de nervio periférico facilitando, en mayor medida, la adhesión y la diferenciación de células de Schwann, elementos cruciales para el guiado y regeneración de los axones. El estudio se focalizó en el procesado de un blend de PCL, PHA y un porogenerador sólido, combinando las buenas propiedades de extrusión del PCL y las características inherentes de biocompatibilidad y regeneración axonal del PHA, abordando por primera vez, el desarrollo y optimización de la tecnología de extrusión hacia la fabricación de NGCs basados en estructuras tubulares micro-porosas combinando poliésteres naturales y sintéticos, controlando a su vez la geometría (espesor de pared a escala micrométrica) y propiedades mecánicas del implante. El porogenerador utilizado, que en este caso fue glucosa para evitar problemas de citotoxicidad derivados del uso de NaCl, permitía su absorción por parte de los tejidos, pudiendo prescindir de la etapa de lixiviación previa a la implantación del NGC. Una vez controlada la influencia de los parámetros de proceso en la geometría, propiedades micro-estructurales y mecánicas del NGC, se fabricaron estructuras tubulares bio-miméticas altamente porosas con propiedades mecánicas similares a las correspondientes del nervio ciático de rata (modelo biológico del ensayo), y con un periodo de degradación tras implantación acorde con el tiempo requerido para el proceso de regeneración del nervio periférico. A su vez, el estudio concluye con una validación de las propiedades de regeneración de dichos implantes *in-vivo*. La capacidad regenerativa del NGC desarrollado a partir de un blend PCL-PHA mediante extrusión fue superior al implante comercial de poli(lactida-co-caprolactona) (PLCL), referencia en este ámbito, demostrando el éxito del implante desarrollado mediante la tecnología de fabricación de alta productividad, objeto de la presente tesis doctoral. Esta novedosa ruta de fabricación fácilmente escalable supone un punto de inflexión en la producción de implantes de nervio periférico.

El Capítulo 5 resume los resultados generales de la tesis, así como una descripción del trabajo futuro que contempla el desarrollo de un diseño avanzado de NGCs que incluye, junto con las características geométricas y micro-estructurales descritas en el presente trabajo, la presencia de micro-canales de guiado axonal en las paredes internas de dichos implantes tubulares. Aunque dicho diseño ha sido propuesto previamente en la literatura, no existe hasta la fecha un estudio que aborde la fabricación de dicho diseño mediante tecnología de micro-extrusión,

el cual podrá realizarse gracias al conocimiento adquirido en el presente trabajo de tesis y la experiencia previa de TEKNIKER y la Universidad del País Vasco (UPV-EHU) en el desarrollo de superficies micro-estructuradas con capacidad de guiado y regeneración celular.

El trabajo realizado durante este trabajo de tesis ha dado lugar a publicaciones en revistas científicas y contribuciones en conferencias internacionales en forma de presentaciones orales, y una solicitud de patente que se detallan a continuación.

Publicaciones:

- Mendibil, X., Llanos, I., Urreta, H. and Quintana, I. In process quality control on micro-injection moulding: the role of sensor location. Int. J. Adv. Manuf. Technol. 2017, 89, 3429-3438. DOI: 10.1007/s00170-016-9300-2.
- Mendibil, X., Ortiz, R., Sáenz de Viteri, V., Ugartemendia, J.M., Sarasua, J.R. and Quintana, I. High throughput manufacturing of bio-resorbable micro-porous scaffolds made of poly(L-lactide-co-ε-caprolactone) by micro-extrusion for soft tissue engineering applications. Polymers. 2019, 12, 34. DOI: 10.3390/polym12010034.
- Mendibil, X., González-Pérez, F., Bazan, X., Díez-Ahedo, R., Quintana, I., Rodríguez, F. J., Basnett, P., Nigmatullin, R., Lukasiewicz, B., Roy, I., Taylor, C. S., Glen, A., Claeyssens, F., Haycock, J. W., Schaafsma, W. González, E., Castro, B., Duffy, P., Merino, S. Bio-resorbable and Mechanically Optimized Nerve Guidance Conduit Based on a Naturally Derived Medium Chain Length Polyhydroxyalkanoate and Poly(ε-Caprolactone) Blend. ACS Biomater. Sci. Eng. 2021, 7, 2, 672-689. DOI: 10.1021/acsbiomaterials.0c01476.

Presentaciones orales en conferencias internacionales:

- Mendibil, X., Llanos, I., Urreta, H. and Quintana, I. Micro-injection quality monitoring using in-mould pressure and temperature sensors. 11th International Conference on Micro Manufacturing. Orange County, California, USA, March 2016.
- Mendibil, X., Ortiz, R., Sáenz de Viteri, V., Ugartemendia, J.M., Sarasua, J.R. and Quintana, I. Validation of the micro-extrusion process for the manufacturing of tubular bio-resorbable porous scaffolds for tissue engineering. EUSPEN, Special Interest Group meeting: Micro/Nano manufacturing. Technical University of Berlin. 27th – 28th November 2019.

Solicitud de patente:

- Merino, S., Quintana, I., Márquez, C., Mendibil, X., Bazan, X., Diez, R., Roy, I., Basnett, P., Nigmatullin, R., Lukasiewicz, B., Haycock, J., Claeyssens, F., Sherborne, C., Glen, A., Taylor, C., Rodriguez, F.J., Gonzalez, F.J. Implantable nerve guidance conduit for nerve repair. PCT/EP2018/054984.

Además de las publicaciones, las participaciones en las conferencias y la solicitud de una patente, el trabajo llevado a cabo durante la tesis ha hecho posible colaborar y contribuir en los siguientes proyectos financiados por la Comisión Europea:

- Minimizing Defects in Micro Manufacturing Applications (MiDeMMA). Grant agreement: 285614, funded under FP7-NMP. (https://cordis.europa.eu/project/id/285614).
- Novel combination of biopolymers and manufacturing technologies for production of a peripheral nerve implant containing an internal aligned channels array (NEURIMP). Grant agreement: 604450, funded under FP7-NMP. (https://cordis.europa.eu/project/id/604450).

Summary and Thesis structure

This thesis is structured in four main sections: scope and objectives; introduction; results and discussion; and general conclusions. The results and discussion section, in turn, is divided into three chapters, sequentially describing the main research activities linked to achieving the defined objectives. The main objective is to establish the scientific-technical knowledge base that guarantees the development of miniaturized and micro-structured tubular components, meeting the functional requirements established by the target application: the regeneration of peripheral nerves. The study has focused on the development of a methodology for the processing of bio-resorbable polymers, under the premise of efficiency, reliability and industrial scalability, considering high-productivity micro-replication technologies. In particular, the methodology considers the combination of micro-extrusion technology and the selection of advanced polyesters, both of synthetic and bacterial origin, showing its suitability for the obtaining of these components. The results obtained show the feasibility of manufacturing implantable, bio-resorbable, and micro-structured tubular components, considering micro-extrusion as a key manufacturing technology in terms of productivity and functionality of the final component.

The introduction, described in Chapter 1, summarizes the current state of the art, presenting the challenges associated with the development of polymeric implants that promote regenerative processes in peripheral nerve lesions, both from a manufacturing and functional point of view. Subsequently, a review of the most widely used bio-resorbable materials, both in academic and commercial terms, in this application is introduced, with special attention to polyesters. Finally, the challenges associated with the implementation of technologies for the fabrication of miniaturized and micro-structured bio-mimetic components that can be used in the target application of this thesis are described.

The review of the state of the art establishes that micrometer-scale geometric features drastically impact the functional properties of peripheral nerve implants (Nerve Guidance Conduits (NGCs)). In particular, the internal micro-structure of the component, in the form of

micro-porosity of controlled size and proportion, improves the biocompatibility of the implant and promotes regenerative processes of the native nerve. This micro-porosity constitutes a protective permeable barrier around the regenerating tissue, protecting and isolating it from the environment while allowing the exchange of nutrients and waste products. The geometry of the implant as a whole, including the presence of micrometric-size, micro-porous and/or micro-structured walls, not only influences the interaction with the tissue, but also its mechanical, chemical and bio-resorption properties, which in turn are dependent on the nature of the selected biopolymer. In order to meet the dimensional specifications established in the design phase of the application, it is necessary to select an appropriate manufacturing technology. This technology must guarantee the production of components whose dimensions satisfy the accuracy requirements established in the design phase, as well as the industrial demands in terms of productivity. Currently, the selection of this technology is the main challenge in the development of NGCs. The technologies for the manufacture of micro-structured polymeric components that, a priori, meet these requirements are those based on replication, such as hot-embossing, micro-injection molding and micro-extrusion. Being the latter the most suitable for the fabrication of tubular components, such as NGCs. To overcome the limitations in the fabrication of components by micro-extrusion, it is necessary to acquire knowledge about the critical quantities that affect the micro-replication properties. This will enable the establishment of a fabrication methodology that ensures accurate replication in different scenarios, including the use of biopolymers and the inclusion of porogenerators in the polymer bulk to induce the desired micro-porosity. Regarding the selection of these biopolymers, polyesters are one of the most widely used and studied families of bio-resorbable polymers in the biomedical field, and they can be found in a multitude of applications. The great diversity of formulations, co-polymerizations, and polymeric blends that can be developed favors the versatility in the selection of the appropriate configuration according to the mechanical requirements, biocompatibility, and degradability established by the target application. The review of the state of the art is focused on those polyesters that have shown intrinsic properties suitable for their use in the development of NGCs. In particular, the analysis focuses on the family of thermoplastic polyesters, because of their greater coexistence with micro-extrusion technology.

Chapter 2 focuses on the study of the common characteristic magnitudes of replication processes, *i.e*., temperature and pressure, as well as their influence on the replication accuracy of micro-structures with geometries characteristic of those required by the target application. This study was carried out considering the plastic micro-injection technology as a test bench for micro-replication processes, given its intrinsic characteristics that allow the implementation of sensors in the workstation, being able to correlate the selected process parameters and the geometrical characteristics of the replicated features. The knowledge of this correlation led to the implementation of a process control and monitoring methodology under the zero-defect manufacturing strategy framework. From this monitoring, a novel design methodology was determined corresponding to the location of the sensors in the system, and it was possible to correlate, in a univocal way, the input parameters of the process, the measurable magnitudes during the process, and the replication degree of the micro-structures of the component. These results allowed the acquisition of new knowledge on the influence of these magnitudes and the validation of the proposed hypotheses. In this sense, it was observed that the temperature setpoint at the entrance of the cavity strongly influenced the quality of the replication by directly conditioning the temperature of the polymer at the beginning of the filling of the cavity and of the micro-structures. The cavity temperature measurement was not observed to vary significantly with polymer inlet temperatures, indicating that the molten polymer was rapidly tempered at the mold temperature because of its low mass and high surface-to-volume ratio characteristic of the presence of the micro-features. The process parameters that could be correlated with critical changes in the quality of the replication and therefore, essential to optimize the process, were the temperature set points corresponding to the nozzle and the fixed part of the mold. These parameters are equivalent to the barrel and nozzle temperature in an extrusion system, positioning them as the main parameters of study in the development of the central research of this thesis work: The optimization of extrusion technology as a unique and reliable tool for the manufacture of bio-resorbable NGCs, characterized by their tubular geometry and the presence of micrometric structures that promote an improvement in the regenerative properties of such implants.

Chapter 3 focuses on the extrusion process of a polyester identified as a 70/30 copolymer of poly(L-lactide) (PLLA) and poly(ε-caprolactone) (PCL), which was additivated with sodium

chloride (NaCl) micro-particles (porogenerators) of controlled size and ratio. This study focused on analyzing how the size and ratio of the solid porogenerator particles affect the mechanical properties, crystallization, and sample size variation of the extruded polyester specimens once the porogenerator is removed by leaching. This analysis was performed as a preliminary step to generate knowledge in the development of micro-porous tubular components made of biocompatible polyesters, which meet the mechanical and geometrical requirements established by the application under study. From the conducted research, it was possible to confirm the feasibility of extrusion for processing biocompatible polyesters with high solid porogenerator loadings. The influence of porosity on mechanical properties was analyzed as a function of the porogenerator size and ratio variables, as well as the effect they have on the leaching efficiency of the porogenerator particles and the size variation due to solvent absorption. The knowledge gained from the study allowed establishing guidelines for selecting the porogenerator ratio and size to fabricate NGCs with the desired size, porosity and mechanical properties. This knowledge, together with the selection of process parameters identified in Chapter 2, was materialized in obtaining a tube of PLLA and PCL copolymer with high loading (70% by weight) of porogenerator and extruded with thin walls, as a demonstrator of the ability of extrusion to manufacture NGCs and to establish extrusion as a platform for obtaining the NGCs manufactured and validated in functional terms in Chapter 4.

Chapter 4 adds one more critical factor in the industrial development of peripheral nerve implants: the use of polyesters of bacterial origin as a critical factor in providing improved biocompatibility and regenerative properties of NGCs. The selected materials are polyhydroxyalkanoates (PHAs), which have demonstrated their suitability in biological terms with respect to their cell adhesion and growth properties, being of great interest in the field of tissue engineering. In particular, these polyesters offer substantial improvements over those of synthetic origin in terms of peripheral nerve regeneration by promoting, to a greater extent, adhesion and differentiation of Schwann cells, crucial elements for axon guidance and regeneration. The study was focused on the processing of a blend of PCL, PHA, and a solid porogenerator, combining the good extrusion properties of PCL and the inherent biocompatibility and axonal regeneration characteristics of PHA, addressing, for the first time, the development and optimization of extrusion technology towards the fabrication of NGCs

based on micro-porous tubular structures combining natural and synthetic polyesters, controlling, in turn, the geometry (wall thickness at micrometer scale) and mechanical properties of the implant. The porogenerator used, which in this case was glucose to avoid cytotoxicity problems derived from the use of NaCl, facilitated its absorption by the tissues, making it possible to skip the leaching stage prior to implantation of the NGC. Once the influence of the process parameters on the geometry, micro-structural and mechanical properties of the NGC were controlled, highly porous bio-mimetic tubular structures were fabricated with mechanical properties similar to those corresponding to the rat sciatic nerve (biological model of the assay), and with a degradation period after implantation in accordance with the time required for the peripheral nerve regeneration process. In turn, the study concludes with a validation of the regenerative properties of these implants *in-vivo*. The regenerative capacity of the NGC developed from a PCL-PHA blend by extrusion was superior to the commercial poly(lactide-co-caprolactone) (PLCL) implant, a reference in this area, proving the success of the implant developed by means of the high throughput manufacturing technology, the object of the present doctoral thesis. This novel and easily scalable manufacturing route represents a turning point in the production of peripheral nerve implants.

The Chapter 5 summarizes the general results of the thesis, as well as a description of future work that involves the development of an advanced design of NGCs that includes, together with the geometrical and micro-structural features described in the present work, the presence of axonal guidance micro-grooves in the inner walls of such tubular implants. Although such design has been previously proposed in the literature, there is no study to date that addresses the fabrication of such design by means of micro-extrusion technology, which will be possible thanks to the knowledge acquired in the present thesis work and the previous experience of TEKNIKER and the University of the Basque Country (UPV-EHU) in the development of micro-structured surfaces with guidance and cell regeneration capabilities.

The work carried out during this thesis work resulted in publications in scientific journals and contributions to international conferences in the form of oral presentations, and a patent request, which are detailed below.

Publications:

- Mendibil, X., Llanos, I., Urreta, H. and Quintana, I. In process quality control on micro-injection moulding: the role of sensor location. Int. J. Adv. Manuf. Technol. 2017, 89, 3429-3438. DOI: 10.1007/s00170-016-9300-2.
- Mendibil, X., Ortiz, R., Sáenz de Viteri, V., Ugartemendia, J.M., Sarasua, J.R. and Quintana, I. High throughput manufacturing of bio-resorbable micro-porous scaffolds made of poly(L-lactide-co-ε-caprolactone) by micro-extrusion for soft tissue engineering applications. Polymers. 2019, 12, 34. DOI: 10.3390/polym12010034.
- Mendibil, X., González-Pérez, F., Bazan, X., Díez-Ahedo, R., Quintana, I., Rodríguez, F. J., Basnett, P., Nigmatullin, R., Lukasiewicz, B., Roy, I., Taylor, C. S., Glen, A., Claeyssens, F., Haycock, J. W., Schaafsma, W. González, E., Castro, B., Duffy, P., Merino, S. Bio-resorbable and Mechanically Optimized Nerve Guidance Conduit Based on a Naturally Derived Medium Chain Length Polyhydroxyalkanoate and Poly(ε-Caprolactone) Blend. ACS Biomater. Sci. Eng. 2021, 7, 2, 672-689. DOI: 10.1021/acsbiomaterials.0c01476.

Oral dissertations in international conferences:

- Mendibil, X., Llanos, I., Urreta, H. and Quintana, I. Micro-injection quality monitoring using in-mould pressure and temperature sensors. 11th International Conference on Micro Manufacturing. Orange County, California, USA, March 2016.
- Mendibil, X., Ortiz, R., Sáenz de Viteri, V., Ugartemendia, J.M., Sarasua, J.R. and Quintana, I. Validation of the micro-extrusion process for the manufacturing of tubular bio-resorbable porous scaffolds for tissue engineering. EUSPEN, Special Interest Group meeting: Micro/Nano manufacturing. Technical University of Berlin. 27th – 28th November 2019.

Patent request:

- Merino, S., Quintana, I., Márquez, C., Mendibil, X., Bazan, X., Diez, R., Roy, I., Basnett, P., Nigmatullin, R., Lukasiewicz, B., Haycock, J., Claeyssens, F., Sherborne, C., Glen, A., Taylor, C., Rodriguez, F.J., Gonzalez, F.J. Implantable nerve guidance conduit for nerve repair. PCT/EP2018/054984.

In addition to publications, conference contributions, and a patent request, the work carried out during the thesis made it possible to collaborate and contribute to the following projects funded by the European Commission:

- Minimizing Defects in Micro Manufacturing Applications (MiDeMMA). Grant agreement: 285614, funded under FP7-NMP. (https://cordis.europa.eu/project/id/285614).
- Novel combination of biopolymers and manufacturing technologies for production of a peripheral nerve implant containing an internal aligned channels array (NEURIMP). Grant agreement: 604450, funded under FP7-NMP. (https://cordis.europa.eu/project/id/604450).

Scope and Objectives

This work, which emerges from the collaboration between the University of the Basque Country (UPV/EHU) and the technological center TEKNIKER, member of the Basque Research and Technology Alliance (BRTA), has as main objective to acquire knowledge and to develop a methodology to achieve the development of micro-structured tubular components made of medical grade bio-resorbable polyesters in an efficient, reliable, and industrially scalable manner.

For this purpose, it is required to meet the following specific targets:

- To identify the key process parameters characteristic of high throughput polymer micro-replication processes and to elucidate the influence of those parameters on the replication quality. This knowledge allows an effective monitoring and control of the process, promoting the quality control in manufacturing of polymer components containing micro-features.
- To establish a method for obtaining bio-resorbable micro-porous and micro-walled tubular components based on polymer extrusion manufacturing technique. It involves not only the determination of the effect of process parameters, porogenerator selection, and biopolymer characteristics on replication quality, but also the influence of those parameters on the porosity distribution and physicochemical properties of the final product. This information turns out extremely helpful to produce porous tubular components that fulfill the dimensional and mechanical requirements that must be satisfied by NGCs.
- To transfer the knowledge acquired to the development and validation, in terms of physicochemical and biological properties, of an advanced bio-resorbable micro-porous NGC made of a novel blend of polyesters of synthetic and bacterial origin, that provides better outcomes in terms of biocompatibility and nerve regeneration capacity.

Table of contents

Chapter 1

Introduction

1.1 Background

The emergence of micro-manufactured components, which started in the 1990s, had an unprecedented impact in a vast amount of different areas [1], and there is a shared consensus that medical applications have the greatest potential to benefit from the use of those components [2,3]. Micro-manufactured components not only allow the reduction in size of the systems, which leads to a reduction in weight and number of used materials, but also enable new synergistic functionalities through their micro-features [4,5].

A micro-manufactured component is an element or system with at least one of its functional dimensions in the micrometer range, although the overall dimensions can be up to several millimeters [6–8]. This definition of micro-component implies that there is an enormous number of medical application examples that benefit from the implementation of these components. The self-evident medical application of micro-components lies in their use in minimally invasive surgery (MIS), where the reduction of the dimensions and the integration of functionalities can result in a significant change in procedures such as laparoscopy or arthroscopy, minimizing the incisions, related pain, and recovery time of patients. [2,9,10]. Additionally, the miniaturization and customization of surface micro-structuring leads to other derived effects, such as micro-fluidic properties and modulation of interactions between tissue cells and topography of the micro-component. These effects enable further development in technological areas such as drug discovery, biosensor development and tissue engineering [5,11–16].

Micro-manufactured components used in medical applications are challenging parts for several reasons; first, the medical application where they are going to be used defines very tight requirements of size, quality, and physicochemical properties; second, the materials suitable for the medical application may present intrinsic properties that define and narrow the manufacturing methods suitable for being applied to the specific application; third and last, the manufacturing processes necessary to produce the micro-manufactured components also show their own peculiarities and limitations. In particular, one of the applications where a large number of requirements converge, making it necessary to develop an optimized micro-

fabrication methodology, is the fabrication of implantable guide conduits for peripheral nerve regeneration.

This chapter begins by defining the nerve guidance conduits used in surgical procedures for the regeneration of peripheral nerves. The challenges and requirements for these implants are reviewed, along with the current solutions and a brief overview of different researched alternatives found in the literature in which the micro-structuration plays an important role in the performance of the implant. Then, the most used polymers for peripheral nerve regeneration applications are explored, with a particular emphasis on polyesters. The technical introduction concludes with an overview of the replication technologies that can be used to obtain micro-fabricated components, and specifically in tubular form, since these replication processes allow for high throughput manufacturing.

1.2 Nerve guidance conduits

A nerve guidance conduit (NGC) is a manufactured implantable tubular scaffold used to repair a damaged nerve. The use of this type of implants is one of the alternatives for the surgical repair of medium size gap injuries of peripheral nerves.

Peripheral nerves are those motor-sensory nerves that do not belong to the central nervous system, *i.e.*: the brain, brain stem and the spinal cord. They are present all over the body and can be damaged by a variety of reasons, with trauma being the most common cause. Although peripheral nerve injury is typically not life-threatening, it significantly impacts the patient's quality of life, which has significant socio-economic consequences [17,18].

The common surgical technique to repair a severed peripheral nerve is to join both two ends of the nerve together by means of suture or fibrin glue, but this method requires no tension on the nerve, as excessive tension can prevent axon regeneration and jeopardize blood flow to the nerve. In practice, this means gaps shorter than 10 mm [19,20]. For longer gap distances, the use of autograft is considered the gold standard. However, this approach has a number of downsides, including the loss of sensation at donor site, the need for an additional incision to collect the graft tissue, the development of scars at donor site, neuropathic pain, limited

availability, and complications related to the size and fascicle mismatch [21,22]. Nerve allografts and xenografts, which can be used to avoid availability problems and donor morbidity, are decellularized extracellular matrices obtained from human or animal nerve tissue which are later seeded with cells from the patient. Although the use of allo- and xenografts can overcome some of the drawbacks of the autografts, they require a systemic immunosuppression therapy [18,21,22]. Figure 1.1 (a) schematically shows the implantation of a nerve segment to repair a gap between two sections of damaged nerve. The origin of the nerve used determines whether it is classified as an autograft, allograft, or xenograft. Allografts make use of nerves of human origin while xenografts utilize nerves of porcine or bovine origin.

Figure 1.1. (b) schematically shows an implanted NGC covering the gap between the two nerve stumps. These artificial implants are proposed as an alternative to address all the issues that nerve grafts have. An ideal NGC requires a series of characteristics that conflict with each other, such for example: it must provide support and mechanical strength to immobilize both ends of the damaged nerve during the healing process and avoid kinking problems when flexed by the surrounding tissue and at the same time be flexible and exert no forces on the nerve that is being regenerated. It must have an internal structure to guide the axons and at the same time should not hinder cell migration and the growth of the tissue. It must isolate the internal part of the conduit to concentrate the growth factors and at the same time it must be porous and permeable to allow the exchange of nutrients and waste products [17,20,22,23]. No single NGC can meet all requirements in an ideal way, which in turn, results in a wide variety of commercial solutions and an active field of research in which a compromise between requirements is pursued to optimize the nerve regeneration.

The following section corresponds to a brief overview of the commercially available NGCs on the market and design approaches currently being studied that involve micro-features. The fabrication methods considered to create such micro-features are also reviewed.

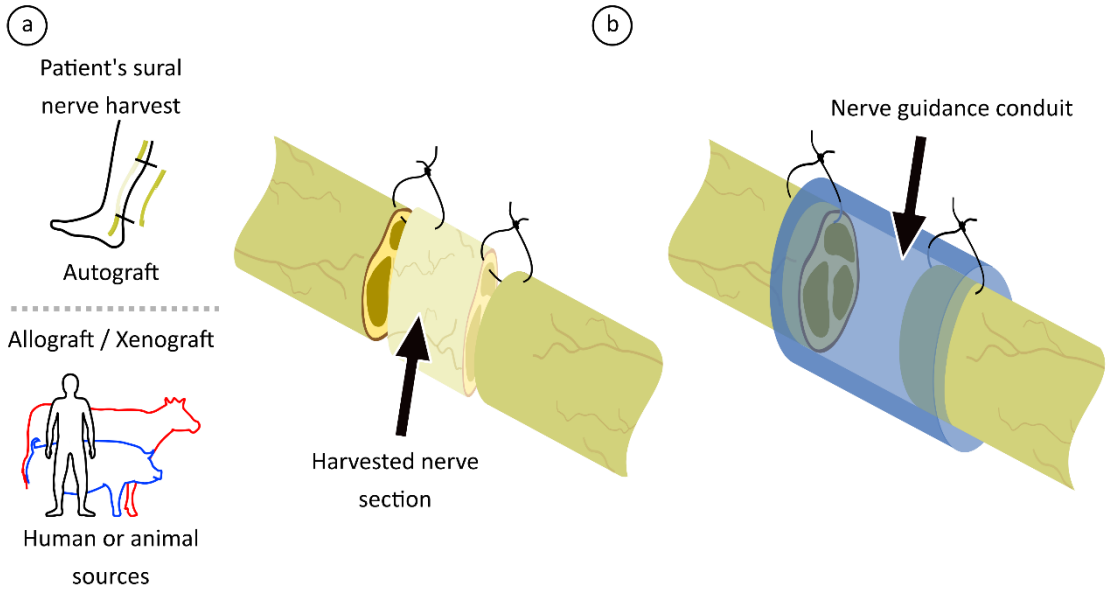

Figure 1.1 Type of implanted nerve according to its source, autograft, allograft, or xenograft and harvested nerve sutured between the two nerve stumps to bridge the gap (a). Nerve guidance conduit sutured to both nerve stumps (b).

1.2.1 Commercial NGCs

Table 1.1 lists the commercially available NGCs that have been found in the literature. This table does not include some products that, despite being found in the updated literature, are still in clinical trials or have disappeared from the market.

Commercially available NGCs include Neurotube®, a highly porous NGC made of a woven mesh of polyglycolic acid (PGA) fibers that was the first NGC of synthetic origin to be approved by the FDA [24]. More recently Nerbridge®, also composed by a PGA filament fabric, is commercialized with its lumen filled with collagen [25]. In this regard, the NeuraGen 3D Nerve Guide Matrix® was the first FDA-approved NGC available on the market to include intra-luminar filler, which is claimed to enhance the regeneration of the nerve in contrast to the hollow NGC [17]. NeuroFlex™ has the unique feature of being designed to bend up to 140° and not to kink, which renders it suitable for repair nerves in joints. Neurolac® is the only FDA approved NGC that is

Table 1.1 Commercially available NGCs, data collected and adapted from Houshyar *et al*. [20], Taylor *et al*. [21], Gu *et al*. [26] and Kehoe *et al*. [24].

Product name	Diameter (d) (mm) Length (L) (mm)	Biomaterial	Degradation Time (months)	Manufactured by
Neurotube®	d= 2.3 – 8 L= 20 – 40	Polyglycolic acid (PGA)	6 – 12	Synovis Micro Companies Alliance
Nerbridge®	d= 1 – 4 L=25	Polyglycolic acid (PGA)	3	Toyobo
NeuraGen®	d= 1.5 – 7 L= 20 – 30	Collagen type I	36 – 48	Integra Life Sciences
NeuraGen 3D Nerve Guide Matrix®	d= 1.5 – 7 L= 20 – 30	Collagen type I	--	Integra Life Sciences
NeuroFlex™	d= 2 – 6 L= 25	Collagen type I	4 - 8	Collagen Matrix Inc.
NeuroMatrix™	d= 2 – 6 L= 25	Collagen type I	4 - 8	Collagen Matrix Inc.
Neurolac®	d= 1.5 - 10 L= 30	Poly(lactide-caprolactone) (PLCL)	16	Polyganics

translucent and that shows comparable results to autograft in lesions involving gaps up to 20 mm [19,24]. Nevertheless, due to the lack of standardization of preclinical models and their evaluation, it is rather complex to compare the data obtained in the conducted trials with the different NGCs [27,28]. Among the NGCs available on the market, those that are not made of animal-derived materials such as collagen, are made of synthetic polyesters like PGA and poly(lactide-caprolactone) (PLCL).

1.2.2 NGC developments involving micro-manufacturing

There is extensive literature on the development of next-generation NGCs that aim to overcome the limitations of FDA-approved NGCs which, except the NeuraGen 3D Nerve Guide Matrix®, are hollow tubes made of natural or synthetic materials [29]. There is active research focused on introducing biochemical agents and cues inside NGCs to guide, promote, or facilitate the propagation of tissue regenerating cells inside them. Example of these biochemical techniques is the filling of the tube lumen with hydrogels containing a variety of components (proteins, peptides, etc.) to improve regeneration [17,23]. These biochemical techniques are far from the scope of this work, and herein only those developments involving physical modifications of the

NGC that imply challenges in their manufacturing route will be reviewed, specifically: intraluminal structures and fillers, wall porosity, and intraluminal grooves. Figure 1.2 shows the modifications that can be made to the wall of the NGC, *i.e.*: porosity and inner micro-grooves, in (a), and the different fillers that can be used to fill the lumen of the NGC in (b).

- Intraluminal fillers/structure

Hollow NGCs potentially face problems in the nerve regeneration process because of difficulties derived from the dispersion of the regenerating axons [30], consequently, different alternatives have been studied to fill the NGC lumen with structures that perform the scaffold function to longitudinally guide the axons in the inner volume of the NGC, although some authors claim that NGC fillers do not improve their performance over the hollow tubes [23]. These intraluminal structures can be divided into three main groups, multi-channel structures, sponges, and fibers. Regardless of which of the filling alternatives is adopted, the method of inserting the structures/fillers into the tubular NGC remains highly dependent on the skill of the handler, being difficult to industrialize/automatize.

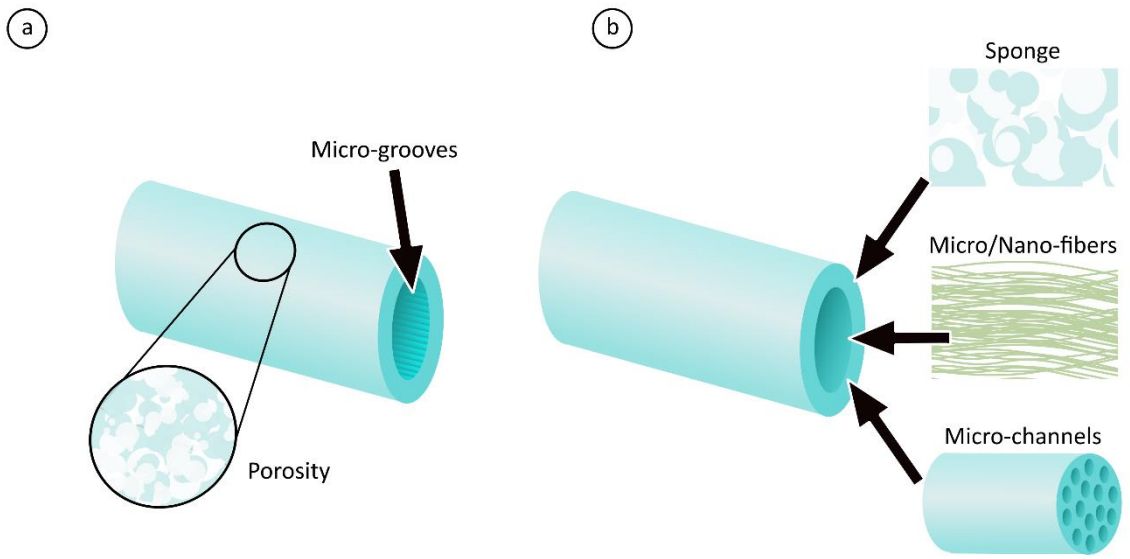

Figure 1.2 Porosity and inner micro-grooves as NGC wall modifications (a). Different types of fillers to introduce in the lumen of the NGC (b).

- *Multi-channel structures*

The NGC lumen is arranged into smaller sections to increase the contact surface and reduce axon dispersion mimicking the natural compartmented structure of the nerves [27,30]. Different approaches exist in the literature to create the micro-channels, but most are based on molding or adding material around parts that are later removed to create the micro- channels. Sundback *et al*. [31] and Diez-Ahedo *et al*. [32] used molding to create highly porous multi-channel structures. Lee *et al*. [33] used sucrose rods over which they wrapped a fiber mesh created by electrospinning. This method allowed to obtain an array of micro-channels made of electrospinned fiber once the rods were removed by dissolution. Pawelec *et al*. [34] used the dip coating method to create micro-tubes that after being bundled and inserted into the NGC serve as the micro-channels inside. These processes designed to obtain the micro-channels are very rudimentary and require great skill to roll or insert the materials to obtain the structures. The described molding processes could potentially be more easily industrialized, but as described in the literature, they involve time consuming assembly and demolding of the elements used to create the micro-channels, which requires a lot of manual handling of the NGCs and consequent risk of breakage, failure, and lack of reproducibility.

- *Sponges*

Sponges are highly porous structures made of biocompatible materials and mostly created by the freeze-drying method [30]. The use of these kind of sponges have shown positive results with respect to neural stem cell adhesion and proliferation, indicating that they are good candidates to be used as fillers for NGCs [30,35,36]. Toba *et al*. [37] poured a collagen solution inside a woven PGA and by means of freeze drying they obtained a highly porous intraluminal sponge. This sponge filled NGC succeeded in regenerating 80mm gap nerve injury in dog model. Similarly, Tonda-Turo *et al*. [35] used the freeze-drying method to create a gelatin sponge inside custom-made porous poly(ε-caprolactone) (PCL) tubes. The in-vitro tests yielded promising results indicating that the proposed solution was suitable for peripheral nerve regeneration. In addition, they observed and measured the mechanical properties of the PCL tube and their dependance on the degree of porosity. More recently Huang *et al*. [38] prepared a longitudinally oriented inner filler in form of a collagen-chitosan sponge made using directional freezing, which was later inserted in a electrospun PCL sheath to build the filled NGC. This NGC was reported to

yield better regeneration results than hollow tubes. Freeze drying is a powerful method to obtain structures with high porosity and directional pore morphology. This process however requires the preparation of the dissolution or obtaining the precursor of the component that constitutes the sponge. This preparation is then poured inside the NGC, or in the mold used to shape the sponge, which requires to be sealed to avoid leakages before the process of solidifying and creating the sponge begins. In this process it is difficult to control the pore size, interconnection, and shape. The time required to freeze-dry and dehydrate the specimen can be in the range of several hours to a few days.

- *Fibers*

The fibers, usually manufactured by electrospinning, can range in size from a few microns to hundreds of nanometers. The aligned electrospun fibers are longitudinally inserted along the NGC. This intraluminal structure provides a longitudinal guide and enables cell anchoring, eventually causing an elongation of the cells along the length of the fibers, an effect that is dependent on the diameter of the fibers [39]. This structure made from micro- or nanofibers mimics the necessary frameworks for nerve regeneration [21,30,40], which leads to enhanced regeneration results comparable to autografting [22,36]. Behbehani *et al.* [41] threaded over six thousand PCL micro-fibers into a non-degradable polyethylene glycol tube made by means of micro-stereolithography to investigate the applicability of a new 3D in-vitro model for the analysis of intraluminal scaffolds. Taylor *et al*. [39] using the 3D in-vitro model from Behbehani tested different diameter micro-fibers, made of a blend of polyhydroxyalkanoates (PHAs), a bacterial origin polyester, obtaining an increased neural cell attachment compared to PCL fibers, which indicated the suitability of PHAs for peripheral nerve regeneration. The insertion of the fibers into the NGC presents difficulties because of the required manipulation for their placement inside the conduit. This manipulation can lead to entanglements and accumulation of fibers, producing undesirable results. Additionally, there also exist challenges in the arrangement of the fibers within the NGC, including keeping them in position and ensuring an even distribution.

- Porosity

Porosity is a required property in the manufacture of scaffolds as it is critical to ensure the supply of nutrients [42]. This permeability, achieved by the insertion of pores, has been shown to be critical for peripheral nerve regeneration and it has been reported to improve the performance of NGCs. This has led to the conclusion that non-porous NGCs are obsolete [22,28]. Different methods of manufacturing porous components are available, such as leaching, freeze drying, gas foaming and phase separation. Gas foaming and phase separation methods present potential problems of lack of interconnectivity of the pores, and incompatibility with drugs or living cells because of the use of organic solvents. Therefore, particle leaching and freeze-drying methods are the most suitable methods for the manufacture of scaffolds [43]. Widmer *et al*. [44] back in 1998 experimented with the creation of porous NGCs using a blend of dissolved poly(DL-lactic-glycolic acid) (PLGA) and poly(L-lactic acid) (PLLA) to which they added table salt. This mixture, once the solvent evaporated, was forced through a heated nozzle using a hydraulic piston to push the material and form a tubular shape. They achieved highly porous tubes, demonstrating that the thermal processing of particle loaded polymer and the salt leaching technique are valid techniques for creating porous tubular scaffolds. Manoukian *et al*. [45] prepared a NGC made of chitosan loaded with a neurotransmitter release promoting drug. They achieved tubes with highly porous walls by means of freeze drying. As result, they obtained porous degradable NGCs with a sustained drug release, with the added feature that the longitudinally arranged pores of the walls could act as guides for the regenerating axons. The incorporation of porosity through the utilization of solid porogenerators is a simple and effective method. By ensuring a homogeneous mixture of particles with the polymer and preventing particle agglomeration, a porous structure can be achieved. The size, shape, and pore ratio can be easily controlled by manipulating the corresponding properties of the porogenerator. The use of solid porogenerators presents several potential drawbacks. Firstly, not all generated pores may be interconnected. Secondly, during the porogenerator removal process, there is a possibility that some particles may remain embedded within the polymer matrix. Additionally, in the case of thermal processing, the melting point of the porogenerator must be considered as it may impose limitations. With regards to the freeze-drying method for pore production, the

processing considerations are similar to those for obtaining spongy fillers as previously described.

- Grooves

The topography of implant surfaces in contact with the tissues affects the behavior of the living cells in interaction with it. Adhesion, proliferation, and differentiation of cells can be altered by means of physical modification of surfaces. With the objective of promoting and guiding the regenerating axons, the inner part of the NGCs can be micro-patterned. The most studied pattern for peripheral nerve regeneration is based on the parallel arrangement of micro or nanogrooves in the inner surface of the NGC [17]. Li *et al*. [46] carved thin titanium foils with parallel micro-groove pattern using laser machining. The thin foils were later rolled to form a tube, where polydimethylsiloxane (PDMS) was casted in to form micro-patterned rods. Using the PDMS micro-patterned rods as mold cores, chitosan porous NGCs were obtained by means of solvent casting and freeze-drying. They observed better regeneration on the patterned NGCs they tested compared to those without patterning. Kim *et al*. [47] also used parallel micro-grooves in their design to manufacture NGCs. They prepared micro-patterned flat films made of a mixture of PLGA and table salt by means of solvent evaporation method, to subsequently roll up the obtained films to form tubes. They compared NGCs with and without the micro-patterning, yielding an enhanced proliferation and accelerated regeneration on the patterned NGC. Wang *et al*. [48] and more recently Yang *et al*. [49] used the dry-jet wet spinning method to manufacture highly porous tubes with micro-grooves in their inner surfaces. The base polymeric material was dissolved in dimethyl sulfoxide to later push the mixture through a micro-patterned nozzle into deionized water bath were the polymer coagulated to form the porous tube. Both studies found that the NGC with micro-grooves NGCs performed better than NGCs with smooth inner surfaces. Mold-based methods, including those involving the assembly of a mold by means of master rolling and those involving the creation of a flat film with microgrooves prior to rolling, are relatively artisanal. Such methods do not guarantee high repeatability and depend on the skill of the operator in assembling the molds and rolling the NGCs. In contrast to these molding-based methods, the dry-jet spinning technique has significant potential for creating micro-grooves in tubular fashion without limitations on the

length of the tube. Additionally, the use of low-toxicity solvents makes this technique suitable for creating implants such as NGCs. However, as a result of the precipitation of the polymer during phase inversion process, a structure appears on the walls of the profiles manufactured in this way, showing internal and external dense surfaces with a highly porous middle layer with irregular macro-voids [50], which, in the case of an NGC, may compromise the mechanical behavior and the dynamics of resorption owing to an irregular degradation process derived from the heterogeneity of the walls of the implant.

The totality of the papers found in the literature describing the developments on NGCs report advantages in nerve regeneration, claiming that the strategy adopted and developed in each of these studies is the appropriate one to create a better NGC. However, few of these papers describe how to recreate the achievements in a robust and repeatable way to create an industrializable manufacturing process. Among the reviewed developments, those involving the insertion of fillers into the conduit are not easily automatable and require a significant amount of skilled manual manipulation to produce NGC samples. In contrast, strategies for adding porosity and/or grooves to NGC walls involving processes such as polymer extrusion and wet spinning (or its wet spinning variant with dry jetting) are better suited to establish an easily industrializable and highly productive manufacturing route to create improved NGCs.

1.3 Bio-resorbable polymers

The selection of the material for a medical application must consider a series of short and long-term factors from the mechanical, physical, chemical, biological and boundary conditions point of view. Moreover, these considerations must be addressed for the entire life of the device, *i.e.*: processing, assembly, packaging, storage and transport, sterilization, and final use.

Polymers are one of the most comprehensive biomaterial class, being used in a wide range of medical applications, such as sutures, scaffolds, medical implants, drug eluting devices, disposable elements, housings, and part of surgical tools [51,52]. The main advantages of the polymers are that they are easy to manufacture, and that they have flexibility to be modified to tune their physical-mechanical properties. Polymers are the primary material used in soft tissue

engineering and drug delivery and are slowly beginning to replace metals and ceramics in hard tissue replacement applications [51]. There are hundreds of polymers that can be synthesized and used in medical applications; however the current use is limited to around 20 types that can be found in diverse applications, from disposable elements to durable implants [52].

Out of these few polymers used in medical applications, only a small number are biodegradable by the body, of which polyesters are the leading group. They present hydrolytically degradable ester bonds in their main chain and, most of them degrade in bulk, which is characterized by water penetrating in the polymer mass, where the polymer degrades by hydrolysis. The byproducts are usually carboxylic acids, which reduce the local pH, leading to autocatalysis of the polymer and further decrease in pH. Despite the local increase in acidity they can generate, they are the most commercially available and studied polymers for medical applications [51–55]. In fact, as mentioned before, the only commercially available resorbable NGCs, that are not made from animal-derived collagen, are those made from polyester (see Table 1.1). Furthermore, the polyesters relevant for medical applications are thermoplastics, and can be processed using conventional polymer processing methods, namely injection molding and extrusion [55]. The ability of these polyesters to be absorbed by the body is optimal for the peripheral nerve regeneration application since it allows to avoid a second intervention to remove the non-absorbed NGC once the nerve has been regenerated. The optimal material must also present mechanical properties similar to the soft tissue that is regenerating. The NGC must be flexible and elastic without transmitting tensions to the nerve, while protecting the regenerating tissue from the environment. These high elasticity requirements eliminate those rigid and brittle materials, which are normally used for other applications such as biodegradable staples or screws.

The following section summarizes the use of polyesters for the manufacture of resorbable NGCs, listing both synthetic and bacterial origin polyesters, as well as the manufacturing route selected. The used methods, to manufacture NGCs made of each polymer, will be highlighted.

1.3.1 Bio-resorbable synthetic polyesters

Most of the synthetic origin polyesters are based on petroleum-derived carbohydrates, but some are synthetized from renewable sources, for example from lactic acid, and can therefore be identified as polymers of natural origin, but they should not be confused with natural occurring polyesters such as those bio-synthesized by bacteria, which are discussed in the following section. Polyesters can be easily synthetized by ring opening or condensation polymerization and they show tailorable properties, low toxicity and high processability.

Table 1.2 shows the synthetic polyesters registered in the literature to be used to fabricate and test NGCs, or at least proven to be compatible with nerve cells. The table includes *in-vivo* bio-resorption times and published mechanical and thermal properties.

The reviewed synthetic polyesters have been found to be beneficial for nerve tissue regeneration and the fabrication of NGCs. However, some are more promising than others because of their intrinsic properties. Degradation time is an important factor, as an NGC must protect the nerve during the long period of nerve regeneration (time ≥ 12 months). Not all reviewed polyesters meet this condition. Mechanical properties are also important, as the NGC must mimic the properties of the nerve to avoid causing stresses on the tissue and maintain these properties over time. This excludes materials that rapidly lose their properties in *in-vivo* conditions. Although by design and the addition of porosity to the material, it is possible to make the material more flexible, those materials with high rigidity are also discarded for the manufacture of high-performance NGCs. These considerations lead to the identification of PCL and PLCL among the group of synthetic polyesters that are more attractive for the fabrication of flexible NGCs with long degradation times.

The processability of synthetic polyesters is crucial for efficient and reliable production of NGCs in an industrial scale. These reviewed polyesters are thermoplastics and technically can be processed by industrial thermal methods such as injection molding, hot melt extrusion or

Table 1.2 Synthetic polyesters used or researched for nerve tissue regeneration.

Polyester	Degradation time (months)	Properties	Tested	NGC manufacturing route
Polyglycolic acid (PGA)	3 [56] 6-12 with strength loss in less than a month [51,55,57]	E = 12 GPa [58]. T_g = 35-40°C T_m > 200°C [24]	Commercial NGC [59]	Extrusion [60] Woven mesh [24] Wrapping [61]
Poly(p-dioxanone) (PDS)	12 with property loss in less than 2 months [57,62]	T_g = -10°C T_m = 127°C [63]	*In vitro* [64–66]	Electrospinning [64,65] Freeze drying [66]
Poly(L-lactic acid) (PLLA)	24 [51,55] 60 [62]	E= 4.8 GPa [51,62] T_g = 62°C T_m = 170°C [67]	*In vitro* [68] *In vivo* [69]	Freeze drying [68] Solvent casting [69]
Poly(D, L-lactic acid) (PDLLA)	2-12 [70]	E = 1.9 GPa [51,62] T_g = 55°C [71]	*In vivo* [72]	Dip coating [73] Solvent casting [72,74]
Poly(lactic-co-glycolic acid) (PLGA)	1-6 [62]	E = 1-4GPa [55]	*In vivo* [47]	Freeze drying [31] Plunger extrusion [44] Solvent casting [47]
Poly(ε-caprolactone) (PLC)	>36 [55]	T_g = -60°C T_m = 60°C [55]	*In vivo* [32]	Electrospinning [75] Solvent casting [32]
Poly(lactide-co-ε-caprolactone) (PLCL)	Tunable form days to years [76]	T_g = 10-20C T_m = 135-155C E = 0.04 GPa [77]	*In vivo* [78]	Dip coating [78,79] Electrospinning [80,81]

Glass transition temperature (T_g); Melting temperature (T_m); Young's modulus (E).

thermo-forming. However, there are no examples in the literature of their use to manufacture NGCs by injection molding or hot melt extrusion. The study presented by Rosen *et al*. [60] is, to the best of our knowledge, the only one in which it is stated that the NGC, made of PGA, was extruded, but they do not specify details on the fabrication method. The methods found in the literature that are used to create NGCs with these polyesters are mainly laboratory techniques which are not easily industrializable, such as solvent casting or freeze drying.

1.3.2 Bio-resorbable bacterial origin polyesters

Polyhydroxyalkanoates (PHAs) are polyesters produced by certain varieties of micro-organisms, which generate these polymers as internal energy storage and accumulate them within the cytoplasm as intracellular inclusions. PHAs can be produced from renewable carbon sources by means of bacterial fermentation, are biocompatible and degrade into non-toxic byproducts via surface erosion [82,83].

Depending on the type of micro-organism used, process conditions and carbon source, different types of PHAs are available. These PHAs differ in their composition, structure, and number of carbon atoms in their monomeric unit, characteristics that directly affect their mechanical, biocompatibility, and bio-resorption properties [84]. PHAs with respect to other bio-resorbable materials exhibit better biocompatibility because they cause lower local acidity resulting from the degradation, and facilitate cell attachment and growth [39,84]. There are over 160 different types and combinations of PHAs [85], which can be classified broadly into two types, short chain length (SCL) or medium chain length (MCL) [86,87]. Because of their excellent biocompatibility, PHAs have been extensively researched for tissue engineering, where copolymerization and blends of SCL-PHAs and MCL-PHAs have been used to tailor the properties of PHAs to suit the needs of the application. Here the focus will remain on formulations to fabricate NGCs or to promote neuronal cell growth.

Table 1.3 shows the bacterial origin polyesters that are identified in the literature to be used to fabricate and test NGCs, or at least proven to be compatible with nerve cells. The table includes *in-vivo* bio-resorption times and some mechanical and thermal properties reported in the literature.

PHAs are of great interest for the fabrication of NGCs because of their high biocompatibility with nerve cells. Some PHA copolymers and MCL-PHAs have an elastic behavior that can be convenient for designing NGCs with suitable mechanical properties to further improve the compatibility with the damaged nerve. Although PHAs can be produced on a large scale, their production volume is much lower than that of synthetic polyesters, and the production cost

Table 1.3 Bacterial origin polyesters researched for nerve tissue regeneration.

Polyester	Degradation time (months)	Properties	Tested	NGC manufacturing route
Poly(3-hydroxybutyrate) (P(3HB))	>6 [88]	T_g = 2°C T_m = 150-180°C [89,90] E = 3.5 GPa [86]	*In vivo* [88]	Wrapping [88,91]
Poly(3-hydroxyoctanoate) (P(3HO))	24-30 [92]	T_g = -33°C T_m = 40-58°C [93] E = 17 MPa [86]	*In vivo* [92]	Solvent evaporation [92]
P(3HO)/P(3HB) Blend	--	E = 1.3-140 Mpa [89]	*In vitro* [89] *Ex vivo* [39]	Solvent casting flat films [89] Electrospinning [39,40]
Poly(3-hydroxybutyrate-co-3-hydroxyvalerate) (P(3HB-V))	>4 [94]	E = 2,4 GPa T_g = -1°C T_m = 130-153°C [90,95]	*In vivo* [96,97]	Wrapping [98] Electrospinning [96] Solvent casting [97]
Poly(3-hydroxybutyrate-co-3-hydroxyhexanoate) (P(3HB-HHx))	>6 [86]	E = 155-630 KPa [86] Tm = 54°C [90]	*In vivo* [99]	Dip-coating [99]
Poly(3-hydroxyoctanoate-co-3-hydroxydecanoate-co-3-hydroxydodecanoate) (P3HO-3HD-3HDD)	--	E = 2 Mpa T_g = -45°C T_m = 25-56°C [100]	*In vitro* [100]	Solvent casting flat films [100]

Glass transition temperature (T_g); Melting temperature (T_m); Young's modulus (E).

doubles that of PLA production [101]. Therefore, to control biodegradability and mechanical properties, it may be useful to use PHAs as additives by combining them with synthetic polyesters. Consequently, large quantities of a blend with optimized properties can be obtained to manufacture NGCs for nerve regeneration. In the literature, there are examples where PHAs have been blended with PCL to improve their properties, in particular to increase the toughness of Poly(3-hydroxybutyrate) (P3HB) and Poly(3-hydroxybutyrate-co-3-hydroxyhexanoate) (P(3HB-HHx)) [102–104].

Among the manufacturing methods that have been found in the literature for making NGCs or test scaffolds, thermal processing methods such as extrusion and injection are not found. Although PHAs are claimed to be processed by these thermal methods to make, for example, bio-resorbable sutures, staples, and drug delivery components [105], they are difficult to process as the degradation temperatures are very close to melting temperatures. Such narrow processing windows leads to, at least with SCL-PHAs, the addition of plasticizers. Other

strategies that are done to lower their melting temperature and ease their processing are: increase their molecular weight; copolymerization such as Poly(3-hydroxybutyrate-co-3-hydroxyvalerate) (P(3HB-V)) or P(3HB-HHx); blending with MCL -PHAs and blending with synthetic origin polyesters, such as PCL [90,102,106].

1.4 High throughput micro-replication techniques

The previous sections explored the current advancements in the field of NGCs and provided an overview of the use of polyesters in their fabrication. Various methodologies for producing NGCs have been introduced, being most of them classified as laboratory techniques, which are used for generating test specimens. These methods were adapted to accommodate the specific requirements of NGCs and facilitate their obtention.

The fabrication of NGCs with the attributes and features described in Section 1.2 requires the use of high-throughput micro-manufacturing techniques, specifically polymer micro-replication methodologies, as they enable the production of micro-structured components composed of the materials discussed in Section 1.3. These replication methodologies represent the most industrially efficient approaches to produce micro-structured components with non-planar geometries, such as the NGCs.

In Figure 1.3 a schematic classification of main micro-manufacturing processing technologies is shown. These can be classified into three main subdivisions, replication, mechanical cutting, and energy assisted machining technologies [7,107–111].

Of the three technological areas into which micro-manufacturing can be divided, replication is the one that is recognized as suitable for mass production [112]. Furthermore, micro-injection molding and micro-extrusion are the most suitable methods to manufacture tubular geometries such as NGCs.

The capabilities of polymer replication technologies are virtually limited only by the constraints of the micro-machining manufacturing processes needed for the manufacture of the tooling used during the replication process. Therefore, depending on the geometry of micro-features to be replicated, a specific manufacturing route must be adopted to produce the molds or dies

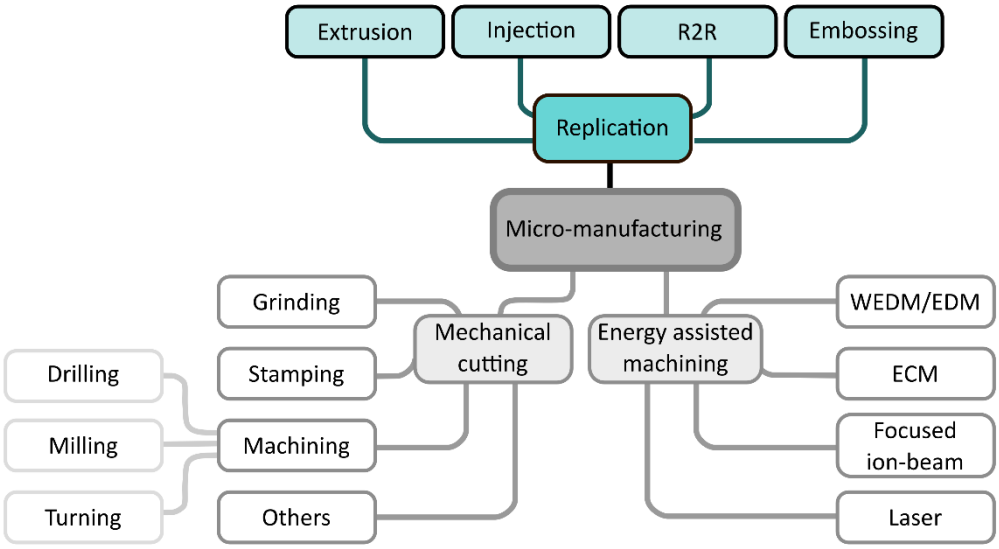

Figure 1.3 Classification of micro-manufacturing technologies.

that meet those geometrical requirements. These manufacturing routes are identified as Mechanical cutting and Energy assisted machining in Figure 1.3.

The replication processes are based on transferring the geometry of a master or mold to a substrate material. This transference can be carried out by means of heat, pressure, chemical activation, or other methods. The obtained workpiece copies the shape of the tool. There is no subsequent removal nor elimination of material, allowing to obtain micro-manufactured components at one thousandth of the cost of other micro-manufacturing techniques such as micro-milling or laser micro-machining.

The micro-replication processes selected in this thesis for the study of the manufacturability of NGCs at industrial scale are micro-injection and micro-extrusion. Here a brief description of each technology is made, specifying its characteristics, advantages, drawbacks, and main challenges. In addition, a literature review is made, where these technologies have been used to manufacture components with the geometrical requirements described in Section 1.2 and, where the materials listed in Section 1.3 have been correctly processed.

1.4.1 Micro-injection molding

- Process description

Injection molding process is a manufacturing process in which the material in plastic state is introduced into a rigid mold, where the material solidifies copying its geometry. Subsequently, the mold is opened to demold the piece and closed again, once empty, to be ready for the next load of material. Injection molding is a high throughput manufacturing technology capable of producing highly repeatable and precisely shaped parts of virtually freeform geometry. This manufacturing process has extremely high production rate, being the most widely used technology for producing components made of polymeric materials [113,114].

- Machine characteristics

Modern micro-injection machines are equipped with systems and added sub-process steps to decouple the stages of material transport, melting, accumulation, and injection, making it possible to control each of them separately. Schematic representation of a micro-injection machine with differentiated metering system is shown in Figure 1.4, where the injection piston, the screw and the metering systems are highlighted. This new architecture of micro-injection

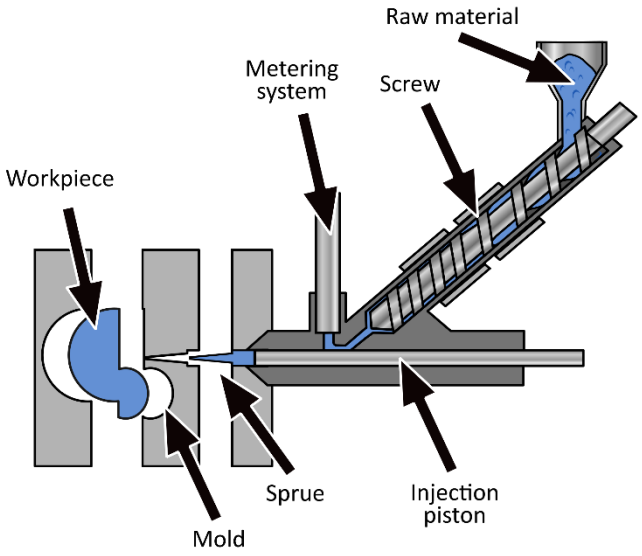

Figure 1.4 Schematic representation of polymer micro-injection machine with differentiated screw, metering system and injection piston.

dedicated machines have brought other advantages, such as the reduction of runner and sprue sizes, and therefore reduced material waste, which is of great interest when expensive materials such as the bacterial origin PHAs described in Section 1.3 are used [115–119].

- Key advantages

Because of its production rate and high repeatability, the injection process is also positioned as one of the key technologies to produce micro-manufactured components. The cost of fabrication of micro-injected components is mostly influenced by the complexity of the design, which directly affects the complexity of the mold and its manufacturing route, that can reach the limits of the micro-machining techniques needed to produce it. Anyhow, once the mold is made and ready, it can usually enable the replication of several thousands to millions of parts, implying that the cost of the mold has a minimal impact on the unit cost of each part for large batches. Similarly, from a cost point of view, micro-injected parts, because of the small amount of material they require, are suitable to be made of high-cost materials, since the amount material in each part can be considered negligible [114,116,120,121]. Although the manufacture of expensive micro-structured molds is required to achieve some of the NGC features described in Section 1.2, and the use of biocompatible and bio-resorbable materials can be expensive, such as some of the most exotic materials mentioned in Section 1.3, the polymer micro-injection technology could allow the production of NGCs at a competitive price, based on the reasons outlined above.

By injection molding almost any geometry can be replicated, considering that the polymer must be able to properly fill the cavity under certain processing conditions (temperature, pressure, shear stress, etc.) in which it is not degraded, being of major concern the rheological properties of the polymer.

- Main drawbacks

One of the main drawbacks is the need of considering “by design” several mold split lines, slides and movable elements to guarantee part ejection without destroying the part. This causes not only an increment on the manufacturing costs of the mold but also the appearance of marks, misalignments, flashes, or burrs in the injected part. These defects, in case of micro-

manufactured components can be in the same dimension range as the micrometric features or tolerances to be replicated, making their appearance a critical failure. Additionally, the increase of precision assembly of the mold movable parts, and the reduction of gaps between them, deters the proper evacuation of the air inside the cavity, causing incomplete filling, leading to defective parts. Moreover, if the temperature and pressure inside the mold cavity during the injection are high enough, the ignition of the trapped air can happen, causing located burn marks in the injected component. To avoid these defects, air vents are added to the cavity, usually in the split line between main mold parts, and preferably in the last-to-fill area of the cavity. However, in micro-injection molding the size of these vents (typically 25 micrometers depth and several millimeters wide) can be comparable to the size of the features to be replicated, being extremely difficult to avoid vent filling. In the literature, other strategies have been applied, such as vacuum venting of the cavity to reduce the resistance to filling caused by trapped air. However, it is not clear that the application of vacuum improves the replication of micrometric features, because of the reduction of the mold surface temperature caused by the removal of the hot air inside the cavity, which ultimately hinders the flow of the polymer front, solidifying it before the complete filling [122].

Micro-injected parts generally show very large surface to volume ratio because of the reduced size of the part and the presence of micro-sized features. This large surface area proportion has a dual negative effect: first, it leads to a high cooling rate of the part, which can cause premature solidification, and cause skin-core effects [122,123]; second, once the cavity is filled, the relatively high proportion of part surface in contact with the mold causes an increment of adherence and local friction, which has to be overcome by the force applied by the ejectors without damaging the replicated part [124]. Consequently, the demolding process of injected thin-walled NGCs having high surface – to – volume ratio, either with or without internal structuring, can raise problems. This implies that injection molding may not be the most suitable method for the fabrication of tubular thin wall geometries such as NGCs. To face the challenges linked to the micro-injection molding of micro-scale features with such a high surface – to – volume ratio, a deep study on the influence of process parameters (input and temperature and pressure signals eventually registered by sensors located in strategic zones of the mold) on replication quality is mandatory.

The replication quality of micro-injected components is mainly influenced by the melt and mold temperatures, along with the injection speed. By increasing the injection speed, the mold pressure is also increased, while the cavity filling time is reduced. High cavity pressures imply an improved replication. However, the use of high injection speeds can worsen the quality of replication by amplifying the differences in replication along the component, function of distance from the polymer inlet point. High melt and mold temperatures improve the degree of replication but at the expense of increasing the cycle time, which reduces productivity. In the literature, there are disparities in the identification of the process parameters with the greatest impact on the variations in replication quality. Such discrepancies in results are attributed to differences in the configurations of the reported studies, in which different polymers and replication geometries were analyzed [125–127].

The quality control of micro-injected components is complex because of two main factors: the size of the features to be controlled and the inspection time. Because of the size, time consuming microscopy measurements are needed to control the produced parts and thus, the quality control becomes the bottleneck of the process. In bibliography it can be found that there is a real effort to find a correlation between measurable process parameters and the replication quality to enable an in-process quality control [125,128]. The conventional control of regular injection process, based on the machine setpoint parameters, is not enough in micro-injection molding to ensure the stability of the process, because of the effect the inherent process noise has on the consistency of the replicated components [129,130]. The architectures of the new micro-injection machines enable to have the stages of the process decoupled to facilitate their control, but despite this, comprehensive monitoring strategies are needed to achieve zero defect manufacturing. These strategies include the control of the machine parameters, which are usually the mold temperature and injection speed, and the monitoring of the process signals, pressure, and temperature inside the mold cavity, attempting to link these parameters and signals with the obtained replication quality in order to define an in-process control of the micro-injected parts. Anyhow, micro-injection is a well-established manufacturing process in the industry, and it is a well characterized micro-manufacturing process with a plethora of available studies compared to micro-extrusion.

- Micro-injection capabilities

Here, the literature background on micro-injection capabilities is described, both to obtain micro-features similar to those described in Section 1.2, that are required to obtain NGCs with advanced functionalities and, in the research to process the bio-resorbable polyesters listed in Section 1.3.

- *Multi-channel structures*

In order to obtain an NGC with an inner structure composed of micro-channels by micro-injection molding, it is necessary to prepare a mold that resembles the negative geometry of the multi-channeled NGC. This implies that the mold must have the elements that create these micro-channels inside it. These elements must be removed during demolding or in later stages to create the micro-channels in the injected part. The size of the channels required in NGCs can range from tens to hundreds of micrometers with lengths of several centimeters, which determines the size of these components in the mold. Their micro size dimensions and slender geometry make it extremely difficult to position them inside the mold, their handling, and demolding. To confirm this fact, to the best of our knowledge, there is no literature describing the fabrication of components with internal micro-channels with similar arrangement to that shown in Figure 1.2 (b) by micro-injection molding.

- *Porosity*

Porosity in micro-injection can be achieved by using porogenerator elements blended with the polymer, such as solid particles or other polymers, which can then be selectively removed by means of solvents. Other methods used industrially are gas foaming or micro-cellular injection molding, both of which obtain very good porosity results, but the type of pore obtained is closed, which resembles a group of bubbles inside a foam without any type of interconnection that could allow the flow and exchange of fluids and nutrients, which eventually limits their utility in the generation of scaffolds for tissue engineering [131]. There are some examples in the literature that implemented these methods to obtain porous specimens considering synthetic polyesters, such as the studies of Ghosh *et al*. [132], Teng *et al.* [133], and Kramschuster *et al.* [134].

- *Grooves*

In the literature related to the addition of grooves in NGCs, a great diversity of sizes and arrangements can be found. These groove sizes can range from sub-cellular to supra-cellular sizes with depths that can vary from a few tens up to about fifty micrometers [135].

There are multiple examples reported in the literature, where grooves of these sizes are replicated, either with bio functionality or with other functionalities such as microfluidics for instance [126,136]. Therefore, it is reasonable to assume that this type of surface structuring is not a particular challenge for micro-injection.

In a nutshell, although micro-injection seems to present critical drawbacks that make it difficult to be implemented as the most suitable micro-manufacture method to obtain tubular geometries such as NGCs, its similarities to micro-extrusion, a more convenient technologies as we describe later, and the extensive bibliography behind it, make it a useful platform for studying the parameters that influence micro-replication, and that can be implemented in the optimization of micro-extrusion.

1.4.2 Micro-extrusion

- Process description

Extrusion is the primary thermal processing method for polymers, where the polymer in molten or heat softened state is continuously forced through a die to shape it, producing a part with constant profile and unlimited length, as long as the feed of material continues [137]. This technology allows the transformation of the material, that can be in the form of pellets or powder, turning it into shapes of different geometries, such as rods, filaments, sheets, films, complex profiles, and tubes, which is particularly useful for manufacturing NGCs.

- Machine characteristics

The basic parts of an extrusion machine are the hopper, where the material is introduced, the screw, the extruder barrel heaters and the die. The extruder screw has several functions: first, it conveys the solid material from the hopper to the extruder; second, it melts, blends,

compresses and degasses the polymer; and third, it conveys the molten polymer to the die. Finally, the die defines the shape by means of an appropriate orifice geometry. A schematic representation of an extrusion machine is shown in Figure 1.5.

An extrusion system usually includes additional peripheral components. A cooling system for the extrudate, usually consisting of a water bath. A pulling system to maintain the extrudate under constant tension to counteract the die-swelling effect, with the objective of obtain the required dimensions by means of the appropriate speed control, and a system for cutting or spooling the extrudate depending on its specific geometry and storage mode [138].

The extrusion process is controlled by the screw speed parameter and the temperature set points along the extruder barrel and nozzle. The extrudate pulling speed is also another parameter to be controlled in those extrusion systems that are equipped with this peripheral system. The screw speed strongly influences the pressure of the molten polymer reaching the nozzle, with the pressure increasing as the screw speed increases. However, while lower screw speeds result in improved extrusion quality, they also lead to reduced productivity. On the other hand, increasing the temperature decreases the viscosity of the polymer which causes the pressure to also decrease [139,140].

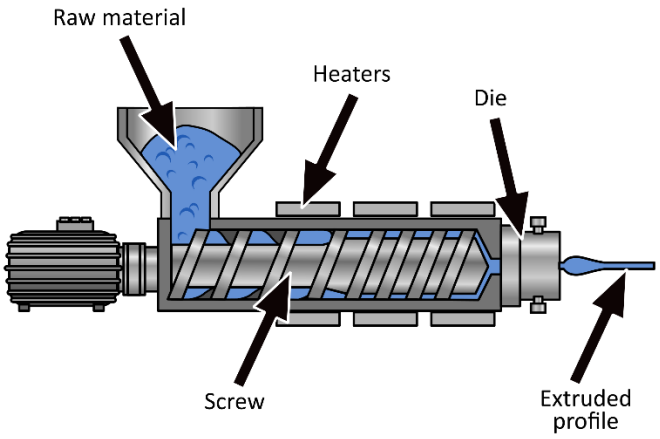

Figure 1.5 Schematic representation of extrusion machine.

- Key advantages

The parts that can be obtained by extrusion are characterized by a constant cross-section along its entire length. This apparent limitation, on the contrary, allows the manufacture of components with constant geometry with unlimited length, which is very useful for the manufacture of filaments, wire coatings, tubes and profiles with high manufacturing capacity and reliability. In addition, this process allows to process blends and particle doped materials, which can be of great interest for the inclusion of porogenerator agents, producing porous structures. Micro-extrusion is widely applied to manufacture micro-tubes to be used as catheters in medicine, micro-capillary reactors, micro-needles, micro-heat exchangers, micro-structured profiles for low friction applications, surgical sutures, etc., being able to obtain, for example, tubes with diameters down to 100 micrometers and miniature multi-lumen catheters, which suggests a high potential for the manufacture of NGCs.

- Main drawbacks

When processing the polymer, it undergoes high temperatures and high shear ratios, which can be limiting to extrude certain temperature-sensitive polymers, such as some polymers for bio applications. Moreover, the minimum polymer quantity needed for extrusion increases with the size of the extruder, since both screw(s) and die have a dead volume that must be filled with polymer to generate extrusion pressure and mass continuity. A polymer quantity equal to this dead volume is lost in the extrusion process, which can be not negligible and be a great concern for small extrusion batches of expensive materials. Most industrial extruders have a length to diameter ratio (L/D) between 30 and 36. Higher values of this ratio favor productivity and melt homogeneity, but sensitive materials may show more degradation when processed on long machines.

The design of the extruder screw and the nozzle directly affect the pressures that can be reached inside the extruder during the process. The geometry of these elements must be designed according to the production needs and the type of polymer to be used. The parameters that are controlled during the process are the screw speed and the barrel and nozzle temperatures. High screw speed is required for high productivity and setting temperatures are

expected to be adequate to not degrade the polymer and to offer a compromise between good flowability and the reproduction of the shape of the nozzle at the outlet. The increase of the screw speed causes an increment in pressure because of the higher polymer flow rate forced through the nozzle, additionally, the shear rate applied to the polymer increases, which in turn causes the apparent viscosity of the polymer to decrease. This reduction in apparent viscosity causes a loss of proportionality in the pressure variation caused by the screw speed, with the increase becoming progressively smaller as the screw speed increases. The increase in screw speed also causes an increase in the amplitude of the pressure oscillation caused by the rotation of the screw helix, which results in pulsating pressure and creates instabilities in the extrudate, compromising the extrudate quality. These pressure instabilities caused by screw rotation can be minimized using nozzles designed with appropriate land lengths, that result in larger pressure drops, which can counteract this effect at the cost of lower productivity and possible degradation of the polymer. On the other hand, as polymer viscosity is temperature dependent, thermal homogeneity of the melt is crucial to minimize inconsistency in melt properties. The temperature heterogeneity on the melt polymer may eventually cause pressure instabilities and lead to undesirable changes in the extrudate [137,139–143]. Although significant improvements have been made in the extrusion process in recent years, monitoring and controlling the temperature and pressure inside the extruder is still a challenge to be faced and, there are not many techniques that allow to control the process according to measurable temperature and pressure characteristics of the melt [144].

Even though there is a wide variety of micro-extruded components used as medical components, there is a gap in the literature where this technology is not being studied to process materials with bio-advanced capabilities, such as those described in Section 1.3, and with geometries that are capable of meeting the challenges of the micro-features described in Section 1.2, with the goal of fabricating high-performance NGCs in an industrial way [7,145–153].

- Micro-extrusion capabilities

Here, in a similar approach to that used for micro-injection, the literature background on micro-extrusion capabilities is described, both in obtaining micro-features similar to those described

in Section 1.2 that are required to obtain NGCs with advanced functionalities and, in the research on micro-extrusion processing of the bio-resorbable polyesters listed in Section 1.3.

- *Multi-channel structures*

The extrusion dies used to manufacture hollow or tubular profiles, have at least one core that is surrounded by the melt polymer before it exits the die to form, this way, a seamless hollow or tubular section profile. These cores can be vented to add an air supply to the inner part of the profile. This airflow can be controlled by pressure to swell the profile or counteract the shrinkage of the polymer as it cools down. For the extrusion of multi-channeled tubes, the extrusion die must have the same number of cores, ideally vented.

Extruded multi-channel tubing solutions of reduced diameter are available commercially, *e.g.*: Zeus, Raumedic, and GenX Medical. These tubing are of great utility and interest for medical catheters and as components for endoscopes, for instance. These components are manufactured by means of polymer melt extrusion, which indicates that this process is capable of generating this type of complex internal geometries. In the literature some examples can also be found where both, the design of the die and the effect of the process parameters, on the achievement of the required dimensions in the manufacture of multi-channel tubes by micro-extrusion are studied. In particular, the effect of nozzle temperature and screw speed on the extrudate quality has been studied, being reported that the increase of both parameters negatively affects the quality of the tubes with multi-channels, causing problems on channel ovality. It was also observed that high screw speed causes an increase on the anisotropy of the die-swelling that eventually, deforms the geometry of the extrudate. [145,154].

- *Porosity*

Porosity is a characteristic that is simple to implement in extruded profiles by means of gas foaming. This method is based on the addition of gas into the molten polymer inside the extruder and as it exits through the die, at atmospheric pressure, the gas expands to form bubbles [138]. But similar to injection molding, this method of creating porosity produces closed pores with no interconnection, which is not convenient for creating components to be used in tissue engineering. Other methods for creating interconnected pore extruded profiles are the equivalent to those used in injection molding which are based on adding leachable components

(particles or other polymers) that will be removed by dissolution once the profile has been extruded. Several studies can be found in the literature related to micro-extrusion, where the pores are obtained by means of particle or polymer leaching, with or without the addition of gas foaming to obtain highly interconnected porous profiles made of bio-resorbable polyesters [155–157].

- *Grooves*

To our knowledge, there is not much literature on the use of extrusion to produce micro-grooves. Among the limited information that has been found, there is a patent that specifically describes polymer extrusion as a method for manufacturing components with micro-grooves that function as a capillary tube to be used in pen tips. Later, the company that applied for that patent used the same technology in the medical sector for the controlled dosing of liquid medicines [158]. Regarding research literature*, Cannon et al.* [150] and Villacorta *et al*. [151] used extrusion to successfully obtain components with micro-grooves, which were meant to reduce the friction coefficient of the components containing the micro-grooves on their surface, instead of aiming for interactions with cells.

- *Bio-resorbable polyesters*

Micro-extrusion, like micro-injection, is a fundamental technique in the processing of thermoplastic polymers, such as those listed in section 1.3. Explicit examples of the use of extrusion for the processing of PLLA, PLGA, P(3HB-V) and P3HB copolymers can be found in the literature, giving an idea of the versatility of this process to work with different grades of polymers [44,156,157,159–161].

In conclusion, micro-extrusion enables the manufacture of tubular components, even with multiple channels and high porosity, grooves and the potential to process several of the polymers of interest, making it a very suitable manufacturing process to obtain NGCs in an efficient and easily industrializable way. However, the process shows critical limitation in terms of control, due to the parameters intercorrelation and complexity on measuring the actual temperature variations in the screw zone and the pressure front in the nozzle. Hence, the application of extrusion to obtain a complex component, such as an advanced NGC where multiple requirements are needed, is not a straightforward process. Therefore, there is an

opportunity for the research and industrial community to implement a methodology to produce these types of advanced components via micro-extrusion, which has been also proved by the lack of works in the literature.

1.5 References

[1] Alting L, Kimura F, Hansen HNN, Bissacco G. Micro Engineering. CIRP Ann 2003;52:635–57. https://doi.org/10.1016/S0007-8506(07)60208-X.

[2] Dario P, Carrozza MCMC, Allotta B, Guglielmelli E. Micromechatronics in medicine. IEEE/ASME Trans Mechatronics 1996;1:137–48. https://doi.org/10.1109/3516.506150.

[3] Masuzawa T. State of the art of micromachining. CIRP Ann - Manuf Technol 2000;49:473–88. https://doi.org/10.1016/S0007-8506(07)63451-9.

[4] Mohd Ghazali FA, Hasan MN, Rehman T, Nafea M, Mohamed Ali MS, Takahata K. MEMS actuators for biomedical applications: a review. J Micromechanics Microengineering 2020;30:073001. https://doi.org/10.1088/1361-6439/ab8832.

[5] Aguilo J, Millan J, Villa R. Micro and nano technologies in medical applications: a challenge. 2001 Int. Semicond. Conf. CAS 2001 Proc. (Cat. No.01TH8547), vol. 1, IEEE; 2001, p. 247–55. https://doi.org/10.1109/SMICND.2001.967456.

[6] Hansen HN. Micro Manufacturing – Process and Part Quality Control Process variations 2013:5–8.

[7] Cora ÖN, Koç M. Micromanufacturing. Mod. Manuf. Process., Hoboken, NJ, USA: John Wiley & Sons, Inc.; 2019, p. 149–84. https://doi.org/10.1002/9781119120384.ch7.

[8] Uhlmann E, Mullany B, Biermann D, Rajurkar KP, Hausotte T, Brinksmeier E. Process chains for high-precision components with micro-scale features. CIRP Ann - Manuf Technol 2016;65:549–72. https://doi.org/10.1016/j.cirp.2016.05.001.

[9] Dario P, Menciassi A, Stefanini C, Accoto D. Miniaturization of biomedical micromachines. 2nd Annu. Int. IEEE-EMBS Spec. Top. Conf. Microtechnologies Med. Biol. Proc. (Cat. No.02EX578), IEEE; 2002, p. 291–6. https://doi.org/10.1109/MMB.2002.1002332.

[10] Guber AE. Potential of microsystems in medicine. Minim Invasive Ther 1995;4:267–75. https://doi.org/10.3109/13645709509152805.

[11] Yao X, Peng R, Ding J. Cell-Material Interactions Revealed Via Material Techniques of Surface Patterning. Adv Mater 2013;25:5257–86. https://doi.org/10.1002/adma.201301762.

[12] Desai TA. Micro - and nanoscale structures for tissue engineering constructs. Med Eng Phys 2001;22:595–606. https://doi.org/10.1016/S1350-4533(00)00087-4.

[13] Pečar B, Resnik D, Možek M, Vrtačnik D. Microfluidics: a review. Inf MIDEM - J Microelectron Electron Components Mater 2021;51:3–23. https://doi.org/10.33180/InfMIDEM2021.101.

[14] Barbillon G. Engineering of Micro/Nano Biosystems. 1st ed. 20. Singapore: Springer Singapore; 2020. https://doi.org/10.1007/978-981-13-6549-2.

[15] Šalić A, Tušek A, Zelić B. Application of microreactors in medicine and biomedicine. J Appl Biomed 2012;10:137–53. https://doi.org/10.2478/v10136-012-0011-1.

[16] De Chiffre L, Kunzmann H, Peggs GNN, Lucca DAA. Surfaces in Precision Engineering, Microengineering and Nanotechnology. CIRP Ann 2003;52:561–77. https://doi.org/10.1016/S0007-8506(07)60204-2.

[17] Carvalho CR, Oliveira JM, Reis RL. Modern Trends for Peripheral Nerve Repair and Regeneration: Beyond the Hollow Nerve Guidance Conduit. Front Bioeng Biotechnol 2019;7:1–30. https://doi.org/10.3389/fbioe.2019.00337.

[18] Narayan SK, Arumugam M, Chittoria R. Outcome of human peripheral nerve repair interventions using conduits: a systematic review. J Neurol Sci 2019;396:18–24. https://doi.org/10.1016/j.jns.2018.10.012.

[19] Deumens R, Bozkurt A, Meek MF, Marcus MAE, Joosten EAJ, Weis J, et al. Repairing injured peripheral nerves: Bridging the gap. Prog Neurobiol 2010;92:245–76. https://doi.org/10.1016/j.pneurobio.2010.10.002.

[20] Houshyar S, Bhattacharyya A, Shanks R. Peripheral Nerve Conduit: Materials and Structures. ACS Chem Neurosci 2019;10:3349–65. https://doi.org/10.1021/acschemneuro.9b00203.

[21] Taylor CS, Haycock JW. Biomaterials and Scaffolds for Repair of the Peripheral Nervous System, 2022, p.

245–79. https://doi.org/10.1007/978-3-030-21052-6_3.

[22] Vijayavenkataraman S. Nerve guide conduits for peripheral nerve injury repair: A review on design, materials and fabrication methods. Acta Biomater 2020;106:54–69. https://doi.org/10.1016/j.actbio.2020.02.003.

[23] Wieringa PA, Gonçalves de Pinho AR, Micera S, van Wezel RJA, Moroni L, Wezel RJA, et al. Biomimetic Architectures for Peripheral Nerve Repair: A Review of Biofabrication Strategies. Adv Healthc Mater 2018;7:1701164. https://doi.org/10.1002/adhm.201701164.

[24] Kehoe S, Zhang XF, Boyd D. FDA approved guidance conduits and wraps for peripheral nerve injury: A review of materials and efficacy. Injury 2012;43:553–72. https://doi.org/10.1016/j.injury.2010.12.030.

[25] Fujimaki H, Matsumine H, Osaki H, Ueta Y, Kamei W, Shimizu M, et al. Dedifferentiated fat cells in polyglycolic acid-collagen nerve conduits promote rat facial nerve regeneration. Regen Ther 2019;11:240–8. https://doi.org/10.1016/j.reth.2019.08.004.

[26] Gu X, Ding F, Williams DF. Neural tissue engineering options for peripheral nerve regeneration. Biomaterials 2014;35:6143–56. https://doi.org/10.1016/j.biomaterials.2014.04.064.

[27] Du J, Chen H, Qing L, Yang X, Jia X. Biomimetic neural scaffolds: A crucial step towards optimal peripheral nerve regeneration. Biomater Sci 2018;6:1299–311. https://doi.org/10.1039/c8bm00260f.

[28] Parker BJ, Rhodes DI, O'Brien CM, Rodda AE, Cameron NR. Nerve guidance conduit development for primary treatment of peripheral nerve transection injuries: A commercial perspective. Acta Biomater 2021;135:64–86. https://doi.org/10.1016/j.actbio.2021.08.052.

[29] Bell JHA, Haycock JW. Next generation nerve guides: Materials, fabrication, growth factors, and cell delivery. Tissue Eng - Part B Rev 2012;18:116–28. https://doi.org/10.1089/ten.teb.2011.0498.

[30] Chiono V, Tonda-Turo C. Trends in the design of nerve guidance channels in peripheral nerve tissue engineering. Prog Neurobiol 2015;131:87–104. https://doi.org/10.1016/j.pneurobio.2015.06.001.

[31] Sundback C, Hadlock T, Cheney M, Vacanti J. Manufacture of porous polymer nerve conduits by a novel low-pressure injection molding process. Biomaterials 2003;24:819–30. https://doi.org/10.1016/S0142-9612(02)00409-X.

[32] Diez-Ahedo R, Mendibil X, Márquez-Posadas MC, Quintana I, González F, Rodríguez FJ, et al. UV-Casting on Methacrylated PCL for the Production of a Peripheral Nerve Implant Containing an Array of Porous Aligned Microchannels. Polymers (Basel) 2020;12:971. https://doi.org/10.3390/polym12040971.

[33] Lee DJ, Fontaine A, Meng X, Park D. Biomimetic nerve guidance conduit containing intraluminal microchannels with aligned nanofibers markedly facilitates in nerve regeneration 2016. https://doi.org/10.1021/acsbiomaterials.6b00344.

[34] Pawelec K, Koffler J, Shahriari D, Galvan AR, Tuszynski M, Sakamoto JS. Microstructure and in vivo characterization of multi-channel nerve guidance scaffolds. Biomed Mater 2018;in press. https://doi.org/10.1088/1748-605X/aaad85.

[35] Tonda-Turo C, Audisio C, Gnavi S, Chiono V, Gentile P, Raimondo S, et al. Porous Poly(ε-caprolactone) Nerve Guide Filled with Porous Gelatin Matrix for Nerve Tissue Engineering. Adv Eng Mater 2011;13:B151–64. https://doi.org/10.1002/adem.201080099.

[36] Sarker M, Naghieh S, McInnes AD, Schreyer DJ, Chen X. Strategic Design and Fabrication of Nerve Guidance Conduits for Peripheral Nerve Regeneration. Biotechnol J 2018;13:1700635. https://doi.org/10.1002/biot.201700635.

[37] Toba T, Nakamura T, Shimizu Y, Matsumoto K, Ohnishi K, Fukuda S, et al. Regeneration of canine peroneal nerve with the use of a polyglycolic acid-collagen tube filled with laminin-soaked collagen sponge: A comparative study of collagen sponge and collagen fibers as filling materials for nerve conduits. J Biomed Mater Res 2001;58:622–30. https://doi.org/10.1002/jbm.1061.

[38] Huang L, Zhu L, Shi X, Xia B, Liu Z, Zhu S, et al. A compound scaffold with uniform longitudinally oriented guidance cues and a porous sheath promotes peripheral nerve regeneration in vivo. Acta Biomater 2018;68:223–36. https://doi.org/10.1016/j.actbio.2017.12.010.

[39] Taylor CS, Behbehani M, Glen A, Basnett P, Gregory DA, Lukasiewicz BB, et al. Aligned Polyhydroxyalkanoate Blend Electrospun Fibers as Intraluminal Guidance Scaffolds for Peripheral Nerve Repair. ACS Biomater Sci Eng 2023;9:1472–85. https://doi.org/10.1021/acsbiomaterials.2c00964.

[40] Lizarraga-Valderrama LR, Taylor CS, Claeyssens F, Haycock JW, Knowles JC, Roy I. Unidirectional neuronal cell growth and differentiation on aligned polyhydroxyalkanoate blend microfibres with varying diameters. J Tissue Eng Regen Med 2019;13:1581–94. https://doi.org/10.1002/term.2911.

[41] Behbehani M, Glen A, Taylor CS, Schuhmacher A, Claeyssens F, Haycock JW. Pre-clinical evaluation of advanced nerve guide conduits using a novel 3D in vitro testing model. Int J Bioprinting 2018;4:1–12. https://doi.org/10.18063/IJB.v4i1.123.

[42] Kirillova A, Yeazel TR, Asheghali D, Petersen SR, Dort S, Gall K, et al. Fabrication of Biomedical Scaffolds Using Biodegradable Polymers. Chem Rev 2021;121:11238–304. https://doi.org/10.1021/acs.chemrev.0c01200.

[43] Loh QL, Choong C. Three-Dimensional Scaffolds for Tissue Engineering Applications: Role of Porosity and Pore Size. Tissue Eng Part B Rev 2013;19:485–502. https://doi.org/10.1089/ten.teb.2012.0437.

[44] Widmer MS, Gupta PK, Lu L, Meszlenyi RK, Evans GR. D, Brandt K, et al. Manufacture of porous biodegradable polymer conduits by an extrusion process for guided tissue regeneration. Biomaterials 1998;19:1945–55. https://doi.org/10.1016/S0142-9612(98)00099-4.

[45] Manoukian OS, Arul MR, Rudraiah S, Kalajzic I, Kumbar SG. Aligned microchannel polymer-nanotube composites for peripheral nerve regeneration: Small molecule drug delivery. J Control Release 2019;296:54–67. https://doi.org/10.1016/j.jconrel.2019.01.013.

[46] Li G, Xue C, Wang H, Yang X, Zhao Y, Zhang L, et al. Spatially featured porous chitosan conduits with micropatterned inner wall and seamless sidewall for bridging peripheral nerve regeneration. Carbohydr Polym 2018;194:225–35. https://doi.org/10.1016/j.carbpol.2018.04.049.

[47] Kim SM, Lee MS, Jeon J, Lee DH, Yang K, Cho SW, et al. Biodegradable Nerve Guidance Conduit with Microporous and Micropatterned Poly(lactic- co -glycolic acid)-Accelerated Sciatic Nerve Regeneration. Macromol Biosci 2018;18:1800290. https://doi.org/10.1002/mabi.201800290.

[48] Wang Z, Wu Y, Xiang Y, Kruth MB, Wei P, Dai G, et al. Efficacy of Large Groove Texture on Rat Sciatic Nerve Regeneration In Vivo Using Polyacrylonitrile Nerve Conduits. Ann Biomed Eng 2021;49:394–406. https://doi.org/10.1007/s10439-020-02560-7.

[49] Yang X, Liu X, Xu F, Ji S, Sun Y, Song Z, et al. Fabrication of microgroove poly(lactic-co-glycolic acid) nerve guide conduit using dry-jet wet spinning for rat laryngeal recurrent nerve regeneration. Mater Des 2022;223:111151. https://doi.org/10.1016/j.matdes.2022.111151.

[50] Long Y, Zhang N, Huang Y, Wen X. Formation of highly aligned grooves on inner surface of semipermeable hollow fiber membrane for directional axonal outgrowth. J Manuf Sci Eng 2008;130:0210111–8. https://doi.org/10.1115/1.2896111.

[51] Damodaran VB, Bhatnagar D, Murthy NS. Biomedical Polymers: An Overview. Biomed. Polym., Cham: Springer International Publishing; 2016, p. 1–22. https://doi.org/10.1007/978-3-319-32053-3.

[52] Park J, Bronzino J. Biomaterials: principles and applications. Boca Raton: CRC Press; 2002.

[53] Daher E, Souza FG, Carelo J, Brandão V. Drug delivery polymers: An Analysis Based on Literature Text Mining. Brazilian J Exp Des Data Anal Inferent Stat 2021;1:40–55. https://doi.org/10.29327/232092.1.1-9.

[54] Yaszemski M, Trantolo DJ. Biomaterials in Orthopedics. New York: Marcel Dekker; 2004.

[55] Duffy P, McMahon S, Wang X, Keaveney S, O'Cearbhaill ED, Quintana I, et al. Synthetic bioresorbable poly-α-hydroxyesters as peripheral nerve guidance conduits; a review of material properties, design strategies and their efficacy to date. Biomater Sci 2019;7:4912–43. https://doi.org/10.1039/C9BM00246D.

[56] Jiang X, Lim SH, Mao H, Chew SY. Current applications and future perspectives of artificial nerve conduits. Exp Neurol 2010;223:86–101. https://doi.org/10.1016/j.expneurol.2009.09.009.

[57] Zhang Z, Ortiz O, Goyal R, Kohn J, Hubbell JA. Principles of Tissue Engineering. Princ. Tissue Eng. Fourth Edi, Elsevier; 2014, p. 83–123. https://doi.org/10.1016/B978-0-12-398358-9.00006-9.

[58] Dalamagkas K, Tsintou M, Seifalian AM. Advances in peripheral nervous system regenerative therapeutic strategies: A biomaterials approach. Mater Sci Eng C 2016. https://doi.org/10.1016/j.msec.2016.04.048.

[59] Waitayawinyu T, Parisi DM, Miller B, Luria S, Morton HJ, Chin SH, et al. A Comparison of Polyglycolic Acid Versus Type 1 Collagen Bioabsorbable Nerve Conduits in a Rat Model: An Alternative to Autografting. J Hand Surg Am 2007;32:1521–9. https://doi.org/10.1016/j.jhsa.2007.07.015.

[60] Rosen JM, Hentz VR, Kaplan EN. Fascicular Tubulization: A Cellular Approach to Peripheral Nerve Repair. Ann Plast Surg 1983;11:397–411. https://doi.org/10.1097/00000637-198311000-00007.

[61] Mackinnon SE, Dellon AL. Clinical Nerve Reconstruction with a Bioabsorbable Polyglycolic Acid Tube. Plast Reconstr Surg 1990;85:419–24. https://doi.org/10.1097/00006534-199003000-00015.

[62] Nasution AK, Hermawan H. Degradable Biomaterials for Temporary Medical Implants, 2016, p. 127–60. https://doi.org/10.1007/978-3-319-14845-8_6.

[63] Sabino MA, Feijoo JL, Müller AJ. Crystallisation and morphology of poly(p-dioxanone). Macromol Chem Phys 2000;201:2687–98. https://doi.org/10.1002/1521-3935(20001201)201:18<2687::aid-macp2687>3.0.co;2-%23.

[64] Chow WN, Simpson DG, Bigbee JW, Colello RJ. Evaluating neuronal and glial growth on electrospun polarized matrices: bridging the gap in percussive

spinal cord injuries. Neuron Glia Biol 2007;3:119–26. https://doi.org/10.1017/S1740925X07000580.

[65] Wu S, Qi Y, Shi W, Kuss M, Chen S, Duan B. Electrospun conductive nanofiber yarns for accelerating mesenchymal stem cells differentiation and maturation into Schwann cell-like cells under a combination of electrical stimulation and chemical induction. Acta Biomater 2022;139:91–104. https://doi.org/10.1016/j.actbio.2020.11.042.

[66] Wu H, Zhang J, Luo Y, Wan Y, Sun S. Mechanical properties and permeability of porous chitosan–poly(p-dioxanone)/silk fibroin conduits used for peripheral nerve repair. J Mech Behav Biomed Mater 2015;50:192–205. https://doi.org/10.1016/j.jmbbm.2015.06.016.

[67] Sarasua J-RR, López-Rodríguez N, Zuza E, Petisco S, Castro B, Del Olmo M, et al. Crystallinity assessment and in vitro cytotoxicity of polylactide scaffolds for biomedical applications. J Mater Sci Mater Med 2011;22:2513–23. https://doi.org/10.1007/s10856-011-4425-1.

[68] Yang F, Murugan R, Ramakrishna S, Wang X, Ma YX, Wang S. Fabrication of nano-structured porous PLLA scaffold intended for nerve tissue engineering. Biomaterials 2004;25:1891–900. https://doi.org/10.1016/j.biomaterials.2003.08.062.

[69] Evans GR., Brandt K, Niederbichler AD, Chauvin P, Hermann S, Bogle M, et al. Clinical long-term in vivo evaluation of poly(L-lactic acid) porous conduits for peripheral nerve regeneration. J Biomater Sci Polym Ed 2000;11:869–78. https://doi.org/10.1163/156856200744066.

[70] Narayanan G, Vernekar VN, Kuyinu EL, Laurencin CT. Poly (lactic acid)-based biomaterials for orthopaedic regenerative engineering. Adv Drug Deliv Rev 2016;107:247–76. https://doi.org/10.1016/j.addr.2016.04.015.

[71] Yi Q, Wen X, Li L, He B, Nie Y, Wu Y, et al. The chiral effects on the responses of osteoblastic cells to the polymeric substrates. Eur Polym J 2009;45:1970–8. https://doi.org/10.1016/j.eurpolymj.2009.04.018.

[72] Hsu SH, Ni HC. Fabrication of the microgrooved/microporous polylactide substrates as peripheral nerve conduits and in vivo evaluation. Tissue Eng - Part A 2009;15:1381–90. https://doi.org/10.1089/ten.tea.2008.0175.

[73] Xu H, Holzwarth JM, Yan Y, Xu P, Zheng H, Yin Y, et al. Conductive PPY/PDLLA conduit for peripheral nerve regeneration. Biomaterials 2014;35:225–35. https://doi.org/10.1016/j.biomaterials.2013.10.002.

[74] Dai LG, Huang GS, Hsu SH. Sciatic nerve regeneration by cocultured schwann cells and stem cells on microporous nerve conduits. Cell Transplant 2013;22:2029–39. https://doi.org/10.3727/096368912X658953.

[75] Schnell E, Klinkhammer K, Balzer S, Brook G, Klee D, Dalton P, et al. Guidance of glial cell migration and axonal growth on electrospun nanofibers of poly-ε-caprolactone and a collagen/poly-ε-caprolactone blend. Biomaterials 2007;28:3012–25. https://doi.org/10.1016/j.biomaterials.2007.03.009.

[76] Sabbatier G, Larrañaga A, Guay-Bégin A-A, Fernandez J, Diéval F, Durand B, et al. Design, Degradation Mechanism and Long-Term Cytotoxicity of Poly(L -lactide) and Poly(Lactide-co-ε-Caprolactone) Terpolymer Film and Air-Spun Nanofiber Scaffold. Macromol Biosci 2015;15:1392–410. https://doi.org/10.1002/mabi.201500130.

[77] McMahon S, Bertollo N, Cearbhaill EDO, Salber J, Pierucci L, Duffy P, et al. Bio-resorbable polymer stents: a review of material progress and prospects. Prog Polym Sci 2018;83:79–96. https://doi.org/10.1016/j.progpolymsci.2018.05.002.

[78] Den Dunnen WFAA, Stokroos I, Blaauw EH, Holwerda A, Pennings AJ, Robinson PH, et al. Light-microscopic and electron-microscopic evaluation of short-term nerve regeneration using a biodegradable poly(DL-lactide-ε-caprolacton) nerve guide. J Biomed Mater Res 1996;31:105–15. https://doi.org/10.1002/(sici)1097-4636(199605)31:1<105::aid-jbm13>3.0.co;2-m.

[79] Meek MF, Den Dunnen WFA. Porosity of the wall of a Neurolac® nerve conduit hampers nerve regeneration. Microsurgery 2009;29:473–8. https://doi.org/10.1002/micr.20642.

[80] Yoo J, Park JWJH, Kwon YW, Chung JJ, Choi IC, Nam JJ, et al. Augmented peripheral nerve regeneration through elastic nerve guidance conduits prepared using a porous PLCL membrane with a 3D printed collagen hydrogel. Biomater Sci 2020;8:6261–71. https://doi.org/10.1039/d0bm00847h.

[81] Lee HS, Jeon EY, Nam JJ, Park JH, Choi IC, Kim SH, et al. Development of a regenerative porous PLCL nerve guidance conduit with swellable hydrogel-based microgrooved surface pattern via 3D printing. Acta Biomater 2022;141:219–32. https://doi.org/10.1016/j.actbio.2022.01.042.

[82] Malafaya PB, Silva GA, Reis RL. Natural–origin polymers as carriers and scaffolds for biomolecules and cell delivery in tissue engineering applications. Adv Drug Deliv Rev 2007;59:207–33. https://doi.org/10.1016/j.addr.2007.03.012.

[83] Balart R, Garcia-Garcia D, Fombuena V, Quiles-Carrillo L, Arrieta MP. Biopolymers from natural resources. Polymers (Basel) 2021;13:1–9. https://doi.org/10.3390/polym13152532.

[84] Fornasari BE, Carta G, Gambarotta G, Raimondo S. Natural-Based Biomaterials for Peripheral Nerve Injury Repair. Front Bioeng Biotechnol 2020;8. https://doi.org/10.3389/fbioe.2020.554257.

[85] Muthuraj R, Valerio O, Mekonnen TH. Recent developments in short- and medium-chain- length Polyhydroxyalkanoates: Production, properties, and applications. Int J Biol Macromol 2021;187:422–40. https://doi.org/10.1016/j.ijbiomac.2021.07.143.

[86] Rai R, Keshavarz T, Roether JA, Boccaccini AR, Roy I. Medium chain length polyhydroxyalkanoates, promising new biomedical materials for the future. Mater Sci Eng R Reports 2011;72:29–47. https://doi.org/10.1016/j.mser.2010.11.002.

[87] Basnett P, Nigmatullin R, Lukasiewicz B, Rodriguez FJ, Pacharra S, Mendibil X, et al. Polyhydroxyalkanoates : A Family of Natural Polymers , for Medical Implant Development and Disease Modelling, 2019.

[88] Ljungberg C, Johansson-Ruden G, Boström KJ, Novikov L, Wiberg M. Neuronal survival using a resorbable synthetic conduit as an alternative to primary nerve repair. Microsurgery 1999;19:259–64. https://doi.org/10.1002/(SICI)1098-2752(1999)19:6<259::AID-MICR1>3.0.CO;2-Q.

[89] Lizarraga-Valderrama LR, Nigmatullin R, Taylor C, Haycock JW, Claeyssens F, Knowles JC, et al. Nerve tissue engineering using blends of poly(3-hydroxyalkanoates) for peripheral nerve regeneration. Eng Life Sci 2015;15:612–21. https://doi.org/10.1002/elsc.201400151.

[90] Puppi D, Pecorini G, Chiellini F. Biomedical Processing of Polyhydroxyalkanoates. Bioengineering 2019;6:108. https://doi.org/10.3390/bioengineering6040108.

[91] Hazari A, Wiberg M, Johansson-Rudén G, Green C, Terenghi G. A resorbable nerve conduit as an alternative to nerve autograft in nerve gap repair. Br J Plast Surg 1999;52:653–7. https://doi.org/10.1054/bjps.1999.3184.

[92] Hazer DB, Bal E, Nurlu G, Benli K, Balci S, Öztürk F, et al. In vivo application of poly-3-hydroxyoctanoate as peripheral nerve graft. J Zhejiang Univ Sci B 2013;14:993–1003. https://doi.org/10.1631/jzus.B1300016.

[93] Rai R, Yunos DM, Boccaccini AR, Knowles JC, Barker IA, Howdle SM, et al. Poly-3-hydroxyoctanoate P(3HO), a Medium Chain Length Polyhydroxyalkanoate Homopolymer from Pseudomonas mendocina. Biomacromolecules 2011;12:2126–36. https://doi.org/10.1021/bm2001999.

[94] Volova T, Shishatskaya E, Sevastianov V, Efremov S, Mogilnaya O. Results of biomedical investigations of PHB and PHB/PHV fibers. Biochem Eng J 2003;16:125–33. https://doi.org/10.1016/S1369-703X(03)00038-X.

[95] Rivera-Briso AL, Serrano-Aroca Á. Poly(3-Hydroxybutyrate-co-3-Hydroxyvalerate): Enhancement strategies for advanced applications. Polymers (Basel) 2018;10:1–28. https://doi.org/10.3390/polym10070732.

[96] Biazar E, Keshel SH, Pouya M. Efficacy of nanofibrous conduits in repair of long-segment sciatic nerve defects. Neural Regen Res 2013;8:2501–9. https://doi.org/10.3969/j.issn.1673-5374.2013.27.001.

[97] Karimi M, Biazar E, Keshel SH, Ronaghi A, Doostmohamadpour J, Janfada A, et al. Rat Sciatic Nerve Reconstruction Across a 30 mm Defect Bridged by an Oriented Porous PHBV Tube With Schwann Cell as Artificial Nerve Graft. ASAIO J 2014;60:224–33. https://doi.org/10.1097/MAT.0000000000000044.

[98] Durgam H, Sapp S, Deister C, Khaing Z, Chang E, Luebben S, et al. Novel degradable co-polymers of polypyrrole support cell proliferation and enhance neurite out-growth with electrical stimulation. J Biomater Sci Polym Ed 2010;21:1265–82. https://doi.org/10.1163/092050609X12481751806330.

[99] Bian YZ, Wang Y, Aibaidoula G, Chen GQ, Wu Q. Evaluation of poly(3-hydroxybutyrate-co-3-hydroxyhexanoate) conduits for peripheral nerve regeneration. Biomaterials 2009;30:217–25. https://doi.org/10.1016/j.biomaterials.2008.09.036.

[100] Basnett P, Marcello E, Lukasiewicz B, Panchal B, Nigmatullin R, Knowles JC, et al. Biosynthesis and characterization of a novel, biocompatible medium chain length polyhydroxyalkanoate by Pseudomonas mendocina CH50 using coconut oil as the carbon source. J Mater Sci Mater Med 2018;29. https://doi.org/10.1007/s10856-018-6183-9.

[101] Chen G-Q. A microbial polyhydroxyalkanoates (PHA) based bio- and materials industry. Chem Soc Rev 2009;38:2434. https://doi.org/10.1039/b812677c.

[102] Duarte MAT, Hugen RG, Martins ES, Pezzin APT, Pezzin SH. Thermal and mechanical behavior of injection molded Poly(3-hydroxybutyrate)/Poly(epsilon-caprolactone) blends. Mater Res 2006;9:25–8. https://doi.org/10.1590/S1516-14392006000100006.

[103] Garcia-Garcia D, Ferri JM, Boronat T, Lopez-Martinez J, Balart R. Processing and characterization of binary poly(hydroxybutyrate) (PHB) and poly(caprolactone) (PCL) blends with improved impact properties. Polym Bull 2016;73:3333–50. https://doi.org/10.1007/s00289-016-1659-6.

[104] Katsumata K, Saito T, Yu F, Nakamura N, Inoue Y. The toughening effect of a small amount of poly(ε-caprolactone) on the mechanical properties of the poly(3-hydroxybutyrate-co-3-hydroxyhexanoate)/PCL blend. Polym J 2011;43:484–92.

https://doi.org/10.1038/pj.2011.12.

[105] Chen G-Q, Wu Q. The application of polyhydroxyalkanoates as tissue engineering materials. Biomaterials 2005;26:6565–78. https://doi.org/10.1016/j.biomaterials.2005.04.036.

[106] Bugnicourt E, Cinelli P, Lazzeri A, Alvarez V. Polyhydroxyalkanoate (PHA): Review of synthesis , characteristics , processing and potential applications in packaging. Express Polym Lett 2014;8:791–808. https://doi.org/10.3144/expresspolymlett.2014.82.

[107] Venkatesh V, Swain N, Srinivas G, Kumar P, Barshilia HC. Review on the machining characteristics and research prospects of conventional microscale machining operations. Mater Manuf Process 2017;32:235–62. https://doi.org/10.1080/10426914.2016.1151045.

[108] Debnath S, Kunar S, Anasane SS, Bhattacharyya B. Non-traditional Micromachining Processes: Opportunities and Challenges, 2017, p. 1–59. https://doi.org/10.1007/978-3-319-52009-4_1.

[109] Razali AR, Qin Y. A review on micro-manufacturing, micro-forming and their key issues. Procedia Eng 2013;53:665–72. https://doi.org/10.1016/j.proeng.2013.02.086.

[110] Dimov S, Brousseau E, Minev R, Bigot S. Micro- and nano-manufacturing: Challenges and opportunities. Proc Inst Mech Eng Part C J Mech Eng Sci 2012;226:3–15. https://doi.org/10.1177/0954406211422972.

[111] Dimov SS, Matthews C, Glanfield A, Dorrington P. A roadmapping study in Multi-Material Micro Manufacture. 4M 2006 - Second Int. Conf. Multi-Material Micro Manuf., Elsevier; 2006, p. xi–xxv. https://doi.org/10.1016/B978-008045263-0/50001-5.

[112] Hansen HN, Hocken RJ, Tosello G. Replication of micro and nano surface geometries. CIRP Ann - Manuf Technol 2011;60:695–714. https://doi.org/10.1016/j.cirp.2011.05.008.

[113] Baruffi F, Calaon M, Tosello G, Charalambis A, Elsborg R. Comparison of micro and conventional injection moulding based on process precision and accuracy. Procedia CIRP 2018;75:149–54. https://doi.org/10.1016/j.procir.2018.04.046.

[114] Giboz J, Copponnex T, Mélé P. Microinjection molding of thermoplastic polymers: a review. J Micromechanics Microengineering 2007;17:R96–109. https://doi.org/10.1088/0960-1317/17/6/R02.

[115] Tosello G. Micro Injection Molding. Munich: Hanser Publishers; 2018.

[116] Tosello G, Hansen HN. Micro-Injection-Molding. Micromanufacturing Eng. …, 2010, p. 90–113. https://doi.org/10.1016/B978-0-8155-1545-6.00006-5.

[117] Surace R, Trotta G, Bellantone V, Fassi I. the Micro Injection Moulding Process for Polymeric Components Manufacturing. New Technol - Trends, Innov Res 2012. https://doi.org/10.5772/35299.

[118] Bellantone V, Surace R, Trotta G, Fassi I. Replication capability of micro injection moulding process for polymeric parts manufacturing. Int J Adv Manuf Technol 2012;67:1407–21. https://doi.org/10.1007/s00170-012-4577-2.

[119] Surace R, Bellantone V, Trotta G, Fassi I. Replicating capability investigation of micro features in injection moulding process. J Manuf Process 2017;28:351–61. https://doi.org/10.1016/j.jmapro.2017.07.004.

[120] Mélé P, Giboz J. Micro-injection molding of thermoplastic polymers: Proposal of a constitutive law as function of the aspect ratios. J Appl Polym Sci 2017;45719:45719. https://doi.org/10.1002/app.45719.

[121] Muanchan P, Ito H. Replication of Micro- / Nanostructures. In: J. Yan, editor. Micro Nano Fabr. Technol. Springer N, 2018, p. 1–29. https://doi.org/https://doi.org/10.1007/978-981-10-6588-0_19-1.

[122] Sorgato M, Babenko M, Lucchetta G, Whiteside B. Investigation of the influence of vacuum venting on mould surface temperature in micro injection moulding. Int J Adv Manuf Technol 2017;88:547–55. https://doi.org/10.1007/s00170-016-8789-8.

[123] Tosello G, Lucchetta G, Hansen HN, Gava A. Mechanical properties test and microstructure analysis of polyoxymethylene (POM) micro injection moulded standard parts. Multi-Material Micro Manuf 2009:231–5. https://doi.org/10.1243/17547164C0012009045.

[124] Griffiths CA, Dimov SS, Brousseau EB, Chouquet C, Gavillet J, Bigot S. Investigation of surface treatment effects in micro-injection-moulding. Int J Adv Manuf Technol 2010;47:99–110. https://doi.org/10.1007/s00170-009-2000-4.

[125] Sha B, Dimov SS, Griffiths CA, Packianather MS. Micro-injection moulding: Factors affecting the achievable aspect ratios. Int J Adv Manuf Technol 2006;33:147–56. https://doi.org/10.1007/s00170-006-0579-2.

[126] Lucchetta G, Sorgato M, Carmignato S, Savio E. Investigating the technological limits of micro-injection molding in replicating high aspect ratio micro-structured surfaces. CIRP Ann - Manuf Technol 2014;63:521–4. https://doi.org/10.1016/j.cirp.2014.03.049.

[127] Vera J, Brulez A-C, Contraires E, Larochette M, Trannoy-Orban N, Pignon M, et al. Factors influencing microinjection molding replication quality. J Micromechanics Microengineering

2018;28:015004. https://doi.org/10.1088/1361-6439/aa9a4e.

[128] Tosello G, Gulcur M, Whiteside B, Coates PD, Luca A, Riemer O, et al. Micro product and process fingerprints for zero-defect net-shape micromanufacturing, Bilbao: 2019.

[129] Attia UM, Alcock JR. Evaluating and controlling process variability in micro-injection moulding. Int J Adv Manuf Technol 2011;50:533–42. https://doi.org/10.1007/s00170-010-2547-0.

[130] Michaeli W, Schreiber A. Online Control of the Injection Molding Process Based on Process Variables. Adv Polym Technol 2009;28:65–76. https://doi.org/10.1002/adv.

[131] Mi HY, Jing X, Turng LS. Fabrication of porous synthetic polymer scaffolds for tissue engineering. J Cell Plast 2014;51:165–96. https://doi.org/10.1177/0021955X14531002.

[132] Ghosh S, Viana JC, Reis RL, Mano JF. Development of porous lamellar poly(l-lactic acid) scaffolds by conventional injection molding process. Acta Biomater 2008;4:887–96. https://doi.org/10.1016/j.actbio.2008.03.001.

[133] Teng P-T, Chern M-J, Shen Y-K, Chiang Y-C. Development of novel porous nasal scaffold using injection molding. Polym Eng Sci 2013;53:762–9. https://doi.org/10.1002/pen.23317.

[134] Kramschuster A, Turng L-S. An injection molding process for manufacturing highly porous and interconnected biodegradable polymer matrices for use as tissue engineering scaffolds. J Biomed Mater Res - Part B Appl Biomater 2010;92:366–76. https://doi.org/10.1002/jbm.b.31523.

[135] Simitzi C, Ranella A, Stratakis E. Controlling the morphology and outgrowth of nerve and neuroglial cells: The effect of surface topography. Acta Biomater 2017;51:21–52. https://doi.org/10.1016/j.actbio.2017.01.023.

[136] Liparoti S, Speranza V, Pantani R. Replication of micro- and nanofeatures in injection molding of two PLA grades with rapid surface-temperature modulation. Materials (Basel) 2018;11. https://doi.org/10.3390/ma11081442.

[137] Abeykoon C, Martin PJ, Kelly AL, Brown EC. A review and evaluation of melt temperature sensors for polymer extrusion. Sensors Actuators, A Phys 2012;182:16–27. https://doi.org/10.1016/j.sna.2012.04.026.

[138] Giles HF, Wagner JR, Mount EMI. Extrusion : The Definitive Processing Guide. 2005.

[139] Gao Y Lou, Wang X, Zhou L. The effect of screw speed on extrusion quality of the single-screw extruder. Adv Mater Res 2014;941–944:1715–9. https://doi.org/10.4028/www.scientific.net/AMR.941-944.1715.

[140] Jin G, Zhao D, Wang M, Jin Y, Tian H, Zhang J. Study on design and experiments of extrusion die for polypropylene single lumen micro tubes. Microsyst Technol 2015. https://doi.org/10.1007/s00542-015-2426-6.

[141] Abeykoon C, Kelly AL, Vera-Sorroche J, Brown EC, Coates PD, Deng J, et al. Process efficiency in polymer extrusion: Correlation between the energy demand and melt thermal stability. Appl Energy 2014;135:560–71. https://doi.org/10.1016/j.apenergy.2014.08.086.

[142] Abeykoon C, Kelly AL, Martin PJ, Li K. Dynamic modelling of die melt temperature profile in polymer extrusion. Proc IEEE Conf Decis Control 2013;38:2550–5. https://doi.org/10.1109/CDC.2013.6760264.

[143] Xiaochun Y, Sai L, Guangjian H, Guizhen Z, Jinping Q. Experimental Study of the Extrusion Characteristic of a Vane Extruder Based on Extensional Flow. Adv Polym Technol 2016;35:215–20. https://doi.org/10.1002/adv.21545.

[144] Abeykoon C. Single screw extrusion control: A comprehensive review and directions for improvements. Control Eng Pract 2016;51:69–80. https://doi.org/10.1016/j.conengprac.2016.03.008.

[145] Jin G, Wang M, Zhao D, Tian H, Jin Y. Design and experiments of extrusion die for polypropylene five-lumen micro tube. J Mater Process Technol 2014;214:50–9. https://doi.org/10.1016/j.jmatprotec.2013.07.016.

[146] Jin G, Jin Y, Zhao D, Dai G, Zhang Q. Cross-section design of multi-lumen extrusion dies: study on the effects of die swell and gas flow rate of the lumen. Microsyst Technol 2017;23:5093–104. https://doi.org/10.1007/s00542-017-3489-3.

[147] Perale G, Pertici G, Giordano C, Daniele F, Masi M, Maccagnan S. Nondegradative microextrusion of resorbable polyesters for pharmaceutical and biomedical applications: The cases of poly-lactic-acid and poly-caprolactone. J Appl Polym Sci 2008;108:1591–5. https://doi.org/10.1002/app.27875.

[148] Qin Y, Zhao J, Anyasodor G, Hansen KS, Calderon I, Konrad K, et al. Forming of Polymeric Tubular Micro-components. Micromanufacturing Eng. Technol. Second Edi, Elsevier; 2015, p. 179–200. https://doi.org/10.1016/B978-0-323-31149-6.00008-6.

[149] Cho S, Lee E, Jo S, Kim GM, Kim W. Extrusion Characteristics of Thin Walled Tubes for Catheters Using Thermoplastic Elastomer. Polymers (Basel) 2020;12:1628. https://doi.org/https://doi.org/10.3390/polym12081628.

[150] Cannon AH, King WP, Toub M. Extrusion of low friction and low tack microstructured surfaces on silicone rubber. Rubber World 2013;248:26–8.

[151] Villacorta BS, Hulseman S, Cannon AH, Hulseman R, Ogale AA. Continuously Extruded Micro-Textured Polypropylene Films. Polym Eng Sci 2014;54:2147–54. https://doi.org/10.1002/ pen.23762.

[152] Sahmel O, Siewert S, Schmitz KP, Arbeiter D, Grabow N, Kreiner CF, et al. Extrusion as a manufacturing process for polymer micro-tubes for various bio-medical applications. Curr Dir Biomed Eng 2019;5:489–91. https://doi.org/10.1515/cdbme-2019-0123.

[153] Casalini T, Perale G. Durability and Reliability of Medical Polymers. Woodhead; 2012. https://doi.org/10.1533/9780857096517.2.225.

[154] Tian H, Zhao D, Wang M, Jin G, Jin Y. Study on extrudate swell of polypropylene in double-lumen micro profile extrusion. J Mater Process Technol 2015;225:357–68. https://doi.org/10.1016/j.jmatprotec.2015.06.015.

[155] Washburn NR, Simon CG, Tona A, Elgendy HM, Karim A, Amis EJ. Co-extrusion of biocompatible polymers for scaffolds with co-continuous morphology. J Biomed Mater Res 2002;60:20–9. https://doi.org/10.1002/jbm.10049.

[156] Reignier J, Huneault MA. Preparation of interconnected poly(ε-caprolactone) PCL porous scaffolds by a combination of polymer and salt particulate leaching. Polymer (Guildf) 2006;47:4703–17. https://doi.org/10.1016/j.polymer.2006.04.029.

[157] Peng X-F, Mi H-Y, Jing X, Yu P, Qu J-P, Chen B-Y. Preparation of highly porous interconnected poly(lactic acid) scaffolds based on a novel dynamic elongational flow procedure. Mater Des 2016;101:285–93. https://doi.org/10.1016/j.matdes.2016.03.156.

[158] Corporation A. EP0131207B1_Method of manufacturing synthetic resin pen nibs, 1988.

[159] Yin H-M, Qian J, Zhang J, Lin Z-F, Li J-S, Xu J-Z, et al. Engineering Porous Poly(lactic acid) Scaffolds with High Mechanical Performance via a Solid State Extrusion/Porogen Leaching Approach. Polymers (Basel) 2016;8:213. https://doi.org/10.3390/polym8060213.

[160] Le Moigne N, Sauceau M, Benyakhlef M, Jemai R, Benezet J-C, Rodier E, et al. Foaming of poly(3-hydroxybutyrate-co-3-hydroxyvalerate)/organo-clays nano-biocomposites by a continuous supercritical CO2 assisted extrusion process. Eur Polym J 2014;61:157–71. https://doi.org/10.1016/j.eurpolymj.2014.10.008.

[161] Ventura H, Laguna-Gutiérrez E, Rodriguez-Perez MA, Ardanuy M. Effect of chain extender and water-quenching on the properties of poly(3-hydroxybutyrate-co-4-hydroxybutyrate) foams for its production by extrusion foaming. Eur Polym J 2016;85:14–25. https://doi.org/10.1016/j.eurpolymj.2016.10.001.

Chapter 2

In process quality control on micro-injection molding: the role of sensor location

2.1 Introduction

High performance miniaturized components offer unique advantages linked to their low cost and maximal functionalities in the minimal space. Hence, there is a strong demand for miniaturized components from diverse industries such as electronics, optics, medical components, and consumer goods, among others [1,2]. In this scenario, reliable and economical micro manufacturing processes are required in order to fulfil those market demands [3]. In particular, microinjection molding is a well – established high throughput manufacturing technology capable of producing micro systems, 3D micro sized parts or even larger components with features in the range of a few to several hundred micrometers [4,5].

Both, micro and conventional, injection molding processes are based on pushing molten polymer into a cavity where the material is cooled down to a temperature where it solidifies and can be ejected from the mold without damaging it [6]. The final shape of the replicated part is directly related to the dimensional accuracy of the mold, material shrinkage, internal stresses, and molten material volume in the mold. Some of the mechanical properties of the injected part, *i.e.*: ultimate tensile strength, elongation at break and storage modulus, relate to the polymer pressure and temperature evolution during the injection molding cycle [7,8].

The micro machining technologies commonly used to manufacture microinjection molds, *i.e.*: micro-milling, µEDM milling, laser ablation, etc., are capable of machining features sized of 100µm or less, with accuracies around 5µm [9,10]. Mold accuracy is not considered the main source of defective replicated parts, being those aspects linked to the material and the injection process itself the most important factors contributing to part quality deviations [11]. Because of variation on these factors, even when the injection machine and process are properly set, inspection of the injected parts is currently mandatory to assure quality of procured components. In microinjection, due to the nature of some polymeric raw materials (an amorphous polymer is typically clear in appearance) and micro-feature dimensions, part quality inspection involves expensive and time-consuming microscopy or machine vision methods [10,12], being this inspection the bottleneck of the microinjection molding process in terms of productivity.

Cavity pressure monitoring has been reported as a common strategy to detect injection process deviations during a production cycle [12–15]. Commercially available pressure sensors are usually too big to be fitted inside the mold cavities used in microinjection without varying the cavity geometry. Hence, indirect pressure detection in the cavity is performed by arranging these sensors outside the cavity, covering different locations of the machine and mold. In particular, a common strategy is to measure the microinjection process pressure behind the injection pin, in the runner system or by means of ejector pins [13–16]. Apart from the deviations on proper cavity pressure values obtained by such sensors because of the locations far from the cavity, in microinjection, the runner to cavity volume ratio is bigger than in regular injection. This volume ratio can affect even more, the reliability of the pressure monitoring on the cavity via sensor signal acquisition from the runner system. However, it is worth to note that this approach is a very versatile method of controlling the quality of the process when the micro cavity geometry cannot be altered to arrange a specific sensor [17].

There are several studies that analyze the effect of process parameters on the replication quality of microinjected parts [4,18–22], as well as the correlation between these input parameters and output sensing pressure signals [11,13–16,23]. Among them, only two research papers have analyzed the correlation between pressure signal value and part quality deviation [14,15]. Those studies conclude that pressure, is directly linked to part quality and, despite not being as reliable as in conventional injection, it can be used for process monitoring and optimization.

In the study reported in this chapter, pressure and temperature sensors were implemented at two different locations: the cavity of the mold and the runner system. Part quality deviations were correlated to sensor signal variations and input process parameters. The micro-injected parts were classified according to their replication quality level; those quality control results were cross matched with the collected sensor signals to analyze the correlation between signal variations and micro-part quality variations.

The effect of the sensors location on their capacity to detect signal differences regarding the micro-injected part quality was addressed, as well as the identification of the input parameters that play the main role on the quality of the final injected part.

2.2 Materials and methods

The mold used in the study is a three-plate mold that allows using a pin-point gate runner system. This kind of runner system is often used in microinjection molding because of the lack of additional or intermediate process stages needed to achieve finished injected parts. In this scenario, the runner system is split from the injected part during mold opening.

The sensors used to monitor the injection molding process have been arranged in both sides of the pin-point gate: The runner system (pre-gate location) and the cavity, (post-gate position).

The plastic part selected to be tested in the study, is a simple demonstrator comprising several micro sized pillars which have been designed bearing in mind several aspects such as machining limitations, micro-mold design guidelines [1,9] and typical dimensions of micro- features that are considered in real micro-injected components. The micro pillars of this test part have been arranged setting a matrix of (60) pillars with different diameter size, covering dimensions from 350µm down to 65µm as shown in Figure 2.1 (a). Two values for the height of the pillars were considered: 100 and 50µm.

To arrange the in-cavity sensors without affecting the final shape of the micro-featured zone of the injected part, a supplementary cavity branch was considered in the design. This sensor branch has been designed with identical size, volume, and entrance geometry to the micro-featured cavity. The sensor located at the runner system, was also arranged in a branch added to the sprue. Those sensor locations are highlighted in Figure 2.1 (b).

The equipment used to perform the experiments was the "Battenfeld Microsystems 50" microinjection machine (1cm^3 maximum shot volume; 50kN maximum closing force) from Wittmann Battenfeld [24]. The thermo-plastic material used was polyoxymethylene (POM) "ULTRAFORM W2030 003 UNC Q600" (Melt temperature range 190-230°C; mold temperature range 60-120°C) from BASF [25].

The three-plate mold used in the study, is an interchangeable inserts mold which facilitates replicating variable shaped parts by inter-changing mold parts and inserts instead of developing a completely new mold. The inserts and supplementary mold components were designed and

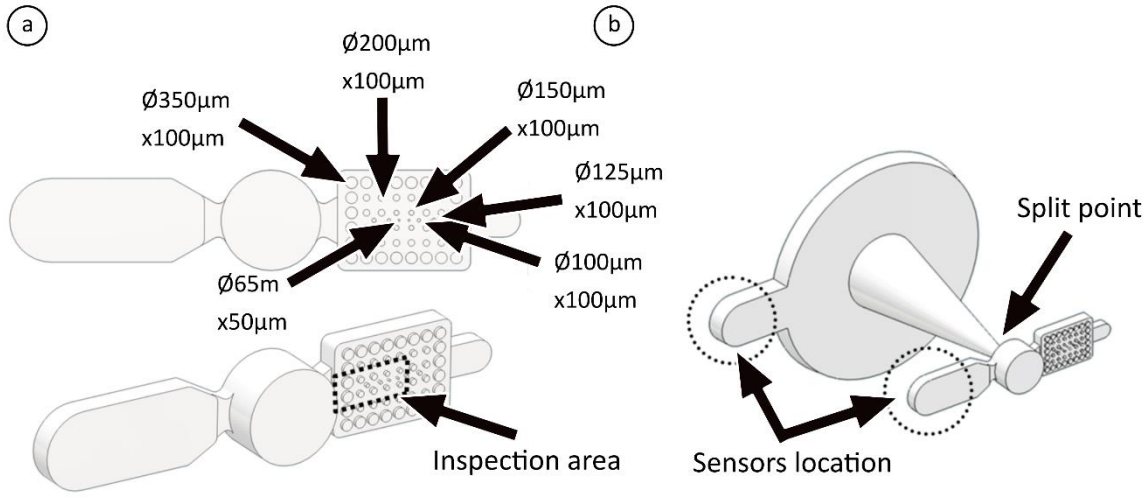

Figure 2.1 CAD images of the designed part and arrangement and dimensions of the micro pillars (a). CAD image of injected part and the runner system (b).

manufactured bearing in mind both the design of the micro-featured part and the arrangement of the sensors (Figure 2.2). The mold inserts were made of Orvar Supreme tool steel, from Uddelholm [26] hardened to 54HRC and machined using different micromachining equipment available at Tekniker: Micro-milling technology for manufacturing the mold cavity and the negative shape of the designed part (including the micro-features). Wire electro discharge machining (WEDM) was used to machine the cone of the sprue and the holes where the ejector pins and sensors will be positioned. Two types of sensors were used in this work, regular pressure and combined pressure and temperature (p-T) sensors. The regular pressure sensor was set in the runner system and the hybrid p-T sensor in the branch of the cavity. The sensors and their signal amplifiers were “KISTLER 6182B”, charge amplifier 5039A222 and “KISTLER P-T 6189A”, charge amplifier 5155A22B1 [27]. Signals from sensors were collected with an acquisition card “DAQ NATIONAL INSTRUMENTS NI usb-6210” connected to a laptop running LabView based “General Acquisition Software V1.02” developed by Tekniker. The sampling rate was 100Hz. The trigger and reset signals were wired from the machine PLC to the amplifiers and measurement outputs were connected to the NI-DAQ card. The regular pressure sensor output was also connected to the machine PLC for sensor calibration purposes.

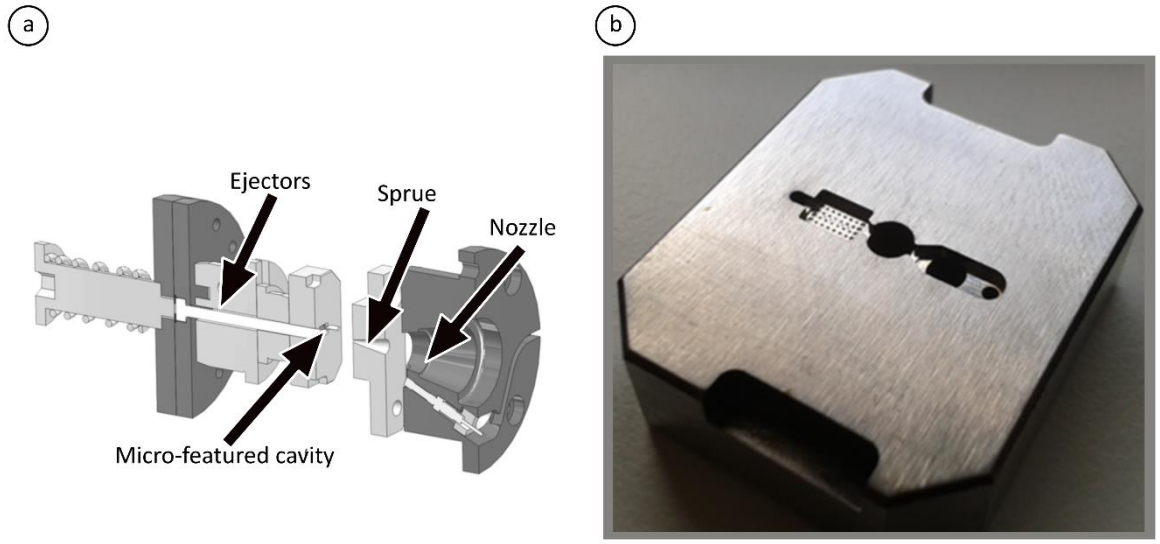

Figure 2.2 Section view of CAD design of the inserts and inner components of the mold (a). Picture of the micro-machined mold insert (b).

The collected data are the maximum values of each signal curve provided by the sensors. The use of the maximum values of each signal implies information loss but enables and facilitates the use of DOE methodology.

The design of experiment approach (DOE) is being currently used to evaluate and control the effect of process input parameters on the quality level of microinjected parts [16,28,29]. In this research, the approach considers the use of fractional factorial DOE to determine the relationship between input parameters and output signals, carrying out less experiments than full factorial approach [18,30].

The experiment was designed following 2 level and 6 inputs half fractional factorial methodology [31]. The 6 inputs (process parameters) correspond to the temperature values at 5 different locations of the microinjection machine (Figure 2.3) and to the speed of the injection ram, which defines the polymer transfer rate into the mold. The holding pressure and the transferred polymer volume, that have significant effects in replication quality [32], were kept constant.

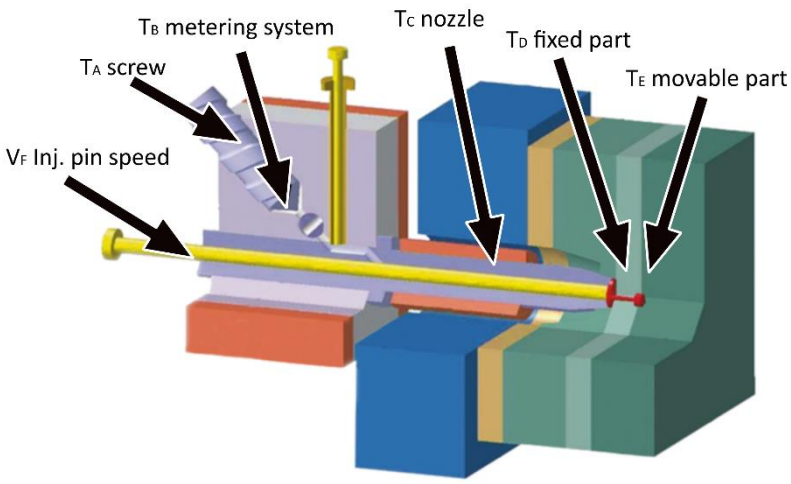

Figure 2.3 Microsystem 50 scheme for input parameters identification.

The process parameters were named T for temperature and V for speed. Locations are identified in the text by the sub-indexes A to F (T_A, T_B...T_E and V_F). Output signals correspond to pressure and temperature signals collected by the sensors at different locations as indicated in Figure 2.1 (b).

The fractional experimental design consisted in $2^{(6-1)} = 32$ configurations; in each test configuration, 5 parts were injected and discarded, to let the process stabilize, and then 5 parts were injected, monitored, and saved to subsequent quality check. 160 monitored parts, in 32 different process input parameter conditions, were obtained and checked by means of confocal microscopy.

The upper and lower-level values of the inputs were defined according to the experience acquired during preliminary screening injection tests as described by Attia *et al*. [21]. During those tests the limits of the process window were identified as the limits where the microinjection was feasible, leading to fully replicated parts, but quality differences in the micro pillar zone were noticeable to the naked eye. Those values are shown in Table 2.1.

Table 2.1 Lower (-1) and Upper (+1) values for each input variable used in the experiment.

	$T_{(A,B,C)}$ [°C]	$T_{(D,E)}$ [°C]	V_F [mm/s]
-1	190	75	280
+1	205	85	350

2.3 Results and discussion

2.3.1 Parameters and signals analysis

The micro-injection trials were conducted following the DOE methodology, varying process inputs and collecting signals from the sensors in the cavity and in the runner system. The collected data was analyzed to determine the correlation between input parameters and monitored output signals deviation. Significant pressure variations caused by some of the input values were detected and, in case of the measured temperatures, an interaction between input parameters was also noticeable.

In Figure 2.4 half normal plots of the absolute normalized effect weights of input parameters are shown. Those plots are useful to determine the input parameters having impact on the output signal variation [33,34].

As it can be analyzed from the half normal plots of the effects on pressure signals (Figure 2.4 (a), (b)), the parameters T_C and T_D, corresponding to the temperatures of the machine nozzle and the fixed part of the mold, cause significant effects on both output pressure signals. Additionally, the parameter T_B, which is the metering system input temperature, seems to have a slightly significant effect on cavity pressure signal. Regarding the effects on cavity temperature (Figure 2.4 (c)), it is worth to note that parameters T_D, T_E, and their interaction DE show the most noticeable effects, showing the straightforward correlation between the mold temperatures and the cavity temperature signals. Temperature input values in the metering system (T_B) and

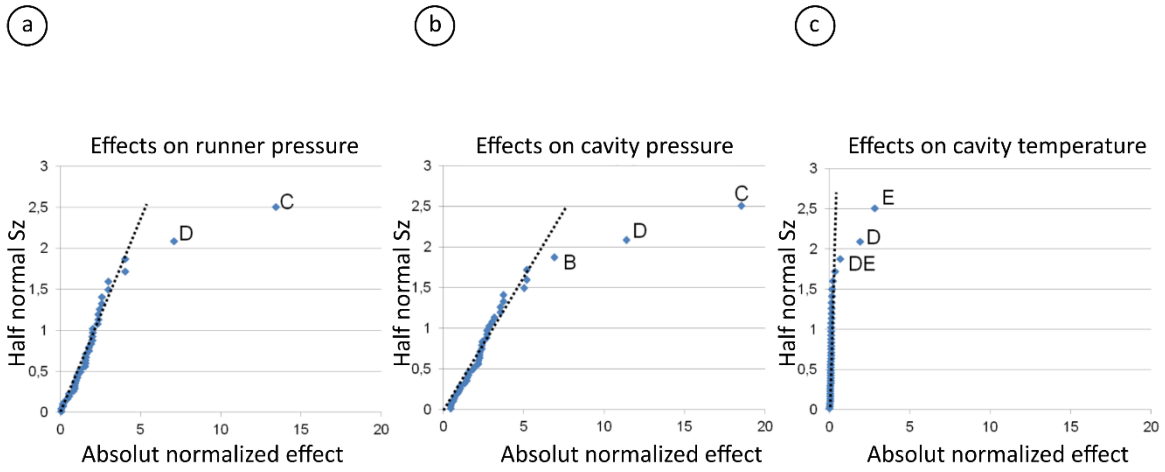

Figure 2.4 Half normal plots of normalized effects.

nozzle (T_C), in contrast to the effect they show on pressure signals, show no influence on temperature output. The effects caused by those inputs that are not significant, are within the range of the normal variability of the process.

Figure 2.5 gives additional information regarding the value and sign of the effects of the six input parameters on the output signals, as well as the interaction of different input parameters on the cavity temperature signal. In those line-charts it is worth to note that both, nozzle (T_C) and fixed part (T_D) input temperatures, have a positive effect on the pressure value, the increment of the input temperature will rise the expected pressure signal.

The use of a pressure sensor directly inside the cavity of the mold, which is an innovative monitoring strategy in microinjection, has shown to be more sensitive than pressure monitoring in the runner system which is a common and almost standard strategy. The pressure signal variations in the cavity are bigger than those in the runner system. The same input parameter change cause bigger and more noticeable effect in the cavity signal than in the runner system.

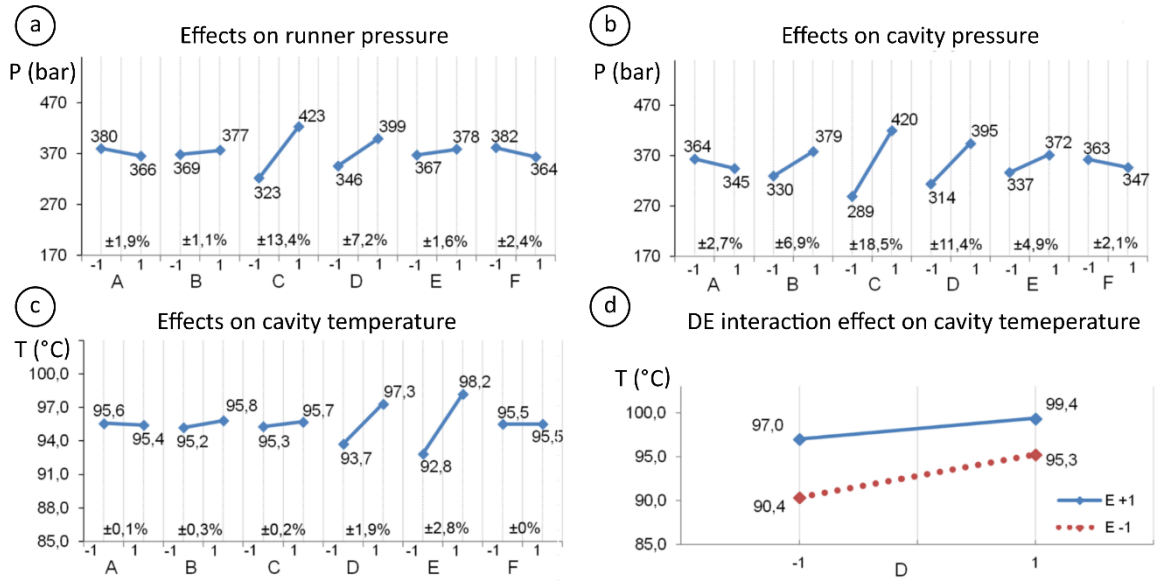

Figure 2.5 Plots of input parameters effects on measured pressure and temperature values.

The pressure signal in the cavity is also sensitive to other input variations, for example the input temperature of the metering system (T_B), and although it was disregarded by the half normal plot (Figure 2.4), the input temperature of the movable part of the mold (T_E) can cause a variation of almost 5% on the cavity pressure value.

As it was indicated in Figure 2.3, the screw temperature T_A, sets the polymer temperature helping to plasticize and melt it, whereas the metering system and machine nozzle temperature input values, T_B and T_C, determine the temperature of the melted polymer previous to be injected into the mold. Additionally, the temperature value of the fixed part of the mold, T_D, sets the temperature of the mold part where the runner system is located. Hence, higher temperatures of mold and melted polymer, cause polymer viscosity reduction, preventing premature solidification and helping to completely fill the cavity, which can lead to higher pressure values [10]. This correlation between temperature input parameters and measured pressures is not a general rule as it depends on the type of material and other different inputs as it can be derived from the study carried out by Griffiths *et al*. [16].

Mold temperature input values, T_D and T_E, show a remarkable effect on cavity temperature readings (Figure 2.5 (c)). This can be explained by the cooling rate of the molten polymer when it touches the mold cavity walls. In a warmer mold, the polymer flow front reaches the sensor

location at higher temperature which leads to higher temperature output signals [10,29]. The observed DE significant interaction (Figure 2.5 (d)) shows that the rise in cavity temperature caused by changing T_D input from (-1) to (+1) is more relevant when T_E is set (-1) than when it is set (+1). It may be explained in terms of the arrangement of the cavity temperature sensor. As it was mentioned previously, this sensor is in the mold part which temperature values are set by the input T_E. Hence the effect caused by T_D in the micro-featured cavity temperature, can be somehow masked by T_E when high temperature levels are considered (+1). Furthermore, the system has a big inertia, and the temperature sensor may not be fast enough to record the actual temperature of the polymer. To analyze polymer fast temperature changes inside the micro-featured cavity, other kinds of sensors may be used.

Figure 2.4 and Figure 2.5 show that the input parameters T_A and V_F, corresponding to the temperature of the screw and the injection speed, cause no detectable effect on output signals in both mold locations. The use of other kind of sensors and the analysis of the evolution of the recorded signal could provide more information about the effect caused by the variation of those input parameters.

The temperature changes in the screw, causes no effect in the pressure and temperature signals probably, because the screw is the place where polymer heats up, as it plasticizes. Posterior heat-controlled zones, such as the metering zone and nozzle, have greater effect on melt temperature.

Changes on the pressure and temperature signals were expected at high injection speeds, because of the direct relationship of this parameter with the shear rate and the shear induced heating in the polymer. This induced heating improves the flow into the cavity, leading to a better filling and packing of the part. Along with that, higher injection speeds promote quicker filling of the cavities which prevents early freezing of the melt [16,35]. The reasons why pressure variations caused by injection speed changes were not detected in our study might be related to the values selected for speed levels. Those high- and low-level values, despite the differences observed on part replication during preliminary screening tests, seemed to be not different enough to induce changes in the output signals.

Another reason behind these results may be the configuration of the injection speed on the machine. Acceleration and deceleration rates of the injection ram are set by defining several set points in a velocity - distance table. In this study the deceleration profile of the final part of the stroke, was kept constant.

2.3.2 Part quality analysis

The microinjected parts obtained during the experiment were measured by confocal microscopy. The measuring area was set considering the wide range of pillar dimensions defined in the part design (Figure 2.1 (a)).

The confocal images were analyzed with numerical computation software [36] to sort out the parts according to their replication quality level. The information obtained via confocal microscopy is collected on a matrix that includes the position and height of each pixel. In the performed part quality analysis, the replication quality level of each part, was correlated with a certain number of pixels per image (area) which height values were above a certain threshold (Figure 2.6 (b)). The height and area thresholds, to consider a part properly replicated, were set at 70% and 90% respectively.

Figure 2.7 (a) (b) is SEM and confocal images of a replicated part identified as "low quality", where the pillar edge roundness and wrinkles are highlighted. Figure 2.7 (c) and (d) show SEM and confocal images of a properly replicated part (high quality). It is worth to note that even for high quality parts, the confocal image shows some missed height data, represented by black areas around each pillar; this data loss, can be correlated to steep walls of the pillars and/or low reflective surface at the bottom of the pillars.

Figure 2.8 shows the P and T values obtained at different sensor locations as a function of the replication quality level of the injected parts and their frequency. Figure 2.8 (a) and (b) show low- and high-quality part frequency distribution along pressure. Both histograms show a quite spread pressure range where high quality and low-quality parts are overlapped. The histograms show the signal maximum values, measured during the DOE experiment, where 32 different

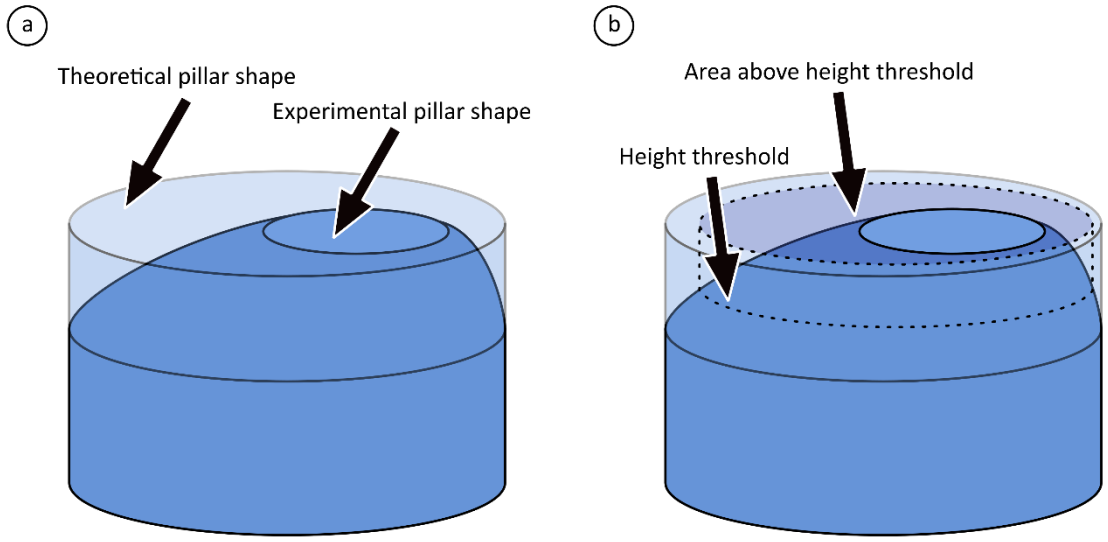

Figure 2.6 Pillar shape and projected area above the height threshold scheme.

input parameter combinations were tried. A spread and even experimental distribution was expected due to the low repeatability of the inputs of the process. However, despite the consistency lack in the process parameters input, some trends and part grouping were found to be worthy of note.

In Figure 2.8 (a) and (b), high quality parts are grouped around higher-pressure values while low quality parts are around lower pressure values and distributed in spreader range, showing a tail of the distribution overlapping the high-pressure values where high-quality parts are found.

Figure 2.8 (c) shows that there was no evidence of a trend of high-quality part distribution with the output temperature measured during the trials. The histogram data is distributed into two groups, one group is distributed around 90°C while the other group can be found around 97°C. The high quality to low quality part ratio is slightly bigger at higher cavity temperatures. It is more probable to obtain a high-quality part when high cavity temperatures are read.

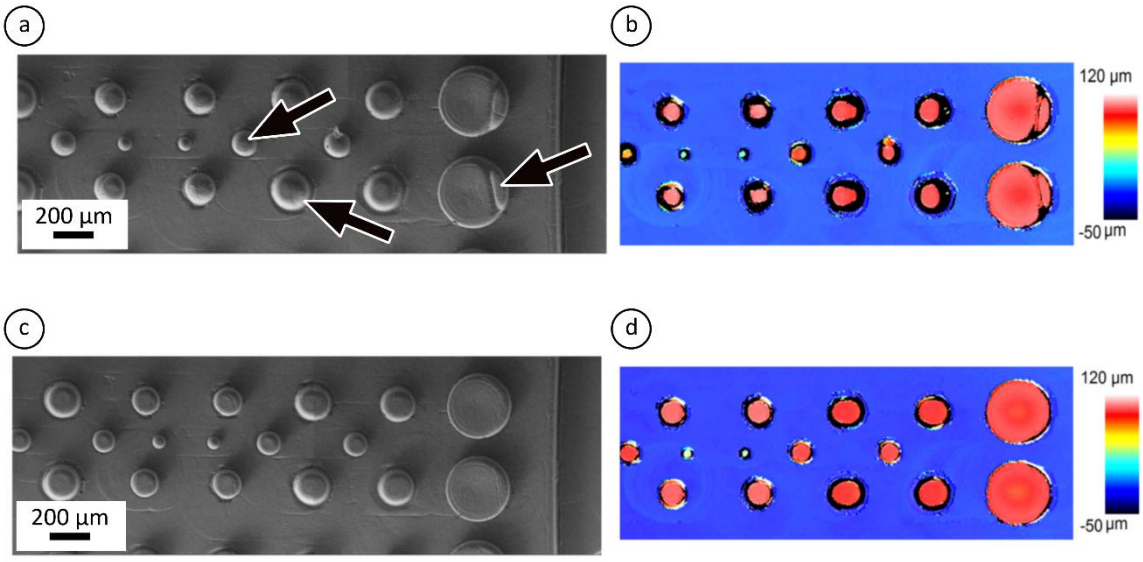

Figure 2.7 Confocal and SEM images of two injected parts showing different replication quality levels.

The histograms show that during the micro-injection experiment, pressures from 138bar to 556bar were acquired in the cavity and, of about 227bar to 502bar in the runner. From the data plotted in the histograms, defining a quality objective of 90 % of injected parts to be high-quality parts, the pressure thresholds would fit to: 450 bar in the runner signal and 480 bar in the micro-featured cavity.

Although some signal variation was expected due to the repeatability of the process and machine, such wide range was caused by the variation of the input parameters during the experiment. In order to evaluate the effect of sensor location on quality deviation detection, the pressure difference (ΔP) between cavity and runner system signals was analyzed and represented in the histogram showed in Figure 2.8 (d). Both high- and low-quality part frequency histograms can be fitted to Gaussian curves which show an overlapping region in the range of -35 to 25 bars. Higher values of ΔP increase the probability of producing high quality parts while lower ΔP values are associated to low quality replication. Hence, the analysis of the pressure signals obtained by the sensors at different locations taking into account the two Gaussian bell curves presented in Figure 2.8 (d) would lead to a direct and fast identification of the part quality in an injection cycle.

The runner and cavity pressure histograms (Figure 2.8 (a) and (b)) are quite similar, both show that higher pressure values lead to properly replicated parts, and both show a wide overlapped range of pressures where high quality and low-quality parts can be found.

For higher values of the pressure, the probability of obtaining high-quality micro-part increases, this relation has been observed in both runner system and in cavity. Similar process behavior was stated by Kuek [12] who observed that better filling up of the cavity generate higher peak pressure in the cavity. Additionally, Tsai *et al*, [17] reported that there is a strong correlation between cavity and runner system pressures and depending on the runner system design and sensor location, both pressure signals can behave similarly to same input variations. Similar results have been observed in present study, where runner and cavity pressures respond in the same way to input parameter variations (Figure 2.5 (a) and (b)) and show analogous pressure histograms regarding part quality levels (Figure 2.8 (a) and (b)).

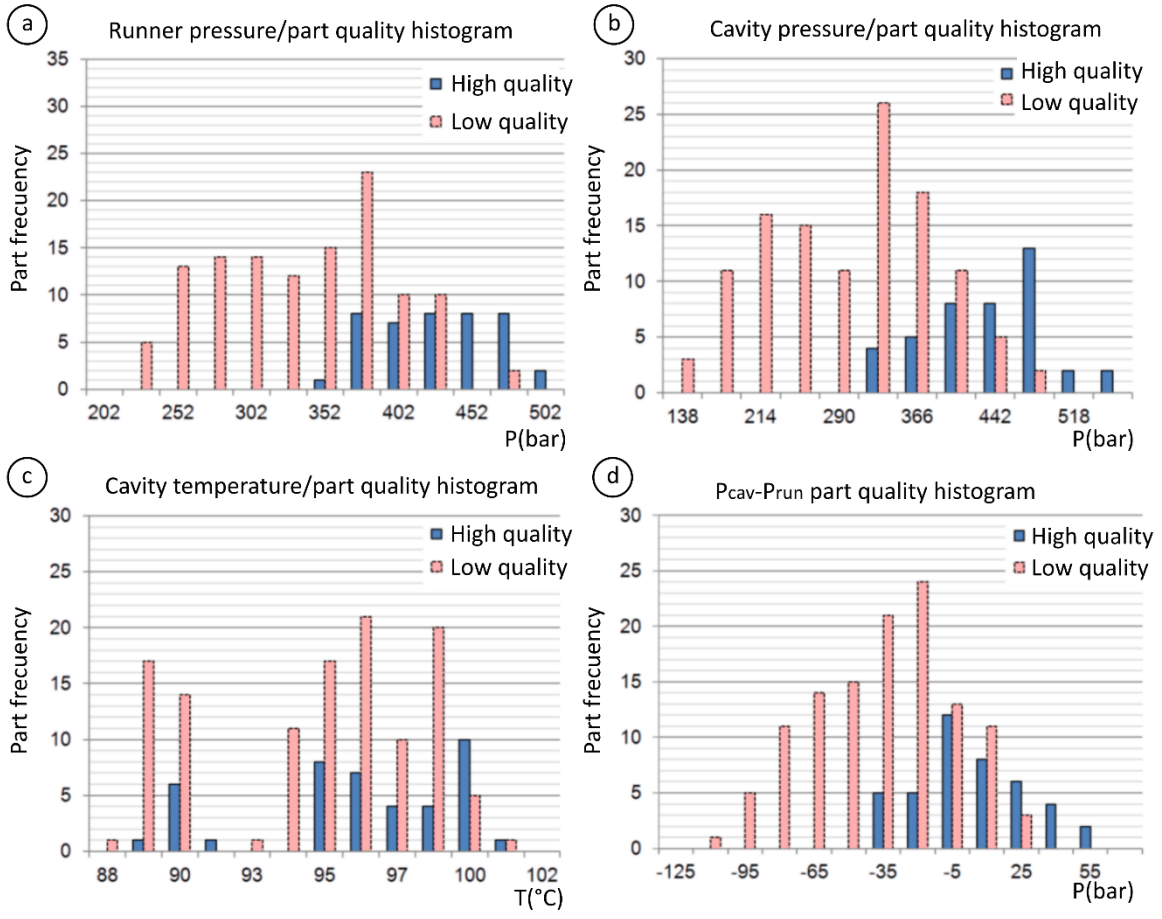

Figure 2.8 Part quality differentiated pressure and temperature frequency histograms.

Low quality parts showing cavity pressures lower than runner pressures, could be correlated to a premature polymer solidification at the gate of the cavity, causing a pressure build up in the runner [10,35]; whereas cavity pressures higher than runner ones, can be explained due to the proper cavity filling and packing while runner melt polymer still flows [17]. It is worth to note that runner and cavity pressure values ratio correlation is mold design dependent, as different runner designs can induce different pressure drops [10].

The use of a pressure and temperature sensor directly arranged into the cavity of the mold, which is an innovative monitoring strategy in micro-molding, has been seen to be more sensitive to input parameter variations than runner pressure sensor (Figure 2.4 and Figure 2.5), however, both pressure monitoring strategies show comparable performance in terms of part quality monitoring and differentiation.

Both pressure/quality histograms (Figure 2.8 (a) and (b)), show similar low to high quality part quantity ratio (65 and 60%) in the overlapped range. The sensors in the cavity and in the runner system provide comparable information and confidence level to determine if a microinjected part is properly injected or not. The use of a cavity pressure sensor, which comprises increased difficulty in micro-mold design and sensor installation, provides same information, in terms of part quality control, the runner system pressure sensor does.

However, the addition of the cavity pressure sensor can be useful to improve process optimization tasks, as it is sensitive to input variations, the sensor in the runner cannot sense. The use of the additional sensor can be used to measure the pressure drop in the gate. The analysis of the pressure difference (ΔP) between cavity and runner, which is a monitoring strategy relatively easy to implement to the process, can provide additional information to detect defective parts or process misbehaviors.

The measured cavity temperature signal seems not to be correlated to the micro-part quality level; the histogram of part distribution shown in Figure 2.8 (c), shows a completely overlapped quality groups along the temperature axis. The measurement of the temperature value inside the cavity as the polymer fills it, seems to be not suitable for evaluating part quality. However, the additional information provided by the temperature sensor can be used to assess and

reduce the cooling cycle and to control the thermal evolution in those cases where those parameters can affect the performance of the injected part [10,37].

2.4 Conclusions

The experiment reported in the present chapter, studies the effects caused by the variation of the input parameters, on pressure and temperature signals in different locations inside the mold, and their linkage to the replication quality level of a micro-featured part, have been studied. The main conclusions of the study are the following:

Both runner and cavity pressure values are strongly related to replication quality level of the micro parts. Higher pressure signal values show higher chance to obtain a properly replicated part. The location of the pressure sensor does not affect the reliability on defective part detection. It has been observed that both sensors, arranged in runner and cavity, show similar performance in terms of micro-part quality level assessment.

The input parameters which cause the most important changes on measured pressure peak values, and therefore on micro-part quality level, are the setting temperatures of the nozzle and fixed part of the mold. Those temperature inputs set the molten polymer temperature and can change its cooling rate, causing variations on the filling up of the cavity.

The sensor arranged inside the cavity, showed higher sensitivity to process variations than the sensor in the runner. Same input variations caused bigger effects in pressure signals inside cavity than in the runner. Cavity sensor has been seen to be able to detect some input variations that were not detected by runner sensor, *e.g.*: changes on metering system setting temperature. The enhanced sensitivity of this sensor arrangement can be used to perform better process monitoring or to improve the setting up of the injection process.

The analysis of the value differences between two pressure sensors, located inside the cavity and in the runner, can be useful to determine the quality level of the micro-injected parts. Most of the low-quality parts obtained in the study, shown runner pressure values greater than cavity ones, whereas high quality parts, shown similar values for cavity and runner pressures, and in some cases, cavity pressures slightly higher than runner ones. The relation between those

pressure values de- pends on the size and design of the molding, and observed results cannot be used to draw conclusions that could be ap- plied to other micro-part design.

The temperature signal measured using the sensor inside the cavity has not shown a clear trend or linkage to the replication quality level of the micro-injected parts. The read temperature values have been seen to be strongly linked to the mold setting temperature inputs, and they seem not to be affected by other process input variations.

2.5 References

[1] Yang C, Yin X-H, Cheng G-M. Microinjection molding of microsystem components: new aspects in improving performance. J Micromechanics Microengineering 2013;23:093001. https://doi.org/10.1088/0960-1317/23/9/093001.

[2] Dimov SS, Gardner D, Loibl H, Anson S, Dessors S, Hast J, et al. Advanced manufacturing of multi material multi functional products towards 2020 and beyond (4M2020). Multi-Material Micro Manuf., 2013, p. 978–81. https://doi.org/10.3850/978-981-07-7247-5.

[3] Heckele M, Schomburg WK. Review on micro molding of thermoplastic polymers. J Micromechanics Microengineering 2004;14:R1–14. https://doi.org/10.1088/0960-1317/14/3/R01.

[4] Sha B, Dimov SS, Griffiths CA, Packianather MS. Investigation of micro-injection moulding: Factors affecting the replication quality. J Mater Process Technol 2007;183:284–96. https://doi.org/10.1016/j.jmatprotec.2006.10.019.

[5] Michaeli W, Opfermann D. Micro Assembly Injection Moulding: Potential Application in Medical Science. In: Dimov SS, Menz W, editors. Multi-Material Micro Manuf., Elsevier; 2005, p. 1–4.

[6] Berry M, Schott N. Process Monitoring and Process Control: An Overview. Appl Plast Eng Handb 2011:359–73. https://doi.org/10.1016/B978-1-4377-3514-7.10020-0.

[7] Tosello G, Lucchetta G, Hansen HN, Gava A. Mechanical properties test and microstructure analysis of polyoxymethylene (POM) micro injection moulded standard parts. Multi-Material Micro Manuf 2009:231–5. https://doi.org/10.1243/17547164C0012009045.

[8] Baldi F, Bongiorno A, Pagano C, Riccò T, Surace R, Tescione F. Process – Property – Structure Relationship in Miniaturized Injection Moulded Polyoxymethylene Samples. Polym Eng Sci 2014. https://doi.org/10.1002/pen.

[9] Uriarte LG, Herrero A, Ivanov A, Oosterling H, Staemmler L, Tang PT, et al. Comparison between microfabrication technologies for metal tooling. Proc Inst Mech Eng Part C J Mech Eng Sci 2006;220:1665–76. https://doi.org/10.1243/09544062JMES220.

[10] Giboz J, Copponnex T, Mélé P. Microinjection molding of thermoplastic polymers: a review. J Micromechanics Microengineering 2007;17:R96–109. https://doi.org/10.1088/0960-1317/17/6/R02.

[11] Chen Z, Turng L-S. A review of current developments in process and quality control for injection molding. Adv Polym Technol 2005;24:165–82. https://doi.org/10.1002/adv.20046.

[12] Kuek S-C. An investigaiton of cavity pressure as process and quality indicator in the micro injection moulding process. Clemson University, 2007.

[13] Chu J, Kamal M. Characterization of the microinjection molding process. Polym Eng Sci 2010:1–12. https://doi.org/10.1002/pen.

[14] Whiteside BR, Martyn M, Coates P. Micromoulding: process evaluation. ANTEC-CONFERENCE 2004:3–7.

[15] Zhao J, Chen G, Juay YK. Development of Process Monitoring Technologies for Polymer Micro Moulding Process 2003:1–6.

[16] Griffiths CA, Dimov SS, Scholz SG, Hirshy H, Tosello G. Process Factors Influence on Cavity Pressure Behavior in Microinjection Moulding. J Manuf Sci Eng 2011;133:031007. https://doi.org/10.1115/1.4003953.

[17] Tsai K-M, Lan J-K. Correlation between runner

pressure and cavity pressure within injection mold. Int J Adv Manuf Technol 2015:14–23. https://doi.org/10.1007/s00170-014-6776-5.

[18] Sha B, Dimov SS, Griffiths CA, Packianather MS. Micro-injection moulding: Factors affecting the achievable aspect ratios. Int J Adv Manuf Technol 2006;33:147–56. https://doi.org/10.1007/s00170-006-0579-2.

[19] Annicchiarico D, Attia UM, Alcock JR. Part mass and shrinkage in micro injection moulding: Statistical based optimisation using multiple quality criteria. Polym Test 2013;32:1079–87. https://doi.org/10.1016/j.polymertesting.2013.06.009.

[20] Mani MR, Surace R, Ferreira P, Segal J, Fassi I, Ratchev S. Process Parameter Effects on Dimensional Accuracy of Micro-Injection Moulded Part. J Micro Nano-Manufacturing 2013;1:031003. https://doi.org/10.1115/1.4025073.

[21] Attia UM, Alcock JR. An evaluation of process-parameter and part-geometry effects on the quality of filling in micro-injection moulding. Microsyst Technol 2009;15:1861–72.

[22] Rodgers JW, Casey ME, Jedlicka SS, Coulter JP. Effect of Micro-Injection Molding Processing Conditions on the Replication and Consistency of a Dense Network of High Aspect Ratio Microstructures. J Micro Nano-Manufacturing 2014;2:011006. https://doi.org/10.1115/1.4026606.

[23] Zhang N, Gilchrist MD. Characterization of microinjection molding process for milligram polymer microparts. Polym Eng Sci 2014;54:1458–70. https://doi.org/10.1002/pen.23677.

[24] Wittmann Battenfeld n.d. http://www.wittmann-group.com/.

[25] BASF n.d. http://iwww.plasticsportal.com/products/products.html.

[26] Uddeholms AB n.d. http://www.uddeholm.com/.

[27] Kistler Holding AG n.d. http://www.kistler.com/.

[28] Attia UM. Micro-injection moulding of three-dimensional integrated microfluidic devices. Cranfield University, 2009.

[29] Guarise M. Filling of micro injection moulded parts: an experimental investigation. 2007.

[30] Bellantone V, Surace R, Trotta G, Fassi I. Replication capability of micro injection moulding process for polymeric parts manufacturing. Int J Adv Manuf Technol 2012;67:1407–21. https://doi.org/10.1007/s00170-012-4577-2.

[31] Prat-Bartés A, Tort-Martorell-Llabrés X, Grima-Cintas P, Pozueta-Fernández L. Métodos estadísticos: control y mejora de la calidad. Univ. Politèc. de Catalunya; 2004.

[32] Zhao J, Mayes RH, Chen G, Xie H, Chan PS. Effects of process parameters on the micro molding process. Polym Eng Sci 2003;43:1542–54. https://doi.org/10.1002/pen.10130.

[33] Montgomery DC. Design and analysis of experiments· 5th ed. John Wiley & Sons; 2001.

[34] Daniel C. Use of Half-Normal Plots in Interpreting Factorial Two-Level Experiments. Technometrics 1959;1:311–41. https://doi.org/10.1080/00401706.1959.10489866.

[35] Griffiths CA, Dimov SS, Scholz SG, Tosello G, Rees A. Influence of Injection and Cavity Pressure on the Demoulding Force in Micro-Injection Moulding. J Manuf Sci Eng 2014;136:031014. https://doi.org/10.1115/1.4026983.

[36] Scilab n.d. http://www.scilab.org/ (accessed August 18, 2015).

[37] Mendoza R. Morphologies induites dans les pièces en polyoléfine moulées par injection 2005.

Chapter 3

High throughput manufacturing of bio-resorbable micro-porous scaffolds made of poly(L-lactide-co-ε-caprolactone) by micro-extrusion for soft tissue engineering applications

3.1 Introduction

Elastomeric bio-resorbable scaffolds are of great interest for soft tissue engineering as they can be synthesized to show proper biocompatibility, low immunogenicity, and a proper resorption rate to degrade into products that can be eliminated from the host's body [1–3]. The performance of those scaffolds can be tailored to provide suitable mechanical properties during tissue healing and regeneration [4–6] fostering the adhesion, proliferation, and differentiation of cells. Another usual requirement for scaffold manufacturing is porosity, which is needed to promote cell migration, nutrient transport, and waste removal through the material, while maintaining adequate mechanical properties. Numerous attempts to produce highly porous scaffolds by several techniques and different materials can be found in the literature [7–9]. Generally, pores of diameter greater than 100 μm are suitable for cell colonization and migration, while smaller diameters are intended to provide favorable physiological liquid and nutrient interchange [10,11].

In this regard, poly(L-lactide-co-ε-caprolactone) (PLCL) arises as a promising material, due to its tailorable mechanical properties, degradation rate [12–17], and its easy processing to manufacture scaffolds in which porosity can be produced and controlled [18–24]. The lactide to caprolactone proportion of the PLCL can be varied to match the aimed tissue properties for different clinical applications [25]. In particular, the PLCL with 70/30 L-lactide/ε-caprolactone proportion enhances the proliferation of Schwann cells and is commonly used for neural guide conduit fabrication for peripheral nerve healing [26–28]. Particle leaching is the most common technique to create porous scaffolds [29–41]. This technique allows to produce scaffolds with well interconnected pores, whose characteristics are controlled by particle proportion, size, and distribution. Some of the advantages of this technique are that non-specialized equipment is needed, and that pore size and porosity can be effectively controlled by varying the size and quantity of leachable particles. The polymeric scaffold is immersed in water to dissolve the porogenerator particles, which generally are salt particles of sodium chloride (NaCl) or other soluble porogenerator such as sucrose or starch [30]. NaCl salt particles, contrary to other

particle materials, show thermal stability in the range of polymer processing temperatures and good resistance to the organic solvents typically used in polymer handling and processing.

Most of the current porous scaffold manufacturing techniques are based on obtaining films [4,34,35] or more complex three-dimensional (3D) geometries (like tubes) [6,18,23] by means of solvent exchange or evaporation, or more novel technologies like 3D printing [42,43] and electrospinning [44], which consist of material deposition. These methods allow to produce a high degree of porosity, up to 90% [4,10,23,32,33,36], and are successfully used to prepare testing samples. However, they show low manufacturing throughput, limitations in size and resolution, and are difficult to implement in industrial processes. For example, Jeong *et al*. [18] used a cylindrical mold where, after introducing a mixture of sieved salt and PLCL solved in chloroform, the lumen of the tube was shaped by means of a home-made tool before a solvent was allowed to evaporate, obtaining a 6 mm outer diameter tube and around 20-mm length. This procedure is like the industrial indirect extrusion, where billets of material are pushed by a ram to obtain the desired profile, but the productivity of this process is limited by the length of the ram and material billet size. On the contrary, extrusion is a high throughput manufacturing method where a polymer is processed to obtain unrestricted-length 3D components characterized by a constant cross section, such as tubes, profiles, and films [37,38]. The micro-extrusion process is focused on the manufacturing of profiles and tubes containing dimensions and features in the sub millimeter range, which can be of great interest for tissue engineering of certain tissues as veins, nerves, and tendons, where long micro-structured scaffolds are usually needed. In addition, the micro extruders, due to their inherent small size, use low amounts of material and show low material residence times, which makes this technique highly appropriate to process thermal sensitive materials, polymers under development, and expensive polymers.

There is very little information regarding the extrusion of bio-resorbable polymers with the objective of manufacturing soft tissue healing scaffolds. For example, Salmoria *et al*. [45] successfully extruded tubes of 1.5 mm in diameter made of polycaprolactone loaded with silver particles, to be used as tubular guides to promote the self-regeneration of injured peripheral nerves. The tubes were not porous, and the flexural moduli of the obtained tubes were over 200 MPa, which is not appropriate for most soft tissues. Other authors extruded the polymer

and the porogenerator to prepare a mixture, which was later processed by other means, to obtain the test samples. Washburn *et al*. [46] used the extruder to blend two immiscible polymers which were later hot pressed to obtain thick films. Further, Etxabide *et al*. [38] extruded fish gelatin mixed with lactose to promote its crosslink to subsequently inject the test samples.

Here, a simple particle leaching method was combined with micro-extrusion processing as a high throughput manufacturing technique to obtain porous bio-resorbable scaffolds made of PLCL. Samples of PLCL containing different salt particle sizes and proportions were micro-extruded to analyze the post leaching residual porogenerator amount, the geometric variation of the porous micro-extruded parts, their mechanical properties, and the polymer ageing. A micro-extruded porous PLCL tube with 400 µm wall thickness was produced in order to investigate the capabilities of this technique to manufacture porous tubes made of an elastomeric biodegradable material as scaffolds for vascular tissue engineering [19,23,24] or implants to promote the healing of tendons [39,40] and nerves [31,41,47].

3.2 Materials and methods

3.2.1 Materials

Purasorb PLC 7015 (PLCL with 70/30 L-lactide/ε-caprolactone proportion copolymer) was supplied by Corbion Purac (Amsterdam, The Netherlands). The melting temperature of the polymer is 107.3–112.4 °C. The polymer was stored in sealed bags in a freezer at −20 °C.

Analysis grade Sodium Chloride (NaCl) salt provided by Scharlab (Barcelona, Spain) was used as porogenerator. The salt was milled in a blender, sieved using 25, 50, and 100 µm mesh sizes, and kept in silica-gel desiccator at room temperature (RT).

3.2.2 Methods

- Sample preparation and characterization

The extrusion of PLCL/NaCl was carried out using a Thermo Scientific Haake Minilab II micro extruder (Waltham, MA, USA). The processing parameters were constant for all the performed extrusions, applying a barrel temperature of 140 °C and a screw rotating speed of 10rpm. Neither cooling nor pulling were used at the outlet during test sample extrusion. Only when extruding the final tube (which was flexible and fragile when warm) was a conveyor belt was placed next to the nozzle to facilitate handling.

Table 3.1 presents a description of the samples, particle sizes, and amount of porogenerator considered for the study, and their identifier numbers. This includes nine different mixtures, comprising the combination of 3 different salt/copolymer proportions (50/50, 60/40 and 70/30 % in weight) and 3 different particle size ranges (0–50 µm, 25–50 µm and 50–100 µm). The outcome of particles smaller than 25 µm was negligible and non-viable for material preparation, therefore, the range including particles smaller than 25 µm (0–50 µm) was obtained mixing 50/50% in weight of 0–25 µm and 25–50 µm sieved salt to guarantee that at least the 50 wt.% of the particles were smaller than 25 µm. Particle size ranges and proportions were defined in preliminary extrusion tests whereby it was found that was not possible either to successfully extrude samples of polymer and NaCl mixtures containing porogenerator proportions higher than 80 wt.% with the defined experimental set. Prior to each extrusion,

Table 3.1 Identifier numbers of the considered porogenerator amounts and particle size ranges. Mixtures containing 50%, 60%, and 70% in weight of salt particles in 0–50 µm, 25–50 µm and 50–100 µm size ranges were prepared.

	Particle size range [µm]		
Amount of porogenerator [%]	00-50	25-50	50-100
70	005070	255070	501070
60	005060	255060	501060
50	005050	255050	501050

copolymer and sieved salt were weighed using a precision analytical balance from Mettler Toledo (Columbus, OH, USA). Subsequently, 14 g of each mixture were mechanically stirred and directly put in the micro-extruder feeder to manufacture 1400 mm length rods of each mixture with section of 1 × 4 mm, which were cut into 100 mm long pieces for handling purposes. The obtained salt/copolymer profiles, were stored in sealed bags in a desiccator at RT. From each mixture, 5 samples of 10 mm length (considering samples from the beginning, middle and ending sections of the extruded rod) were collected and prepared for characterization.

Dimensions of the extruded samples were measured by a 10 µm resolution digital gauge from Mitutoyo (Kawasaki-shi, Japan) and their mass was measured using an analytical balance from Mettler Toledo (Columbus, OH, USA). The samples were later rinsed in 50 mL of deionized water for 5 days to dissolve and leach the salt particles from the extruded rod. The water was refreshed every 24 h. The samples were dimensionally characterized right after the leaching process using the gauge to keep record of dimensional changes. They were dried at RT wrapped in blotter paper for 3 days. Then, the samples were put in a desiccator at RT for at least one week and, once the samples were completely dry, they were dimensionally controlled and weighted. Leached and non-leached samples were cryogenic cut in liquid nitrogen to inspect the breakage surface using scanning electron microscopy (FE-SEM ZEISS ULTRA plus Gemini, Oberkochen, Germany). Pore size was characterized using ImageJ software, measuring the Feret diameter of ellipsoids adjusted to the shape of not less than 50 pores for scaffolds with big particles, and up to 500 pores in the case of scaffolds made with the smallest particles.

- Mechanical Tests

Tensile test samples made of neat PLCL (without porogenerator) were prepared following the method applied by Ugartemendia *et al*. [48]. Porous scaffolds obtained from leached extruded parts were also used as samples for performing mechanical tests. These were performed by means of an Instron Model 3369K2004 (Norwood, MA, USA) applying the following test conditions: RT, 1KN, 5 mm/min, 50 mm clamp distance. Secant modulus was calculated at 2% of elongation.

- Thermal Tests

Thermal analysis of leached and non-leached samples stored in a desiccator at RT for 12 weeks were characterized by differential scanning calorimetry (DSC, Mettler Toledo GC 200 Star System, Columbus, OH, USA), applying a ramp from −60 °C to 180 °C at 20 °C/min.

3.3 Results

3.3.1 Leaching performance

Figure 3.1 (a) shows the differences observed in scaffold weight after the leaching process for the considered three particle size ranges. The weight losses were (42 ± 5%) for samples containing 50 wt.% salt proportion, (55 ± 2%) for samples with a 60 wt.% of salt, and (67 ± 3%) for samples having 70 wt.%. No weight loss differences were attributable to particle size when same salt proportion was considered. Figure 3.1 (b) shows the sample weight loss deviation, which was calculated as the weight loss normalized to the theoretical maximum loss (*i.e.*: 50%, 60% and 70%), showing the percental amount of porogenerator that remained in the leached sample. Samples containing 70 wt.% of salt showed a remnant of around (4 ± 5%), whereas for samples having 60 wt.% and 50% of salt, the remnant slightly increased up to (6 ± 5%) and (13 ± 8%) respectively.

Figure 3.2 shows SEM images of leached samples of each mixture. SEM images of pre and post leached samples are shown in Appendix A Figures A1 to A9. Most of the non-leached samples showed uniform particle distribution with no aggregates and particle sizes inside the expected range for each mixture. Some samples showed the formation of a continuous polymer skin (without presence of particles or pores) on the top and bottom surfaces of the scaffolds. After leaching there were no residual particles, as expected, due to the good leaching efficiency observed in weight loss analysis. Table 3.2 shows pore mean sizes measured by ImageJ in leached scaffolds, showing that the observed values were consistent with the porogenerator particle size used to prepare each scaffold.

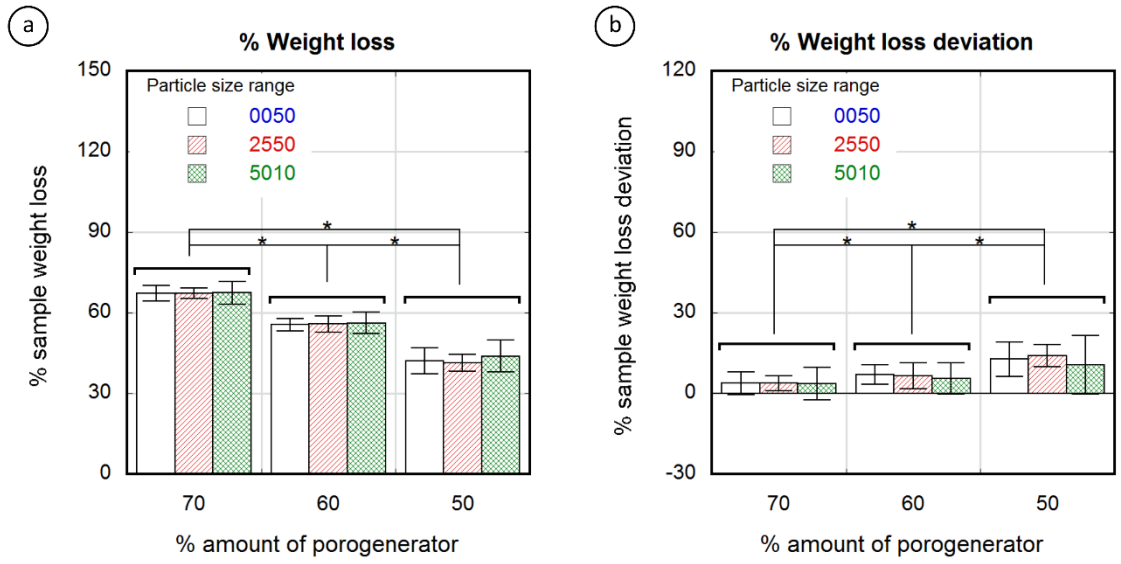

Figure 3.1 Percental weight loss after leaching of samples containing different salt particle sizes (white 0–50 µm, stripe pattern 25–50 µm and cross pattern 50–100 µm) as a function of the theoretical percental amount of porogenerator (a); Percental deviation from theoretical to experimental weight loss of samples containing different particle sizes (white 0–50 µm, stripe pattern 25–50 µm and cross pattern 50–100 µm) as a function of the theoretical percental amount of porogenerator (b). Significance level according to the Student t-test *p<0.05.

Although there was a good correspondence between pore and particle sizes, SEM images show pores with elongated shapes along the scaffold length instead of the expected cube-shaped pores that should be formed after particle leaching.

3.3.2 Dimensional Variations

Figure 3.3 and Figure 3.4 and 4 show the percentage change in scaffold dimensions for wet (Figure 3.3and dry (Figure 3.4) leached samples obtained using different salt weight proportions and particle sizes. The pre-leached samples originally measured 1 × 4 × 10 mm. The dimensional variations of the scaffolds in length, width, and thickness were plotted separately: change in scaffold length and width is shown in Figure 3.3 (a) and Figure 3.4 (a) and change in scaffold thickness is shown in Figure 3.3 (b) and Figure 3.4 (b), for wet and dry samples, respectively. Wet scaffolds showed an isotropic increase in their dimensions (swelling) for all particle sizes and proportions.

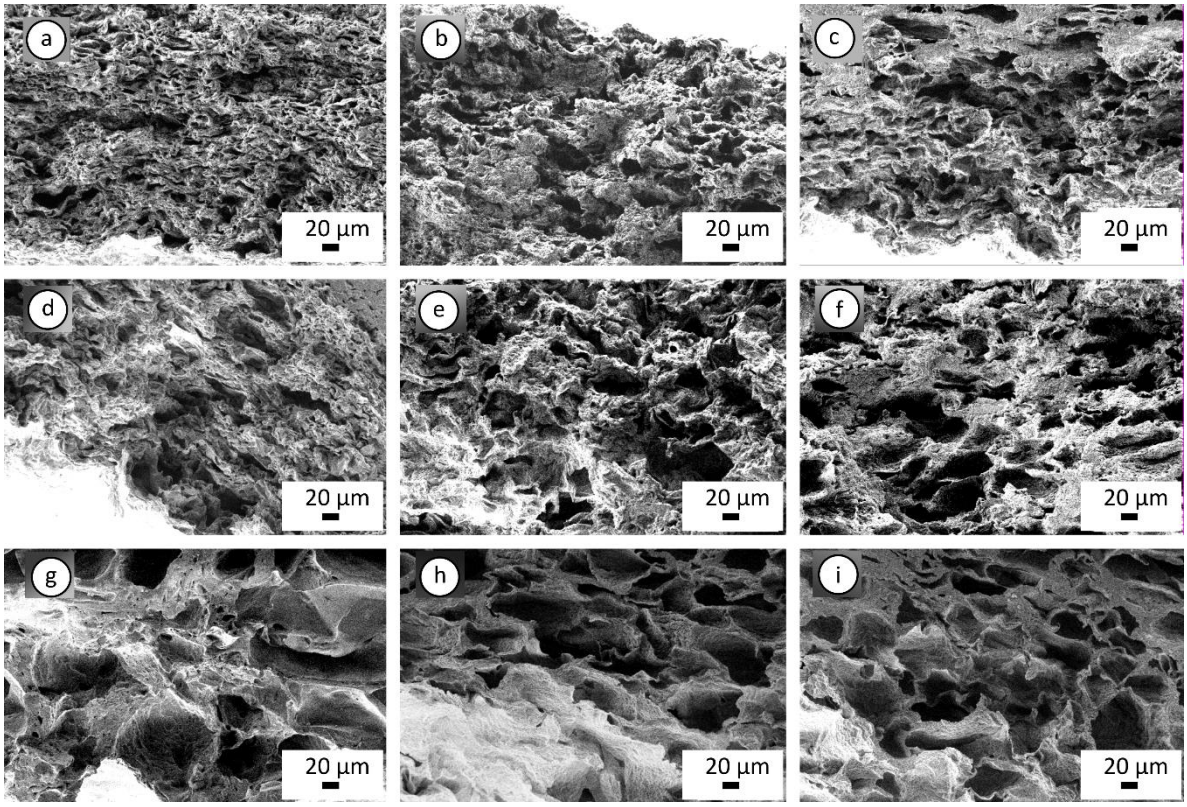

Figure 3.2 SEM images of nine different leached scaffolds arranged by their particle size range (row) and porogenerator weight proportion amount (column). Scaffolds made with particles in 0–50 µm range and proportion of 50 wt.% (a); 60 wt.% (b); and 70 wt.% (c); scaffolds made with particles in 25–50 µm range and proportion of 50 wt.% (d); 60 wt.% (e); 70 wt.% (f); scaffolds made with particles in 50–100 µm range and proportion of 50 wt.% (g); 60 wt.% (h), and 70 wt.% (i).

Table 3.2 Mean values and standard deviation of Feret diameter of ellipsoids adjusted to the pore shapes in leached samples with 50%, 60% and 70 wt.% of pore densities and particle sizes in 0–50, 25–50, and 50–100 µm ranges.

	Particle size range [µm]		
Amount of porogenerator [%]	00-50	25-50	50-100
70	20 ± 10	30 ± 20	50 ± 30
60	20 ± 10	30 ± 20	50 ± 20
50	12 ± 8	20 ± 20	60 ± 40

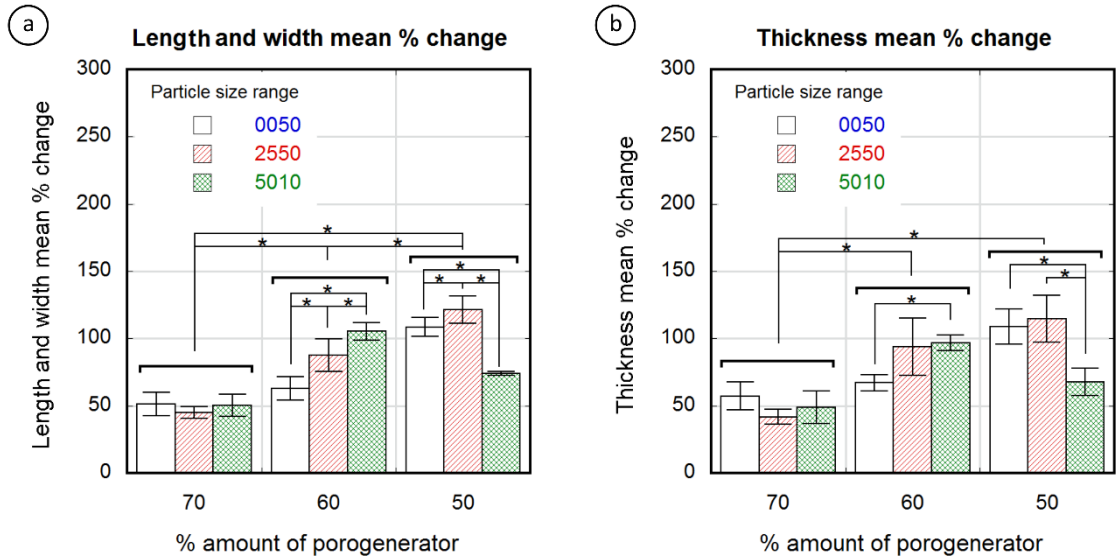

Figure 3.3 Dimensional variation in percental values for wet scaffolds obtained from different particle sizes (white 0–50 µm, stripe pattern 25–50 µm, cross pattern 50–100 µm) and proportions as a function of the theoretical percental amount of porogenerator: Scaffold length and width mean % change (a); scaffold thickness mean % change (b). Significance level according to the Student t-test *p<0.05.

The swelling for the most porous scaffolds produced with 70 wt.% of porogenerator was constant (50 ± 8%) regardless salt particle size, and the lowest compared to scaffolds with lower porosity. However, scaffolds produced with 60 wt.% of porogenerator showed a swelling of (63 ± 9%) for 0–50 µm particle size range, (88 ± 12%) for 25–50 µm particle size range and (105 ± 6%) for 50–100 µm particle size range, revealing an increase of swelling rate with the salt particle size. This did not happen to 50 wt.% samples, which showed an increase in swelling from small to medium particle size ranges ((109 ± 7%) for 0–50 µm and (121 ± 10%) for 25–50 µm), but a decrease for the 50–100µm particle size range (74 ± 1.4%).

Unlike wet scaffolds, dry scaffolds showed an anisotropic change in their dimensions. Scaffolds with highest porosity (70 wt.% porogenerator) showed negligible length and width variation, while less porous scaffolds (50 wt.%) showed a maximal swelling of about (25 ± 9%) with a non-significant dependence on pore size. The change in scaffold thickness was similar and negative (about −30%) for all the measured samples, with no significant differences between scaffolds with different pore sizes and proportions.

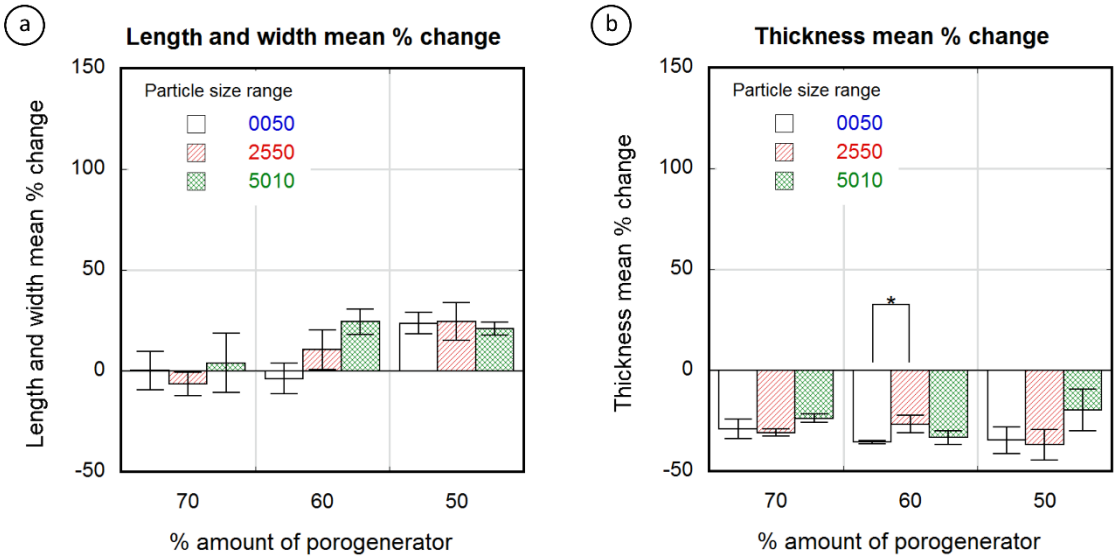

Figure 3.4 Dimensional variation in percentage values for dry scaffolds obtained from different particle sizes (white 0–50 µm, stripe pattern 25–50 µm, cross pattern 50–100 µm) and proportions as a function of the theoretical percental amount of porogenerator: scaffold length and width mean % change (a); scaffold thickness mean % change (b). Significance level according to the Student t-test *p<0.05.

3.3.3 Mechanical Properties

Table 3.3 shows the mechanical properties of porous scaffolds produced using different porogenerator sizes and proportions compared to neat PLCL. Samples containing 70 wt.% and 50 wt.% of particles in the 0–50 µm range showed secant modulus ($E_{2\%}$) values similar and even greater than the neat PLCL ((19 ± 4) and (11.9 ± 0.5) MPa compared to 12 MPa), while the rest of the samples showed lower $E_{2\%}$ values. All the porous samples showed ultimate strengths (σ_u) and elongations at break (ε_u) lower than the neat PLCL (maximums of (8.7 ± 1.5) MPa and (201 ± 9%) compared to 17 MPa and 441%). Values of $E_{2\%}$ and σ_u of samples of the same porosity were observed to decrease with the increase in pore size. Variations from (19 ± 4) to (6 ± 2) MPa, from (8.5 ± 0.6) to (2.8 ± 0.2) MPa and from (11.9 ± 0.5) to (7 ± 4) MPa were observed for values of $E_{2\%}$, and from (8.7 ± 1.5) to (4.7 ± 0.6) MPa, from (7.5 ± 2) to (3.1 ± 0.5) MPa and from (8.5 ± 0.4) to (4.2 ± 0.3) MPa in the case of σ_u values. The ultimate strength was similar for scaffolds with the same pore size but different porosity, indicating no influence of pore density in this mechanical property. The elongation at break (ε_u) did not seem to follow a clear trend with the change in porosity nor dimensions, showing a nearly constant value of about 200%.

Table 3.3 Secant modulus E2% (MPa), ultimate strength σu (MPa) and elongation at break εu (%), measured by tensile tests, of porous scaffolds produced using 50, 60 and 70 wt.% of porogenerator and particle sizes in 0–50, 25–50 and 50–100 µm size ranges, and compared to neat PLCL.

		Material property		
Amount of porogenerator [wt.%]	Sample	$E_{2\%}$ [MPa]	σ_u [MPa]	ε_u [%]
70	005070	19 ± 4	8.7 ± 1.5	187 ± 6
	255070	9.7 ± 1.1	7.2 ± 0.8	218 ± 7
	501070	6 ± 2	4.7 ± 0.6	215 ± 20
60	005060	8.5 ± 0.6	7.5 ± 2	204 ± 3
	255060	6.4 ± 1.4	5.7 ± 1	190 ± 20
	501060	2.8 ± 0.2	3.1 ± 0.5	180 ± 20
50	005050	11.9 ± 0.5	8.5 ± 0.4	201 ± 9
	255050	10 ± 1	6.7 ± 0.8	190 ± 10
	501050	7 ± 4	4.2 ± 0.3	150 ± 30
0	PLCL	12	17	441

3.3.4 Thermal Analysis

Figure 3.5 shows the thermal behavior of leached (a) and non-leached (b) samples aged for 12 weeks at RT, considering different salt weight proportions and particle sizes. Leached samples appeared to be slightly crystalline with a cold crystallization peak (Tc) at 60 °C, melting temperature at Tm= 100 °C, and glass transition temperature at Tg=18.5 °C. All non-leached samples were amorphous, showing a single Tg at 23 °C (TGA (Appendix A Figure A10) and DSC (Appendix A Figures A11 to A28).

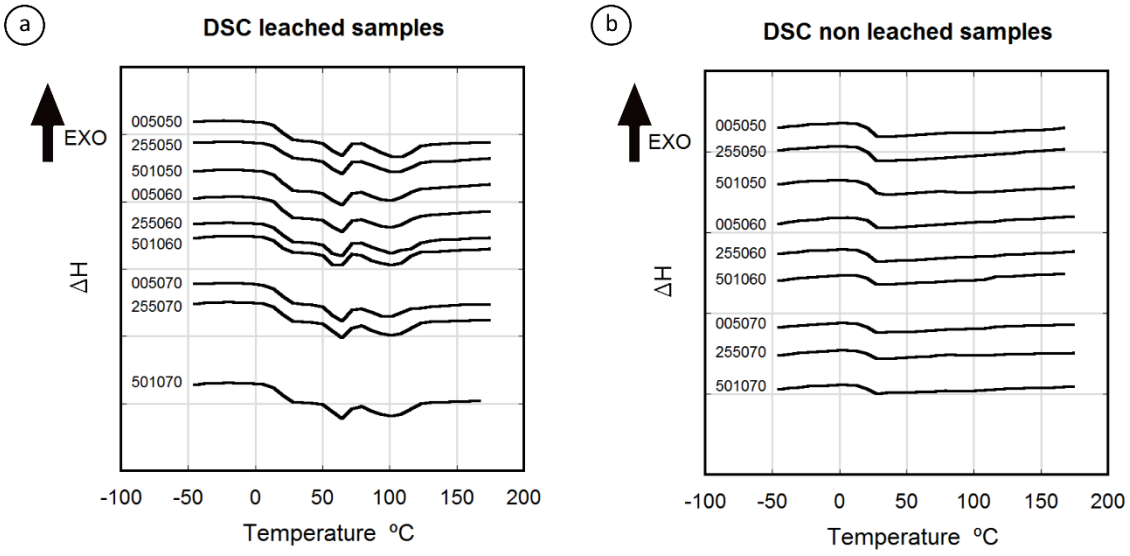

Figure 3.5 Thermograms of leached (a) and non-leached (b) aged samples (12 weeks at RT) produced using different porogenerator proportions and particles sizes (exothermic behavior upwards).

3.4 Discussion

Non-significant differences in weight loss due to different particle sizes were observed, which suggests that the efficiency of the leaching was not dependent on particle size but on initial porogenerator amount. Also, a modest but significant increase in weight loss deviation was observed when decreasing the salt proportion, with a maximum remnant salt value of approximately 13%. Considering the high standard deviation values, the measured remnants were close to that reported for the applied sample preparation method (<4 wt.%) [49] and no noticeable effect can be attributable to the presence of skin effect observed in some of the samples. Samples with low salt proportions contained non-porous copolymer volumes in the matrix where no salt was present (Figure 3.6 (a)), leading to poorly connected salt particles, that eventually remained embedded in the copolymer matrix after the leaching process (Figure 3.6(b)). According to Reignier *et al*. [50] and Hou *et al*. [51], these isolated particles could be more difficult to leach from the polymeric matrix due to the decrease in contact points between particles. Particle volume fraction (ϕ_v) was calculated from the weight fraction (ϕ_w) and particle

and polymeric matrix densities (ρ_p and ρ_m, respectively) (see Equation A1 in Appendix A for detailed information). Due to the difference between the PLCL and the NaCl particle densities (ρ_m = 1.22g/cm3, from Corbion Purac safety data sheet and ρ_p = 2.165g/cm3), there was a noticeable change between volumetric and weight fractions, *e.g.*: for a porogenerator weight proportion of 50 wt.%, the fraction of total volume attributable to leachable particles is around 36 vol.%, which is far from the maximum packing fraction for cubic or even spherical particles (around 64 vol.% [52]). This means that some pores or particles could be not well connected to the porous network [50,51].

Wet porous PLCL scaffolds swelled isotropically and up to 100% for some of the considered pore density and size combinations. The swelling of the scaffolds could be caused either by the polymer matrix absorbing water, despite the low hydrophilicity of the PLCL (with a contact angle of 81°) [53], or by the osmotic pressure, where the polymer matrix acted as a membrane causing water penetration into the scaffold and prevented the free flow of the solution. Low pore density scaffolds showed higher swelling percentages than scaffolds with greater porosities. This could be due to the higher proportion of polymeric material liable to absorb water in those low porosity scaffolds, leading to a greater swelling than in scaffolds with higher porosities. However, scaffolds with the lowest pore density and biggest pore sizes (501050) did not follow this trend. The defects observed in particle distribution inside the polymeric matrix of this scaffold (Figure 3.6(a)) are detrimental to pore interconnectivity, which could cause a more restricted interchange with the leaching media. The non-porous volumes inside the copolymer matrix of this scaffold were in a more restrictive situation to get access to humidity and to freely swell than in the case of a uniform well-interconnected porous structure. Swelling ratios of scaffolds obtained with 50 and 60 wt.% porogenerator amounts were proportional to the particle size, but this did not occur in samples containing 70 wt.% salt. This fact could also be related to the scaffold pore amount and interconnectivity, since for higher proportions of porogenerator, greater homogeneity and pore interconnectivity can be achieved, and less polymeric material is liable to absorb humidity, eventually veiling the effect of particle size. These findings could be of great interest to scaffold design, since high porosities and implantation in wet state (physiological conditions) [31,54] are usually required.

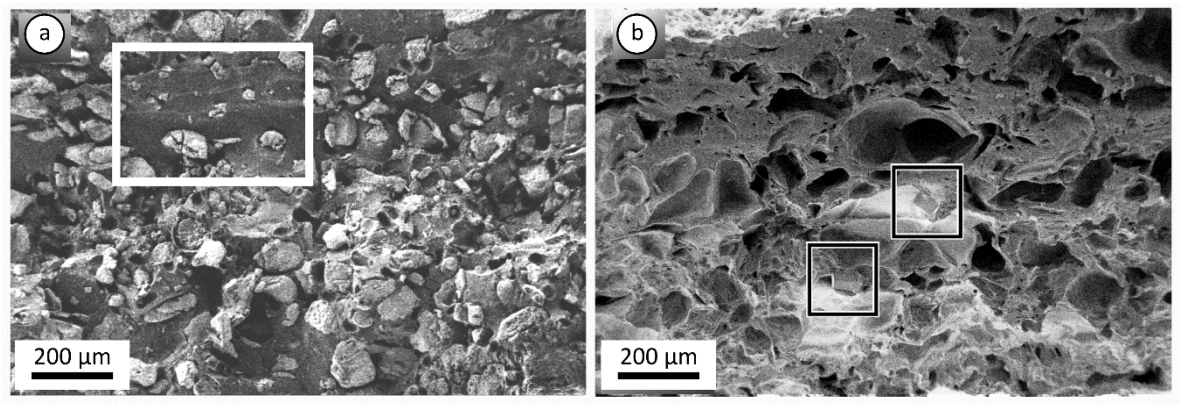

Figure 3.6 SEM images of cross-section surfaces of 501050 non-leached samples (a) and leached samples (b) showing non-porous polymer regions (outlined by a white rectangle in (a)) and remaining salt particles (outlined by squares in (b)).

Strong residual deformation anisotropy was observed in dry scaffolds, which showed length and width variations inversely proportional to their pore density, (as observed in wet conditions), but a negative thickness variation for all the scaffold preparation conditions (around −30%). The scaffolds that did not follow the observed trend in wet conditions (501050), once dry, exhibited similar length and width deformation (maximum of (25 ± 9%)) to scaffolds with different pore sizes but the same pore density (50 wt.%). This could be due to a lower recovery capacity of the deformed material due to the lesser elasticity of the observed non-porous volumes inside the matrix compared to the spongy porous structure. The measured negative thickness variation indicated the occurrence of a collapse during the drying process, which is also noticeable in the shape of the observed pores, which are elongated instead of cubic. The scaffolds were dried by placing them over blotter paper for three days before being put into a desiccator, producing the differential deformation measured in the thickness variation measurement and in the directional pore deformation observed in SEM cross section images of the scaffolds (Figure 3.7).

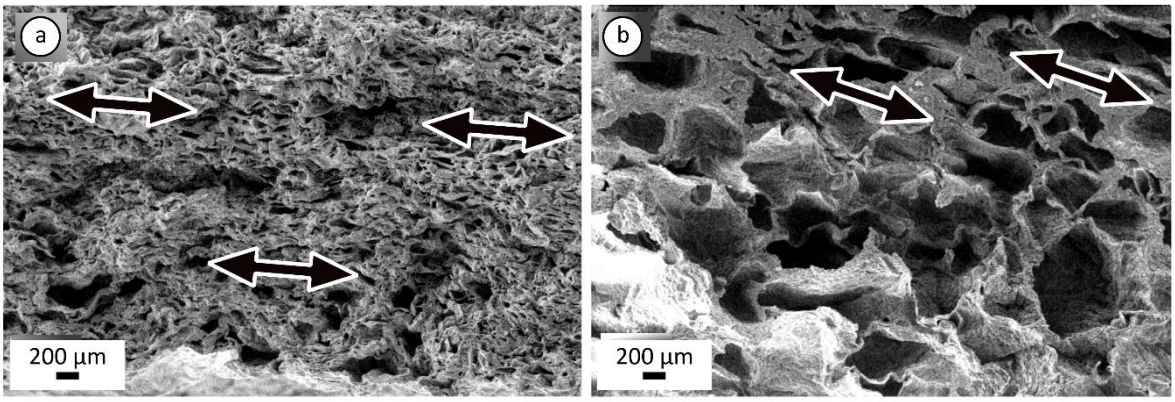

Figure 3.7 SEM images of cross-section surfaces of 005050 (a) and 501070 (b) scaffolds, showing the observed directional pore deformation highlighted by white arrows.

Tensile tests showed that the ultimate strength (σ_u) and elongation (ε_u) values of the porous scaffolds were lower than bulk PLCL, as expected. On the contrary, the secant modulus ($E_{2\%}$) of some scaffolds (005070 and 005050) yielded values comparable and even greater than the bulk material (12 MPa). This effect of material stiffening (increase of $E_{2\%}$ up to 60%) can be related to the manufacturing process, where the polymer was extruded with a remarkable quantity of rigid particles which eventually could cause a stretching and orientation of the material. All the tested scaffolds yielded similar values of elongation at break (ε_u) around 200%, showing no clear trend related to neither porosity nor pore size. Pore size seemed to directly affect the resistance of the samples (in terms of ultimate strength and secant modulus), the samples with smaller pores being more resistant than those having bigger pores. The decrease in σ_u as the pore size increases, (strength loss of 46% for samples with 70 wt.%, 59% for samples with 60 wt.% and 50% for samples with 50 wt.%), could be due to a more heterogeneous structure of scaffolds with bigger pores, which makes them more prone to stress intensification. On the other hand, the ultimate strength of the scaffolds was observed to be independent of pore proportion, opposed to the results stated on literature, where the ultimate tensile strength is strongly dependent on the porosity degree [10,18,20,30,51,55,56], decreasing as the porosity increases. The discrepancy between our findings and the data reported in the literature could be attributable to the porosity rates considered in our study (50, 60 and 70 wt.%), which were lower than those stated in literature (up to 90 wt.%), and to the manufacturing process applied

here, in contrast to currently applied laboratory techniques for film preparation. In addition, it is important to highlight that porous structure deformation and break mechanisms are complex, as reported by Gibson *et al*. [57], who commented on the different and diverse deformation mechanisms a foam can undergo (pore wall bending, pore face bending, collapse of pores, elastic buckling, brittle crushing etc.). Further studies must be carried out to investigate the effect of pores on the mechanical properties of extruded samples, *e.g*.: compressive strength test, fracture toughness test, etc. Nevertheless, from the obtained results it can be inferred that mechanical properties of the obtained porous scaffolds were tailorable and similar to that of human soft tissues (human nerve E: (16 ± 2) MPa, σ_u: (7 ± 0.6) MPa [31]; Skin E: 7.6 MPa, Cartilage E: 3 MPa [58]; Aortic valve E: (15 ± 6) MPa, Cerebral vein E: 7 MPa [59]).

Non-leached samples, aged for at least 12 weeks at RT, showed no crystallinity, being completely amorphous. The presence of NaCl particles seemed to directly affect the mobility and evolution of the PLCL chains, preventing the crystallization of the material. The presence of the particles in the matrix caused a delay in copolymer crystallization, similar to that reported by Wurm *et al*. [60] and Kiersnoswki *et al*. [61], who observed a retard in the crystallization of different polymers (PA6 and poly-ε-caprolactone) due to the presence of inorganic particles. On the contrary, leached samples underwent clear crystallization, revealing the characteristic Tg and crystallization peak of aged PLCL (70% LA 30%CL proportion) [12,35,48,62]. This crystallization behavior corresponds to the crystal form due to the L-lactide building blocks of the copolymer [13,63]. The presence of salt particles in the pre-leached samples and its age delaying effect should be considered for the storage and shelve life strategies of implantable products made by the presented method, as the PLCL evolves to crystalline structure once the salt is removed and could lead to variations in mechanical properties and resorption rates.

PLCL tubes with an inner diameter of 1.5mm, a wall thickness below 500-µm, and a length of 300-mm were extruded, proving the feasibility of the micro-extrusion process to manufacture porous elastomeric biodegradable scaffolds (Figure 3.8). This tube was extruded using NaCl particles of 0–50-µm size with a 70 wt.% proportion. To the best of our knowledge, this study reports for the first time the manufacturing of a microtube made of porous, biocompatible and bio-resorbable PLCL and manufactured by means of a continuous extrusion process. The production of porous tubular scaffolds made of bio-resorbable polymers by means of high

throughput manufacturing techniques can have an important impact in scaffold manufacturing as it allows to produce several meters of product in a few hours. The validation of this kind of industrial production technique for scaffold manufacturing helps to narrow the gap between the laboratory and market, reducing the production costs and improving the repeatability and reliability of the manufactured products. Further experiments regarding in vitro cell culture tests such as cytotoxicity and cell viability assays and/or bio-mechano-reactor tests will be carried out to investigate the use of those micro-extruded scaffolds in soft tissue engineering, mimicking the conditions of the *in-vivo* environment in the final application (cell type, culture media, blood flow conditions, etc.).

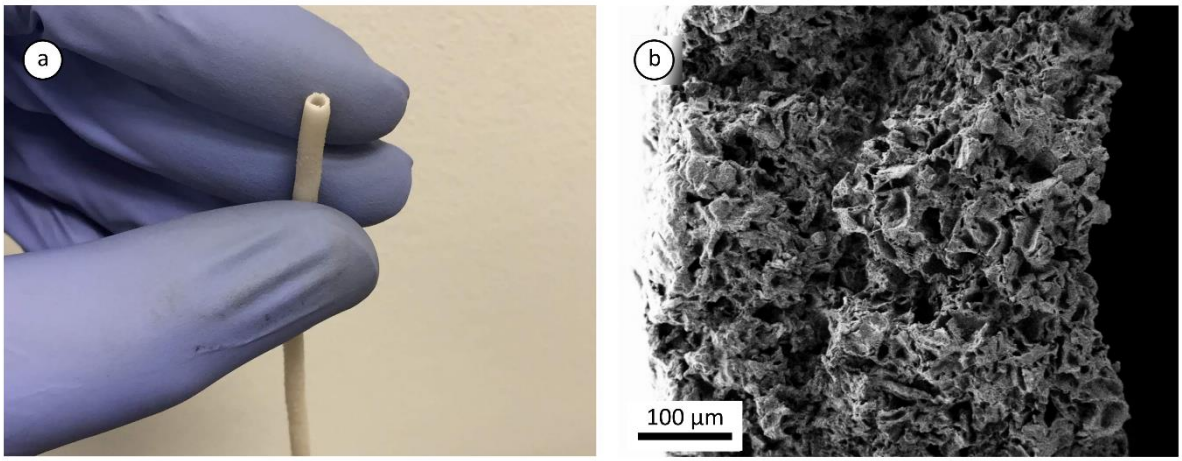

Figure 3.8 Tube with an inner diameter of 1.5-mm, a wall thickness of 400-µm, and a length of 300-mm produced by micro-extrusion (a); SEM image of a section of the tube wall (<500-µm) showing its porous structure (b).

3.5 Conclusions

Porous scaffolds made of medical grade of Poly(L-lactide-co-ε-caprolactone) were manufactured by continuous extrusion using a twin-screw micro extruder. The copolymer was mixed with different proportions and particle sizes of NaCl, extruded, and subsequently leached in distilled water to obtain scaffolds with different porosity degrees and pore sizes. The leaching efficiency improved for higher porosities, being independent on the resultant pore size. Scaffold

swelling was inversely affected by its porosity, *i.e.*: lower porosities swelled more when wet. Once dry, only scaffolds which had highest porosities (70 wt.%) recovered their initial length and width values, while the rest of the scaffolds showed residual deformation. All the tested scaffolds exhibited thickness reduction once dry. Pore size and proportion seemed to influence scaffold mechanical properties, the scaffolds with smallest pores being the most resistant and stiff. More importantly, the secant modulus and ultimate tensile strength of the produced scaffolds were tailorable by varying the pore size and porosity degree, and similar to human soft tissues such as nerves, veins, or skin. This study sets down for the first time the processing of medical grade PLCL by means of continuous extrusion to produce scaffolds with tailorable porosity and mechanical properties. A sub-millimeter walled porous tube up to 300 mm in length was extruded, proving the capability of the micro-extrusion process as a high throughput manufacturing technique for the production of elastomeric biodegradable scaffolds appropriate for the reconstruction and healing of nerves, veins, and other soft tissues.

3.6 References

[1] Siddiqui N, Asawa S, Birru B, Baadhe R, Rao S. PCL-Based Composite Scaffold Matrices for Tissue Engineering Applications. Mol Biotechnol 2018;60:506–32. https://doi.org/10.1007/s12033-018-0084-5.

[2] Gunatillake PA, Adhikari R, Gadegaard N. Biodegradable synthetic polymers for tissue engineering. Eur Cell Mater 2003;5:1–16; discussion 16. https://doi.org/vol005a01 [pii].

[3] Asghari F, Samiei M, Adibkia K, Akbarzadeh A, Davaran S. Biodegradable and biocompatible polymers for tissue engineering application: a review. Artif Cells, Nanomedicine, Biotechnol 2017;45:185–92. https://doi.org/10.3109/21691401.2016.1146731.

[4] Larrañaga A, Diamanti E, Rubio E, Palomares T, Alonso-Varona A, Aldazabal P, et al. A study of the mechanical properties and cytocompatibility of lactide and caprolactone based scaffolds filled with inorganic bioactive particles. Mater Sci Eng C 2014;42:451–60. https://doi.org/10.1016/j.msec.2014.05.061.

[5] Manavitehrani I, Fathi A, Badr H, Daly S, Negahi Shirazi A, Dehghani F. Biomedical Applications of Biodegradable Polyesters. Polymers (Basel) 2016;8:20. https://doi.org/10.3390/polym8010020.

[6] Salerno A, Guarino V, Oliviero O, Ambrosio L, Domingo C. Bio-safe processing of polylactic-co-caprolactone and polylactic acid blends to fabricate fibrous porous scaffolds for in vitro mesenchymal stem cells adhesion and proliferation. Mater Sci Eng C 2016;63:512–21. https://doi.org/10.1016/j.msec.2016.03.018.

[7] Gandolfi MG, Zamparini F, Degli Esposti M, Chiellini F, Fava F, Fabbri P, et al. Highly porous polycaprolactone scaffolds doped with calcium silicate and dicalcium phosphate dihydrate designed for bone regeneration. Mater Sci Eng C 2019;102:341–61. https://doi.org/10.1016/j.msec.2019.04.040.

[8] Cho YS, Hong MW, Quan M, Kim SY, Lee SH, Lee SJ, et al. Assessments for bone regeneration using the polycaprolactone SLUP (salt-leaching using powder) scaffold. J Biomed Mater Res - Part A 2017;105:3432–44. https://doi.org/10.1002/jbm.a.36196.

[9] Peng X-F, Mi H-Y, Jing X, Yu P, Qu J-P, Chen B-Y. Preparation of highly porous interconnected poly(lactic acid) scaffolds based on a novel dynamic elongational flow procedure. Mater Des 2016;101:285–93. https://doi.org/10.1016/j.matdes.2016.03.156.

[10] Kumar A, Nune KC, Murr LE, Misra RDK. Biocompatibility and mechanical behaviour of three-dimensional scaffolds for biomedical devices: process–structure–property paradigm. Int Mater Rev 2016;61:20–45. https://doi.org/10.1080/09506608.2015.1128310.

[11] Lin ST, Kimble L, Bhattacharyya D. Polymer Blends and Composites for Biomedical Applications. In: Li Q, Mai Y-W, editors. Biomeaterials Implant. scaffolds, vol. 8, Berlin, Heidelberg: Springer Berlin Heidelberg; 2017, p. 195–235. https://doi.org/10.1007/978-3-662-53574-5_7.

[12] Fernández J, Etxeberria A, Sarasua J-R. Synthesis, structure and properties of poly(L-lactide-co-ε-caprolactone) statistical copolymers. J Mech Behav Biomed Mater 2012;9:100–12. https://doi.org/10.1016/j.jmbbm.2012.01.003.

[13] Fernández J, Meaurio E, Chaos A, Etxeberria A, Alonso-Varona A, Sarasua J-R. Synthesis and characterization of poly (l-lactide/ε-caprolactone) statistical copolymers with well resolved chain microstructures. Polym (United Kingdom) 2013;54:2621–31. https://doi.org/10.1016/j.polymer.2013.03.009.

[14] Fernández J, Etxeberria A, Ugartemendia JM, Petisco-Ferrero S, Sarasua J-R. Effects of chain microstructures on mechanical behavior and aging of a poly(L-lactide-co-ε-caprolactone) biomedical thermoplastic-elastomer. J Mech Behav Biomed Mater 2012;12:29–38. https://doi.org/10.1016/j.jmbbm.2012.03.008.

[15] Lu XL, Cai W, Gao ZY. Shape-memory behaviors of biodegradable poly(L-lactide-co-ε-caprolactone) copolymers. J Appl Polym Sci 2008;108:1109–15. https://doi.org/10.1002/app.27703.

[16] Jikei M, Takeyama Y, Yamadoi Y, Shinbo N, Matsumoto K, Motokawa M, et al. Synthesis and properties of Poly(L-lactide)-Poly(ε-caprolactone) multiblock copolymers by the self-polycondensation of diblock macromonomers. Polym J 2015;47:657–65. https://doi.org/10.1038/pj.2015.49.

[17] Fernández J, Larrañaga A, Etxeberria A, Wang W, Sarasua J-R. A new generation of poly(lactide/ε-caprolactone) polymeric biomaterials for application in the medical field. J Biomed Mater Res - Part A 2014;102:3573–84. https://doi.org/10.1002/jbm.a.35036.

[18] Jeong SI, Kim SH, Kim YH, Jung Y, Kwon JH, Kim BS, et al. Manufacture of elastic biodegradable PLCL scaffolds for mechano-active vascular tissue engineering. J Biomater Sci Polym Ed 2004;15:645–60. https://doi.org/10.1163/156856204323046906.

[19] Jeong SI, Kwon JH, Lim JI, Cho S-W, Jung Y, Sung WJ, et al. Mechano-active tissue engineering of vascular smooth muscle using pulsatile perfusion bioreactors and elastic PLCL scaffolds. Biomaterials 2005;26:1405–11. https://doi.org/10.1016/j.biomaterials.2004.04.036.

[20] Loh QL, Choong C. Three-Dimensional Scaffolds for Tissue Engineering Applications: Role of Porosity and Pore Size. Tissue Eng Part B Rev 2013;19:485–502. https://doi.org/10.1089/ten.teb.2012.0437.

[21] Mondal D, Griffith M, Venkatraman SS. Polycaprolactone-based biomaterials for tissue engineering and drug delivery: Current scenario and challenges. Int J Polym Mater Polym Biomater 2016;65:255–65. https://doi.org/10.1080/00914037.2015.1103241.

[22] Pangesty AI, Arahira T, Todo M. Development and characterization of hybrid tubular structure of PLCL porous scaffold with hMSCs/ECs cell sheet. J Mater Sci Mater Med 2017;28:165. https://doi.org/10.1007/s10856-017-5985-5.

[23] Jeong SI, Kim B-S, Kang SW, Kwon JH, Lee YM, Kim SH, et al. In vivo biocompatibilty and degradation behavior of elastic poly(l-lactide-co-ε-caprolactone) scaffolds. Biomaterials 2004;25:5939–46. https://doi.org/10.1016/j.biomaterials.2004.01.057.

[24] Sugiura T, Tara S, Nakayama H, Kurobe H, Yi T, Lee YU, et al. Novel Bioresorbable Vascular Graft With Sponge-Type Scaffold as a Small-Diameter Arterial Graft. Ann Thorac Surg 2016;102:720–7. https://doi.org/10.1016/j.athoracsur.2016.01.110.

[25] Sabbatier G, Larrañaga A, Guay-Bégin A-A, Fernandez J, Diéval F, Durand B, et al. Design, Degradation Mechanism and Long-Term Cytotoxicity of Poly(L -lactide) and Poly(Lactide-co-ϵ-Caprolactone) Terpolymer Film and Air-Spun Nanofiber Scaffold. Macromol Biosci 2015;15:1392–410. https://doi.org/10.1002/mabi.201500130.

[26] Kijeńska E, Prabhakaran MP, Swieszkowski W, Kurzydlowski KJ, Ramakrishna S. Interaction of Schwann cells with laminin encapsulated PLCL core–shell nanofibers for nerve tissue engineering. Eur Polym J 2014;50:30–8. https://doi.org/10.1016/j.eurpolymj.2013.10.021.

[27] Sarker M, Naghieh S, McInnes AD, Schreyer DJ, Chen X. Strategic Design and Fabrication of Nerve Guidance Conduits for Peripheral Nerve Regeneration. Biotechnol J 2018;13:1700635. https://doi.org/10.1002/biot.201700635.

[28] Rodriguez FJ, Gomez N, Perego G, Navarro X. Highly permable polylactide-caprolactone nerve guidance enhance peripheral nerve regeneration through long gaps. Biomaterials 1999;20:1489–500.

[29] Jafari M, Paknejad Z, Rad MR, Motamedian SR, Eghbal MJ, Nadjmi N, et al. Polymeric scaffolds in tissue engineering: a literature review. J Biomed Mater Res Part B Appl Biomater 2017;105:431–59. https://doi.org/10.1002/jbm.b.33547.

[30] Hasan SM, Nash LD, Maitland DJ. Porous shape memory polymers: Design and applications. J Polym Sci Part B Polym Phys 2016;54:1300–18. https://doi.org/10.1002/polb.23982.

[31] Chiono V, Tonda-Turo C. Trends in the design of nerve guidance channels in peripheral nerve tissue engineering. Prog Neurobiol 2015;131:87–104. https://doi.org/10.1016/j.pneurobio.2015.06.001.

[32] Li X, Yin HM, Su K, Zheng G Sen, Mao CY, Liu W, et al. Polydopamine-Assisted Anchor of Chitosan onto Porous Composite Scaffolds for Accelerating Bone Regeneration. ACS Biomater Sci Eng 2019;5:2998–3006. https://doi.org/10.1021/acsbiomaterials.9b00209.

[33] Yin HM, Li X, Wang P, Ren Y, Liu W, Xu JZ, et al. Role of HA and BG in engineering poly(ε-caprolactone) porous scaffolds for accelerating cranial bone regeneration. J Biomed Mater Res - Part A 2019;107:654–62. https://doi.org/10.1002/jbm.a.36584.

[34] Hu C, Tercero C, Ikeda S, Nakajima M, Tajima H, Shen Y, et al. Biodegradable porous sheet-like scaffolds for soft-tissue engineering using a combined particulate leaching of salt particles and magnetic sugar particles. J Biosci Bioeng 2013;116:126–31. https://doi.org/10.1016/j.jbiosc.2013.01.011.

[35] Larrañaga A, Aldazabal P, Martin FJ, Sarasua JR. Hydrolytic degradation and bioactivity of lactide and caprolactone based sponge-like scaffolds loaded with bioactive glass particles. Polym Degrad Stab 2014;110:121–8. https://doi.org/10.1016/j.polymdegradstab.2014.08.021.

[36] He Y, Liu W, Guan L, Chen J, Duan L, Jia Z, et al. A 3D-Printed PLCL Scaffold Coated with Collagen Type i and Its Biocompatibility. Biomed Res Int 2018;2018. https://doi.org/10.1155/2018/5147156.

[37] Incarnato L, Di Maio L. Polymeric Extrusion. Wiley Encycl. Compos., Hoboken, NJ, USA: John Wiley & Sons, Inc.; 2012. https://doi.org/10.1002/9781118097298.weoc182.

[38] Etxabide A, de la Caba K, Guerrero P. A novel approach to manufacture porous biocomposites using extrusion and injection moulding. Eur Polym J 2016;82:324–33. https://doi.org/10.1016/j.eurpolymj.2016.04.001.

[39] Wu Y, Wang Z, Fuh JYH, Wong YS, Wang W, Thian ES. Mechanically-enhanced three-dimensional scaffold with anisotropic morphology for tendon regeneration. J Mater Sci Mater Med 2016;27:115. https://doi.org/10.1007/s10856-016-5728-z.

[40] Webb WR, Dale TP, Lomas AJ, Zeng G, Wimpenny I, El Haj AJ, et al. The application of poly(3-hydroxybutyrate-co-3-hydroxyhexanoate) scaffolds for tendon repair in the rat model. Biomaterials 2013;34:6683–94. https://doi.org/10.1016/j.biomaterials.2013.05.041.

[41] Pinho AC, Fonseca AC, Serra AC, Santos JD, Coelho JFJ. Peripheral Nerve Regeneration: Current Status and New Strategies Using Polymeric Materials. Adv Healthc Mater 2016;5:2732–44. https://doi.org/10.1002/adhm.201600236.

[42] Lee S-J, Esworthy T, Stake S, Miao S, Zuo YY, Harris BT, et al. Advances in 3D Bioprinting for Neural Tissue Engineering. Adv Biosyst 2018;2:1700213. https://doi.org/10.1002/adbi.201700213.

[43] Zhang B, Song J. 3D-Printed Biomaterials for Guided Tissue Regeneration. Small Methods 2018;1700306:1700306. https://doi.org/10.1002/smtd.201700306.

[44] Huang L, Zhu L, Shi X, Xia B, Liu Z, Zhu S, et al. A compound scaffold with uniform longitudinally oriented guidance cues and a porous sheath promotes peripheral nerve regeneration in vivo. Acta Biomater 2018;68:223–36. https://doi.org/10.1016/j.actbio.2017.12.010.

[45] Salmoria G V., Paggi RA, Kanis LA. Manufacturing of PCL/SAg tubes by melt-extrusion for nerve regeneration: Structure and mechanical properties. Polym Test 2016;55:160–5. https://doi.org/10.1016/j.polymertesting.2016.08.021.

[46] Washburn NR, Simon CG, Tona A, Elgendy HM, Karim A, Amis EJ. Co-extrusion of biocompatible polymers for scaffolds with co-continuous morphology. J Biomed Mater Res 2002;60:20–9. https://doi.org/10.1002/jbm.10049.

[47] Widmer MS, Gupta PK, Lu L, Meszlenyi RK, Evans GRD, Brandt K, et al. Manufacture of porous biodegradable polymer conduits by an extrusion process for guided tissue regeneration. Biomaterials 1998;19:1945–55. https://doi.org/10.1016/S0142-9612(98)00099-4.

[48] Ugartemendia JM, Muñoz ME, Santamaria A, Sarasua J-R. Supramolecular structure, phase behavior and thermo-rheological properties of a poly (l-lactide-co-ε-caprolactone) statistical copolymer. J Mech Behav Biomed Mater 2015;48:153–63. https://doi.org/10.1016/j.jmbbm.2015.04.007.

[49] Kramschuster A, Turng L-S. An injection molding process for manufacturing highly porous and interconnected biodegradable polymer matrices for use as tissue engineering scaffolds. J Biomed Mater Res - Part B Appl Biomater 2010;92:366–76. https://doi.org/10.1002/jbm.b.31523.

[50] Reignier J, Huneault MA. Preparation of interconnected poly(ε-caprolactone) PCL porous scaffolds by a combination of polymer and salt particulate leaching. Polymer (Guildf) 2006;47:4703–17. https://doi.org/10.1016/j.polymer.2006.04.029.

[51] Hou Q, Grijpma DW, Feijen J. Porous polymeric structures for tissue engineering prepared by a coagulation, compression moulding and salt leaching technique. Biomaterials 2003;24:1937–47. https://doi.org/10.1016/S0142-9612(02)00562-8.

[52] Li S, Zhao J, Lu P, Xie Y. Maximum packing densities of basic 3D objects. Chinese Sci Bull 2010;55:114–9. https://doi.org/10.1007/s11434-009-0650-0.

[53] Lejardi A, López AE, Sarasua J-R, Sleytr UB, Toca-Herrera JL. Making novel bio-interfaces through bacterial protein recrystallization on biocompatible polylactide derivative films. J Chem Phys 2013;139. https://doi.org/10.1063/1.4811778.

[54] Pan Z, Ding J. Poly(lactide-co-glycolide) porous scaffolds for tissue engineering and regenerative medicine. Interface Focus 2012;2:366–77. https://doi.org/10.1098/rsfs.2011.0123.

[55] Guan J, Fujimoto KL, Sacks MS, Wagner WR. Preparation and characterization of highly porous, biodegradable polyurethane scaffolds for soft tissue applications. Biomaterials 2005;26:3961–71. https://doi.org/10.1016/j.biomaterials.2004.10.018.

[56] Odelius K, Plikk P, Albertsson AC. Elastomeric hydrolyzable porous scaffolds: Copolymers of aliphatic polyesters and a polyether-ester. Biomacromolecules 2005;6:2718–25. https://doi.org/10.1021/bm050190b.

[57] Gibson L, Ashby MF. The mechanics of foams : basic results. Cell. Solids Struct. Prop., 1997, p. 175–234. https://doi.org/https://doi.org/10.1017/CBO9781139878326.007.

[58] Park J, Bronzino J. Biomaterials: principles and applications. Boca Raton: CRC Press; 2002.

[59] Chen Q, Liang S, Thouas GA. Elastomeric biomaterials for tissue engineering. Prog Polym Sci 2013;38:584–671. https://doi.org/10.1016/j.progpolymsci.2012.05.003.

[60] Wurm A, Ismail M, Kretzschmar B, Pospiech D, Schick C. Retarded Crystallization in Polyamide/Layered Silicates Nanocomposites caused by an Immobilized Interphase. Macromolecules 2010;43:1480–7. https://doi.org/10.1021/ma902175r.

[61] Kiersnowski A, Kozak M, Jurga S, Pigłowski J. Structure and Crystallization Behaviour of Poly(∈-caprolactone)/Clay Intercalated Nanocomposites. Polym Polym Compos 2004;12:727–37. https://doi.org/10.1177/096739110401200809.

[62] Ugartemendia JM, Larrañaga A, Amestoy H, Sarasua J-R. Supramolecular evolution over an initial period of biodegradation of lactide and caprolactone based medical (co)polyesters. Polym Degrad Stab 2014;108:87–96. https://doi.org/10.1016/j.polymdegradstab.2014.06.004.

[63] Ugartemendia JM, Muñoz ME, Sarasua J-R, Santamaria A. Phase behavior and effects of microstructure on viscoelastic properties of a series of polylactides and polylactide/poly(ε-caprolactone) copolymers. Rheol Acta 2014;53:857–68. https://doi.org/10.1007/s00397-014-0797-8.

Chapter 4

Bio-resorbable and mechanically optimized nerve guidance conduit based on a naturally derived medium chain length polyhydroxyalkanoate and poly(ε-caprolactone) blend

4.1 Introduction

The incidence of trauma cases involving some degree of peripheral nerve injury (PNI) is around fourteen thousand new cases per year in the U.S.A. only, implying that the annual spend in health care to treat such patients can reach nearly $150 Billion [1,2]. Moreover, nerve gap repair remains a significant clinical challenge in terms of functional recovery, which never fully reach the pre-injury level [3]. The peripheral nervous system has an inherent ability to regenerate after injury or damage [4], but in severe PNI cases where the axons and endoneurium have been disrupted, the axons lose the established guidance pathways to regenerate by themselves, and surgical intervention is mandatory. In such cases, direct coaptation of the proximal and distal neve stumps is the preferred treatment method for small discontinuities (< 5 mm). For larger discontinuities (> 10 mm), direct suturing is not possible without incurring tension which affects negatively to nerve regeneration. In such cases, autografting remains the “gold standard” approach today [5–8]. However, the use of autologous nerve is associated with many drawbacks and complications such as a limited source of donor nerves, additional surgical interventions, the sacrifice of a healthy nerve, mismatch of fascicular pattern, size-matching problems, and donor site morbidity [9]. Other approaches such as allografting and xenografting are associated with potential risks such as immune rejection, cross contamination, and other systemic long-term effects [10]. Therefore, surgical alternatives to autografting and allografting remain highly sought after for peripheral nerve repair [1,11].

Different approaches to replace the use of the autograft have been explored [1,5,11,12]. The most practical alternative is based on implantable nerve guide conduits (NGC), which are tubular implantable devices that provide a structural microenvironment, supporting and guiding axons during their growth, while preventing scar tissue from infiltrating the gap. The major advantage of an entubulation technique resides in avoiding most of the drawbacks that the use of autografts present. This includes less surgical trauma, tension-free endoneurial suturing, providing a physical barrier for cellular invasion such as fibroblasts that can initiate fibrosis and scar formation, and facilitating the neurotrophic communication between proximal and distal nerve stumps [13].

To date, various hollow bio-resorbable NGCs have been approved by the US Food and Drug Administration (FDA) for human use [14,15]. These tubular devices include those based on naturally - derived type I collagen: Neuragen™, Neuromatrix™ and Neurawrap™, or those based on synthetic polymers such as Neurotube™ (poly (glycolic acid) (PGA)) or Neurolac™ (poly (D,L-lactide-co-*ε*-caprolactone) (PLCL)) [10]. In the case of collagen-based tubes, limitations related to control mechanical properties during manufacturing, poor water stability and high-production costs are considered main concerns in terms of nerve recovery success and commercial standpoint [16].

For synthetic polymers, mechanical strength can be tuned more easily than in the case of naturally derived materials. However, achieving targeted mechanical and biodegradability properties on NGCs by considering high throughput manufacturing technologies is not straightforward. As an example, commercially available PGA-based tube Neurotube™ showed encouraging statistical results when evaluated in patients with gaps below 30 mm, leading to sufficient functional recovery in the long term [17,18]. However, major limitations of Neurotube™ include the rapid rate of PGA degradation, which may trigger premature failure, as well as its low solubility and potentially acidic degradation product [15]. In the case of Neurolac™ NGC, good clinical reports were obtained for sensory nerve gaps of less than 25 mm, showing a superior behavior in terms of dense axon regeneration in comparison with other commercially available NGCs [19,20]. However, tube rigidity and concerns surrounding the ability of Neurolac™ to be completely resorbed *in-vivo* are behind the complications reported by several authors regarding clinical trials: sensory changes [21], complications in the fixation leading to trauma and/or inflammatory reaction [22,23], swelling and fibrosis as well as concerns about biocompatibility and bio-resorption rate when this commercial solution was modified to generate porosity and tune their mechanical properties [24]. Even though only semi - permeable conduits have been capable of improved regeneration in the clinic, there is currently no consensus on the degree of porosity or size of pores required to guarantee positive outcomes. Similarly, NGCs with thin walls (less than 1 mm) provided longer axons in an *in-vivo* study [25] as well as less neuroma formation linked to the improved elasticity of the device [26] compared to thicker wall NGCs. However, the selection of the appropriate tube dimensions depends mostly on the mechanical properties and porosity of the base polymer

material. Porosity and device geometry (inner diameter and wall thickness) are key parameters to modify in order to tune their mechanical properties, degradation rate and diffusion of nutrients and waste products between inside the conduit and the surrounding tissue.

Until now, none of the commercially available hollow bio-resorbable NGC has demonstrated superior clinical outcomes to an autologous nerve graft. To face this challenge by considering hollow tubular NGCs that can be manufactured by industrially available production technologies, several approaches have been reported in the literature such as the development of porous devices [7,27–29], the use of semi crystalline synthetic poly(*ε*-caprolactone) (PCL) [28,30,31] and the involvement of a new family of aliphatic polyesters: The naturally derived polyhydroxyalkanoates (PHAs) [32,33]. Advances in the biosynthesis of bacterial origin PHA polyesters are attracting general interest for the development of bio-resorbable and highly biocompatible biomaterials with huge potential in a range of different biomedical applications [34–36]. Thus, biocompatibility of neat poly (3-hydroxyoctanoate) (P(3HO)) has been showed to be as good as collagen in terms of cell viability, proliferation and adhesion of neonatal ventricular rat myocytes [37]. A large diversity of PHA monomer units provides materials with a wide range of mechanical properties, from rigid and strong biomaterials to very soft and elastomeric materials [38]. Medium chain length (MCL) PHAs and their copolymers have recently been used to fabricate healthcare-related materials for distinct biomedical applications, including cardiac tissue engineering [37] and peripheral nerve engineering [10,39–41] due to their low crystallinity, low glass transition temperature, low tensile strength and high elongation to break, making them elastomeric/flexible polymers. In addition, they can be commercially produced in large amounts by fermentation processes of both gram-negative and -positive bacteria in carbon-rich environments. More important, PHAs are thermoplastic polyesters liable to be processed by thermoforming techniques such as hot melt extrusion and injection molding [42]. Blends of PHAs and their copolymers have been extensively studied to suit their properties to different therapeutic applications [39,42,43], yet the blending of PHA blended with synthetic origin polymers is scarce. Garcia-Garcia *et al*. [44] and Duarte *et al*. [45] studied the effect of the proportion of PCL in poly (hydroxybutyrate) (P3HB) PCL blends. They observed a decrease in the Young's modulus and in the tensile strength values while the elongation at break and toughness increased notably as the proportion of PCL increased.

Katsumata *et al*. [46] studied P3HB and its copolymer poly (3-hydroxybutyrate-co-3-hydroxyhexanoate) (P(3HB-HHx)) blended with PCL and they observed that proportions of 20 wt% of PCL could increase remarkably the ductility and toughness of the PHA. Constantinides *et al*. [47] reported the *in-vitro* and *in-vivo* results of scaffolds made of MCL-PHA and its blend with 5 wt% PCL showing the potential of the bacterial origing and synthetic polymers blend and the importance of porosity. The PCL is a semi crystalline polyester that can be synthetized by ring opening polymerization, it can be degraded by microorganisms or hydrolytic depolymerization. PCL has previously been used as a biomaterial for the fabrication of approved devices in the repair of injured nerves. It can be easily modified and blended with other polymers to tailor its properties, and obtain desired biological and mechanical responses [34,48–51].

In this research a blend of bacterial origin MCL-PHA poly (3-hydroxyoctanoate-co-3-hydroxydecanoate) (P(3HO-3HD)) and synthetic PCL was developed for the first time to be transformed into a new biomimetic NGC via hot melt extrusion. Mechanical properties, biocompatibility and degradation rate of the new tubular device were tuned to mimic the native nerve tissue performance and match the rate of nerve regeneration or axon re-growth. *In-vitro* assays were conducted to evaluate the influence of the material properties on neuronal and Schwann cell viability, outgrowth and morphology. The influence of material properties, degree of porosity and tube wall thickness on nerve regeneration was examined across 10 mm rat sciatic nerve gap (equivalent to 30 mm gaps in humans [4]) and compared with autografts and Neurolac™-TW (thin wall), the most studied resorbable NGC on the market.

4.2 Materials and methods

4.2.1 Materials synthesis and characterization

Production of P(3HO-3HD) by *Pseudomonas mendocina* CH50 using 20 g/L of glucose was carried out in 15 L bioreactors (Applikon Biotechnology, Tewkesbury, UK). The working volume used in this study was 10 L. Batch fermentation was carried out in two stages. The seed culture was prepared using a single colony of *P. mendocina* CH50 to inoculate sterile nutrient broth. This was incubated for 16 h at 30°C (shaking rate 200 rpm) and used as inoculum (10 %v/v) in the second seed culture in the mineral salt medium (MSM). Second stage seed culture was used to inoculate the final PHA production media [52,53]. Media components were sterilized at 121°C for 15 min, whereas glucose was sterilized at 110°C for 10 minutes. All media components were combined aseptically prior to the inoculation. The culture was grown for 48 h, at 30°C, and 200 rpm. After fermentation, the biomass was isolated by centrifugation and undergone freeze-drying. The biopolymer was extracted from dry biomass in a two-stage Soxhlet extraction. Methanol extraction was used in the first stage to remove impurities soluble in methanol. Extraction of biopolymer from methanol-treated biomass was conducted using chloroform as a PHA solvent. P(3HO-3HD) was isolated by the precipitation of the polymer into chilled methanol.

^{1}H and ^{13}C nuclear magnetic resonance (NMR) and gas chromatography mass spectrometry (GC-MS) were used for the identification of P(3HO-3HD). Bruker Avance III 600 Cryo (Coventry, United Kingdom) equipped with a DCH cryoprobe was used for NMR analysis. GC-MS analysis was conducted using esterified monomers prepared by methanolysis of polymer catalyzed by sulfuric acid in chloroform/methanol mixture (modified from Lageveen *et al*. [54]). GC-MS analysis was carried out using a Varian Chrompack CP-3800 gas chromatograph (Lörrach, Germany) equipped with Elite-5MS capillary column (length: 30 m, I.D: 0.25 mm, Film Thickness: 0.25µm, Temperature Limits: (-60°C) to 325/350°C) (Perkin Elmer, Seer Green, United Kingdom) and Saturn® 2000 GC/MS/MS workstation.

PCL synthesis was achieved through a one-step approach to ring-opening polymerization (ROP) of ε-caprolactone, catalyzed by tin (II) octanoate and using a hydroxy functionalized methoxy

terminated mPEG co-initiator, thus resulting in long chains of PCL connecting to singular mPEG end-groups on one side. After drying in a vacuum oven at 50°C for 2 h, reactants were added to a stainless-steel autoclave in pre-determined amounts and ROP was carried out in bulk at 120°C for at least 24 h in the presence of an inert gas, which is free of oxygen. Magnetic stirring was maintained at 100 rpm throughout. The reaction scheme and structure of the PCL polymer is shown in Appendix B Figure B1.

^{1}H NMR spectroscopy was used for identification of PCL and to confirm a sufficient degree of polymerization in terms of monomer conversion (> 97%). A 300 MHz Bruker NMR (Coventry, United Kingdom) machine was used to obtain the spectra which were analyzed and processed using the MestReC software package and reported in parts per million (ppm) relative to the response of the solvent, Deuterated Chloroform ($CDCl_3$) (7.24 ppm).

Gel Permeation Chromatography (GPC) was used to determine the molecular weight of both PCL and microbially produced PHA. An Agilent triple detector system was used with columns (PLgel 5 µm MIXED-C 300 × 7.5 mm) which were calibrated with polystyrene standards supplied by Agilent Technologies at a concentration of 10 mg/mL. Chloroform (Sigma Aldrich, Arklow, Ireland) was used as the mobile phase with a flow rate of 1.0 $mLmin^{-1}$.

Polymer film samples were tested in dry state using strips of 5 mm width and length of 35-50 mm to examine the mechanical properties of neat materials. Deformation rate was set to 10 mm per minute. The average values for 4 specimens were calculated.

4.2.2 *In-vitro* assays on spin coated films

Polymer films were prepared for *in-vitro* cell culture by spin coating. PCL and P(3HO-3HD) were dissolved in chloroform to produce a 10 wt% solution of each polymer. 100µL of polymer solution was ejected onto a 19 mm^2 glass coverslip and spun using al WS 650 Spin Coater from Laurel (North Walles, USA) at 100 g for 30 seconds under a vacuum and temperature of 25.5 °C. The samples were left to dry before sterilizing with 70% ethanol and washing with phosphate-buffered saline (PBS) before cell culture experiments.

NG108-15 neuronal cells, obtained from the European Collection of Cell Cultures (ECACC), were used between passages 11-20 for experiments on spin coated films. Neuronal cells were grown in Dulbecco's modified Eagle's medium (DMEM) containing 10% fetal calf serum, 1% penicillin / streptomycin, 1% glutamine and 0.5% amphotericin B at 37°C in a humidified atmosphere with 5% CO_2. 40,000 cells were seeded onto films in DMEM containing 10% FCS at 37°C and 5% CO_2 days for 2 days, before switching to serum-free DMEM for a further 5 days.

Rat primary Schwann cells were isolated and cultured by the method described by Kaewkhaw *et al*. [55]. 60,000 rat primary Schwann cells were cultured on polymer films for 6 days in Dulbecco's modified Eagle's medium (DMEM) containing 10% fetal calf serum, 0.01% forskolin (Sigma Aldrich, Madrid, Spain) 1% penicillin / streptomycin, 1% glutamine and 0.5% amphotericin B at 37°C in a humidified atmosphere with 5% CO_2. Culture medium was changed every 2-3 days and cells were used up to passage 7 for experiments.

- Neuronal and Schwann cell viability

Cell viability was assessed using a live/dead assay. Culture medium was removed and replaced with serum-free DMEM, containing 0.001% Syto-9 and 0.0015% propidium iodide (Invitrogen, Carlsbad, USA). Cells were incubated at 37°C and 5% CO_2 for 30 minutes and imaged using an upright Zeiss LSM 510 confocal microscope. An argon ion laser was used to visualize live cells stained with Syto-9 (λ_{ex} = 494 nm / λ_{em} = 515 nm) and a helium-neon laser for dead cells stained with propidium iodide (λ_{ex} = 536 nm / λ_{em} = 617 nm). Three fields of view were imaged per sample and results calculated by cell numbers (live / cells) and by live / dead cells as percentages per polymer sample type.

- Neuronal cell differentiation and Schwann cell phenotype

The samples were washed with PBS, fixed with 3.7% (v/v) paraformaldehyde (PFA) for 20 minutes, permeabilized with 0.1% Triton X-100 for 20 minutes and unreactive binding sites blocked with 3% bovine serum albumin (BSA) in PBS for 30 minutes. NG108-15 neuronal cells were incubated with a mouse anti-β III-tubulin (neurite marker) antibody (1:250) Promega (Chilworth, United Kingdom) and Schwann cells were labelled with a polyclonal rabbit anti-S100β (1:250) from Dako (Glostrup, Denmark) diluted in 1% BSA in PBS and incubated at 4°C for

48 h. After washing with PBS, NG108-15 neuronal cells were labelled with Texas Red-conjugated anti-mouse IgG antibody (1:200 dilution in 1% BSA from Vector Labs, Burlingame, USA) and Schwann cells incubated with a FITC-conjugated secondary anti-rabbit IgG antibody (1:100 dilution in 1% BSA for S100β and p75 staining) for 90 minutes at room temperature. Samples were washed with PBS and incubated with 4,6-diamidino-2-phenylindole dihydrochloride (DAPI) (Sigma Aldrich, Madrid, Spain) (300 nM) for 30 minutes, at room temperature. Samples were imaged with an upright Zeiss LSM 510 confocal microscope, using a helium-neon laser (543 nm) for Texas Red excitation (λ_{ex} = 589 nm / λ_{em} = 615 nm), an argon ion laser (488 nm) for FITC excitation (λ_{ex}= 495 nm / λ_{em} = 521 nm) and a Ti:sapphire laser (800 nm) was used to image DAPI (λ_{ex}= 358 nm / λ_{em} = 461 nm).

- Neurite outgrowth and primary Schwann cell morphology assessment

To determine NG108-15 neuronal cell differentiation, the average neurite outgrowth length and the average number of neurites per neuron, was calculated. Images were analyzed using ImageJ (NIH, Maryland, USA) and neurites were traced using the NeuronJ plugin tracer software from the cell body to the neurite tip [56]. Ninety neurites were measured to determine the average neurite length for each polymer type. Schwann cell morphology was determined by calculating the average Schwann cell length. Using the ruler tool on NIH ImageJ, the cell length was measured from tip to tip [57]. For each condition, 100 primary Schwann cells were measured, and the average Schwann cell length determined for each sample (± SD).

4.2.3 NGC fabrication

- Porogenerator preparation

The porogenerator was prepared by sieving anhydrous D-(+)-glucose (Reagent grade 99.5% purity) provided by Sigma Aldrich (Madrid, Spain). Glucose powder was sieved by means of mechanically shaken stainless-steel wire sieves from CISA (Barcelona, Spain) with pore size between 25 - 50 μm. Sieved glucose was stored in desiccator at room temperature.

- Blend preparation

Polymer blend and glucose particles were premixed using 5 wt% solution of P(3HO-3HD) and PCL mixture (75/25) in chloroform. Required amount of sieved glucose particles were added to the solution in order to obtain 70 wt% of glucose in polymer/glucose mixture. After thorough mixing, the premix was poured in glass trays and solvent was allowed to evaporate at RT. After complete evaporation of the solvent, solidified premix of P(3HO-3HD)/PCL 75/25 with porogenerator was cut into 5×5 mm pieces and kept in a desiccator at RT prior processing.

- Fabrication of neuronal guides

Production of neuronal guides was carried out by hot melt extrusion of the blend with porogenerator into tubular samples, which subsequently were rinsed in deionized water to dissolve the glucose and obtain microporous NGCs. The blend was extruded in a Thermo Scientific HAAKE Minilab II (Waltham, USA), co-rotating conical twin-screw extruder, set at 70 to 80°C range. Various mandrels and die heads were used to obtain different tube wall thicknesses. Extruded tubes of 1.6 mm inner diameter (ID) and wall thicknesses of 0.5 and 0.25 mm were manufactured using a 1.8 mm mandrel, and 2.4 mm and 2.9 mm die-heads respectively. The extruded tube was cooled down using a ring air wipe from Streamtek Corp (Brampton, Canada) and pulled with a controlled variable speed using an in house-built conveyor belt. For leaching the porogenerator, tube portions of 300 mm in length were put in deionized water and kept at RT for 5 days, while water was changed each 24 h. Finally, the tubular porous scaffolds were rinsed and dried for 48 h before being put into a desiccator, ready for sterilization and implantation.

4.2.4 Tube NGC Characterization

- Thermal, mechanical properties and morphology

Thermal analysis of polymers and blend was conducted using differential scanning calorimetry DSC 214 Polyma (Netzsch, Selb, Germany) equipped with Intra-cooler IC70 cooling system. 5 mg

of polymer was heated from -70 to 170°C at a heating rate of 20°C/min. DSC thermograms were analyzed using Proteus 7.0 software (Netzsch). Porogenerator-leached and non-leached samples of the extruded tubes were measured at T_0 (2 weeks after their processing, kept in a desiccator at RT) and at T_1 (aged for 3 months in a desiccator at RT).

Tensile testing was carried out using a 5942 Testing Systems (Instron, Massachusetts, USA) equipped with 500 N load cell at the room temperature. Mechanical properties of the extruded tubes were measured in a wet state adding an incubation step to emulate *in-vivo* environment. Thus, prior to the testing, porogenerator-leached tubular samples were incubated in PBS for 10 minutes whereas samples with porogenerator were incubated in ethanol 70% for 10 minutes to avoid leaching. Tubes of total length around 60 mm were fixed in rubber-coated grips with the separation distance of 44 mm between the grips. Metal mandrels were inserted into the NGCs from both sides to the full gripping length (approximately 8 mm). The area of the tubes was calculated using the Equation B1 shown in Appendix B. Porogenerator-leached porous tubular scaffold sections were inspected using Scanning Electron microscopy (SEM) (FE-SEM ZEISS ULTRA plus Gemini, Oberkochen, Germany), to check the porosity, pore morphology and size. Micro Computerized Tomography (μCT) was performed on a Skyscan 1272 (Bruker, Belgium). The NGC samples were secured vertically by coating the brass platform surface with dental wax and inserting 1 mm of the NGC into dental wax in order to stabilize the sample against toppling during rotation. Hence, long extruded tubular scaffolds were cut in 1.6 mm length for inspection. Samples were scanned without any filters with a voxel size of 9 μm^3 at 50kV/200μA, in 0.70 increments, an exposure time of 303 millisecond (ms) over 360° of the sample. Scanned images were cropped to select only the samples, reconstructed, analyzed, rendered, and visualized with Nrecon (v1.6.9.8 Bruker, Belgium, Feldkamp algorithm), CT analyzer (v 1.14.4.1 Bruker, Belgium), CTvol (v2.2.3.0 Bruker, Belgium) and CTvox (v2.7.0 r990, Bruker, Belgium) respectively. All samples were subject to misalignment compensation and beam hardening correction.

- Cytotoxicity Analysis

The cytotoxicity of the porous scaffold NGC was analyzed following the indirect 3-[4,5-dimethylthiazol-2-yl]-2,5-diphenyl tetrazolium bromide (MTT) assay according to a standard ISO

10993-5 protocol. An L929 mouse fibroblast cell line was used, and cell viability was normalized to cell growth on a negative (inert) control material (high density polyethylene (HDPE)). A positive (toxic) control material (polyvinyl chloride (PVC)) was used in parallel. All samples were sterilized for 1 hour in ethanol 70% before testing. According to the ISO 10993-5, materials are considered cytotoxic when cell viability is reduced to below a 70% threshold.

- Biodegradation Studies

Following an accredited ISO 10993-13 method, samples were sterilized using gamma irradiation (25 kGy). Before start of the degradation assay, the initial weights of the samples were determined using a precision balance after the samples were dried overnight at 37°C in vacuum. Changes in weight were used as a basis for determining the degree of degradation. Samples were fully immersed in closed Falcon tubes in 3% hydrogen peroxide solution (H_2O_2) (described in ISO10993.13-4.1.4.1.3a). To maintain radical concentration, 3% H_2O_2 (0.88M) solution was changed weekly for the entire duration of the experiment (with no metal ions added to catalyze the H_2O_2 degradation) [58]. The final sample weight was measured after 1 and 3 months with n = 4 samples, and, in parallel, a hydrolytic degradation was performed using laboratory grade water with n = 1. Before measuring the final weight, the samples were again dried overnight at 37°C in vacuum.

4.2.5 *In-vivo* characterization of NGC

- Animals

Female Wistar rats (Janvier Labs, Le Genest - Saint Isle, France), aged 12 weeks were used in this experiment. Animals were housed in plastic cages, maintained at standard laboratory conditions at 22°C in a 12 h light/dark cycle and *ad libitum* access to food and water. The experimental procedures were approved by the respective Ethical Committee and followed the rules of the European Communities Council Directive. The Animal Research and well-being committee of National Hospital for Paraplegics in Toledo approved unanimously at the board

meeting that took place on June 13, 2013 the research animal model, assigning it the reference number 106/2013.

- Surgical procedure

All surgical procedures were performed with aseptic operating conditions and under pentobarbital/xylazine anesthesia (40/10 mg/kg i.p. respectively). Autograft, Neurolac™-TW, with 1.5 mm of internal diameter and 0.28 mm of wall thickness, and P(3HO-3HD)/PCL 75/25 NGC in porous and non-porous (with glucose still present) configuration, with two different wall thicknesses (0.5 and 0.25 mm) were tested. Neurolac™-TW tube was introduced in the *in-vivo* characterization because it is a commercial tube derived from PLCL, aiming to improve the high stiffness and low biodegradation rate of PCL. The right sciatic nerve was exposed and cut 6 mm distal to the exit of the gluteal nerve. In the case of the autograft, 10 mm of sciatic nerve was resected, flipped, and sutured back to the remaining stumps with 10-0 epineural sutures. All the tubular scaffolds were sterilized with 70% ethanol for 5 minutes before implantation and washed out with saline solution. Then, 5 mm of sciatic nerve was excised, and 14 mm-length tubular scaffolds were implanted. Proximal and distal stumps were sutured 2 mm inside the tubular devices, creating a 10 mm gap. The tubular scaffolds were filled with sterile physiological saline solution. The muscle plane was sutured with resorbable 5-0 sutures and the skin with 2-0 silk sutures. All animals were treated with amitriptyline (150 mg/L) *ad libitum* in the drinking water for 2 weeks prior to surgery for preventing autotomy [59]. Animals were distributed in the following experimental groups: Autograft (n = 8), Neurolac™-TW (Polyganics Inc. Groningen, Netherlands) (n = 10), P(3HO-3HD)/PCL 500 µm wall thickness leached (n = 8), P(3HO-3HD)/PCL 500 µm wall thickness non-leached (n = 8), P(3HO-3HD)/PCL 250 µm wall thickness leached (n = 8) and P(3HO-3HD)/PCL 250 µm wall thickness non-leached (n = 8). Representative images of the implanted autograft or neural guides assessed in the study are shown in Appendix B Figure B2.

- Electrophysiological analysis

Functional reinnervation of the target muscles (gastrocnemius muscle, tibialis anterior muscle and plantar muscle) was assessed at 60, 90, and 120-days post-injury (dpi). Animals were

anaesthetized with pentobarbital/xylazine anesthesia (40/10 mg/kg i.p.; respectively) and placed on a homoeothermic blanket to maintain their body temperature at 37°C. The sciatic nerve was stimulated with a Grass S88X stimulator (Astro-Med® Inc.) coupled to transcutaneous monopolar electrodes placed in the sciatic notch, by means of single supramaximal electrical pulses of 0.1 ms of duration. The Compound Muscle Action Potential (CMAP) of the target muscles was recorded with a NeuroLog System (Digitimer Ltd., Lauderdale, USA) coupled to a Micro-1401 data acquisition system and the Signal software (Cambridge Electronic Design Ltd., Cambridge, United Kingdom), by means of monopolar needle electrodes placing the active one in the muscle belly and the reference in the 4th toe. Amplitudes of the M-waves were measured using the same software. The contralateral limb of each animal was used as values pre-injury.

- Immunostaining

Four months after injury, animals were euthanized and transcardially perfused with 4% paraformaldehyde (PFA) in PBS. After perfusion, the regenerated nerves were collected and divided in 3 parts. The proximal and distal portions were used for conventional histology (Section 2.5.5). The mid fragment of the regenerated nerves was postfixed in 4% PFA for 4 h and then changed to 30% sucrose in 0.1 M Phosphate buffer (PB) for 3 days. Collected nerves were mounted in OCT frozen medium (Sakura) and cut with a Microm HM506 (Walldorf, Germany) cryostat in 30 µm thick serial cross-sections. Sections were permeabilized with 0.3% Triton in Tris-Buffered Saline (TBS) and incubated overnight in 0.1% Triton-TBS with 1.5% normal goat serum with the following primary antibodies to perform single or double immunofluorescence: i) mouse anti-S100β (1:500, Sigma-Aldrich) to stain Schwann cells; ii) rabbit anti-Neurofilament 200 (1:200, Sigma-Aldrich) to stain myelinated axons; iii) mouse anti-Fibronectin (1:200, Abcam, Cambridge, United Kingdom) to label the extracellular matrix conforming the regenerating nerve. After washes, slides were incubated with the corresponding secondary DyLigth488- or Dylight594-conjugated antibodies (1:200, WAKO Chemicals, Richmond, USA) for 1 h. Finally, sections were sequentially washed in 0.3% Triton-TBS, TBS and TB, incubated for 5 minutes in 4',6-Diamidine-2'-Phenylindole Dihydrochloride (DAPI) (0.1 µg/mL, Sigma-Aldrich) and mounted with Immuno Mount (Thermo Scientific, Waltham, USA). In order to confirm lack of cross reactivity, sections were processed without the corresponding

second primary antibody and used as controls. No non-specific staining was observed. Images were acquired with an Olympus BX61 Motorized Research Microscope (Tokyo, Japan) equipped for epifluorescence and connected to a DP71 (Olympus) digital camera system.

- Histology

The proximal and distal portions of collected nerves were post-fixed in 4% PFA – 3% glutaraldehyde in PBS. Nerves were post-fixed in 2% osmium tetroxide (Sigma) and 10% glucose in PB 0.2 M (1:1) for 90 minutes at RT, washed with distilled water three times and kept overnight at RT. The following day, nerves were dehydrated in ascending series of 50%, 75%, 90% and 100% acetone for 15 minutes in each solution and embedded in Araldite-502 resin (EMS). Embedded nerves were sectioned using an ultramicrotome (Leica EM UC6, Barcelona, Spain) in 1 µm of thickness sections. These sections were stained with toluidine blue and examined under light microscopy. Images were acquired with an Olympus BX61 Motorized Research Microscope coupled to an Olympus DP71 digital camera for the whole nerve at 4×, while sets of images chosen randomly to represent at least the 30% of nerve cross-sectional area were acquired at 60× from mid and distal portions of the regenerated nerves. Measurements of the cross-sectional area, estimation of myelinated fibers and density of myelinated axons were performed using the ImageJ Software.

- Statistical analysis

All data are presented as mean ± SEM. GraphPad (GraphPad Software San Diego, USA) was used to perform the statistical analysis on the collected data. Two-way analysis of variance (ANOVA) with Bonferroni post hoc test was conducted to analyze differences in the electrophysiological data. One-way ANOVA with Bonferroni post hoc test was conducted to analyze differences in the histological data. Data was considered statistically relevant when $p<0.05$.

4.3 Results

4.3.1 Materials and characterization

Generally, most of engineering and processable materials exceed the mechanical properties of peripheral nerves [60]. However, the addition of porosity to the material, besides its biological role, can decrease the strength and stiffness of the material and turn it prone to be used in tissue engineering even though it shows higher mechanical properties in bulk than the tissue. Therefore, the potential material for nerve guidance fabrication should be stronger and stiffer compared with values obtained for peripheral nerves, bearing in mind that its properties can be tuned via addition of porosity for scaffold construction. P(3HO-3HD) is weak, ductile and soft (Table 5.1) and unsuitable for an *in-vivo* implantation due to that it is easily deformed. On the other hand, PCL is an elastomeric synthetic polymer, versatile, produced in large scale, and associated with precise and robust processability [61–63]. However, it is very stiff (Table 5.1) and is often used in load-bearing tissues to enhance stiffness [64]. This property alongside its prolonged degradation time [65] has limited its use for peripheral nerve implants, being only used to ease processability and enhance mechanical properties as combined in blends [44–47]. Following this strategy, a preliminary screening of various blends of P(3HO-3HD) and PCL was conducted to evaluate blend processability and mechanical properties. Blends of P(3HO-3HD)/PCL with 95/5 and 75/25 proportions were prepared and tested (Table 5.1). MCL-PHAs in general and P(3HO-3HD) in particular are slow crystallizing polymers [66], easily deformed and as a result, hot melt extrusion of P(3HO-3HD) is difficult. Blending P(3HO-3HD) with PCL improves processability and robust hot melt extrusion was achieved for blends with PCL content higher than 25 wt.%. For lower wt%, such as 5 wt%, the blend is not stiff enough to be processed by means of hot melt extrusion and its mechanical properties [47] are not suitable to manufacture a porous scaffold that mimics the rat sciatic nerve. When content of PCL exceeded 30 wt.%, PCL started to dominate the mechanical properties of blends resulting in significantly stiffer materials than P(3HO-3HD). Similar behavior was observed by Lizarraga-Valderrama *et al*. [32] for P(3HO)/P(3HB) blends in which the blend showed a remarkable stiffening when the proportion of the stiff component (P3HB) exceeded the 25%.

Table 5.1 Mechanical properties (yield strength (σy), ultimate tensile strength (σu), Young modulus (E), and strain at sample break (εu)) of non-porous films.

Blend	σ_y [MPa]	σ_u [MPa]	E [MPa]	ε_u [%]
P(3HO-3HD)	0.25 ± 0.06	14.3 ± 1.3	8.4 ± 0.4	640 ± 80
PCL	5.9 ± 0.3	10.3 ± 0.4	230 ± 20	15 ± 2
P(3HO-3HD)/PCL 75/25	1.2 ± 0.5	5.9 ± 0.3	110 ± 10	490 ± 40
P(3HO-3HD)/PCL 95/5	-	13.7 ± 1.2	13.7 ± 1.5	620 ± 50
P(3HO-3HD)	0.25 ± 0.06	14.3 ± 1.3	8.4 ± 0.4	640 ± 80

- P(3HO-3HD)

PHA was produced via microbial fermentation using glucose as carbon source. ^{1}H, ^{13}C NMR and GC-MS analysis identified it as a co-polymer of 3-hydroxyoctanoate and 3-hydroxydecanoate, P(3HO-3HD) (Figure B3 and Figure B4 in Appendix B). Microbial synthesis provided consistent batch-to-batch production of P(3HO-3HD) with monomer content approximately 26 and 74 mol% of 3-hydroxyoctanoate and 3-hydroxydecanoate respectively (Figure B5 and Table B1 in Appendix B). Molecular weight (M_w) of P(3HO-3HD) was found to be (370 ± 60) kDa with molar-mass dispersity of (2.6 ± 0.4).

- PCL

For PCL, caprolactone methylenes presented signals around 2.35 and 4.1 ppm while methoxy poly (ethylene glycol) (mPEG) was identified at a chemical shift of 3.6 - 3.65 ppm (Figure B6 in Appendix B). The polymer conversion was calculated based on the integration of CH_2 peaks for the respective polymers and the monomers introduced. Weight average M_w, number average molecular weight (M_n) and molar-mass dispersity data of the synthetized PCL were collected using the refractive index peak height with values <10 mV and were reported as 90.8, 58.0 and 1.56 kDa, respectively (Figure B7 in Appendix B).

- Characterization of neat biomaterials

Mechanical properties of polymeric film samples are summarized in Table 5.1 and in Figure B8 included in Appendix B. P(3HO-3HD) exhibits typical response for elastomeric materials: a short elastic response at small strains transforms into a large strain-hardening region. Such a response

is also characteristic for many biological tissues such as the rat sciatic nerve (average tensile strength (σ_y) of 1.4 to 2.7 MPa and average Young's modulus (E) of 0.58 MPa) [60]. Despite quite high ultimate tensile strength (σ_u around 14 MPa) of P(3HO-3HD), this polymer behaves as extremely soft material with a Young's modulus around 8 MPa and a yielding stress (the onset of plastic deformation) of only 0.25 MPa. The blend of P(3HO-HD) with 5 wt% PCL did not show remarkable variations comparing to the neat P(3HO-3HD), the σ_u maintained around 14 MPa, Young's modulus increased slightly to almost 14 MPa and the elongation showed practically same values as the neat MCL - PHA. By blending this material with 25 wt% PCL, the Young's modulus increased by more than ten times and the yield strength was five times higher compared with neat P(3HO-3HD), making this blend more suitable than neat PCL and P(3HO-3HD) for nerve regeneration. A distinctive yielding behavior was observed for P(3HO-3HD)/PCL 75/25 blend tested as nonporous film. Neat P(3HO-3HD), P(3HO-3HD)/PCL 95/5 and 75/25 blend are highly deformable materials with elongations at break exceeding 400%.

Figure B9 in Appendix B presents the DSC thermograms for individual components of the polymer blend and P(3HO-3HD)/PCL 95/5 and 75/25 blends. Both P(3HO-3HD) and PCL exhibit glass transition and melting event. The DSC instrument used in this study did not allow reliable measurements in the temperature range between (-70°C) and (-60°C). Therefore, glass transition temperature of PCL was not observed but it was determined to be around -60°C by Pintado-Sierra *et al.* [67] for the PCL used in this study. Glass transition temperature of P(3HO-3HD) was observed for both neat copolymer and its blends with PCL in a temperature range between (-45°C) and (-35°C). It appears that for those specific blend compositions the presence of PCL did not change glass transition of P(3HO-3HD) suggesting poor miscibility of two polyesters. Melting of these polymers are observed at very similar temperatures namely P(3HO-3HD) melts between 42°C and 58°C and temperature range for PCL melting is from 60°C to 70°C. As can be seen from Figure B9 in Appendix B, the melting event for the blends gave a complex endothermic peak with quite wide temperature range, from 35°C to 66.2°C Those peaks represent the superimposition of two melting events from the blend components. With melting temperatures of individual polyesters being so close it is impossible to distinguish reliably individual contributions from polymers to the observed melting peak. Enthalpies of melting for samples aged for 7 weeks were (19.3 ± 0.2), (83.8 ± 0.3), (22.5) and (46.1 ± 0.5) J/g for P(3HO-

3HD), PCL, P(3HO-3HD)/PCL 95/5 and P(3HO-3HD)/PCL 75/25 blends respectively. Based on rule of mixtures, the enthalpy of melting for P(3HO-3HD)/PCL 95/5 was 22.5 J/g and for P(3HO-3HD)/PCL 75/25 blend was 35.4 J/g. This calculated value was almost the observed for 95/5 blend and lower than obtained from thermogram for the 75/25 blend.

Because of the observed mechanical properties of P(3HO-3HD)/PCL 95/5 blend, which barely differ from the neat P(3HO-3HD), and its difficulty to be processed by hot melt extrusion, it was decided to discard it and not continue with the *in-vitro* characterization of this particular blend. Additionally, the cytocompatibility behavior of the P(3HO-3HD)/PCL 95/5 blend was reported by Constantinides *et al*. [47].

4.3.2 Suitability of the materials for cell regeneration

- Cell Viability Analysis

NG108-15 neuronal cells were cultured on polymer films to determine the effect of biomaterial type on cell viability. Neuronal cells adhered to all material types, as seen in Appendix B Figure B10 (a-d). Higher numbers of adhered live cells were observed on the PCL film and TCP control, compared to the P(3HO-3HD) and P(3HO-3HD)/PCL 75/25 films. Appendix B Figure B10 (e) confirmed that significantly higher numbers of live cells were observed on the PCL film and TCP control (450 ± 80 and 440 ± 30 cells) compared to the P(3HO-3HD)/PCL 75/25 and P(3HO-3HD) films (430 ± 90 and 300 ± 90 cells). No significant differences were detected between cells when expressed as a percentage of live versus dead cells. All films had a NG108-15 neuronal cell viability higher than 90%.

Primary Schwann cell viability was also assessed on the different biomaterial films (Appendix B Figure B11 (a-d)). Higher numbers of adhered live cells were observed on the PCL, P(3HO-3HD)/PCL 75/25 films and TCP control compared to the P(3HO-3HD) films. This visual observation was further confirmed by quantification of cell number presented in Figure B11 (e) in Appendix B. The P(3HO-3HD)/PCL 75/25, PCL films and TCP control had significantly higher numbers of live cells attached, compared to the P(3HO-3HD) films ((150 ± 30), (185 ± 19) and

(179 ± 17) cells compared to (96 ± 20) cells respectively). When expressed as live versus dead cells, not significant differences were detected between the samples and all films had a primary Schwann cell viability over 90%.

- Neuronal Cell Differentiation

The NG105-18 cells are a hybridoma (Sendai virus mediated fusion of a mouse neuroblastoma and rat glioma cells) with potential to form neurites. They are commonly used to determine experimental differentiation in this context. NG108-15 neuronal cells were stained for βIII-tubulin (neurite visualization) and DAPI (cell nuclei) after 6 days in culture medium on the different polymer films. All materials supported NG108-15 neuronal cell attachment and neurite outgrowth, as seen in the representative confocal micrographs (Figure 5.1 (a-d)). Confocal micrographs were quantified to confirm that all the different material films supported neuronal cell differentiation and cell maturation. Experimental NG108-15 neuronal cell differentiation can be confirmed by measuring the average number of neurites per neuronal cell cultured on a material, as well as the average neurite length of neurites outgrown. Though no significant differences were detected, Figure 5.1 (i) showed that neurite outgrowth per neuronal cell was higher on P(3HO-3HD) and P(3HO-3HD)/PCL 75/25 films compared to the PCL films and TCP control ((1.67 ± 0.15) and (1.52 ± 0.18) neurites per neuronal cell compared to (1.41 ± 0.33) and (1.33 ± 0.18) neurites per neuronal cell respectively). This indicated that all materials support NG108-15 neuronal cell neurite outgrowth, and that it was preferable on P(3HO-3HD) and P(3HO-3HD)/PCL 75/25 films.

The average length of NG108-15 neuronal cell neurites, cultured on the different materials, was determined (Figure 5.1(j)). The longest average neurite length was measured on the P(3HO-3HD)/PCL 75/25 films, followed by the P(3HO-3HD) films (38 ± 5 μm and 33.0 ± 7 μm). The average length of neurites on the P(3HO-3HD)/PCL 75/25 films was significantly longer than the neurites cultured on the TCP control (23 ± 5 μm). However, no significant differences were detected between the different materials. This indicated that the P(3HO-3HD)/PCL 75/25 and P(3HO-3HD) supported NG108-15 neuronal cell differentiation and promoted maturation more efficiently than the PCL films.

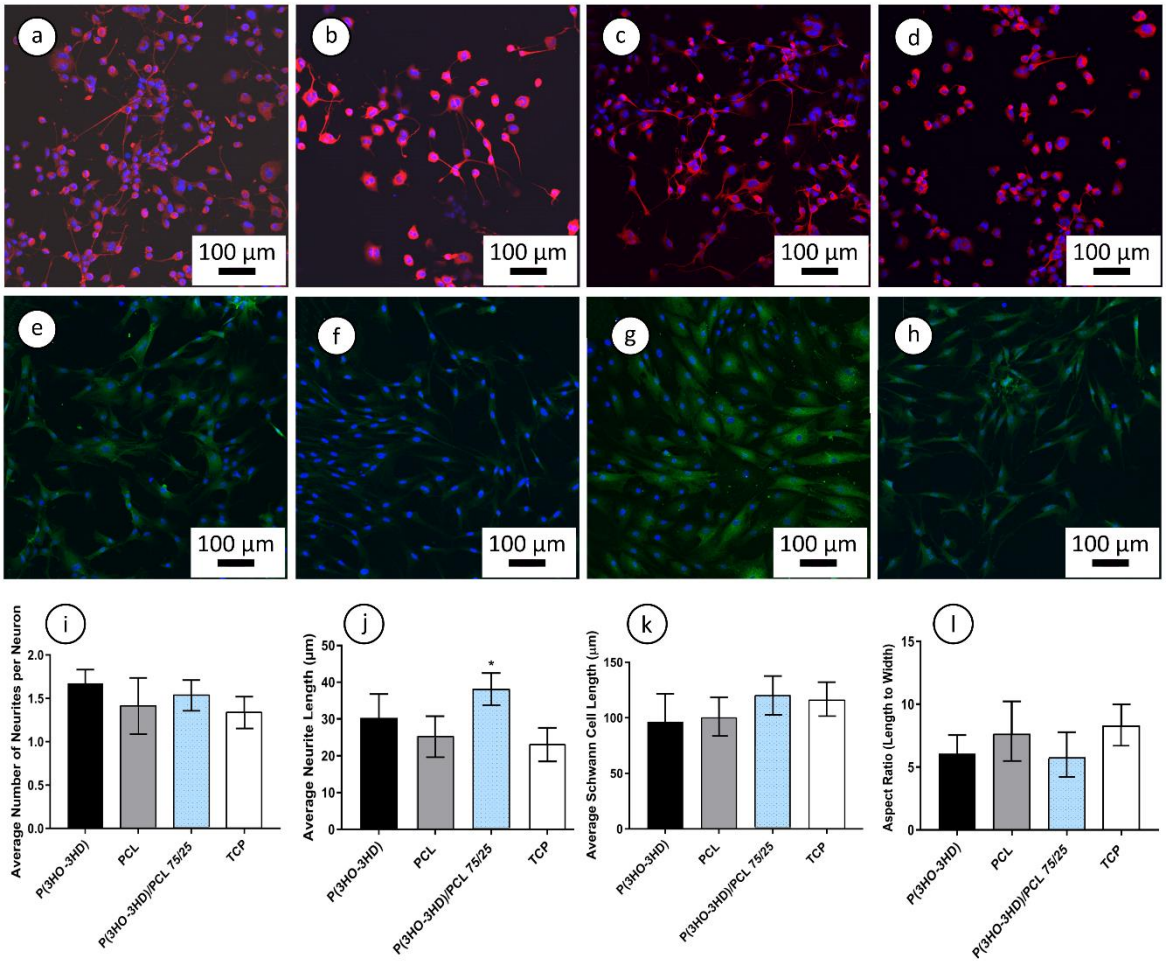

Figure 5.1 Confocal microscopy images of NG108-15 neuronal cells immunolabelled for βIII-tubulin and DAPI on P(3HO-3HD) (a), PCL (b), P(3HO-3HD)/PCL 75/25 (c) films and TCP control (d) (Scale bar = 100 µm). Confocal micrographs of primary Schwann cells immunolabelled for S100β (green) after 6 days of culture on P(3HO-3HD) (e), PCL (f), P(3HO-3HD)/PCL 75/25 (g) films and TCP control (h) (Scale bar = 100 µm). The average number of neurites expressed per neuron (i) (mean ± SD, n=3) and the average neurite length per condition after 6 days in culture (j). The average Schwann cell length (k) and aspect ratio (length/width) (l) were identified to confirm Schwann cell phenotype (mean ± SD, n=3 independent experiments) (mean ± SD, n=3 *p<0.05 against TCP).

- Primary Schwann Cell Phenotype

To confirm a mature phenotype, rat primary Schwann cells were cultured on the different biomaterial films for 7 days and stained with S100β (Schwann cell marker). Figure 5.1 (e-h) showed that all surfaces supported Schwann cell adhesion and positive staining for S100β. Higher numbers of adhered Schwann cells were observed on the P(3HO-3HD)/PCL 75/25 films compared to the other materials. To confirm a maintained phenotype during culture, the average Schwann cell length on each material was determined. Although no significant

differences were detected between the biomaterials, Figure 5.1 (k) indicated a higher average Schwann cell length of Schwann cells cultured on the P(3HO-3HD)/PCL 75/25 films (120 ± 20 µm) compared to the other materials. All the different biomaterials supported Schwann cell attachment, spreading and growth during culture.

The aspect ratio of primary Schwann cells, cultured on the different polymer films and blends, were calculated to determine cell morphology. No statistical differences were detected between substrates. Aspect ratios for the P(3HO-3HD), PCL, P(3HO-3HD)/PCL 75/25 films and TCP control were reported as (6.07 ± 1.48), (7.60 ± 2.63), (5.78 ± 1.99) and (8.22 ± 1.76) respectively. All substrates supported primary Schwann cell adhesion, proliferation and maintained Schwann cell phenotype in culture.

4.3.3 NGC fabrication and characterization

Tubular scaffolds with two different wall thicknesses (0.480 ± 0.020 mm and 0.275 ± 0.025 mm, referenced as P(3HO-3HD)/PCL 500 µm and P(3HO-3HD)/PCL 250 µm, respectively) were produced via hot melt extrusion technique. Optical images of the transversal section of the leached/non-leached thin and thick tubes are showed in Appendix B Figure B12. Figure 5.2 (a) shows a SEM image of a cross section of the porogenerator leached tubular scaffold referenced as P(3HO-3HD)/PCL 250 µm. It is worth to note that removal of glucose (porogenerator) resulted in porous structures with a regular distribution, forming a sponge like structure with pore sizes in the range of 25 to 50 µm. Porogenerator content was around 70% in weight, which corresponded to volumetric porosity around 65% (calculated using the method described by Mendibil *et al*. [68]). This porous structure was further confirmed by µCT, as presented in Figure 5.2 (b) and it is compared with a non-leached tube in Figure B13 in Appendix B, where homogenic distribution of glucose and the polymeric matrix, without remarkable pores nor clumps, can be observed.

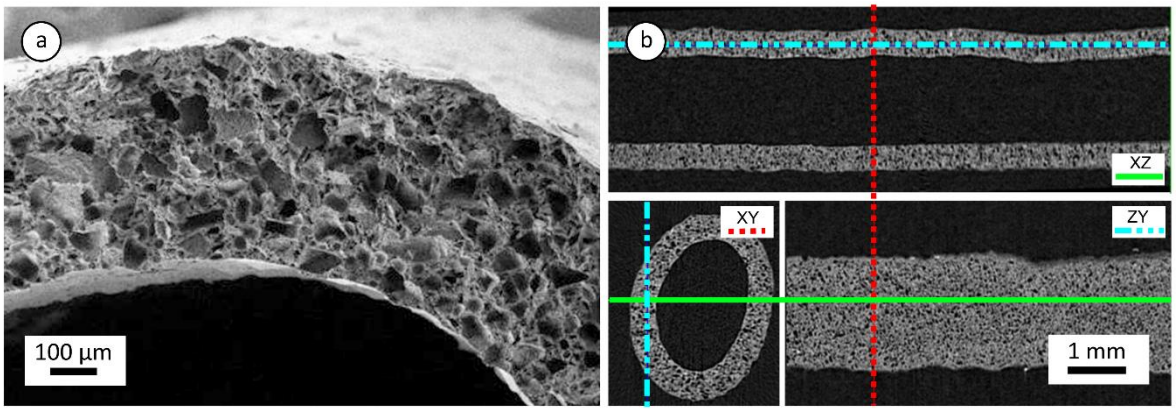

Figure 5.2 SEM image of a cross section of the porogenerator leached NGC referenced as P(3HO-3HD)/PCL 250 µm, showing homogeneous pore distribution through the tube wall (a); µCT images showing several tube sections (b) showing uniform porosity and absence of dense (glucose) particles after the leaching process.

Figure B14 and Figure B15 in Appendix B show the transversal section of leached and non-leached tubes as observed by SEM. Appendix B Figure B16 shows a high magnification SEM image of section of leached tube suggesting a high density of interconnected pores. This fact is also supported by the observation that the leaching of the tube is produced almost immediately (data no showed).

- Mechanical characterization of porous tubular scaffold

Taking into account the superior performance of P(3HO-3HD)/PCL 75/25 in terms of processability and cell regeneration capability (Figure 5.1), mechanical properties of tubular samples were measured and registered in Table 5.2 and Figure B17 in Appendix B. It is worth nothing that in those characterizations thin wall (250 µm) P(3HO-HD)/PCL 75/25 tubes were used and for the calculation, the total cross-sectional area of the tubular sample was used without taking into consideration the porosity of the material in order to characterize the properties of the porous NGC, which are dependent on the material properties, porosity degree and tube geometry. Therefore, the values of tensile strength, elongation and Young's modulus are not comparable to the values obtained for non-porous films. According to Table 5.2, without porogenerator leaching, the P(3HO-3HD)/PCL75/25 +70 wt% glucose tubes were stiff, and brittle as characterized by their high Young's moduli and very low elongation at break values.

Table 5.2 Mechanical properties (yield strength (σy), ultimate tensile strength (σu), Young's modulus (E), and strain at sample break (εu)) of porogenerator leached and non - leached P(3HO-3HD)/PCL 75/25 NGCs in dry and wet conditions.

Blend NGCs	σ_y [MPa]	σ_u [MPa]	E [MPa]	ε_u [%]
P(3HO-3HD)/PCL 75/25 Leached, dry	0.6 ± 0.15	2.06 ± 0.06	2.3 ± 0.7	200 ± 85
P(3HO-3HD)/PCL 75/25 Leached, wet	0.45 ± 0.12	2.07 ± 0.14	3.0 ± 0.6	140 ± 20
P(3HO-3HD)/PCL 75/25 Non-leached, wet	0.7 ± 0.08	2.1 ± 0.7	220 ± 50	3.2 ± 0.8

However, when glucose is removed the resultant porous tubes are highly elastomeric with elongation at break values around 200 and 140% for dry and wet tubes respectively. The yield strength obtained for these porous tubes was more than two times higher than the one obtained for neat P(3HO-3HD) (Table 5.1). Young's modulus and tensile strength values were lower than the ones registered in Table 5.1 for the rest of neat materials analyzed and closer to the native rat sciatic nerve.

- Cytocompatibility and Biodegradation Analysis

Results corresponding to the cytocompatibility assays are presented in Table 5.3, which show that porogenerator non-leached P(3HO-3HD)/PCL 75/25 is considered non-cytotoxic.

Regarding biodegradability assays, Table 5.4 shows the weight loss for both leached and non-leached 500 µm wall thickness P(3HO-3HD)/PCL 75/25 tubular samples over time at 1- and 3-months' period in an oxidative environment. The main weight loss is attributed to the glucose leaching while a mass loss of around 13% is attributed to the polymer degradation at month 3.

Table 5.3 Cytotoxicity assay of P(3HO-3HD)/PCL 75/25 biomaterial and positive control (PVC). Percentage of fibroblast cell viability after 24 hours in culture with conditioned medium is showed. The data showed correspond to the non-leached 500 µm thick wall tubes. Results were normalized to negative control while high density polyethylene. Polyvinyl chloride (PVC) was used as positive control.

Material	% Cell viability (relative to control)
P(3HO-3HD)/PCL 75/25	73±11
Ctrl+	32±6

Table 5.4 Biodegradation study showing the 500 µm thick wall tube's weight loss over time as cultured in a 3% hydrogen peroxide solution. Leached and non-leached tubes' data are showed.

	Sample Mass for tubes [mg]	
Material	Non leached	Leached
P(3HO-3HD)/PCL 75/25	142 ± 18	43 ± 5
P(3HO-3HD)/PCL 75/25 (1 Month)	42 ± 6	41 ± 2
P(3HO-3HD)/PCL 75/25 (3 Month)	37 ± 5	37 ± 3

- Thermal characterization of NGCs

Figure B18 in Appendix B presents thermograms of extruded P(3HO-3HD)/PCL 75/25 tubular samples both porogenerator leached and non-leached at two different ageing stages. The thermograms of extruded tubes are in concordance with results obtained for the solvent cast films. Thermal events (glass transition, melting) which characterize polymers are less prominent in non-leached sample. This is a result of masking from larger scaling required for an additional peak that appeared at 160°C. This peak corresponds to glucose melting which mass fraction (70%) is larger than matrix polymers, which completely disappeared in the leached tubes. The superimposed melting peak, and glass transition for P(3HO-3HD/PCL 75/25 tubes observed between 35 to 65°C and (-45°C) to (-35°C) respectively are in line with results for the solvent-cast blend film. Enthalpy of the polymer melting decreased to (40 ± 5) J/g for the extruded leached tubes compared with (46,1 ± 0.5) J/g for the solvent cast films. This difference might be caused by shorter storage time of the tubes before measurements. Apparent enthalpy of polymer melting for the non-leached was (12.09 ± 0.01) J/g. This corresponded to 40.3 J/g normalized to 0.3 mass fraction of polymer. It appears that the presence of glucose did not affect crystallization of matrix polymer during the storage of non-leached samples.

4.3.4 *In-vivo* results

- Functional recovery

Electrophysiological tests were performed to analyze functional recovery of animals after injury and repair (Figure 5.3, and Appendix B Table B2). Nerve conduction tests performed 7 days post intervention (dpi) demonstrated complete denervation of targeted muscles (gastrocnemius, tibialis anterior and plantar interosseous muscles). At 60 dpi, all autograft-repaired rats showed positive responses and compound muscle action potentials (CMAPs) of gastrocnemius, tibialis anterior and plantar muscles were recorded. This percentage was smaller in tubular-repaired groups. Evidence of reinnervation of gastrocnemius and tibialis anterior muscles was found in 7/10 of Neurolac™-TW repaired animals, 7/8 of P(3HO-3HD)/PCL 500 µm leached (L), 7/8 of P(3HO-3HD)/PCL 500 µm non-leached (NL), 3/8 P(3HO-3HD)/PCL 250 µm leached (L) and 6/8 P(3HO-3HD)/PCL 250 µm non-leached (NL). However,these signals were lower in amplitude and

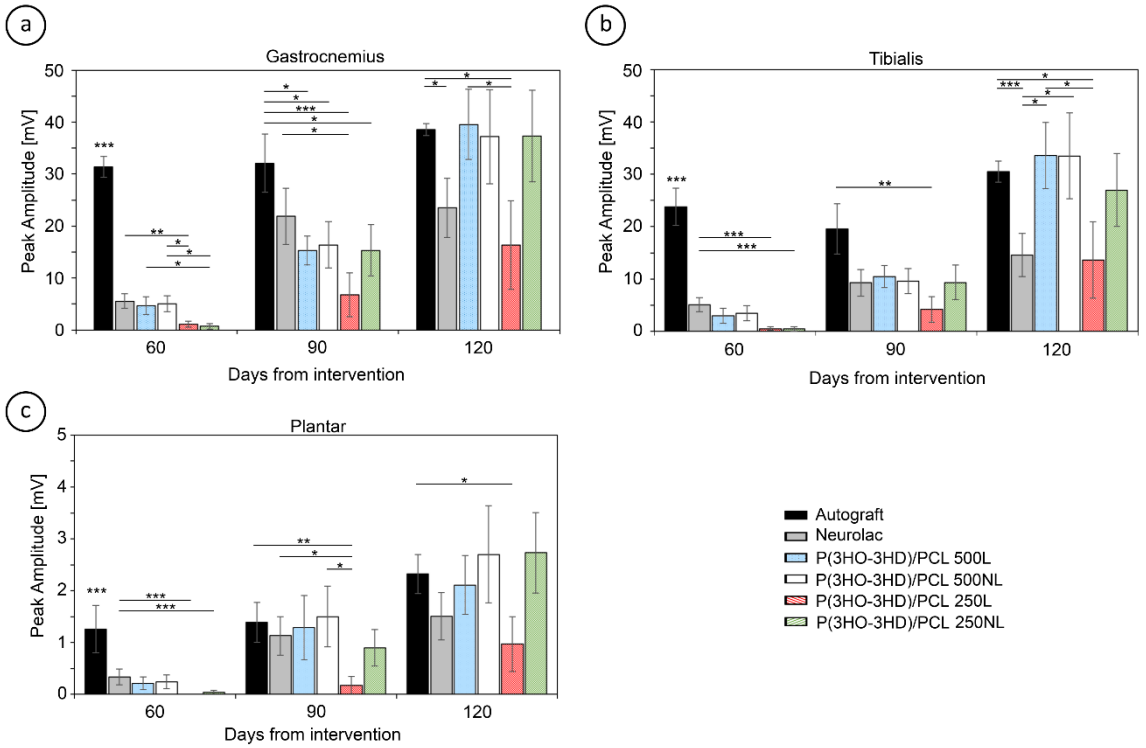

Figure 5.3 Mean amplitude of the Compound Muscle Action Potentials in mV of Autograft (black), Neurolac™ (grey) and different configurations of extruded P(3HO-3HD)/PCL NGCs (blue, white, stripped red and stripped green) in the gastrocnemius (a), tibialis anterior (b) and plantar interosseous (c) muscles at 60, 90 and 120 dpi. Data are presented as Mean ± SEM . *p<0.05, **p<0.01 and ***p<0.005.

slower as recorded with a higher latency from stimulus. Evidence of plantar interosseous muscle reinnervation was observed in 6/10 of Neurolac™-TW repaired animals, 3/8 of P(3HO-3HD)/PCL 500 µm leached, 5/8 of P(3HO-3HD)/PCL 500 µm non-leached, but no signals were recorded in P(3HO-3HD)/PCL 250 µm (either leached or non-leached).

Recordings at longer times post-injury resulted in a steady increase of the onset potentials until the end of the follow-up (120 dpi). The percentage of positive responses of the plantar interosseous muscle increased up to 7/10 of Neurolac™-TW repaired animals, 7/8 of P(3HO-3HD)/PCL 500 µm leached, 6/8 of P(3HO-3HD)/PCL 500 µm non-leached, 3/8 P(3HO-3HD)/PCL 250 µm leached and 6/8 P(3HO-3HD)/PCL 250 µm non-leached.

Significant differences at the final time-point in the gastrocnemius muscle were found between autograft and P(3HO-3HD)/PCL 500 µm (L) vs Neurolac™-TW and P(3HO-3HD)/PCL 250 µm (L) groups, showing less functional recovery in the case of these NGCs compared to autografting. For P(3HO-3HD)/PLC 500 µm (L), values significantly higher than P(3HO-3HD)/PLC 250 mm (L) were obtained and comparable to those obtained for autografting. Hence, wall thickness seems to play an important role on sciatic nerve functional recovery. Similarly, results in the tibialis anterior muscle reveal that for Neurolac™-TW and P(3HO-3HD)/PLC 250 mm (L) the functional recovery is poor compared to autografting, P(3HO-3HD)/PLC 500 mm and P(3HO-3HD)/PLC 250 mm (NL), where peak amplitude values are comparable. Taking into account the numbers corresponding to the rats that showed positive response (Appendix B Table B2), thicker wall thickness seems to enhance the nerve regeneration process.

Results in the plantar interosseous muscle, however, did not show significant differences between autografting and tested NGCs apart from P(3HO-3HD)/PLC 250 mm (L) where the values are significantly lower, not only for such final time-point but also for previous time stages.

- Morphological results of regenerated nerves

Central portions of the regenerated cable were processed for immunohistochemical analysis after 4 months of implantation (Figure 5.4 and Figure 5.5). Interestingly, a large fibronectin-positive extracellular matrix attached to the inner wall of the P(3HO-3HD)/PCL and filling the whole tube lumen was present, in contrast to the Neurolac™-TW devices with a thinner

regenerating cable concentrated in the center of the tube lumen and completely detached from the inner walls of the tube. However, immunohistochemical analysis of myelinated axons (Neurofilament-200) and their wrapping by Schwann cells (S100β) showed a similar total area inside the tube among the groups repaired with either Neurolac™-TW or P(3HO-3HD)/PCL 500 µm, since most of regeneration in the P(3HO-3HD)/PCL 500 µm was also concentrated in the central portion of the regenerated cable. Notably, the total area of regenerating axons was consistently found as significantly higher in the P(3HO-3HD)/PCL guides with a higher wall thickness of 500 than that of 250 µm, which indicated of a more advanced stage of maturation of the regenerated nerves (Figure 5.6).

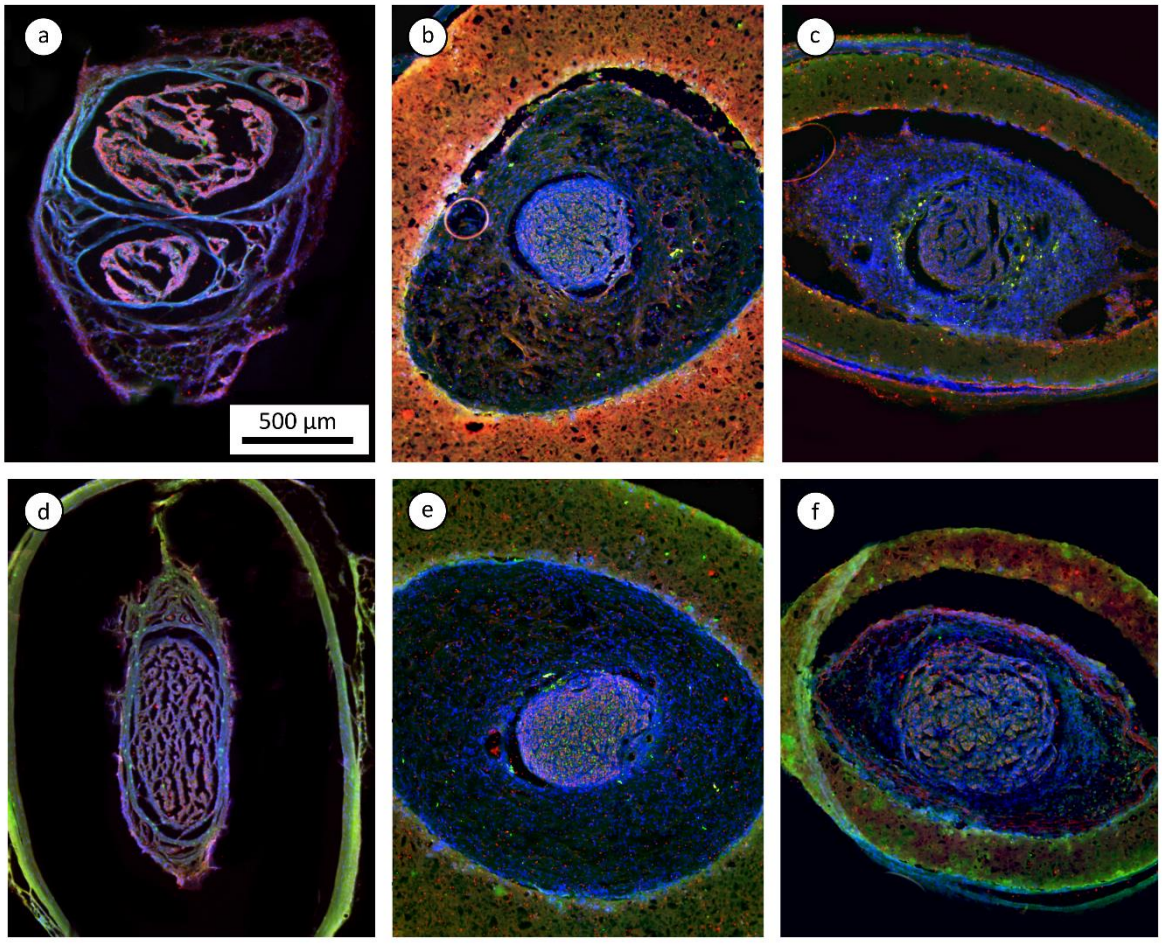

Figure 5.4 Representative cross sectional images of the regenerated nerves at the mid portion of the graft/tube in the Autograft (a), non-leached P(3HO-3HD)/PCL 500 µm wall thickness (b), non-leached P(3HO-3HD)/PCL 250 µm wall thickness (c), Neurolac™-TW (d), leached P(3HO-3HD)/PCL 500 µm wall thickness (e), leached P(3HO-3HD)/PCL 250µm wall thickness (f). Axons are stained with Neurofilament-200 (red), Schwann cells with S100β (green) and cell nuclei with DAPI (blue). Scale bar = 500 µm.

- Histological results

A macroscopic analysis of the regenerated nerves after 4 months of implantation revealed presence of regenerated cable in the 100% of animals repaired with an autograft (8/8), 70% with Neurolac™-TW (7/10), 87.5% with P(3HO-3HD)/PCL 500 µm leached (7/8), 75% with P(3HO-3HD)/PCL 500 µm non-leached (6/8), 37.5 % with P(3HO-3HD)/PCL 250 µm leached (3/8) and 75% with P(3HO-3HD)/PCL 250 µm non-leached (6/8) (Figure 5.7, Appendix B Table B2). Moreover, a careful macroscopic evaluation of their surface evidenced that P(3HO-3HD)/PCL

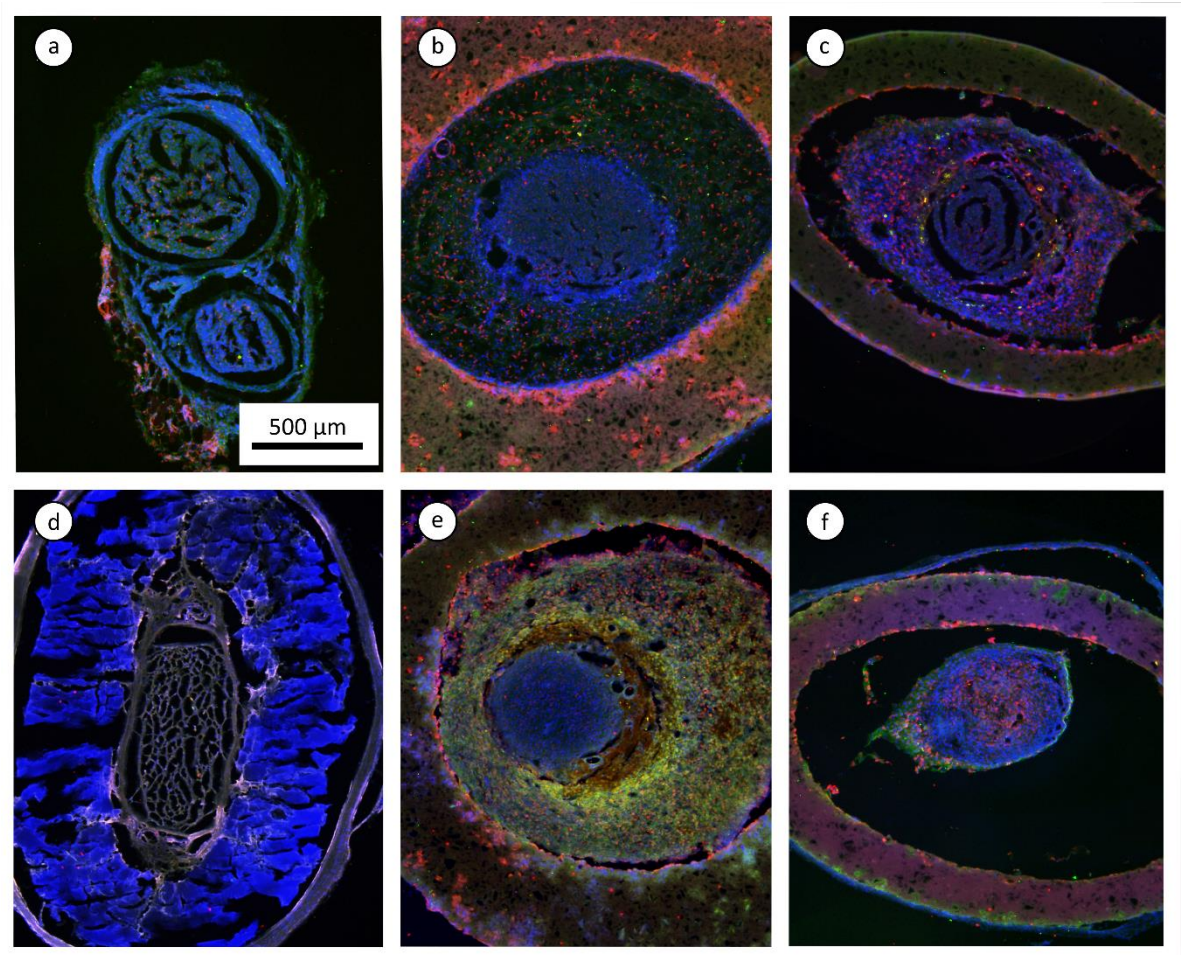

Figure 5.5 Representative cross sectional images of the regenerated nerves at the mid portion of the graft/tube in the autograft (a), non-leached P(3HO-3HD)/PCL 500 µm wall thickness (b), non-leached P(3HO-3HD)/PCL 250 µm wall thickness (c),Neurolac™-TW (d), leached P(3HO-3HD)/PCL 500 µm thickness (e), leached P(3HO-3HD)/PCL 250 µm wall thickness (f). Extracellular matrix presence was stained for fibronectin (green) and macrophages identified by Iba-1 (red). Scale bar = 500 µm.

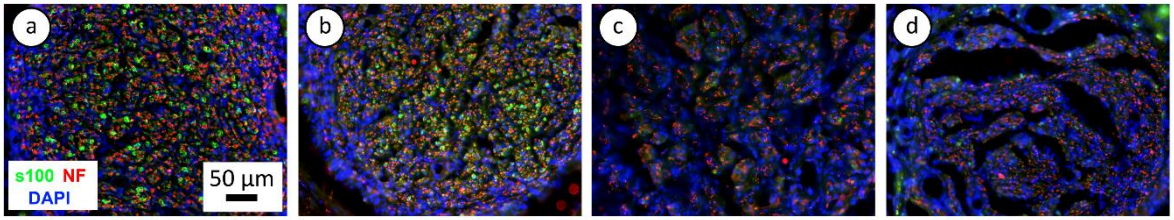

Figure 5.6 High resolution images of the regenerated nerves at the mid portion of the graft/tube in the P(3HO-3HD)/PCL 75/25. Leached P(3HO-3HD)/PCL 500 µm wall thickness (a), non-leached P(3HO-3HD)/PCL 500 µm wall thickness (b), leached P(3HO-3HD)/PCL 250 µm wall thickness (c), non-leached P(3HO-3HD)/PCL 250 µm wall thickness (d). Axons were stained with Neurofilament-200 (red), Schwann cells with S100β (green) and cell nuclei with DAPI (blue). Scale bar = 50 µm.

NGCs are made by long-lasting polymers, since no evident signs of degradation were observed, confirming the results obtained *in-vitro* (Table 5.4).

As mentioned above, the regenerated nerves at the mid-level of the Neurolac™-TW and P(3HO-3HD)/PCL guides are centered in the lumen of the tube. Quantification of the estimated myelinated fibers, density, myelin thickness and axon caliber corroborated the immunohistochemical results described above. A similar performance was found for the Neurolac™-TW, the P(3HO-3HD)/PCL 500 µm and P(3HO-3HD)/PCL 250 µm NL NGCs in contrast

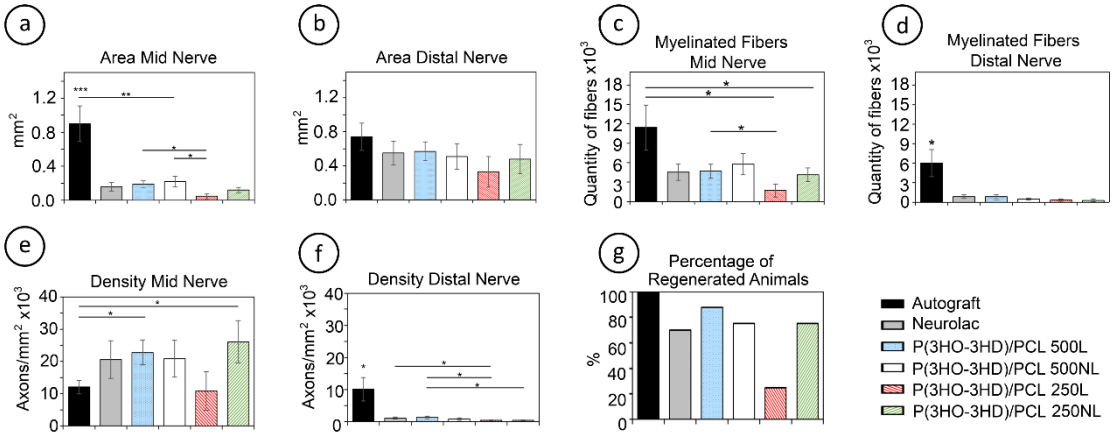

Figure 5.7 Graphs illustrating the area of the regenerated nerve at mid portion (a) and distal portion (b), the estimated number of myelinated fibers at mid portion (c) and distal portion (d), the density of myelinated fibers at mid portion (e) and distal portion (f) and the percentage of animals with successful regeneration (g) of the tested Autograft, Neurolac™ and P(3HO-3HD)/PCL graft/tubes. Data are presented as Mean ± SEM. *p<0.05, **p<0.01 and ***p<0.005.

to the lower values obtained for P(3HO-3HD)/PCL 250 µm L wall (Figure 5.7, Figure 5.8 and Appendix B Table B2). Similar results were observed in the distal level of the conduits, where the data revealed better performance in the Neurolac™-TW, P(3HO-3HD)/PCL 500 µm and P(3HO-3HD)/PCL 250 µm NL NGCs (Figure 5.7, Figure 5.8 and Appendix B Table B2).

4.4 Discussion

The P(3HO-3HD) MCL-PHA biomaterial developed in this research is a soft elastomeric polymer characterized by an ultimate strength of ~14 MPa and large elongation at break ~650 %. These properties agree well with those found in the literature where MCL-PHAs are described as flexible elastomeric polymers with low crystallinity, low glass transition temperature, low tensile strength, and high elongation to break [32,37,53,69–71], which made them extremely attractive

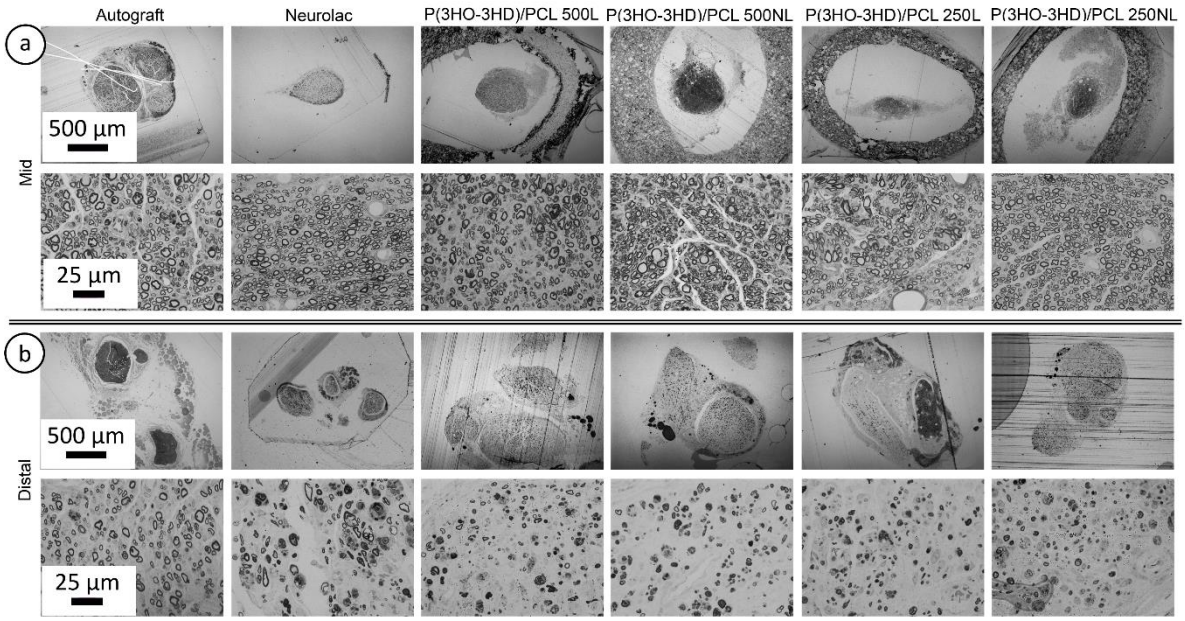

Figure 5.8 Representative images of semithin cross sections at the mid-level (a) and distal portion (3 mm distal) (b) of the graft/tube of regenerated animals in autograft, Neurolac™-TW and P(3HO-3HD)/PCL regenerated nerves. Top panels represent low magnification (4×) images of the whole representation of the regenerated nerves. Scale bar = 500 µm. Higher magnification images (60×) (bottom panels) were used to count the estimation of myelinated fibers and density of axons in the different groups. Scale bar = 25 µ

for soft tissue regeneration. However, low Young's modulus (8.4 MPa) and extremely low yield strength (0.25 MPa) values contribute to its low stiffness, which limits its ability to prevent collapsing of tubular structures under compression stress and, hence, would hinder its use as suitable material for NGC development. To enhance these mechanical properties, P(3HO-3HD) was blended with a synthetic polyester, PCL which is significantly stiffer than P(3HO-3HD) and was specifically synthetized to reach low values of E, σ_y and σ_u while showing good compatibility with that bacterial origin polyester. According to a recent review by Duffy *et al*. [3], the Young´s modulus and tensile strength of PCL are (275 ± 75) MPa and (27 ± 7) MPa, respectively. Table 5.1 shows that PCL was synthetized to reach lower values of the tensile strength and similar values of the Young's Modulus that the ones reported in that review. In terms of compatibility, both bacterial origin and synthetic polyesters presented semi-crystalline nature (Appendix B Figure B9), showing low glass transition temperature which assures a rubbery state of the amorphous phase at room and body temperatures which is a prerequisite for producing high flexible NGCs. Additionally, both polyesters shown melt temperatures below 70°C enabling processing via melt extrusion. Moreover, both polymers are known to degrade in a similar way, namely via surface erosion. According to the DSC results presented in Appendix B Figure B9, the overlapping of temperature ranges of melting for these polymers (42 - 70°C) did not allow drawing conclusions about the polymer compatibility in the blends. However, the observed experimental enthalpy of melting for the 75/25 blend exceeded the theoretical value calculated from the rule of mixing. Moreover, there was a slight shift to lower temperatures for complete melting of the blends compared with the melting temperature of PCL. Thus, promotion of crystallization and decreased melting temperature in the blends could be a result of partial compatibility between the polymers. Higher crystallization is expected to have a positive impact on mechanical stability of tubular structures. A preliminary screening of P(3HO-3HD)/PCL blends related to their processability and mechanical properties resulted in the choice of P(3HO-3HD)/PCL blend with 75 to 25 weight ratio as the blend of choice for this study. Blending of neat P(3HO-3HD) with a proportion of 25% of PCL transformed the material from easily deformable at low stresses to a material where the onset of plastic deformation appeared at strength values 5 times higher than those corresponding to P(3HO-3HD). The Young's modulus increased up to 13 times the value recorded for P(3HO-3HD) and decreased up to 2 times the value measured

for PCL. while the blending of P(3HO-3HD) with only 5% of PCL did no alter notably the mechanical properties nor enhanced its processability by means of hot melt extrusion. (Table 5.1).

As it is shown in Table 5.1, those values are far from the ones corresponding to the native rat sciatic nerve. However, those mechanical properties must be compared with the ones corresponding to the NGC, which is a porous tubular device. Table 5.2 shows that the apparent Young's modulus of porous tubes (2.3 ± 0.7 MPa and 3.0 ± 0.6 MPa for dry and wet conditions, respectively) are much closer to the one reported for rat sciatic nerve (0.58 MPa) [60] while keeping low strength values and large strain at sample break. Stress strain curves of leached and non-leached tubes are shown in Appendix B Figure B17 where the effect of the presence of glucose on the non-leached tubes can be seen. The non-leached tubes are brittle as the glucose particles act as pores at the same time they deter the polymeric matrix to freely deform, due to the presence of solid particles within the material. The leached tubes shown similar ultimate strength to non-leached tubes, as they have the same porosity, but the leached glucose made actual void pores which allow the deformation of the matrix, leading to lower Young's modulus and higher elongation values. Porous NGCs based on P(3HO-3HD)/PCL 75/25 blend did not exhibit the so-called "toe region" in stress/strain curve (Table 5.2 and Appendix B Figure B17 (a)), where large plastic deformation occurs at small stresses as it was observed for films of P(3HO-3HD) (Table 5.1 and Appendix B Figure B8). This should improve the structural stability of implanted device made of P(3HO-3HD)/PCL 75/25 blend under stresses. To the best of our knowledge there is no information regarding the mechanical properties of non-porous Neurolac^{TM}-TW NGCs considered as reference in this study. Selection of P(3HO-3HD)/PCL 75/25 as preferred material was therefore based on a combination of an ability to support neuronal and Schwann cell adhesion, spreading and growth, and mechanical properties of the materials as a candidate for becoming an implantable medical device. The data in Figure 5.1 confirmed that NG108-15 neuronal cells were able to adhere, spread, grow and form neurites on the P(3HO-3HD)/PCL 75/25 blend compared to P(3HO-3HD) alone or PCL alone [72]. Similarly, primary Schwann cells adhered, spread, and grew on P(3HO-3HD)/PCL 75/25 equally as well as P(3HO-3HD) alone or PCL alone.

The extruded tube, as it can be deduced from the inspection by SEM and µCT (Figure 5.2) and Figures B12-B16 in Appendix B, exhibited a uniform porosity and good leaching performance, showing no residual glucose particles in the leached tubes nor areas with differential porosity. The extrusion arises as a valid scalable manufacturing process to produce porous biocompatible tubular components as described by Mendibil *et al*. [68]. Wall porosity allows diffusion of soluble factors, oxygen and nutrients through the tube wall, as well as affecting the migration and organization of myofibroblasts [73], which are responsible for the undesired synthesis of the scar tissue. Thus, the capacity to limit and/or prevent the formation of the contractile capsule of myofibroblasts, as well as a certain grade of permeability are two key factors which must be carefully considered when working on the improvement of the tube wall properties. On the other hand, these requirements should also facilitate the need to prevent the infiltration of inflammatory cells into the conduit and to minimize the diffusion of growth factors out of the conduit. Accordingly, pore sizes in the range of about 20-30 µm were considered optimal [9,28], while pore sizes lower than 38 µm were found to encourage glucose diffusion, and slow protein diffusion and cell migration [74]. Therefore, in this work, the porogenerator particle size was fixed to 25-50 µm, while the largest mass fraction of glucose particles compatible with its processability (70 wt%) was used to ensure interconnectivity in porous structure. After successful leaching of porogenerator, pore volume fraction of the tubes is expected to be around 65%, which agrees well with previous *in-vitro* studies where optimal NGC geometrical configuration was determined (conduit with wall thickness of 0.6 mm and porosity of around 80% and pore size range of 10-40 µm) [67,74]. The target inner diameter was selected according to histological analysis developed previously [48], where the data enabled a target internal diameter above 1.5 mm. Hence, after considering the space needed for suturing without nerve compression, a target diameter of 1.6 mm was considered.

The optimal wall thickness of a nerve guide occurs between the smallest radial thickness that prevents material collapse and occlusion and a wall thickness at which the material swells and causes nerve compression. In the case of PCL tubes, an optimal wall thickness of 600 µm was previously established [74] for 200 and 600 µm wall thickness tubes. For the Neurolac™-TW tube used as reference control, a reduced wall thickness (0.28 mm) instead of the standard (0.43 mm) was chosen to facilitate handling and suturing. For the present study with P(3HO-

3HD)/PCL 75/25 tubes two different wall thickness (250 and 500 μm) covering this range were chosen.

Electrophysiological study revealed that the autograft group has the best performance after injury (Figure 5.3). Onset of responses were earlier (60 dpi) when all animals responded positively to the electrical impulse. At 4 months, these animals reached the plateau phase for muscle reinnervation. Tubular devices instead responded later to the electrical impulse (90 dpi) with lower responses due a slower onset of regeneration of the targeted muscles. This was expected since the maintenance of the physical structure of the implanted graft leads to those regrowing axons may use this structure for rapidly extending their growth cones and easily bridging the gap. In contrast, when using hollow tubular devices for bridging the gap, there is the need for the initial generation of a fibrin/fibronectin cable structure reconnecting the nerve stumps, which is required to support nerve regeneration. This process may take approximately two weeks after the Wallerian degeneration process [10] which causes a delay in nerve regeneration. Indeed, a similar response is obtained at 120 dpi between the autograph and the 500 μm wall thickness P(3HO-3HD)/PCL 75/25 tubular implants. Instead, the lower response observed at 120 dpi in the lower thickness tube was attributed to a poorer fibrin cable formation during regeneration as observed in immuno-histochemical analysis (Figure 5.5). Significant differences were also observed between thicker P(3HO-3HD)/PCL 75/25 and the Neurolac™-TW group in gastrocnemius and tibialis anterior muscles, showing better outcomes in the case of P(3HO-3HD)/PCL 75/25 NGCs. However, as detailed below, this difference in muscle potentials was not translated into significant differences in the histological analysis for the number of myelinated axons at the mid and distal parts of the tube, although there seems to be a better nerve fasciculation in the P(3HO-3HD)/PCL 75/25 NGCs that might partially explain these results (Figure 5.7 and Figure 5.8).

Immunohistochemical analysis and large positive staining for fibronectin (Figure 5.5) demonstrate the biocompatibility of the P(3HO-3HD)/PCL 75/25 blend to support nerve growth, since this protein is essential for both the formation of the initial fibrin/fibronectin clot responsible of the generation of the regenerating nerve cable in the first weeks after injury, as well as the matureness of the regenerated nerve formed in the following weeks with higher contents of fibronectin and other ECM proteins (laminin, collagen) with capacity to promote

axonal regeneration besides Schwann cell migration, proliferation and myelination [75]. On the other hand, fibronectin positive staining was poorer in the 250 µm wall thickness as compared to the NGCs with thicker walls (500 µm), which may be related to a poorer regeneration capacity as observed from the electrophysiological assay (Figure 5.5). This could be explained by considering that the bending stiffness of the hollow tubes was higher (for the same Young's modulus and length) as wall thickness increased for the same inner diameter and any force applied longitudinally or perpendicular to the length of the tube. Hence, an increase in bending for 250 µm wall thickness tubes might inhibit the formation of the fibrin cable during the regeneration stage after implantation. This was also observed as poorer regeneration capacity of leached 250 µm wall thickness, in which the implantation of non-leached tubes initially provides a greater bending stiffness (70×) compared to the leached tubes. The higher bending stiffness helps with fibrin/fibronectin cable formation during the first regeneration steps. It is hypothesized that even though the tube does not lose weight, or its wall thickness does not change significantly as implanted *in-vivo*, the superior bending stiffness of non-leached tubes provides a better mechanical support for fibrin cable formation. High resolution immunohistochemical analysis (Figure 5.6) shows that thicker tubes provide a higher density of Schwann cell and myelinated axons as compared to thinner tubes. Moreover, the large fibronectin-positive obtained with P(3HO-3HD)/PCL 75/25 blend was extended to the whole tube lumen in contrast to the Neurolac™-TW tube's, denoting a mature regenerated nerve with larger area to support axon regeneration through the whole NGC lumen (Figure 5.4).

Histological analysis showed that cross sectional area of regenerated nerves was higher in the autograft group when compared to tubular devices groups (Figure 5.7 and Figure 5.8). This was due to the flip of the graft during the surgery. The trifurcation of the sciatic nerve (tibial, peroneal, and sural branches) which originally (healthy nerve) is located in the distal part, corresponds to the proximal part in the autograft (after surgery), increasing the cross-sectional effective area for nerve regeneration. Even though the number of axons in the mid tube or distal tube might be similar between thicker and non-leached thinner tubes, the histology of the thicker tubes shows the appearance of having the axons structured in fascicles, similar to what we observed in a natural nerve, or those animals repaired with an autograft. In fact, the density of the Schwann cells and axon distribution was characteristic of mature regenerated nerves

(Figure 5.4), with Schwann cells wrapping the axons with the myelin that facilitates and speeds up the conduction of the electrical impulse.

Regarding NGCs biodegradability, wall thickness loss is presented in Figure B19 in Appendix B. Results reveal that the P(3HO-3HD)/PCL 75/25 tubes resulted in long-lasting tubes and the low wall thickness did not affect to the stability and physical structure of the implant. In fact, slight changes in wall thickness were observed in the leached devices (either 500 µm or 250 µm), but no significant differences were observed. *In-vivo* degradation confirms what was observed *in-vitro*, where the mass loss of the tube was estimated around 10-15% as immersed in an oxidative environment for 3 months. This indicates that the tube presents an appropriate biodegradation rate to protect the nerve during the whole regeneration period. Higher biodegradation rates could be desired instead after regeneration to minimize any immune response. However, a moderate mass reduction does not imply that biodegradation may not speed up afterwards. In fact, Iba 1 positive staining demonstrated the presence of macrophage cells, responsible for the primary mechanism of degradation of biopolymers *in-vivo*. It is hypothesized that molecular mass might have decreased. Considering that PHA is hydrophobic, solubility should be achieved only for molecules of quite low molecular weights. Thus, with the decrease of molecular weight, shape can still be preserved due to poor solubility, but mechanical properties should have decreased well before disintegration. Therefore, one can expect that mass loss would be quicker after 4 months (time considered for biodegradation analysis). Degradation might resemble bulk degradation rather than surface erosion, which is usually expected for PHAs and PCL, which indicates that porosity should contribute to such transition, since the ratio of surface material to bulk material drastically increases for porous materials.

4.5 Conclusions

P(3HO-3HD)/PCL 75/25 emerged as a promising blend of bacterial origin and synthetic biomaterials to be used in the manufacturing of hollow nerve guidance conduits able to support peripheral nerve regeneration in 10 mm sciatic nerve gap in rats (equivalent to 30 mm nerve gap in humans). Compatibility of this biomaterial with large-scale manufacturing of NGCs was demonstrated by the production of porous tubular devices via hot melt extrusion, providing two wall thickness values (250 µm and 500 µm) for a fixed inner diameter (1.6 mm). Mechanical properties of NGCs were comparable with those reported for the native rat sciatic nerve. Thicker wall (500 µm) tubular devices shown superior nerve regeneration ability, which is related to the achieved trade-off between porosity and stiffness to guarantee the formation of the fibrin cable from the beginning of the regeneration stage after implantation and enough stiffness, mechanical properties, and selectivity in terms of diffusion of active molecules, nutrients, and oxygen, among others. The devices showed a good porosity/permeability relationship, allowing superior nerve regeneration ability while keeping enough stiffness and low biodegradation rate to protect the nerve during the whole regenerative process. Electrophysiological results shown a similar response after 120 dpi between the autograft and the 500 µm wall thickness P(3HO-3HD)/PCL 75/25 tubular implants, indicating a better performance than the observed for Neurolac™-TW.

Thicker tubes also provided a higher density of Schwann cell and myelinated axons as compared to thinner tubes. Moreover, the large fibronectin-positive obtained with P(3HO-3HD)/PCL 75/25 blend was extended to the whole tube lumen in contrast to the Neurolac™-TW tube's, denoting a mature regenerated nerve with larger area to support axon regeneration through the whole NGC lumen. In a nutshell, a combination of P(3HO-3HD)/PCL 75/25 blend and high throughput manufacturing technologies were applied in this research to produce NGCs with superior mechanical properties, mimicking the native sciatic rat nerve and providing better regenerative capacity than Neurolac™-TW.

[1] Panagopoulos GN, Megaloikonomos PD, Mavrogenis AF. The present and future for peripheral nerve regeneration. Orthopedics 2017;40:e141–56. https://doi.org/10.3928/01477447-20161019-01.

[2] Karsy M, Watkins R, Jensen MR, Guan J, Brock AA, Mahan MA. Trends and Cost Analysis of Upper Extremity Nerve Injury Using the National (Nationwide) Inpatient Sample. World Neurosurg 2019;123:e488–500. https://doi.org/10.1016/j.wneu.2018.11.192.

[3] Duffy P, McMahon S, Wang X, Keaveney S, O'Cearbhaill ED, Quintana I, et al. Synthetic bioresorbable poly-α-hydroxyesters as peripheral nerve guidance conduits; a review of material properties, design strategies and their efficacy to date. Biomater Sci 2019;7:4912–43. https://doi.org/10.1039/C9BM00246D.

[4] Ronchi G, Morano M, Fregnan F, Pugliese P, Crosio A, Tos P, et al. The median nerve injury model in pre-clinical research – A critical review on benefits and limitations. Front Cell Neurosci 2019;13:1–21. https://doi.org/10.3389/fncel.2019.00288.

[5] Vijayavenkataraman S. Nerve guide conduits for peripheral nerve injury repair: A review on design, materials and fabrication methods. Acta Biomater 2020;106:54–69. https://doi.org/10.1016/j.actbio.2020.02.003.

[6] Wieringa PA, Gonçalves de Pinho AR, Micera S, van Wezel RJA, Moroni L. Biomimetic Architectures for Peripheral Nerve Repair: A Review of Biofabrication Strategies. Adv Healthc Mater 2018;1701164:1701164. https://doi.org/10.1002/adhm.201701164.

[7] Papadimitriou L, Manganas P, Ranella A, Stratakis E. Biofabrication for neural tissue engineering applications. Mater Today Bio 2020;6:100043. https://doi.org/10.1016/j.mtbio.2020.100043.

[8] Millesi H. Techniques for nerve grafting. Hand Clin 2000;16:73–91, viii.

[9] Pawelec K, Koffler J, Shahriari D, Galvan AR, Tuszynski M, Sakamoto JS. Microstructure and in vivo characterization of multi-channel nerve guidance scaffolds. Biomed Mater 2018;in press. https://doi.org/10.1088/1748-605X/aaad85.

[10] Arslantunali D, Dursun T, Yucel D, Hasirci N, Hasirci V. Peripheral nerve conduits: Technology update. Med Devices Evid Res 2014;7:405–24. https://doi.org/10.2147/MDER.S59124.

[11] Bell JHA, Haycock JW. Next generation nerve guides: Materials, fabrication, growth factors, and cell delivery. Tissue Eng - Part B Rev 2012;18:116–28. https://doi.org/10.1089/ten.teb.2011.0498.

[12] Pinho AC, Fonseca AC, Serra AC, Santos JD, Coelho JFJ. Peripheral Nerve Regeneration: Current Status and New Strategies Using Polymeric Materials. Adv Healthc Mater 2016;5:2732–44. https://doi.org/10.1002/adhm.201600236.

[13] Muheremu A, Chen L, Wang X, Wei Y, Gong K, Ao Q. Chitosan nerve conduits seeded with autologous bone marrow mononuclear cells for 30 mm goat peroneal nerve defect. Sci Rep 2017;7:44002. https://doi.org/10.1038/srep44002.

[14] Du J, Chen H, Qing L, Yang X, Jia X. Biomimetic neural scaffolds: A crucial step towards optimal peripheral nerve regeneration. Biomater Sci 2018;6:1299–311. https://doi.org/10.1039/c8bm00260f.

[15] Kehoe S, Zhang XF, Boyd D. FDA approved guidance conduits and wraps for peripheral nerve injury: A review of materials and efficacy. Injury 2012;43:553–72. https://doi.org/10.1016/j.injury.2010.12.030.

[16] Doolabh VB, Hertl MC, Mackinnon SE. The role of conduits in nerve repair: A review. Rev Neurosci 1996;7:47–84. https://doi.org/10.1515/REVNEURO.1996.7.1.47.

[17] Donoghoe N, Rosson GD, Dellon AL. Reconstruction of the human median nerve in the forearm with the Neurotube™. Microsurgery 2007;27:595–600. https://doi.org/10.1002/micr.20408.

[18] Rosson GD, Williams EH, Dellon AL. Motor nerve regeneration across a conduit. Microsurgery 2009;29:107–14. https://doi.org/10.1002/micr.20580.

[19] Bertleff MJOE, Meek MF, Nicolai JPA. A prospective clinical evaluation of biodegradable Neurolac nerve guides for sensory nerve repair in the hand. J Hand Surg Am 2005;30:513–8. https://doi.org/10.1016/j.jhsa.2004.12.009.

[20] Shin RH, Friedrich PF, Crum BA, Bishop AT, Shin AY. Treatment of a segmental nerve defect in the rat with use of bioabsorbable synthetic nerve conduits: A comparison of commercially available conduits. J Bone Jt Surg - Ser A 2009;91:2194–204. https://doi.org/10.2106/JBJS.H.01301.

[21] Costa Serrão de Araújo G, Couto Neto B, Harley Santos Botelho R, Carpi Malta M. Clinical Evaluation After Peripheral Nerve Repair With Caprolactone Neurotube. HAND 2017;12:168–74. https://doi.org/10.1177/1558944716643277.

[22] Deal DN, Griffin JW, Hogan M V. Nerve conduits for nerve repair or reconstruction. J Am Acad Orthop Surg 2012;20:63–8. https://doi.org/10.5435/JAAOS-

20-02-063.

[23] Meek MF, Coert JH. Re: Chiriac et al. Experience of using the bioresorbable copolyester poly(DL-lactide-ε-caprolactone) nerve conduit guide Neurolac™ for nerve repair in peripheral nerve defects: report on a series of 28 lesions. J Hand Surg Eur. 2011, 37: 342–9. J Hand Surg (European Vol 2012;37:702–5. https://doi.org/10.1177/1753193412453804.

[24] Meek MF, Den Dunnen WFA. Porosity of the wall of a Neurolac® nerve conduit hampers nerve regeneration. Microsurgery 2009;29:473–8. https://doi.org/10.1002/micr.20642.

[25] Nicoli Aldini N, Fini M, Rocca M, Giavaresi G, Giardino R. Guided regeneration with resorbable conduits in experimental peripheral nerve injuries. Int Orthop 2000;24:121–5. https://doi.org/10.1007/s002640000142.

[26] Meek MF, Robinson PH, Stokroos I, Blaauw EH, Kors G, Den Dunnen WFA. Electronmicroscopical evaluation of short-term nerve regeneration through a thin-walled biodegradable poly(DLLA-ε-CL) nerve guide filled with modified denatured muscle tissue. Biomaterials 2001;22:1177–85. https://doi.org/10.1016/S0142-9612(00)00340-9.

[27] Kim SM, Lee MS, Jeon J, Lee DH, Yang K, Cho SW, et al. Biodegradable Nerve Guidance Conduit with Microporous and Micropatterned Poly(lactic-co-glycolic acid)-Accelerated Sciatic Nerve Regeneration. Macromol Biosci 2018;18. https://doi.org/10.1002/mabi.201800290.

[28] Pawelec KM, Hix J, Shapiro EM, Sakamoto J. The mechanics of scaling-up multichannel scaffold technology for clinical nerve repair. J Mech Behav Biomed Mater 2019;91:247–54. https://doi.org/10.1016/j.jmbbm.2018.12.016.

[29] Huang L, Zhu L, Shi X, Xia B, Liu Z, Zhu S, et al. A compound scaffold with uniform longitudinally oriented guidance cues and a porous sheath promotes peripheral nerve regeneration in vivo. Acta Biomater 2018;68:223–36. https://doi.org/10.1016/j.actbio.2017.12.010.

[30] Jafari M, Paknejad Z, Rad MR, Motamedian SR, Eghbal MJ, Nadjmi N, et al. Polymeric scaffolds in tissue engineering: a literature review. J Biomed Mater Res Part B Appl Biomater 2017;105:431–59. https://doi.org/10.1002/jbm.b.33547.

[31] Manavitehrani I, Fathi A, Badr H, Daly S, Negahi Shirazi A, Dehghani F. Biomedical Applications of Biodegradable Polyesters. Polymers (Basel) 2016;8:20. https://doi.org/10.3390/polym8010020.

[32] Lizarraga-Valderrama LR, Nigmatullin R, Taylor C, Haycock JW, Claeyssens F, Knowles JC, et al. Nerve tissue engineering using blends of poly(3-hydroxyalkanoates) for peripheral nerve regeneration. Eng Life Sci 2015;15:612–21. https://doi.org/10.1002/elsc.201400151.

[33] Basnett P, Nigmatullin R, Lukasiewicz B, Rodriguez FJ, Pacharra S, Mendibil X, et al. Polyhydroxyalkanoates : A Family of Natural Polymers , for Medical Implant Development and Disease Modelling, 2019.

[34] Puppi D, Pirosa A, Lupi G, Erba PA, Giachi G, Chiellini F. Design and fabrication of novel polymeric biodegradable stents for small caliber blood vessels by computer-aided wet-spinning. Biomed Mater 2017;12:035011. https://doi.org/10.1088/1748-605X/aa6a28.

[35] Rydz J, Sikorska W, Kyulavska M, Christova D. Polyester-Based (Bio)degradable Polymers as Environmentally Friendly Materials for Sustainable Development. Int J Mol Sci 2014;16:564–96. https://doi.org/10.3390/ijms16010564.

[36] Deb P, Deoghare AB, Borah A, Barua E, Das Lala S. Scaffold Development Using Biomaterials: A Review. Mater Today Proc 2018;5:12909–19. https://doi.org/10.1016/j.matpr.2018.02.276.

[37] Bagdadi A V., Safari M, Dubey P, Basnett P, Sofokleous P, Humphrey E, et al. Poly(3-hydroxyoctanoate), a promising new material for cardiac tissue engineering. J Tissue Eng Regen Med 2018;12:e495–512. https://doi.org/10.1002/term.2318.

[38] Hazer DB, Kiliçay E, Hazer B. Poly(3-hydroxyalkanoate)s: Diversification and biomedical applications: A state of the art review. Mater Sci Eng C 2012;32:637–47. https://doi.org/10.1016/j.msec.2012.01.021.

[39] Mathuriya AS, Yakhmi J V. Polyhydroxyalkanoates: Biodegradable plastics and their applications. Handb Ecomater 2019;4:2873–900. https://doi.org/10.1007/978-3-319-68255-6_84.

[40] Hazer DB, Bal E, Nurlu G, Benli K, Balci S, Öztürk F, et al. In vivo application of poly-3-hydroxyoctanoate as peripheral nerve graft. J Zhejiang Univ Sci B 2013;14:993–1003. https://doi.org/10.1631/jzus.B1300016.

[41] Mozejko-Ciesielska J, Szacherska K, Marciniak P. Pseudomonas Species as Producers of Eco-friendly Polyhydroxyalkanoates. J Polym Environ 2019;27:1151–66. https://doi.org/10.1007/s10924-019-01422-1.

[42] Zhang J, Shishatskaya EI, Volova TG, da Silva LF, Chen GQ. Polyhydroxyalkanoates (PHA) for therapeutic applications. Mater Sci Eng C 2018;86:144–50. https://doi.org/10.1016/j.msec.2017.12.035.

[43] Możejko-Ciesielska J, Kiewisz R. Bacterial polyhydroxyalkanoates: Still fabulous? Microbiol Res 2016;192:271–82. https://doi.org/10.1016/j.micres.2016.07.010.

[44] Garcia-Garcia D, Ferri JM, Boronat T, Lopez-Martinez J, Balart R. Processing and characterization of binary poly(hydroxybutyrate) (PHB) and poly(caprolactone) (PCL) blends with improved impact properties. Polym Bull 2016;73:3333–50. https://doi.org/10.1007/s00289-016-1659-6.

[45] Duarte MAT, Hugen RG, Martins ES, Pezzin APT, Pezzin SH. Thermal and mechanical behavior of injection molded Poly(3-hydroxybutyrate)/Poly(epsilon-caprolactone) blends. Mater Res 2006;9:25–8. https://doi.org/10.1590/S1516-14392006000100006.

[46] Katsumata K, Saito T, Yu F, Nakamura N, Inoue Y. The toughening effect of a small amount of poly(ε-caprolactone) on the mechanical properties of the poly(3-hydroxybutyrate-co-3-hydroxyhexanoate)/PCL blend. Polym J 2011;43:484–92. https://doi.org/10.1038/pj.2011.12.

[47] Constantinides C, Basnett P, Lukasiewicz B, Carnicer R, Swider E, Majid QA, et al. In Vivo Tracking and 1 H/ 19 F Magnetic Resonance Imaging of Biodegradable Polyhydroxyalkanoate/Polycaprolactone Blend Scaffolds Seeded with Labeled Cardiac Stem Cells. ACS Appl Mater Interfaces 2018;10:25056–68. https://doi.org/10.1021/acsami.8b06096.

[48] Diez-Ahedo R, Mendibil X, Márquez-Posadas MC, Quintana I, González F, Rodríguez FJ, et al. UV-Casting on Methacrylated PCL for the Production of a Peripheral Nerve Implant Containing an Array of Porous Aligned Microchannels. Polymers (Basel) 2020;12:971. https://doi.org/10.3390/polym12040971.

[49] Woodruff MA, Hutmacher DW. The return of a forgotten polymer - Polycaprolactone in the 21st century. Prog Polym Sci 2010;35:1217–56. https://doi.org/10.1016/j.progpolymsci.2010.04.002.

[50] Chiono V, Tonda-Turo C. Trends in the design of nerve guidance channels in peripheral nerve tissue engineering. Prog Neurobiol 2015;131:87–104. https://doi.org/10.1016/j.pneurobio.2015.06.001.

[51] Sarker M, Naghieh S, McInnes AD, Schreyer DJ, Chen X. Strategic Design and Fabrication of Nerve Guidance Conduits for Peripheral Nerve Regeneration. Biotechnol J 2018;13:1700635. https://doi.org/10.1002/biot.201700635.

[52] Basnett P, Lukasiewicz B, Marcello E, Gura HK, Knowles JC, Roy I. Production of a novel medium chain length poly(3-hydroxyalkanoate) using unprocessed biodiesel waste and its evaluation as a tissue engineering scaffold. Microb Biotechnol 2017;10:1384–99. https://doi.org/10.1111/1751-7915.12782.

[53] Rai R, Keshavarz T, Roether JA, Boccaccini AR, Roy I. Medium chain length polyhydroxyalkanoates, promising new biomedical materials for the future. Mater Sci Eng R Reports 2011;72:29–47. https://doi.org/10.1016/j.mser.2010.11.002.

[54] Lageveen RG, Huisman GW, Preusting H, Ketelaar P, Eggink G, Witholt B. Formation of Polyesters by Pseudomonas oleovorans : Effect of Substrates on Formation of Polyesters by Pseudomonas oleovorans : Effect of Substrates on Formation and Composition of Poly- (R) -3-Hydroxyalkanoates and Poly- (R) -3-Hydroxyalkenoates. Appl Enviromental Microbiol 1988;54:2924–32.

[55] Kaewkhaw R, Scutt AM, Haycock JW. Integrated culture and purification of rat Schwann cells from freshly isolated adult tissue. Nat Protoc 2012;7:1996–2004. https://doi.org/10.1038/nprot.2012.118.

[56] Popko J, Fernandes A, Brites D, Lanier LM. Automated analysis of NeuronJ tracing data. Cytom Part A 2009;75A:371–6. https://doi.org/10.1002/cyto.a.20660.

[57] Schneider CA, Rasband WS, Eliceiri KW. NIH Image to ImageJ: 25 years of image analysis. Nat Methods 2012;9:671–5. https://doi.org/10.1038/nmeth.2089.

[58] Dempsey DK, Carranza C, Chawla CP, Gray P, Eoh JH, Cereceres S, et al. Comparative analysis of in vitro oxidative degradation of poly(carbonate urethanes) for biostability screening. J Biomed Mater Res - Part A 2014;102:3649–65. https://doi.org/10.1002/jbm.a.35037.

[59] Navarro X, Butí M, Verdú E. Autotomy prevention by amitriptyline after peripheral nerve section in different strains of mice. Restor Neurol Neurosci 1994;6:151–7. https://doi.org/10.3233/RNN-1994-6209.

[60] Borschel GH, Kia KF, Kuzon WM, Dennis RG. Mechanical properties of acellular peripheral nerve. J Surg Res 2003;114:133–9. https://doi.org/10.1016/S0022-4804(03)00255-5.

[61] Cui Z, Nelson B, Peng Y, Li K, Pilla S, Li W-J, et al. Fabrication and characterization of injection molded poly (ε-caprolactone) and poly (ε-caprolactone)/hydroxyapatite scaffolds for tissue engineering. Mater Sci Eng C 2012;32:1674–81. https://doi.org/10.1016/j.msec.2012.04.064.

[62] Izquierdo R, Garcia-Giralt N, Rodriguez MT, Cáceres E, García SJ, Gómez Ribelles JL, et al. Biodegradable PCL scaffolds with an interconnected spherical pore network for tissue engineering. J Biomed Mater Res - Part A 2008;85:25–35. https://doi.org/10.1002/jbm.a.31396.

[63] Tonda-Turo C, Audisio C, Gnavi S, Chiono V, Gentile P, Raimondo S, et al. Porous Poly(ε-caprolactone) Nerve Guide Filled with Porous Gelatin Matrix for

Nerve Tissue Engineering. Adv Eng Mater 2011;13:B151–64. https://doi.org/10.1002/adem.201080099.

[64] Asghari F, Samiei M, Adibkia K, Akbarzadeh A, Davaran S. Biodegradable and biocompatible polymers for tissue engineering application: a review. Artif Cells, Nanomedicine, Biotechnol 2017;45:185–92. https://doi.org/10.3109/21691401.2016.1146731.

[65] Malikmammadov E, Tanir TE, Kiziltay A, Hasirci V, Hasirci N. PCL and PCL-based materials in biomedical applications. vol. 29. Taylor & Francis; 2018. https://doi.org/10.1080/09205063.2017.1394711.

[66] Basnett P, Marcello E, Lukasiewicz B, Panchal B, Nigmatullin R, Knowles JC, et al. Biosynthesis and characterization of a novel, biocompatible medium chain length polyhydroxyalkanoate by Pseudomonas mendocina CH50 using coconut oil as the carbon source. J Mater Sci Mater Med 2018;29. https://doi.org/10.1007/s10856-018-6183-9.

[67] Pintado-Sierra M, Delgado L, Aranaz I, Marcos-Fernández Á, Reinecke H, Gallardo A, et al. Surface hierarchical porosity in poly (ε-caprolactone) membranes with potential applications in tissue engineering prepared by foaming in supercritical carbon dioxide. J Supercrit Fluids 2014;95:273–84. https://doi.org/10.1016/j.supflu.2014.09.019.

[68] Mendibil X, Ortiz R, Sáenz de Viteri V, Ugartemendia JM, Sarasua J-R, Quintana I. High Throughput Manufacturing of Bio-Resorbable Micro-Porous Scaffolds Made of Poly(L-lactide-co-ε-caprolactone) by Micro-Extrusion for Soft Tissue Engineering Applications. Polymers (Basel) 2019;12:34. https://doi.org/10.3390/polym12010034.

[69] Rai R, Yunos DM, Boccaccini AR, Knowles JC, Barker IA, Howdle SM, et al. Poly-3-hydroxyoctanoate P(3HO), a Medium Chain Length Polyhydroxyalkanoate Homopolymer from Pseudomonas mendocina. Biomacromolecules 2011;12:2126–36. https://doi.org/10.1021/bm2001999.

[70] Rai R, Boccaccini AR, Knowles JC, Mordon N, Salih V, Locke IC, et al. The homopolymer poly(3-hydroxyoctanoate) as a matrix material for soft tissue engineering. J Appl Polym Sci 2011;122:3606–17. https://doi.org/10.1002/app.34772.

[71] Lizarraga-Valderrama LR, Taylor CS, Claeyssens F, Haycock JW, Knowles JC, Roy I. Unidirectional neuronal cell growth and differentiation on aligned polyhydroxyalkanoate blend microfibres with varying diameters. J Tissue Eng Regen Med 2019;13:1581–94. https://doi.org/10.1002/term.2911.

[72] Daud MFB, Pawar KC, Claeyssens F, Ryan AJ, Haycock JW. An aligned 3D neuronal-glial co-culture model for peripheral nerve studies. Biomaterials 2012;33:5901–13. https://doi.org/10.1016/j.biomaterials.2012.05.008.

[73] Cerri F, Salvatore L, Memon D, Martinelli Boneschi F, Madaghiele M, Brambilla P, et al. Peripheral nerve morphogenesis induced by scaffold micropatterning. Biomaterials 2014;35:4035–45. https://doi.org/10.1016/j.biomaterials.2014.01.069.

[74] Kokai LE, Lin YC, Oyster NM, Marra KG. Diffusion of soluble factors through degradable polymer nerve guides: Controlling manufacturing parameters. Acta Biomater 2009;5:2540–50. https://doi.org/10.1016/j.actbio.2009.03.009.

[75] Gonzalez-Perez F, Udina E, Navarro X. Extracellular matrix components in peripheral nerve regeneration. vol. 108. 1st ed. Elsevier Inc.; 2013. https://doi.org/10.1016/B978-0-12-410499-0.00010-1

Chapter 5

General conclusions

5.1 Final remarks

The research carried out in this thesis has achieved a set of advances over the state of the art which have led to an improvement of the manufacturing of advanced NGCs. These improvements include an enhanced micro-injection monitoring strategy and the introduction of new manufacture routes involving high throughput processes for the manufacture of NGCs. These processes were used for the first time to obtain NGCs made of bio-resorbable polymers, with micro-structuration in form of controlled porosity, for their use in medical applications. These remarks are supported by the following results:

- A new strategy for micro-injection monitoring was implemented. This new method showed greater sensitivity to the detection of errors in the replication of micro-features. This development also settled new lines of research, such as for example, the analysis of filling dynamics by the measurement of the pressure in the mold runner and inside the micro-cavity.
- Mechanically tunable porous scaffolds made of medical grade PLCL were obtained by means of extrusion. The porosity was achieved by the addition of soluble particles to the bulk, allowing this way, a direct control of the porosity proportion and pore size of the obtained scaffold, which governs its mechanical properties.
- Porous NGCs, made of a novel blend of bacterial origin and synthetic origin polyesters, were manufactured by means of extrusion. The extruded conduits showed promising *in-vivo* results. That indicated the suitability of the manufactured implants to regenerate the injured nerves, demonstrating the feasibility of extrusion to manufacture implantable micro-structured components by means of an easily scalable manufacturing process.

5.2 Further work

One potential advantage of using extrusion to manufacture NGCs and other tubular implants is the ability to add patterns to both the inner and outer surfaces of the tube. In the case of extruding implantable devices, these surface-modifying patterns can improve their bio-interaction characteristics. This means that the extruded implants including these micro-patterns can better interact with the body and potentially improve their effectiveness.

Superficial micro-features can be added to extruded profiles by micro-machining the extrusion die. This allows for the creation of micro-features that are replicated along the extrusion axis, making it particularly suitable for creating micro-grooves. This type of micro-pattern is commonly used in tissue engineering to guide cell growth and improve their attachment. The ability to produce tubular profiles with this type of micro-patterning through extrusion is not only useful for advanced NGCs but also for other types of tubular implants that benefit from early and correct cell growth on their surface, such as vascular stents.

The next work stages that provide continuity to the present thesis work can be outlined within this new processing challenge, in which it is required to obtain tubes made of bio-resorbable polyesters that include micro-grooves in the inner surface of the tube. Obtaining this type of component with surface micro-patterning designed to obtain a biological response by means of a high-productivity method such as extrusion, can have a major impact on tissue engineering and in particular on the development of new generation of NGCs and vascular stents.

5.3 Additional information

The results of the work performed during this thesis have been disseminated through publications in scientific journals and participations in international conferences via lectures which are cited below.

Publications:

- Mendibil, X., Llanos, I., Urreta, H. and Quintana, I. In process quality control on micro-injection moulding: the role of sensor location. Int. J. Adv. Manuf. Technol. 2017, 89, 3429-3438. DOI: 10.1007/s00170-016-9300-2.
- Mendibil, X., Ortiz, R., Sáenz de Viteri, V., Ugartemendia, J.M., Sarasua, J.R. and Quintana, I. High throughput manufacturing of bio-resorbable micro-porous scaffolds made of poly(L-lactide-co-ε-caprolactone) by micro-extrusion for soft tissue engineering applications. Polymers. 2019, 12, 34. DOI: 10.3390/polym12010034.
- Mendibil, X., González-Pérez, F., Bazan, X., Díez-Ahedo, R., Quintana, I., Rodríguez, F. J., Basnett, P., Nigmatullin, R., Lukasiewicz, B., Roy, I., Taylor, C. S., Glen, A., Claeyssens, F., Haycock, J. W., Schaafsma, W. González, E., Castro, B., Duffy, P., Merino, S. Bio-resorbable and Mechanically Optimized Nerve Guidance Conduit Based on a Naturally Derived Medium Chain Length Polyhydroxyalkanoate and Poly(ε-Caprolactone) Blend. ACS Biomater. Sci. Eng. 2021, 7, 2, 672-689. DOI: 10.1021/acsbiomaterials.0c01476.

Oral presentations in international conferences:

- Mendibil, X., Llanos, I., Urreta, H. and Quintana, I. Micro-injection quality monitoring using in-mould pressure and temperature sensors. 11th International Conference on Micro Manufacturing. Orange County, California, USA, March 2016.
- Mendibil, X., Ortiz, R., Sáenz de Viteri, V., Ugartemendia, J.M., Sarasua, J.R. and Quintana, I. Validation of the micro extrusion process for the manufacturing of tubular bio-resorbable porous scaffolds for tissue engineering. EUSPEN, Special Interest Group meeting: Micro/Nano manufacturing. Technical University of Berlin. 27th – 28th November 2019.

Patent request:

- Merino, S., Quintana, I., Márquez, C., Mendibil, X., Bazan, X., Diez, R., Roy, I., Basnett, P., Nigmatullin, R., Lukasiewicz, B., Haycock, J., Claeyssens, F., Sherborne, C., Glen, A.,

Taylor, C., Rodriguez, F.J., Gonzalez, F.J. Implantable nerve guidance conduit for nerve repair. PCT/EP2018/054984.

In addition to the publications, conference contributions, and the patent request, the work carried out during the thesis has made it possible to work and contribute to the following European Commission granted projects:

- Minimizing Defects in Micro Manufacturing Applications (MiDeMMA). Grant agreement: 285614, funded under FP7-NMP. (https://cordis.europa.eu/project/id/285614).
- Novel combination of biopolymers and manufacturing technologies for production of a peripheral nerve implant containing an internal aligned channels array (NEURIMP). Grant agreement: 604450, funded under FP7-NMP. (https://cordis.europa.eu/project/id/604450).

Appendix A

Supplementary material of Chapter 3

$$\varphi_v = \frac{\rho_m}{\rho_p} \cdot \frac{\varphi_w}{1 + \varphi_w \left(\frac{\rho_m}{\rho_p} - 1 \right)} \qquad \text{(Equation A1)}$$

Equation A1 Equation used to calculate the volume fraction (ϕv) function of matrix density (ρm), particle density (ρp) and weight fraction (ϕw).

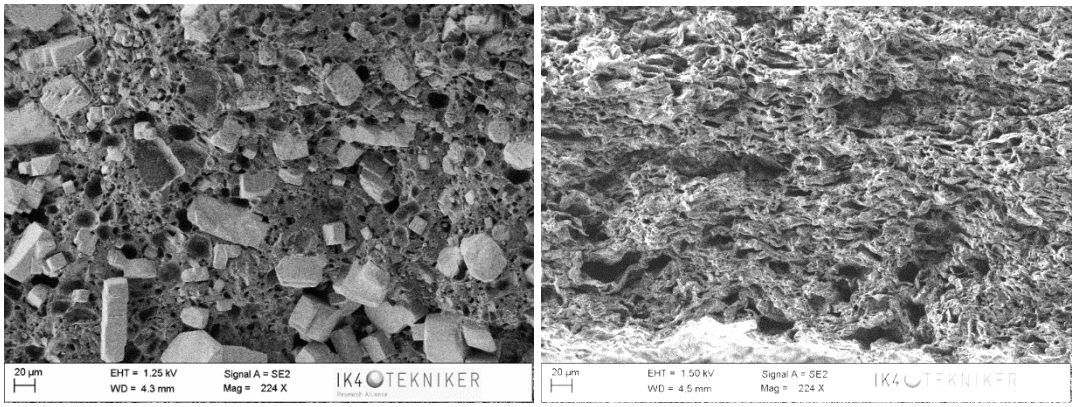

Figure A1 Sample 005050 containing 50 wt.% of salt in 0–50 µm range; non leached (left), leached (right).

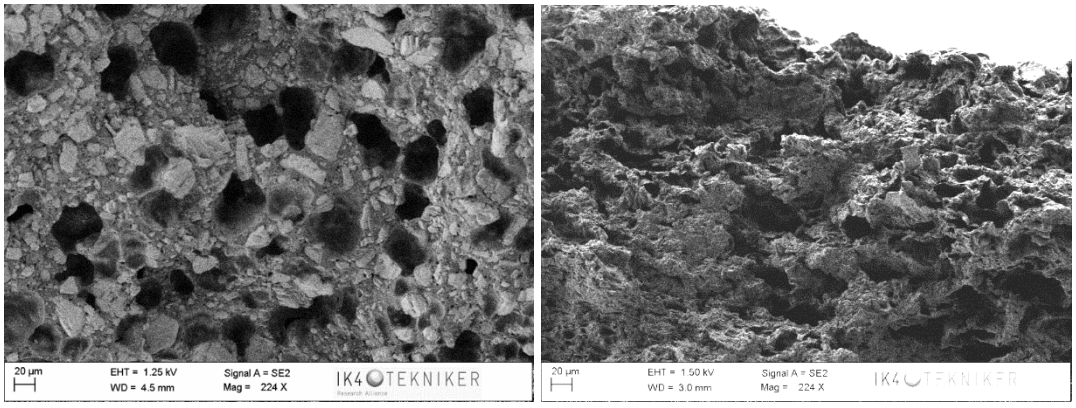

Figure A2 Sample 005060 containing 60 wt.% of salt in 0–50 µm range; non leached (left), leached (right).

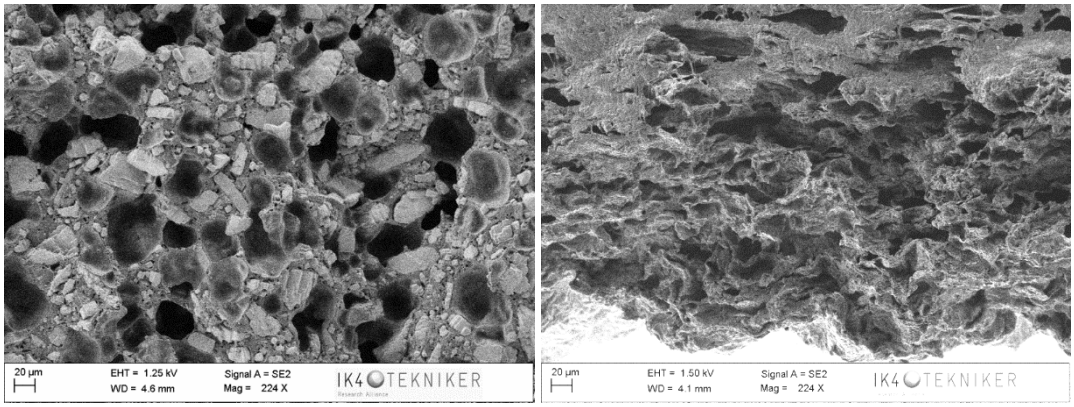

Figure A3 Sample 005070 containing 70 wt.% of salt in 0–50 µm range; non leached (left), leached (right).

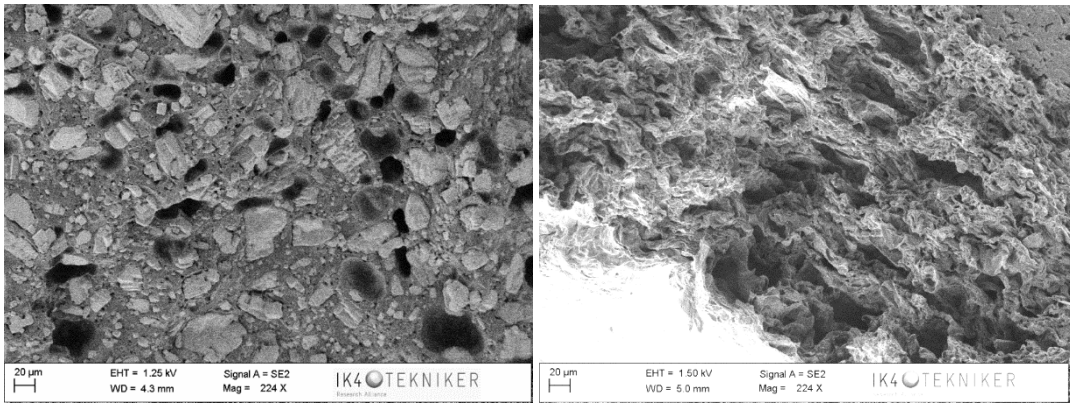

Figure A4 Sample 255050 containing 50 wt.% salt in 25–50 µm range; non leached (left), leached (right).

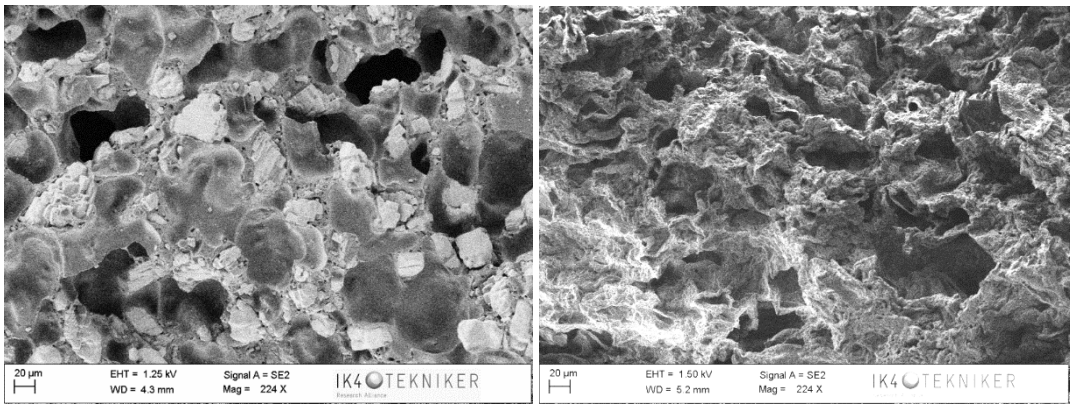

Figure A5 Sample 255060 containing 60 wt.% of salt in 25–50 range; non leached (left), leached (right).

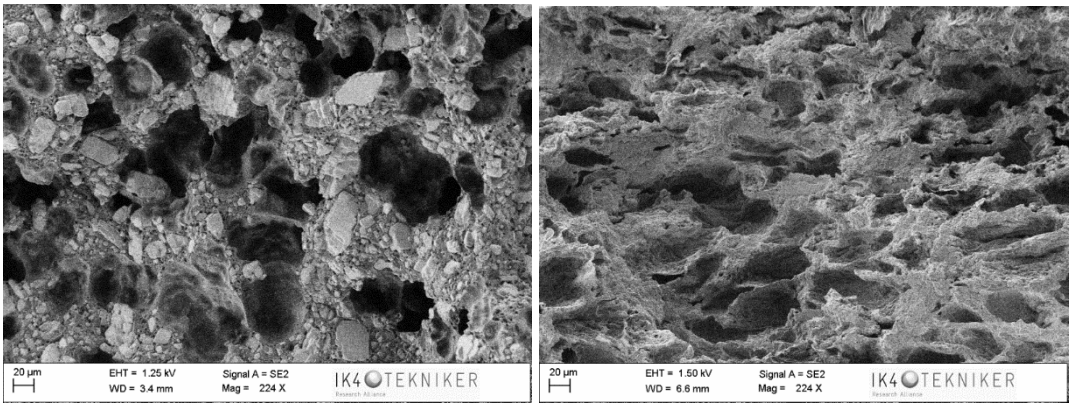

Figure A6 Sample 255070 containing 70 wt.% of salt in 25–50 µm range; non leached (left), leached (right).

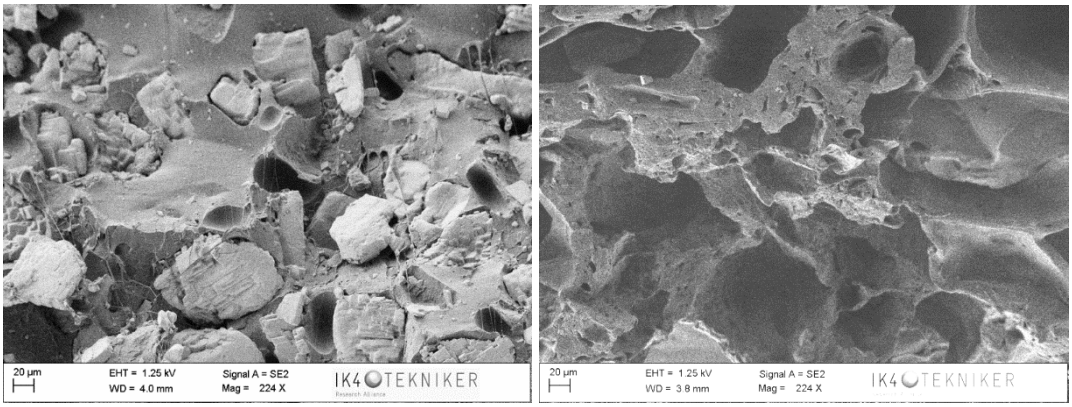

Figure A7 Sample 501050 containing 50 wt.% of salt in 50–100 µm range; non leached (left), leached (right).

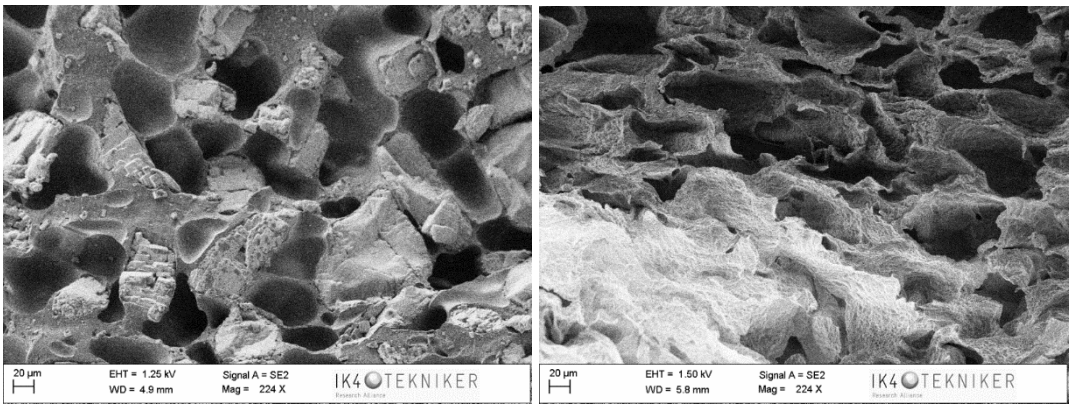

Figure A8 Sample 501060 containing 60 wt.% of salt in 50–100 µm range; non leached (left), leached (right).

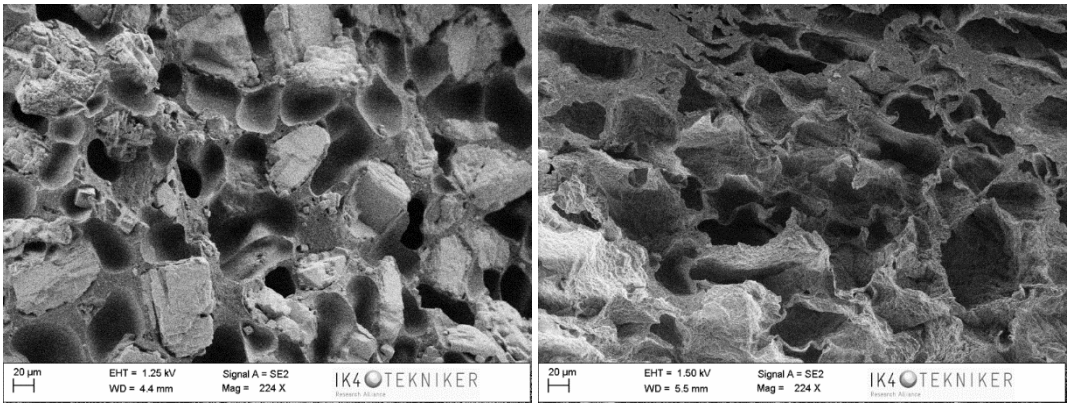

Figure A9 Sample 501070 containing 70 wt.% salt in 50–100 µm range; non leached (left), leached (right).

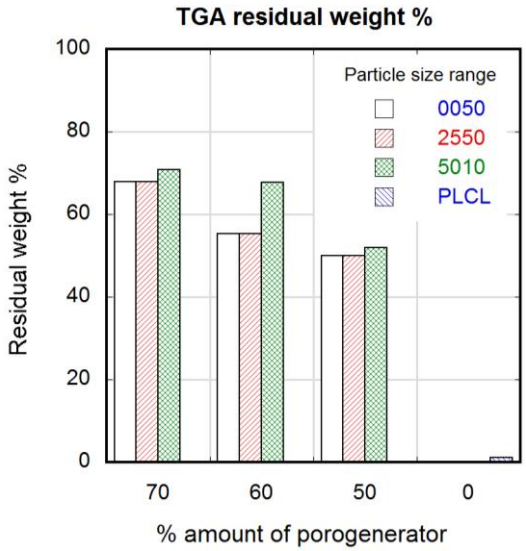

Figure A10 Percental residual weight measured by TGA for samples containing different particle sizes (white 0–50 µm, upwards stripe pattern 25–50 µm, cross pattern 50–100 µm, downwards strip pattern neat PLCL) as a function of the theoretical percental amount of porogenerator.

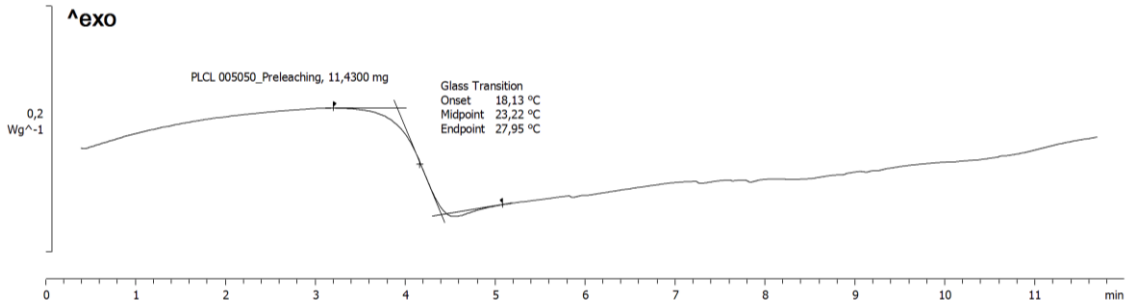

Figure A11 DSC curve of non-leached sample 005050 containing 50 wt.% salt in 0–50 µm range, exothermic upwards.

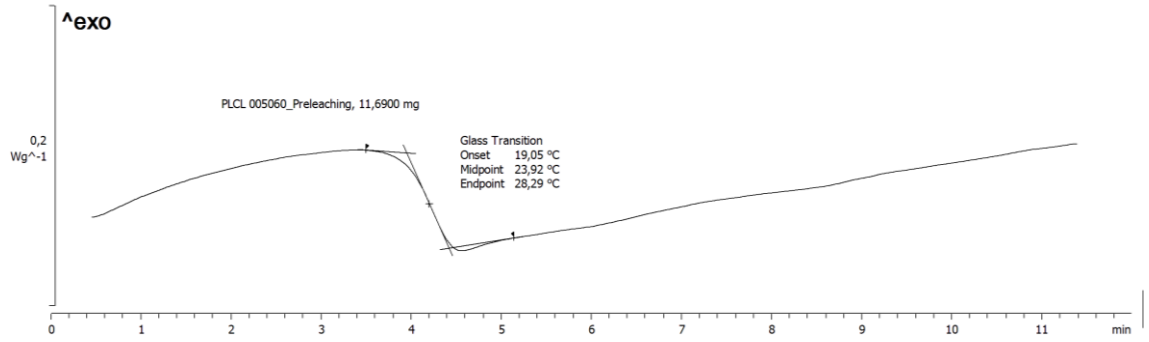

Figure A12 DSC curve of non-leached sample 005060 containing 60 wt.% salt in 0–50 µm range, exothermic upwards.

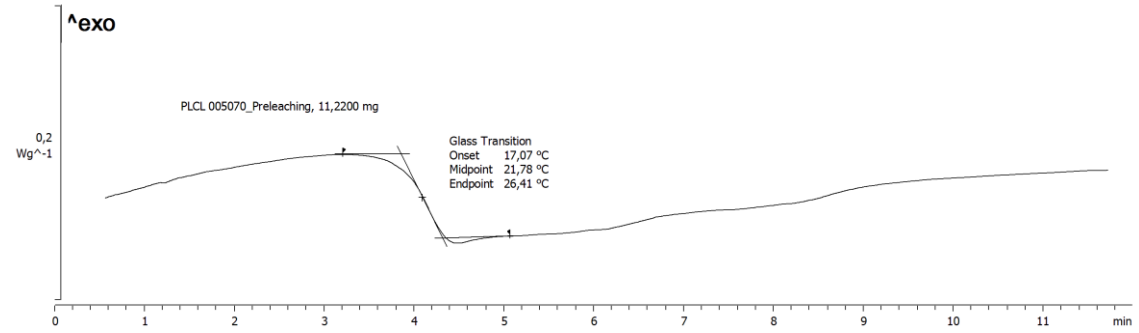

Figure A13 DSC curve of non-leached sample 005070 containing 70 wt.% salt in 0–50 µm range, exothermic upwards.

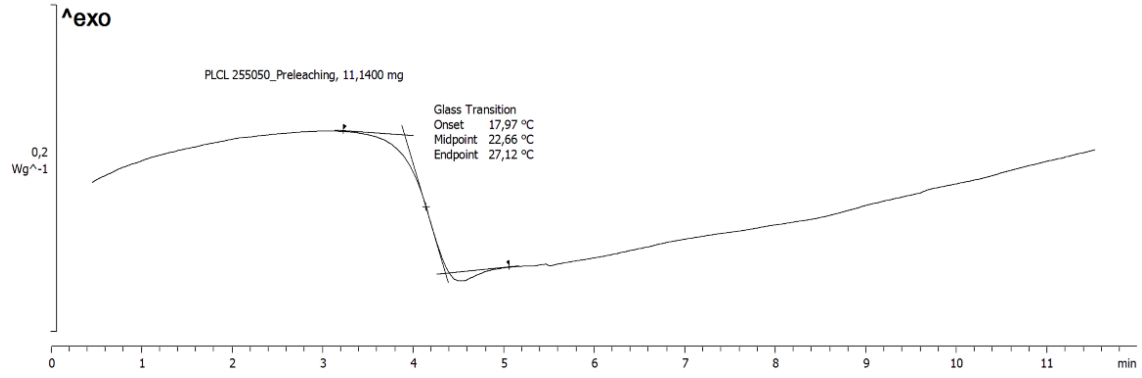

Figure A14 DSC curve of non-leached sample 255050 containing 50 wt.% salt in 25–50 µm range, exothermic upwards.

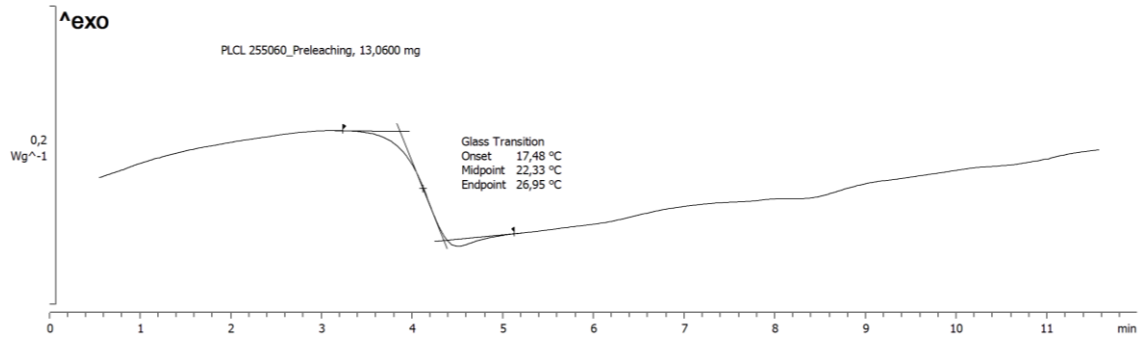

Figure A15 DSC curve of non-leached sample 255060 containing 60 wt.% salt in 25–50 µm range, exothermic upwards.

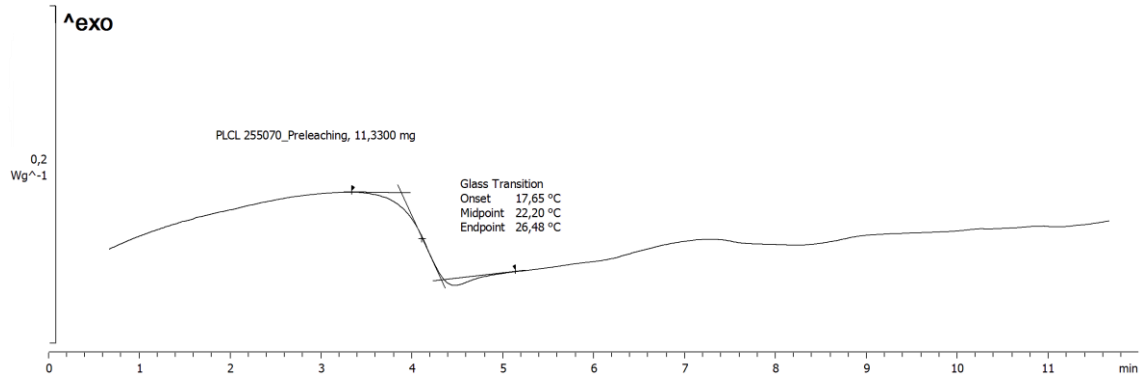

Figure A16 DSC curve of non-leached sample 255070 containing 70 wt.% salt in 25–50 µm range, exothermic upwards.

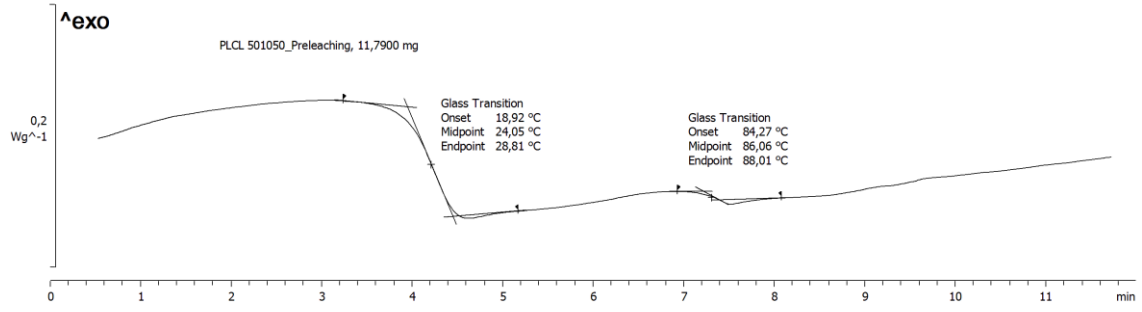

Figure A17 DSC curve of non-leached sample 501050 containing 50 wt.% salt in 50–100 µm range, exothermic upwards.

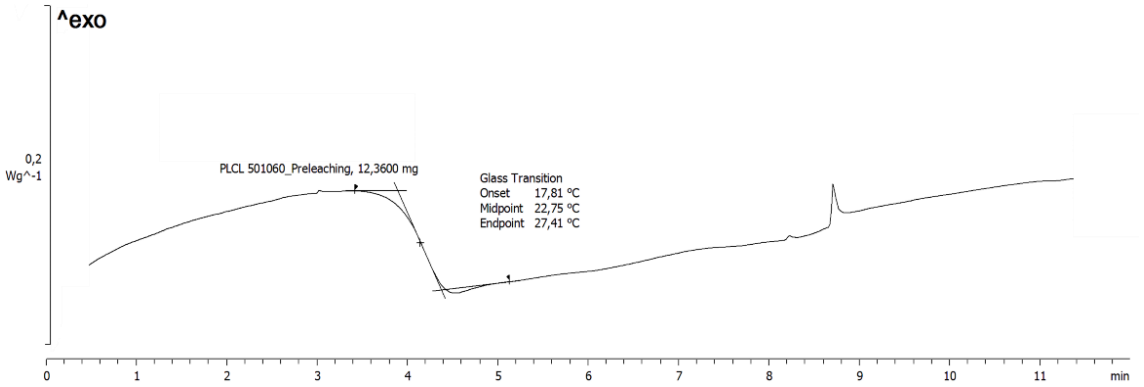

Figure A18 DSC curve of non-leached sample 501060 containing 60 wt.% salt in 50–100 µm range, exothermic upwards.

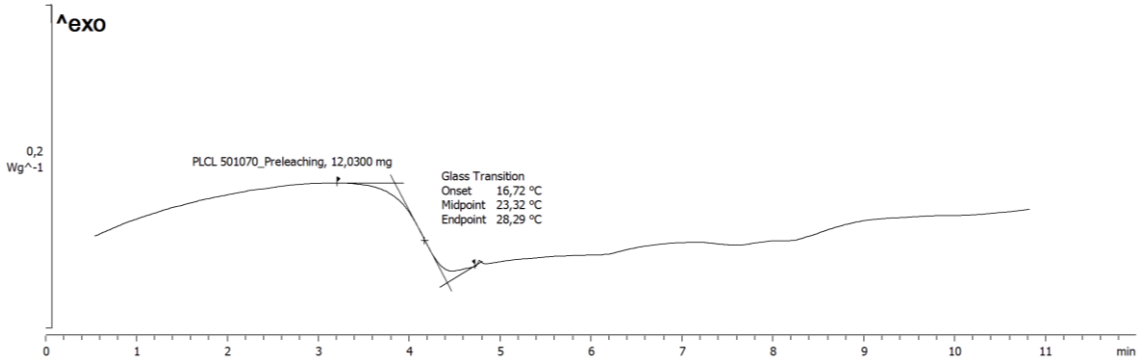

Figure A19 DSC curve of non-leached sample 501070 containing 70 wt.% salt in 50–100 µm range, exothermic upwards.

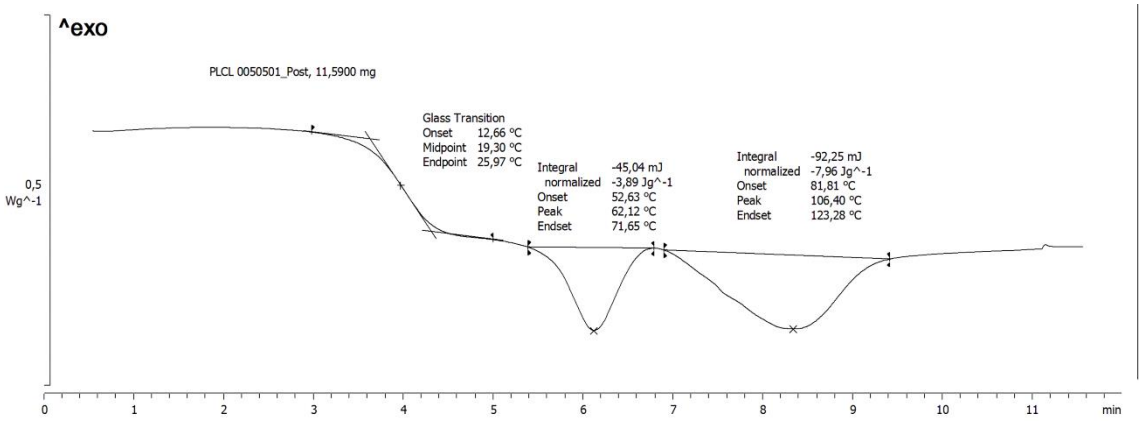

Figure A20 DSC curve of leached sample 005050 containing 50 wt.% salt in 0–50 µm range, exothermic upwards.

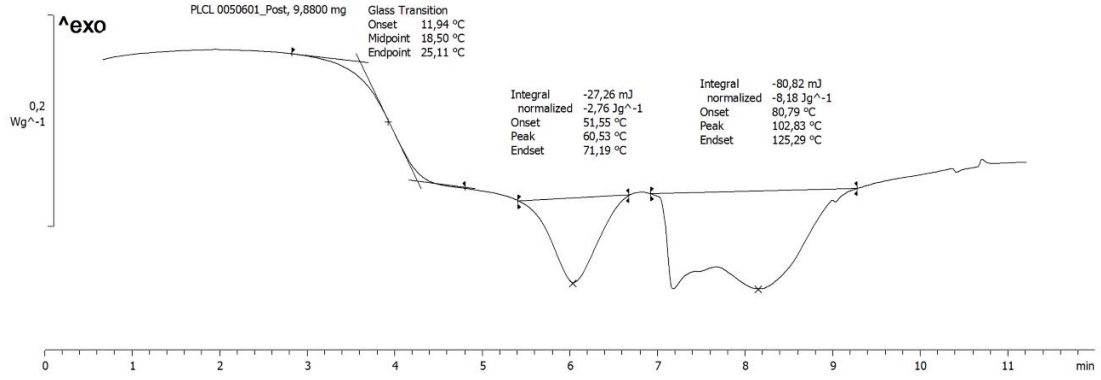

Figure A21 DSC curve of leached sample 005060 containing 60 wt.% salt in 0–50 µm range, exothermic upwards.

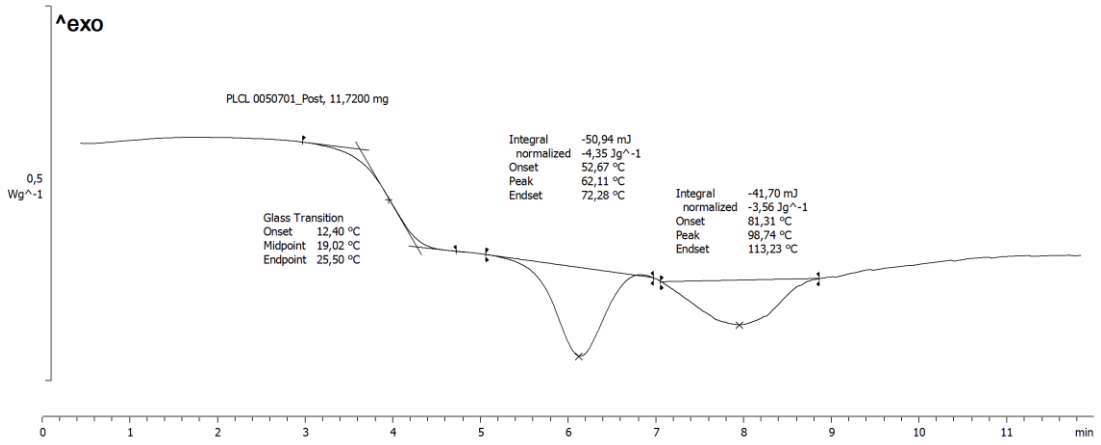

Figure A22 DSC curve of leached sample 005070 containing 70 wt.% salt in 0–50 µm range, exothermic upwards.

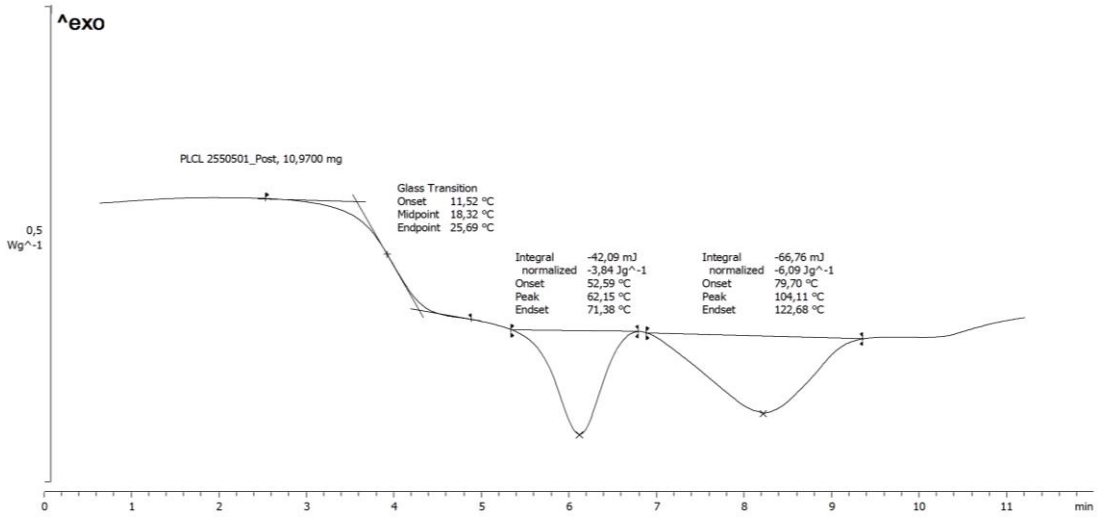

Figure A23 DSC curve of leached sample 255050 containing 50 wt.% salt in 25–50 µm range, exothermic upwards.

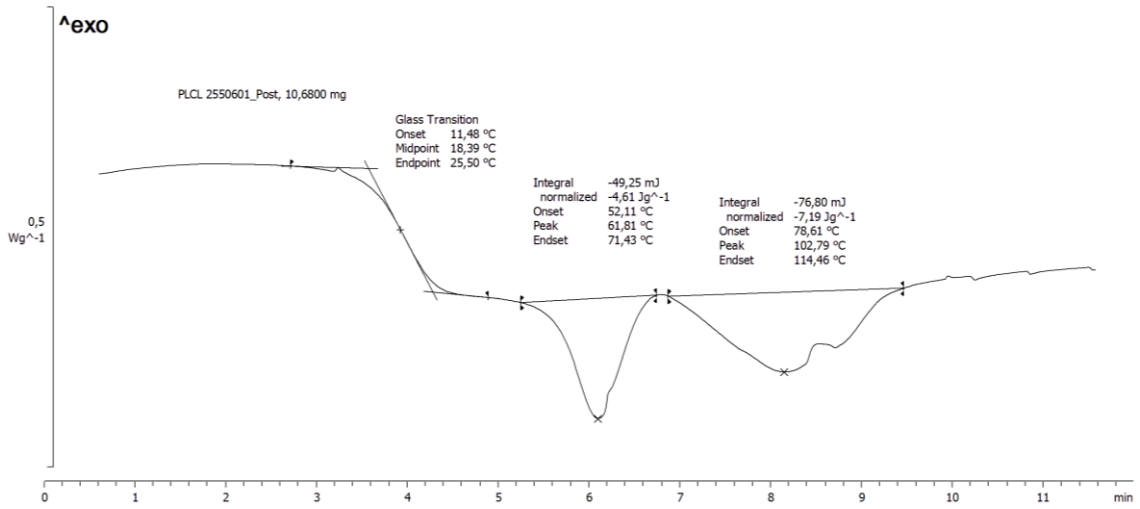

Figure A24 DSC curve of leached sample 255060 containing 60 wt.% salt in 25–50 µm range, exothermic upwards.

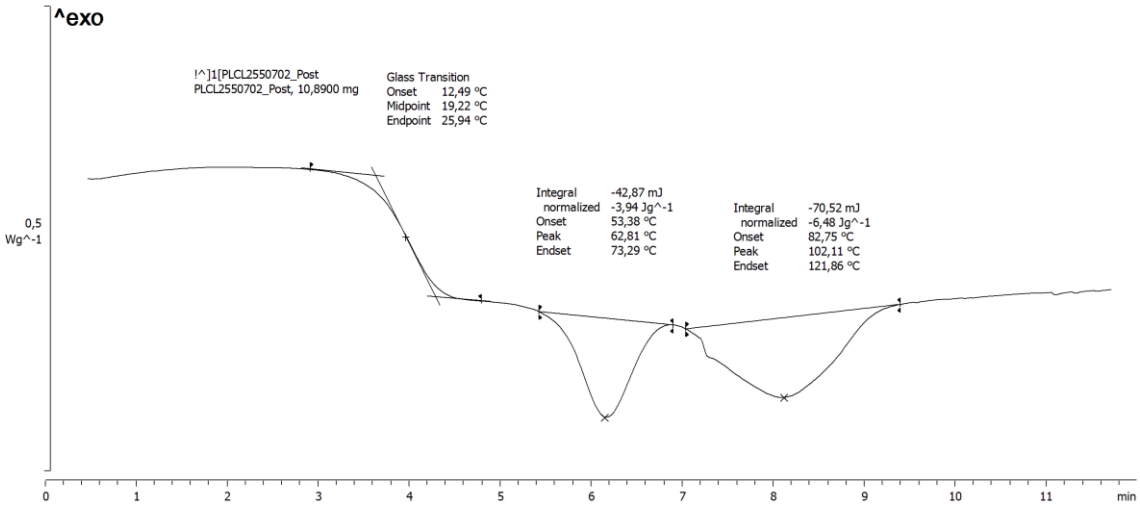

Figure A25 DSC curve of leached sample 255070 containing 70 wt.% salt in 25–50 µm range, exothermic upwards.

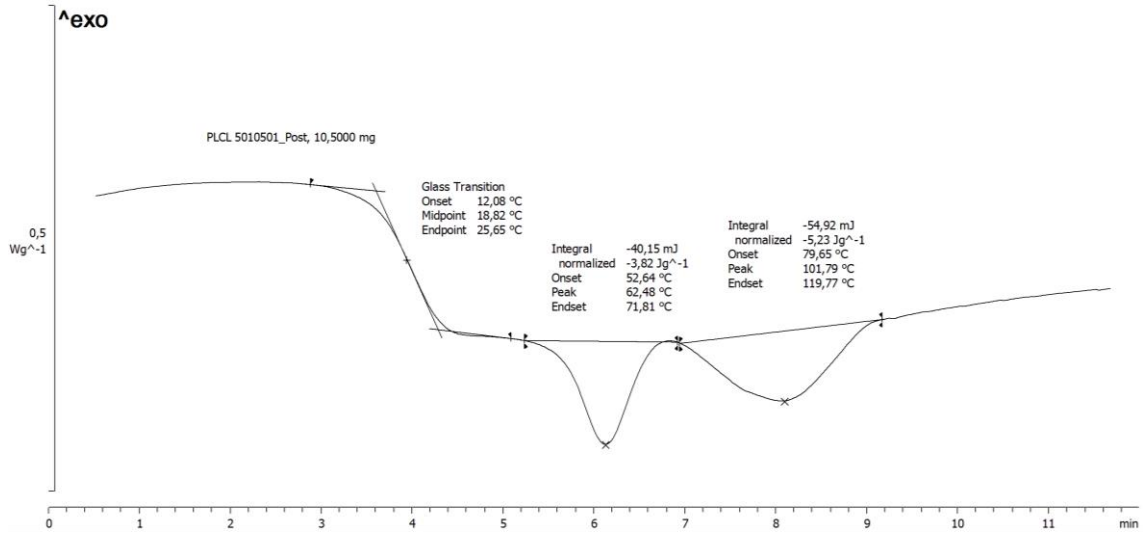

Figure A26 DSC curve of leached sample 501050 containing 50 wt.% salt in 50–100 µm range, exothermic upwards.

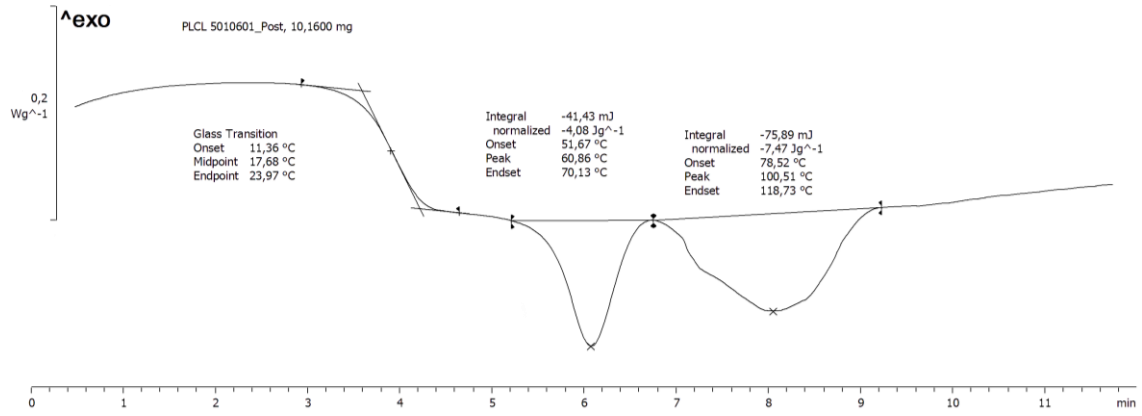

Figure A27 DSC curve of leached sample 501060 containing 60 wt.% salt in 50–100 µm range, exothermic upwards.

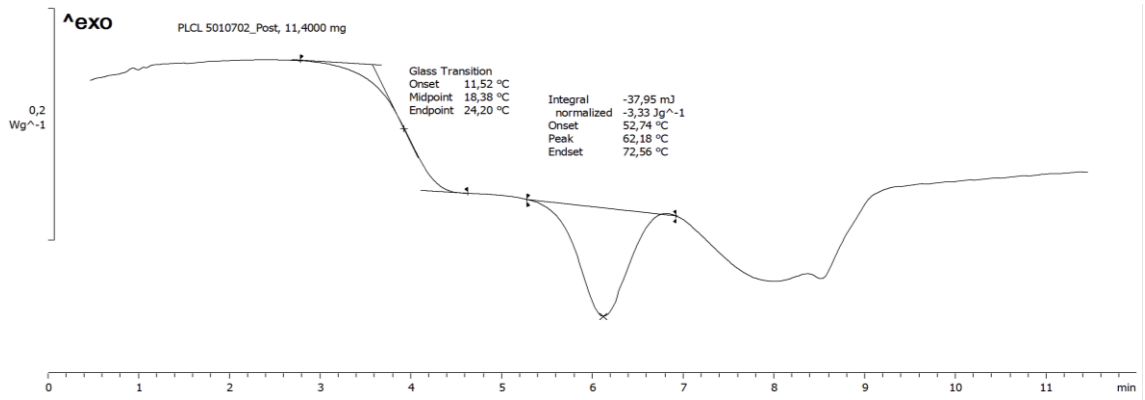

Figure A28 DSC curve of leached sample 501070 containing 70 wt.% salt in 50–100 µm range, exothermic upwards.

Appendix B

Supplementary material of Chapter 4

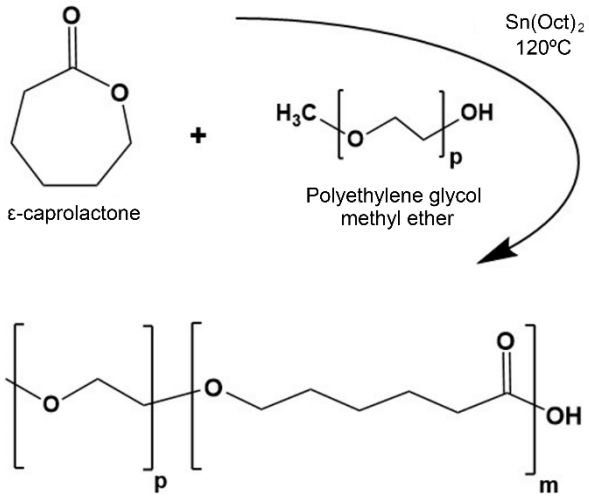

Figure B1 PCL reaction scheme and structure.

$$A = \frac{\pi}{4} \cdot (D_O^2 - D_i^2) \qquad \text{(Equation B1)}$$

Equation B1 Equation used to calculate the area (A) of a tube. D_0 is the outer diameter and D_i the inner diameter.

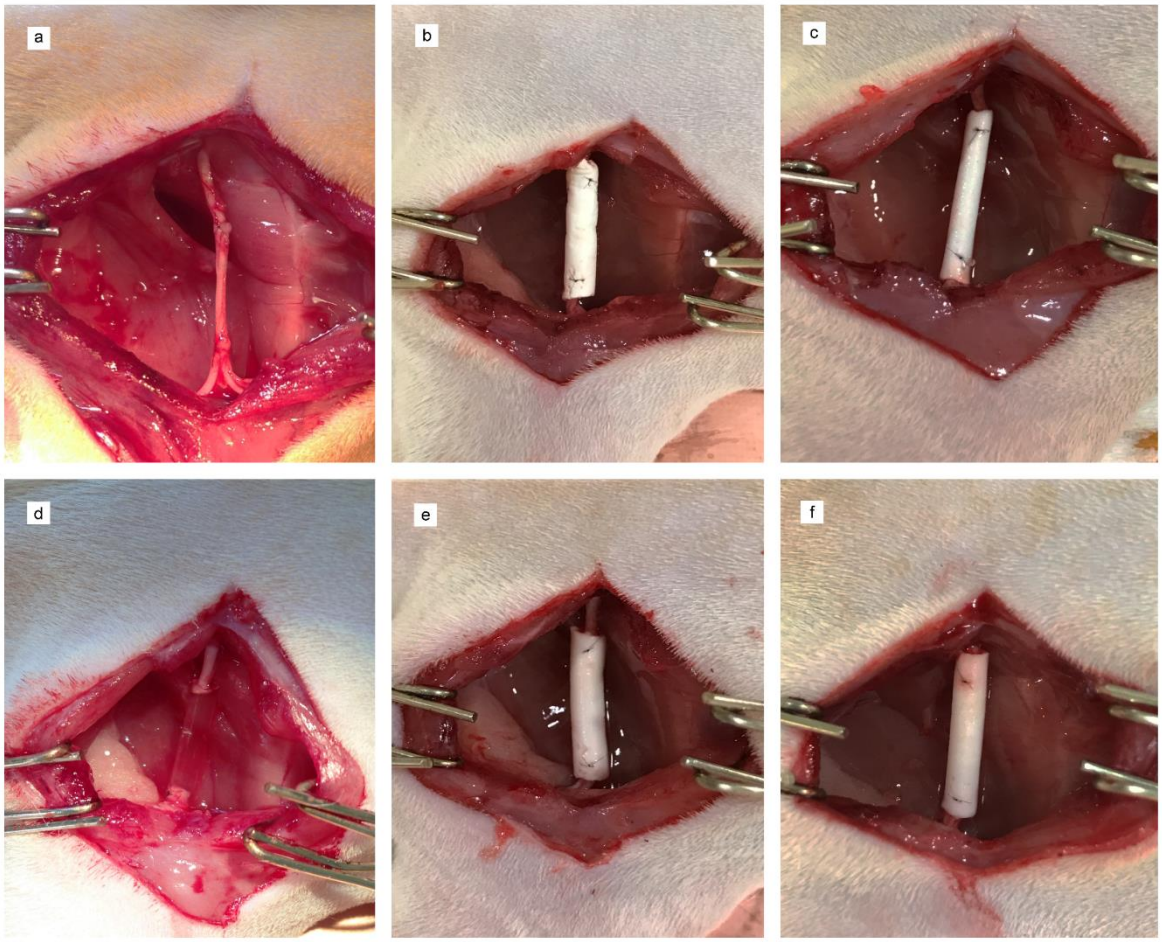

Figure B2 Representative images of surgery implanting Autograft (a), non-leached P(3HO-3HD)/PCL NGC with 500 µm wall thickness (b), and 250 µm wall thickness (c), Neurolac™-TW (d) and leached P(3HO-3HD)/PCL with 500 µm wall thickness (e), and 250 µm wall thickness (f).

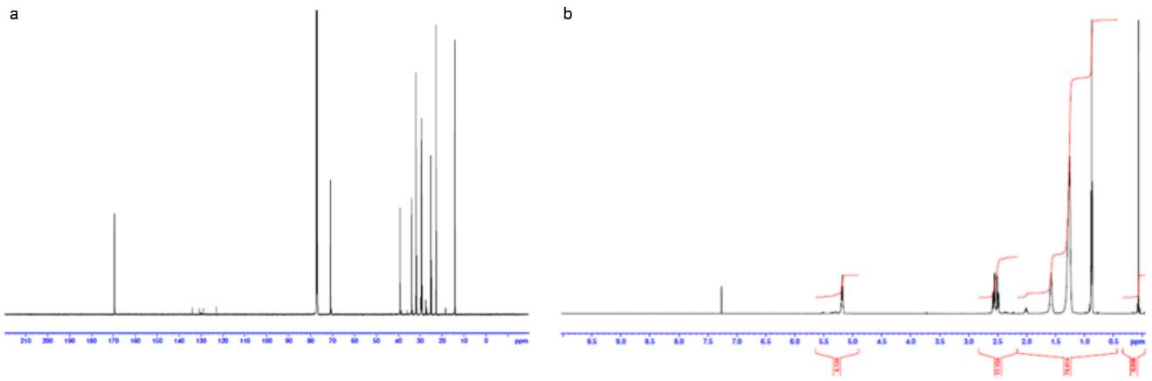

Figure B3 ^{13}C and ^{1}H NMR spectra of microbially produced MCL-PHA. ^{13}C NMR (600 MHz, $CDCl_3$): δ 169.5, 70.9, 39.2, 33.9, 33.8, 31.9, 31.6, 29.5, 29.3, 25.2, 24.8, 22.8, 22.6, 14.2, 14.1 (a). ^{1}H NMR (600 MHz, $CDCl_3$): δ 5.25 (1H, quin), 2.59-2.48 (2H, m), 1.57 (3H, m), 1.25 (m), 0.87 (3H, m) (b).

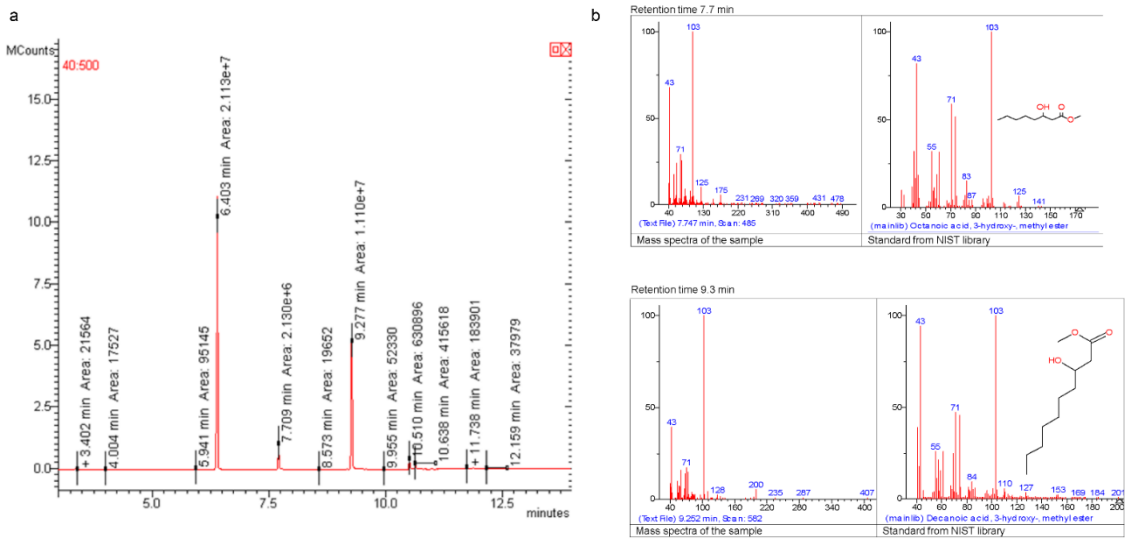

Figure B4 GC-MS analysis of microbially produced MCL-PHA. gas chromatogram (a), mass spectra analysis (b) right column standard spectra from NIST library.

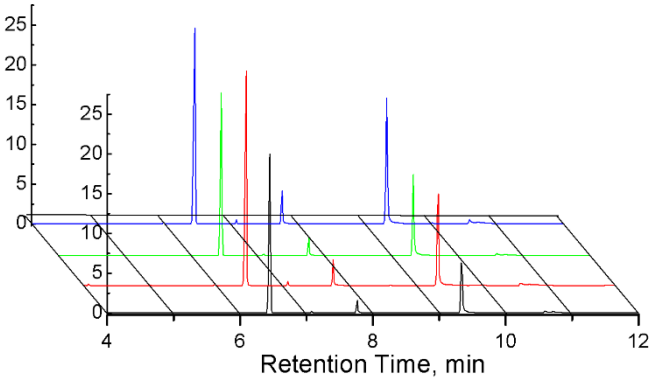

Figure B5 Consistency in microbial production of P(3HO-3HD) – GC-MS spectra of four batches.

Table B1 Consistency in microbial production of P(3HO-3HD) – monomer composition from ^{13}C NMR.

	Monomer content, mol%	
Batch	3-hydroxyoctanoate	3-hydroxydodecanoate
1	24.7	75.3
2	25.1	74.9
3	26.9	73.1
4	26.2	73.8
Mean	26.0	74.3
STD	1.0	1.0

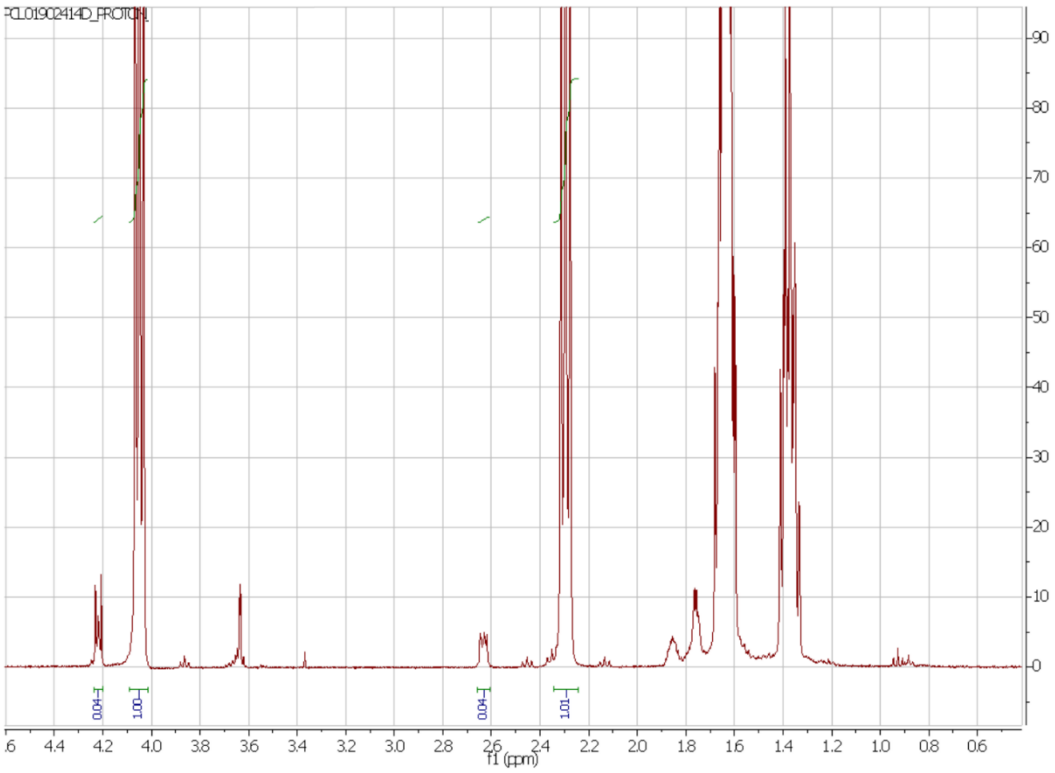

Figure B6 ^{1}H NMR (300 MHz, $CDCl_3$) spectrum of synthetized PCL-PEG. Caprolactone methylenes present signals around 2.35 and 4.1 ppm while mPEG is identified at a chemical shift of 3.6 - 3.65 ppm. The polymer conversion was calculated based on the integration of CH_2 peaks for the respective polymers and monomers introduced.

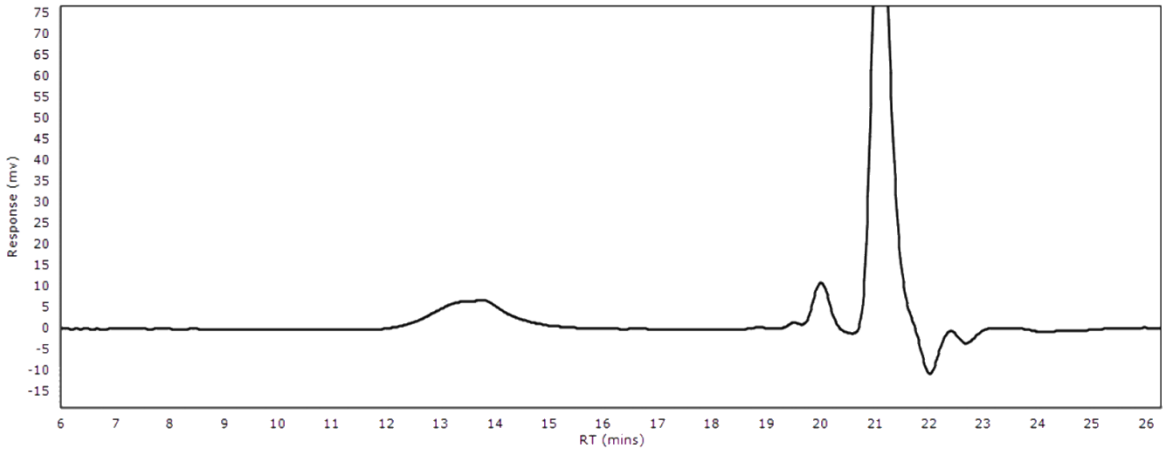

Figure B7 GPC curve of synthetized PCL-PEG. RT (Retention Time).

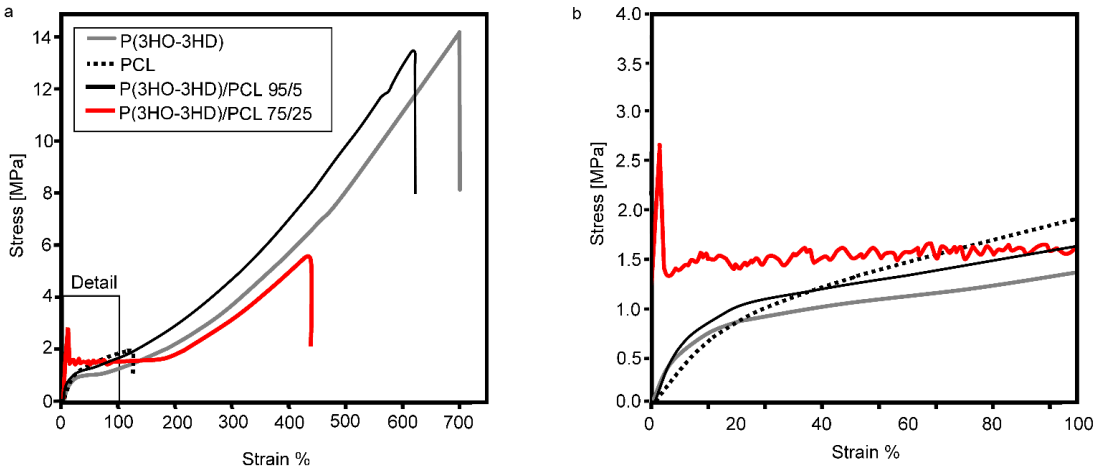

Figure B8 Stress-strain curves for P(3HO-3HD) and PCL non-porous films and blends of P(3HO-3HD)/PCL 95/5 and 75/25 (a). Detail plot of curves with strains between 0 and 100% (b).

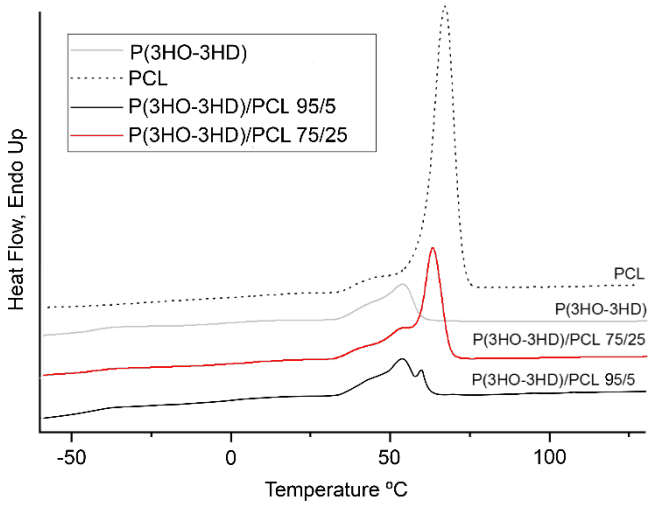

Figure B9 First heating DSC thermograms of aged P(3HO-3HD), PCL and blends of P(3HO-3HD)/PCL with 95/5 and 75/25 proportions. Film samples were stored for 7 weeks at room temperature before DSC experiments. Endothermic heat flow upwards.

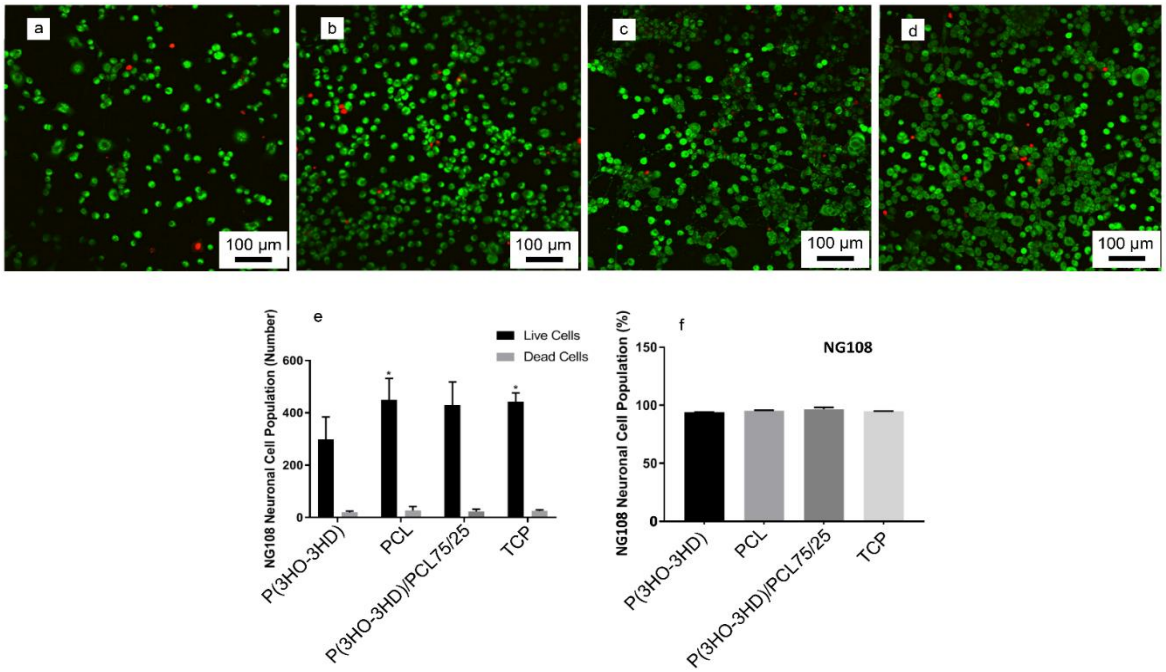

Figure B10 Confocal micrographs illustrating cell viability of NG108-15 neuronal cells cultured on P(3HO-3HD) (a), PCL (b), P(3HO-3HD)/PCL 75/25 (c) films and TCP control (d) (Scale bar = 100 µm). Number of live cells against dead cells per sample (e) and live/dead analysis expressed as a percentage (f) (mean ± SD, n=3 independent experiments, *p<0.05 against P(3HO-3HD).

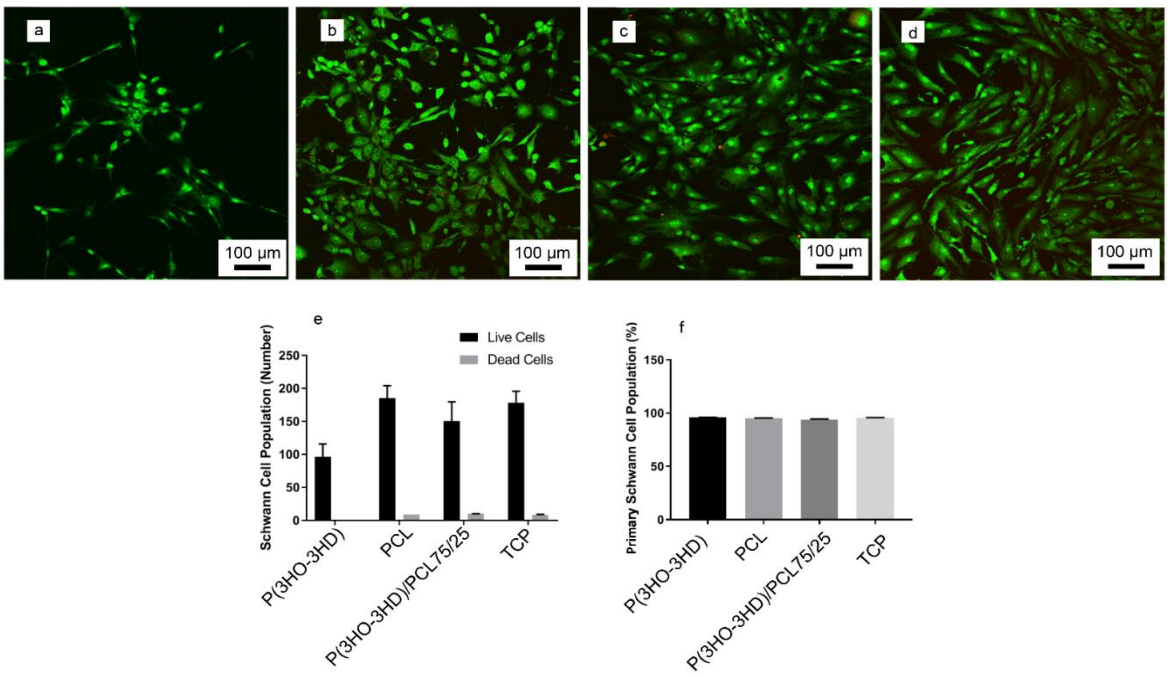

Figure B11 Confocal micrographs illustrating cell viability of primary Schwann cells cultured on P(3HO-3HD) (a), PCL (b), P(3HO-3HD)/PCL 75/25 (c) films and TCP control (d) (Scale bar = 100 µm). Number of live cells against dead cells per sample (e) and live/dead analysis expressed as a percentage (f) (mean ± SD, n=3 independent experiments).

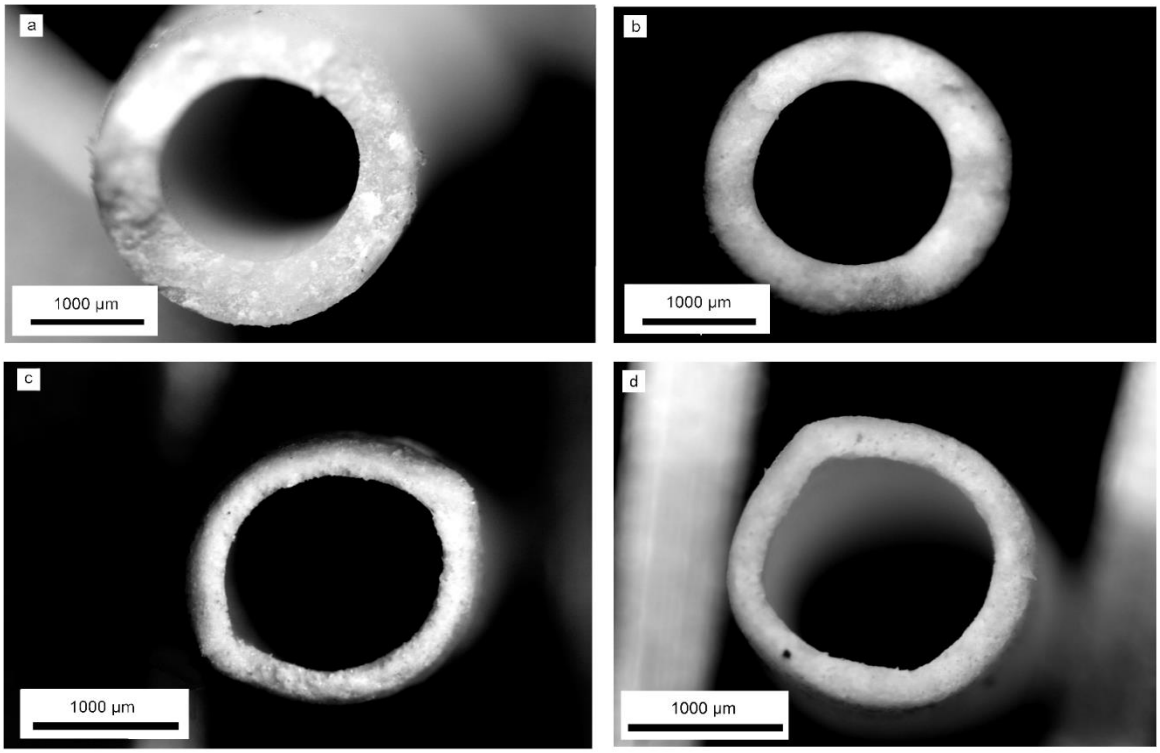

Figure B12 Optical microscope pictures of P(3HO-3HD)/PCL 75/25 tubes with different configurations, 500 µm non-leached (a), 500 µm leached (b), 250 µm non-leached (c) and 250 µm leached (d). Scale bar 1000 µm.

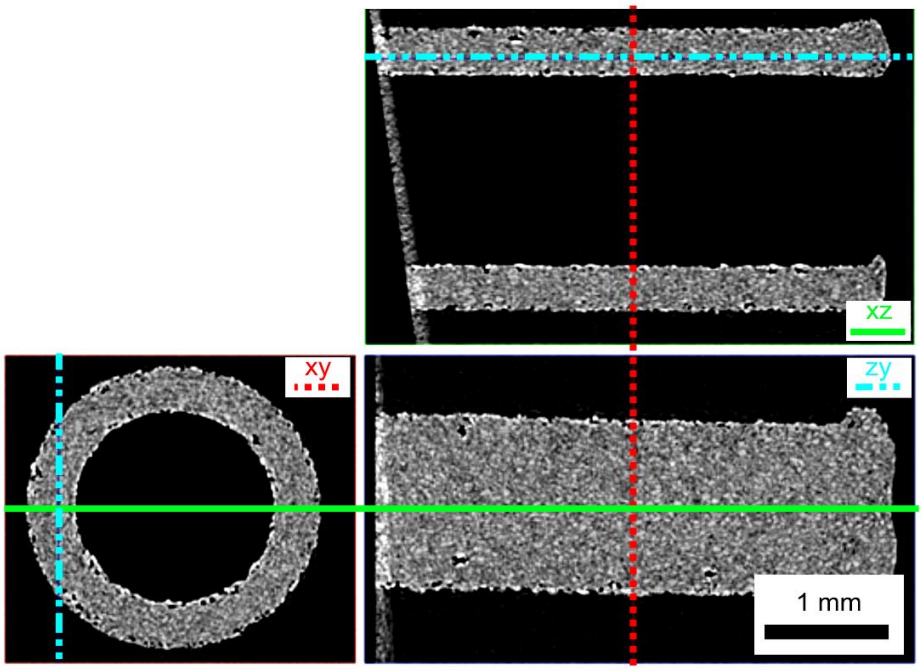

Figure B13 µCT image of non-leached P(3HO-3HD)/PCL 75/25 tube with 250 µm thickness showing the inner structure of the tube where glucose and polymeric matrix shown a homogenic distribution with no remarkable pores nor clumps.

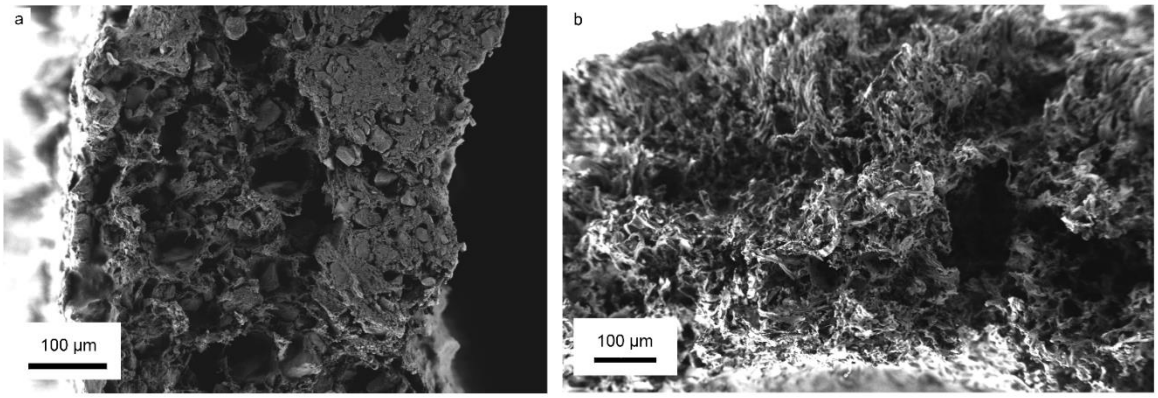

Figure B14 SEM images of P(3HO-3HD)/PCL 75/25 tubes with 500 µm wall thickness, non-leached (a) and leached (b). Scale bar 100 µm.

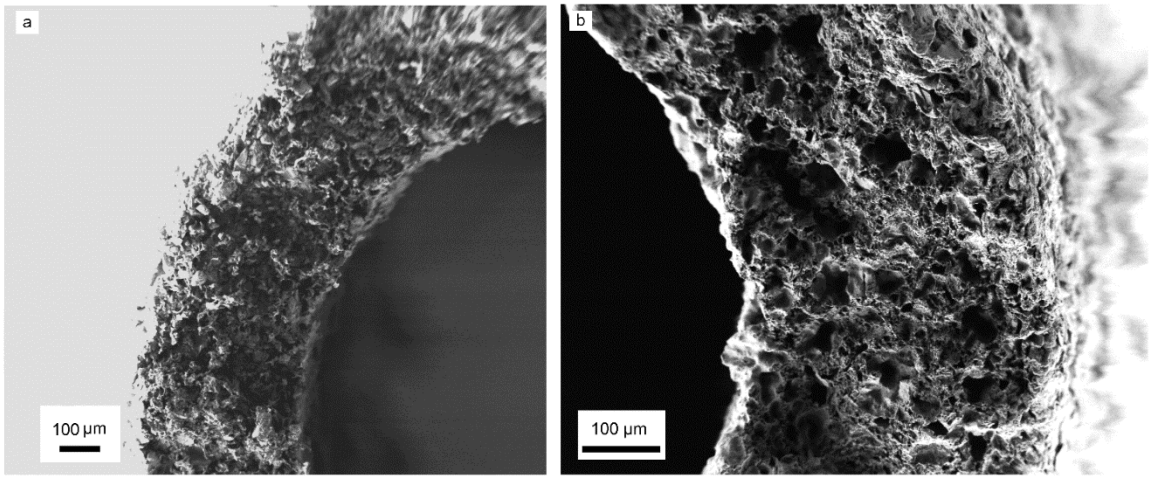

Figure B15 SEM images of P(3HO-3HD)/PCL 75/25 tubes with 250 µm wall thickness, non-leached (a) and leached (b). Scale bar 100 µm.

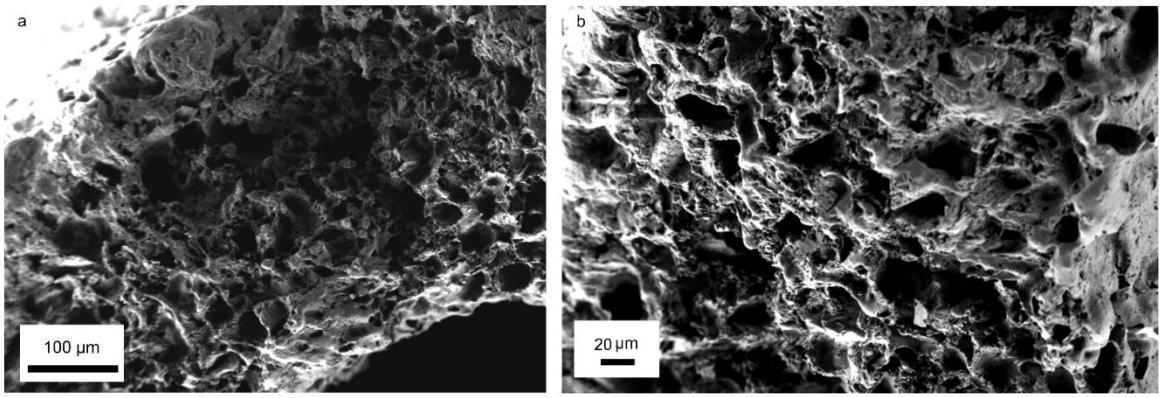

Figure B16 SEM images of P(3HO-3HD)/PCL 75/25 tubes showing the overall distribution of porous structure along the wall (a) and detail of tube section showing uniform and connected pores (b). Scale bar 100 µm in (a) and 20 µm in (b).

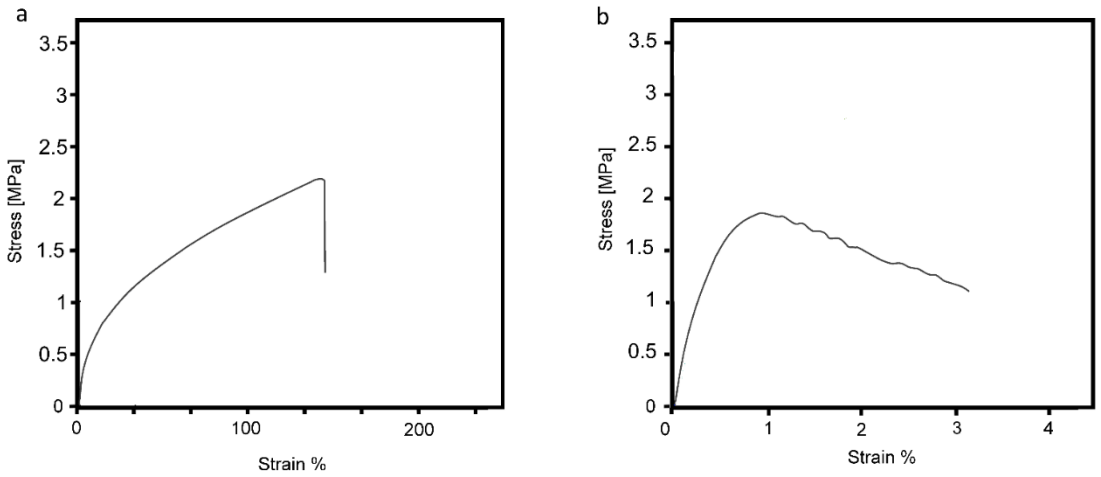

Figure B17 Stress-strain curves for P(3HO-3HD)/PCL 75/25 tubes with 250 µm wall thickness. Leached tubes on (a) and non - leached tubes on (b).

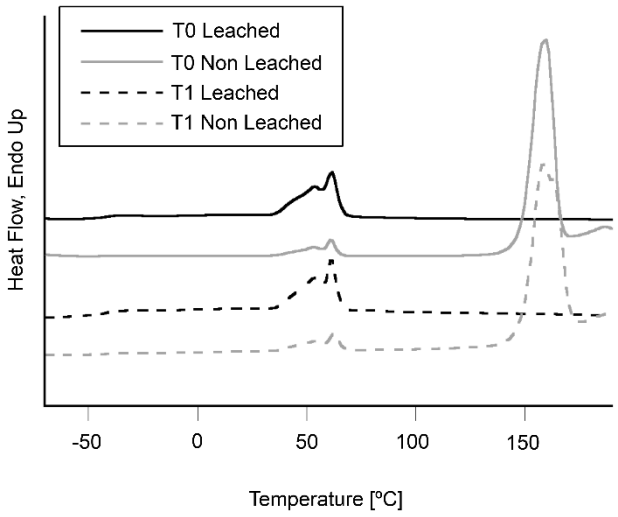

Figure B18 First heating DSC thermograms of extruded P(3HO-3HD)/PCL 75/25 samples in fresh (T0) (continuous line) and aged at room temperature in a desiccator for 3 months (T1) (dashed line). Leached samples are shown with black line and non-leached samples with grey line. Endothermic heat flow upwards.

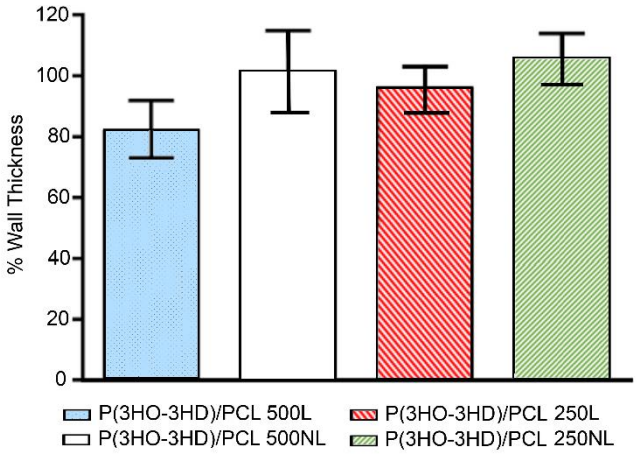

Figure B19 Change in wall thickness after 4 months after injury and repair. Data are presented as mean ± SEM

Table B2 Summary of data. Data are presented as Mean ± SEM

				P(3HO-3HD)/PCL 500 µm wall-thickness		P(3HO-3HD)/PCL 250 µm wall-thickness	
	Group	Autograft	Neurolac™-TW	Leached	Non-Leached	Leached	Non-Leached
	N (% regeneration)	8 (100 %)	10 (70 %)	8 (87.5%)	8 (75 %)	8 (25%)	8 (75 %)
Electrophysiology (60 dpi)	Gastrocnemius (mV)	31.39±1.99	5.53±1.40a	4.68±1.72	5.03±1.51	1.11±0.59	0.67±0.57
	Tibialis anterior (mV)	23.75±3.55	5.12±1.34a	3.00±1.41	3.46±1.44	0.51±0.33	0.50±0.35
	Plantar interosseous (mV)	1.26 ± 0.46	0.33±0.15	0.21±0.12	0.24±0.14	0±0	0.04±0.04
Electrophysiology (90 dpi)	Gastrocnemius (mV)	32.1±5.57	21.87±5.42	15.3±2.77	16.36±4.44	6.75±4.2	15.32±4.91
	Tibialis anterior (mV)	19.6±4.78	9.29±2.51	10.47±2.11	9.61±2.43	4.21±2.45	9.36±3.3
	Plantar interosseous (mV)	1.39±0.38	1.13±0.37	1.29±.62	1.5±0.59	0.17±0.18	0.9±0.35
Electrophysiology (120 dpi)	Gastrocnemius (mV)	38.59±1.12	23.52±5.69	39.57±6.76	37.18±9.09	16.33±8.54	37.32±8.80
	Tibialis anterior (mV)	30.53±2.00	14.57±4.12	33.58±6.34	33.49±8.18	13.63±7.32	26.97±6.96
	Plantar interosseous (mV)	2.32±0.38	1.51±0.46	2.11±0.57	2.70±0.94	0.97±0.53	2.73±0.78
Morphometry (120 dpi) (Mid graft/NGC)	Area (mm2)	0.90±0.21	0.16±0.05	0.19±0.04	0.22±0.06	0.05±0.03	0.12±0.03
	Nº myelinated axons	11432±3468	4520±1271	4693±1066	5756±1624	1711±1004	4139±1035
	Density (Axons/ mm2)	12043±2057	20595±5834	22768±3867	20859±5736	10846±5968	26047 ± 6528
Morphometry (120 dpi) (Distal graft/NGC)	Area (mm2)	0.74±0.16	0.55±0.14	0.57±0.11	0.51±0.15	0.33±0.18	0.48±0.17
	Nº myelinated axons	6017±2081	879±288	859±297	484±157a	301±168	296±168
	Density (Axons/ mm2)	10096±3598	1111±343	1321±383	826±342a	332±174	375±131